

AD-A046 151

AFFDL-TR-73-42

Part III

20070917040

DEVELOPMENT AND EVALUATION OF METHODS OF PLANE STRESS FRACTURE ANALYSIS

Part III. Application of the Residual Strength Prediction Technique to Complex Aircraft Structure

*NORTHROP CORPORATION
AIRCRAFT DIVISION*

AUGUST 1977

TECHNICAL REPORT AFFDL-TR-73-42, PART III,
Report for Period January 1975 – June 1975

Approved for public release; distribution unlimited.

AIR FORCE FLIGHT DYNAMICS LABORATORY
AIR FORCE WRIGHT AERONAUTICAL LABORATORIES
AIR FORCE SYSTEMS COMMAND
WRIGHT-PATTERSON AIR FORCE BASE, OHIO 45433

Best Available Copy

NOTICE

When Government drawings, specifications, or other data are used for any purpose other than in connection with a definitely related Government procurement operation, the United States Government thereby incurs no responsibility nor any obligation whatsoever; and the fact that the Government may have formulated, furnished, or in any way supplied the said drawings, specifications, or other data, is not to be regarded by implication or otherwise as in any manner licensing the holder or any other person or corporation, or conveying any rights or permission to manufacture, use, or sell any patented invention that may in any way be related thereto.

This report has been reviewed by the Office of Information (OI) and is releasable to the National Technical Information Service (NTIS). At NTIS, it will be available to the general public, including foreign nations.

This technical report has been reviewed and is approved for publication.

George P. Sendeckyj

G.P. SENDECKYJ
Project Engineer

R.M. Bader

ROBERT M. BADER, Chief
Structural Integrity Br
Structural Mechanics Division

FOR THE COMMANDER

Howard L. Farmer

HOWARD L. FARMER, Colonel, USAF
Chief, Structural Mechanics Division

Copies of this report should not be returned unless return is required by security considerations, contractual obligations, or notice on a specific document.

UNCLASSIFIED.

SECURITY CLASSIFICATION OF THIS PAGE (When Data Entered)

REPORT DOCUMENTATION PAGE		READ INSTRUCTIONS BEFORE COMPLETING FORM
1. REPORT NUMBER AFFDL-TR-73-42, Part III	2. GOVT ACCESSION NO.	3. RECIPIENT'S CATALOG NUMBER
4. TITLE (and Subtitle) DEVELOPMENT AND EVALUATION OF METHODS OF PLANE STRESS FRACTURE ANALYSIS Part III Application of the Residual Strength Prediction Technique to Complex Aircraft Structure		5. TYPE OF REPORT & PERIOD COVERED Part III (Phase III) Final Report--Jan. 1975 - June 1975
7. AUTHOR(s) M. M. Ratwani and D. P. Wilhem		6. PERFORMING ORG. REPORT NUMBER NOR 75-86 8. CONTRACT OR GRANT NUMBER(s) F33615-72-C-1796
9. PERFORMING ORGANIZATION NAME AND ADDRESS Northrop Corporation, Aircraft Division 3901 West Broadway, Hawthorne, California 90250		10. PROGRAM ELEMENT, PROJECT, TASK AREA & WORK UNIT NUMBERS Project 486U Task 0204
11. CONTROLLING OFFICE NAME AND ADDRESS Air Force Flight Dynamics Laboratory Wright-Patterson Air Force Base, Ohio 45433		12. REPORT DATE August 1977
14. MONITORING AGENCY NAME & ADDRESS(if different from Controlling Office)		13. NUMBER OF PAGES 148 15. SECURITY CLASS. (of this report) Unclassified 15a. DECLASSIFICATION/DOWNGRADING SCHEDULE
16. DISTRIBUTION STATEMENT (of this Report) Approved for Public Release; Distribution Unlimited.		
17. DISTRIBUTION STATEMENT (of the abstract entered in Block 20, if different from Report)		
18. SUPPLEMENTARY NOTES		
19. KEY WORDS (Continue on reverse side if necessary and identify by block number) Structural Residual Strength Prandtl-Reuss Material Behavior Finite Element Fracture Mechanics Analysis J-Integral Modeling Elastic-Plastic Analysis $\sqrt{J_R}$ Resistance Curve Dugdale Model Plane Stress Fracture Biaxial Loading Mixed Mode Fracture		
20. ABSTRACT (Continue on reverse side if necessary and identify by block number) Using the residual strength technique presented in Part II of this report, uniaxially loaded, angle stiffened wing panels were analyzed and fracture strengths determined. Excellent correlation was obtained between experimental and analytical data for an initially intact and broken central stringer for a six bay aluminum panel with thin skin, a thick (0.193 inch) skin aluminum panel, and an all titanium panel. Both crack arrest and fracture could be (See over)		

UNCLASSIFIED

SECURITY CLASSIFICATION OF THIS PAGE(When Data Entered)

20. ABSTRACT (Continued)

predicted using the tangency conditions between the crack driving force curves (\sqrt{J}) and the crack growth resistance curve ($\sqrt{J_R}$). The influence of biaxial load ratio (tension fields) on crack opening displacement, plastic zone size and load transfer was examined for an all aluminum fuselage panel with a crack in the skin located normal to the longerons and parallel to the frames. Comparisons are made between analytical and experimental strain and residual strength data for biaxially loaded structure.

A summary of the technique is presented which will enable analytical predictions of amount of slow tear, crack arrest, and residual strength, as well as defining when a stiffener or skin critical condition prevails. A comparison of the accuracy of the method with experimental residual strength data shows that predictions can be made which are well within the scatter in the material crack growth resistance data which is ± 5 percent.

UNCLASSIFIED

SECURITY CLASSIFICATION OF THIS PAGE(When Data Entered)

PREFACE

This report was prepared by Northrop Corporation, Aircraft Division, Hawthorne, California, under Air Force Contract F33615-72-C-1796. The project was initiated under Project Number 486U, Task 0204, "Advanced Metallic Structures," Advanced Development Program. The work reported herein was administered under the direction of the Air Force Systems Command, Wright-Patterson Air Force Base, Ohio, by Dr. George Sendeckyj (FBEC) and Captain George F. Zielsdorff (ASD), Project Engineers.

The research was conducted between January 1975 and June 1975 as a conclusion to Phase III and the overall program. This report was submitted by the authors M. M. Ratwani and D. P. Wilhem in June 1975 for AFFDL review. The report has been assigned NOR 75-86 for internal control at Northrop Corporation.

The authors wish to acknowledge the support of P. Finwall, J. FitzGerald, and B. J. Mays for their assistance during the structural testing program, and to Messrs. V. C. Frost and P. W. Warren for assistance in structural test specimen design and construction. The secretarial assistance of Lessie Speciale is also acknowledged.

TABLE OF CONTENTS

SECTION		PAGE
I	INTRODUCTION	1
II	STIFFENED UNIAXIALLY LOADED PANELS	2
	2.1 GENERAL INTRODUCTION	2
	2.2 BROKEN AND INTACT STRINGER-THIN SKIN	2
	2.2.1 Description of Test Panel(s)	2
	2.2.2 Finite Element Modeling and Analysis	5
	2.2.2.1 Finite Element Modeling of Intact and Broken Stringer Panels	5
	2.2.2.2 Elastic and Elastic-Plastic Analysis of Panels with Intact and Broken Stringer	8
	2.2.3 Experimental Results and Discussion	14
	2.2.3.1 Test Arrangement - General	14
	2.2.3.2 Fatigue Precracking, Strain Data and Fracture of Broken and Intact Stringer Cases	18
	2.2.3.3 Comparison of Experimental and Analytical Strains	28
	2.2.4 Residual Strength Prediction	36
	2.2.4.1 Residual Strength of Panel with Intact Central Stringer	36
	2.2.4.2 Residual Strength of Panel with Broken Central Stringer	40
	2.3 TITANIUM PANEL	40
	2.3.1 Description of Test Panel	40
	2.3.2 Finite Element Modeling and Analysis	41
	2.3.2.1 Finite Element Modeling of the All Titanium Panel	43
	2.3.2.2 Elastic and Elastic-Plastic Analyses of All Titanium Panel	43

TABLE OF CONTENTS (CONTINUED)

SECTION	PAGE
2.3.3 Experimental Results and Discussion	43
2.3.3.1 $\sqrt{J_R}$ Crack Growth Resistance Data for Beta Mill Annealed Ti-6Al-4V	47
2.3.3.2 Fatigue Precracking, Strain Data and Fracture of Titanium Panel	47
2.3.3.3 Comparison of Experimental and Analytical Strains	56
2.3.4 Residual Strength Prediction	56
2.4 INTACT STRINGER - THICK SKIN	65
2.4.1 Description of Test Panel	65
2.4.2 Finite Element Modeling and Analysis	67
2.4.3 Experimental Results and Discussion	67
2.4.3.1 Fatigue Precracking Strain Data and Fracture of Thick Skin Panel	67
2.4.3.2 Comparison of Experimental and Analytical Strains	78
2.4.4 Residual Strength Prediction	78
III STIFFENED BIAXIALLY LOADED PANELS	84
3.1 GENERAL INTRODUCTION	84
3.2 DESCRIPTION OF TEST PANEL(S)	85
3.3 FINITE ELEMENT MODEL AND ANALYSIS	89
3.3.1 Finite Element Modeling of Biaxially Loaded Panels	89
3.3.2 Elastic and Elastic-Plastic Analysis of the Biaxial Panel	89
3.3.2.1 Elastic Analysis of Biaxial Panel	89
3.3.2.2 Elastic-Plastic Analysis of Biaxial Panel	99

TABLE OF CONTENTS (CONTINUED)

SECTION		PAGE
	3.4 EXPERIMENTAL RESULTS AND DISCUSSION	99
	3.4.1 Fatigue Precracking, Strain Data and Fracture of Biaxial Loaded Panels	103
	3.4.2 Comparison of Experimental and Analytical Data	120
	3.5 RESIDUAL STRENGTH PREDICTION	128
IV	SUMMARY OF OVERALL PROGRAM AND PREDICTION METHODS	132
	4.1 PROGRAM SUMMARY	132
	4.2 PREDICTIVE PROCEDURE (STEPS)	133
V	CONCLUSIONS	134
	5.1 GENERAL TRENDS	134
	5.2 OVERALL ACCURACY OF THE METHOD	134
	REFERENCES	136

LIST OF ILLUSTRATIONS

<u>Figure</u>		<u>Page</u>
1	Drawing of Wing Panel - Angle Stiffened	3
2	Basic Finite Element Model for Angle Stiffened, Lower Wing Panels	7
3	Contours for J Integral Calculations - Angle Stiffened, Lower Wing Panels	9
4	Comparison of Square Root of J Values for Intact and Broken Central Stringer Cases - Thin Skin	10
5	Crack Opening Displacement for Broken (-23) and Intact (-15) Stringers, Angle Stiffened Panels	11
6	Prediction of Broken Stringer Panel Stress From Intact Stringer Analysis	12
7	Stress in Central Stringer as a Function of Applied Stress Based on Elastic and Elastic-Plastic Analysis - Intact Stringer	13
8	Square Root of J as a Function of Applied Stress for Varying Crack Lengths - Intact Stringer	15
9	Square Root of J as a Function of Crack Length - Intact Stringer	16
10	View of Test Panel in 500,000 Pound Load Frame	17
11	Overall View of Skin Side of Wing Panel Angle Stiffened, Lower (Center Stringer Broken)	19
12	Overall View of Skin Side of Wing Panel Angle Stiffened, Lower (Center Stringer Intact)	20
13	Overall View of Angle Stiffened Side of Wing Panel Angle Stiffened, Lower (Center Stringer Broken)	21
14	Overall View of Angle Stiffened Side of Wing Panel Angle Stiffened, Lower (Center Stringer Intact)	22
15	Strain Gage Locations -23 and -15 Panels	25
16	Load-Displacement Curves for -23 Panel Angle Stiffened, Lower (Center Stringer Broken)	26

LIST OF ILLUSTRATIONS (CONTINUED)

<u>Figure</u>		<u>Page</u>
17	Load-Displacement Curves for -15 Panel Angle Stiffened, Lower (Center Stringer Intact)	27
18	View of Fracture Surface from Skin Side, Wing Panel Angle Stiffened, Lower (Center Stringer Initially Broken)	29
19	View of Fracture Surface from Skin Side, Wing Panel Angle Stiffened, Lower (Center Stringer Initially Intact)	30
20	View of Fracture Surface from Stringer Side, Wing Panel Angle Stiffened, Lower (Center Stringer Initially Broken)	31
21	View of Fracture Surface from Stringer Side, Wing Panel Angle Stiffened, Lower (Center Stringer Initially Intact)	32
22	Strain in Central Stringer for -15 Panel, Angle Stiffened, Lower	33
23	Strains in Central Attached Angle Away from the Crack Plane as a Function of Applied Stress for -15, Intact Angle Stiffened Panel	34
24	Strain in Central Stringer for -23 Panel, Angle Stiffened, Lower	35
25	Strain in Central and Outer Attached Angles as a Function of Applied Stress for Broken (-23) and Intact (-15) Stiffened Panels	37
26	Residual Strength Prediction Plot for -15 Panel (Intact Stringer)	39
27	Strain Gage Locations - Titanium Panel	42
28	Elastic and Elastic Plastic Analysis of All Titanium Panel	44
29	Square Root of J as a Function of Applied Stress for Varying Crack Lengths - All Titanium Panel	45
30	Square Root of J as a Function of Crack Length - Titanium Panel	46
31	$\sqrt{J_R}$ Crack Growth Resistance Data - Ti-6Al-4V (Beta Mill Annealed) - .053", LT	48

LIST OF ILLUSTRATIONS (CONTINUED)

<u>Figure</u>		<u>Page</u>
32	$\sqrt{J_R}$ Crack Growth Resistance Data - Ti-6Al-4V (Beta Mill Annealed) - .053", TL	49
33	$\sqrt{J_R}$ Crack Growth Resistance Data - Ti-6Al-4V (Beta Mill Annealed) - .187", LT	50
34	$\sqrt{J_R}$ Crack Growth Resistance Data - Ti-6Al-4V (Beta Mill Annealed) - .187", TL	51
35	Overall View of Skin Side of Wing Panel Angle Stiffened, Lower (All Titanium Panel)	52
36	Overall View of Angle Stiffened Side of Wing Panel Angle Stiffened, Lower (All Titanium Panel)	53
37	Strain Gage Locations - Titanium Panel	55
38	Load-Displacement Curves for Titanium Wing Panel Angle Stiffened, Lower	57
39	View of Fracture Surface From Skin Side, Wing Panel Angle Stiffened, Lower (All Titanium Panel)	58
40	View of Fracture Surface From Stringer Side, Wing Panel Angle Stiffened, Lower (All Titanium Panel)	59
41	Strain in Central Stringer for All Titanium Panel, Angle Stiffened, Lower	60
42	Strain in Central Attached Angle Away From the Crack Plane as a Function of Applied Stress for All Titanium Panel	61
43	Elastic and Elastic-Plastic Stress in Central Stringer as a Function of Applied Stress - All Titanium Panel	62
44	Residual Strength Prediction Plot for All Titanium Panel	64
45	Strain Gage Locations - Thick Skin (-1) Panel	66
46	Elastic and Elastic-Plastic \sqrt{J} Values for Thick Skin, -1 Panel as a Function of Applied Stress	68
47	Elastic and Elastic-Plastic Stress in Central Stringer as a Function of Applied Stress -1 Panel	69

LIST OF ILLUSTRATIONS (CONTINUED)

<u>Figure</u>		<u>Page</u>
48	Overall View of Skin Side of Wing Panel Angle Stiffened, Lower (Thick Skin)	71
49	Overall View of Angle Stiffened Side of Wing Panel Angle Stiffened, Lower (Thick Skin)	72
50	Load-Displacement Curves for Thick Skin - 7075-T73 Wing Panel Angle Stiffened, Lower	74
51	Load-Displacement Curves to Fracture for Thick Skin - 7075-T73 Wing Panel Angle Stiffened, Lower	75
52	View of Panel Fracture From Stringer Side, Wing Panel Angle Stiffened, Lower (Thick Skin)	76
53	Close-up View of Fractured Angles, Wing Panel Angle Stiffened, Lower (Thick Skin)	77
54	Strain Gage Locations - Thick Skin (-1) Panel	79
55	Strain in Central Stringer for Thick Skin, -1 Panel, Angle Stiffened, Lower	80
56	Strain in Central Stringer as a Function of Applied Stress -1 Panel	81
57	Residual Strength Prediction Plot for Thick Skin, -1 Panel	82
58	Fuselage Panel-Frame and Stringer Stiffened (Biaxial Panel)	87
59	Finite Element Model of Biaxial Panel(s)	90
60	Contours Used to Evaluate J for Biaxial Panels	91
61	Square Root of J for Varying Crack Lengths as a Function of Applied Stress - Biaxial Panel	93
62	Stress in the Central Longeron as a Function of Gross Area Panel Stress for Varying Crack Length - Biaxial Panel	94
63	Elastic \sqrt{J} Values as a Function of Applied Stress for Two Biaxial Load Ratios	95
64	Stress in the Central Longeron as a Function of Applied Stress for Two Biaxial Load Ratios	96

LIST OF ILLUSTRATIONS (CONTINUED)

<u>Figure</u>		<u>Page</u>
65	Total Crack Surface Displacements as a Function of Distance Along the Crack for Two Biaxial Load Ratios	97
66	Stresses in Adjacent Longerons for Two Biaxial Load Ratios	98
67	Square Root of J for Varying Biaxial Load Ratios Using Prandtl-Reuss Material Assumptions	100
68	Stress in Central Longeron for Varying Biaxial Load Ratios Using Prandtl-Reuss Material Assumptions	101
69	Plastic Zone Sizes for Three Biaxial Load Ratios Using Prandtl-Reuss Material Assumptions	102
70	Stiffener-Side View of Loading Arrangement for Biaxial Panels	104
71	Side View of Lateral Loading Arrangement for Biaxial Panels	105
72	Skin-Side View of Biaxial Test Panel	107
73	Longeron and Frame Side View of Biaxial Test Panel	108
74	Strain Gage Locations - Biaxial Panels	110
75	Load-Displacement Curves for Biaxial Panel 2-2 During Strain Survey and Slow Tear	112
76	Load-Displacement Curve for Biaxial Panel 2-2 to Fracture After Slow Tear	113
77	Load-Displacement Curve for Biaxial Panel 2-3 to Fracture	114
78	Fracture Sequence for 2-2 Biaxially Loaded Panel (60 kips Lateral Load)	115
79	Fracture Sequence for 2-3 Biaxially Loaded Panel (120 kips Lateral Load)	118
80	View of Fracture Surface From Skin Side, 2-2 Biaxially Loaded Panel	121
81	View of Fracture Surface From Longeron/Frame Side, 2-2 Biaxially Loaded Panel	122
82	View of Fracture Surface From Skin Side, 2-3 Biaxially Loaded Panel	123

LIST OF ILLUSTRATIONS (CONTINUED)

<u>Figure</u>		<u>Page</u>
83	View of Fracture Surface From Longeron/Frame Side, 2-3 Biaxially Loaded Panel	124
84	Strain in Central Longeron Away From the Crack at Three Biaxial Load Ratios	125
85	Strain in Longeron(s) at 0.6 Inches Away from the Crack, Biaxial Panel 2-2	126
86	Strain in Frame Member as a Function of Applied Stress for Three Biaxial Load Ratios	127
87	Total Crack Opening Displacements for Two Biaxial Load Ratios as a Function of Applied Stress	129
88	Square Root of J Versus Crack Length Curve for Biaxial Panel	130

LIST OF TABLES

<u>Tables</u>		<u>Page</u>
I	THIN SKIN-ANGLE STIFFENED WING PANEL AREAS AND MATERIAL IDENTIFICATION	6
II	FATIGUE PRECRACKING AND CRACK LENGTH DATA, -23 AND -15 PANELS	18
III	STRAIN GAGE DATA, -23 WING PANEL ANGLE STIFFENED, LOWER (CENTER STRINGER BROKEN)	23
IV	STRAIN GAGE DATA, -15 WING PANEL ANGLE STIFFENED, LOWER (CENTER STRINGER INTACT)	24
V	TITANIUM SKIN-ANGLE STIFFENED WING PANEL AREAS AND MATERIAL IDENTIFICATION	41
VI	FATIGUE PRECRACKING AND CRACK LENGTH DATA - TITANIUM PANEL	47
VII	STRAIN GAGE DATA, TITANIUM WING PANEL STIFFENED, LOWER	54
VIII	THICK SKIN (-1) - ANGLE STIFFENED WING PANEL AREAS AND MATERIAL IDENTIFICATION	65
IX	FATIGUE PRECRACKING AND CRACK LENGTH DATA - THICK SKIN PANEL	70
X	STRAIN GAGE DATA, -1 THICK SKIN WING PANEL ANGLE STIFFENED, LOWER	73
XI	FRAME-LONGERON STIFFENED PANEL AREAS AND MATERIAL IDENTIFICATION	85
XII	FATIGUE PRECRACKING AND CRACK LENGTH DATA, 2-2 AND 2-3 BIAXIAL PANELS	103
XIII	STRAIN GAGE DATA, 2-2 BIAXIAL PANEL	109
XIV	STRAIN GAGE DATA, 2-3 BIAXIAL PANEL	111
XV	COMPARISON OF PREDICTED AND MEASURED RESIDUAL STRENGTHS FOR PHASE II AND PHASE III PANELS	135

I INTRODUCTION

This report describes the research conducted during Phase III of a three-phase investigation into the development of an improved method of thin section residual strength prediction of cracked aircraft structure (where conditions of plane stress or mixed mode fracture prevail). Phases I and II summarized the current state-of-the-art of structural residual strength prediction and established an analytical procedure and fracture criterion to predict residual strength (Reference 1). Using a flexible fastener model and the Bueckner/Hayes approach to Dugdale type elastic-plastic analysis good predictions of residual strength for both skin and stringer critical conditions were made in Phase II for two-bay, uniaxially loaded panels. The studies undertaken during Phase III were aimed at defining the limits of the technique as well as proving (and improving) its ability to predict both crack arrest and fracture in multi-bay construction and multi-axis loading.

In Section II the following structural test panels were analyzed and tested: Thin skin (all aluminum) panel(s) with both intact and broken stringers, a thick skin (all aluminum) panel with mixed mode fracture behavior, and an all titanium panel. All loading was performed in uniaxial tension and excellent correlation was obtained with the experimental data. Both crack arrest and stringer critical conditions could be predicted.

Two biaxially loaded panels are discussed in Section III where a complete Prandtl-Reuss analysis was performed for the crack length of test. The influence of biaxial stress on crack opening displacement, plastic zone size, and load transferred to the stiffener were determined. Prediction of residual strength for the one panel which failed in the test area were made based on certain approximations with a good degree of success. The unknowns associated with the biaxial failure criterion were also examined and means proposed to study load interaction effects.

A summary of the overall three-phase program effort is included in Section IV, which contains the ten steps required to predict structural residual strength.

In Section V, a short summary is presented of the conclusions to the Phase III research. Also included is a table which compares analytical and experimental results for both phases of the program which indicates an average difference of approximately four percent in predicted versus measured residual strength for all panels tested.

It must again be noted that the proposed method of analysis given in Section 4.2 is not intended for use in performing parametric studies (i.e., stiffener spacing, rivet pitch, etc.) which could be more cheaply accomplished using linear elastic assumption and closed form solutions. However, the proposed method does offer the ability to predict residual strength accurately for a "fatigue sized" structure which is expected to fracture with large amounts of slow, stable tear and plasticity prior to structural failure.

II STIFFENED UNIAXIALLY LOADED PANELS

To demonstrate the utility of the residual strength prediction method for those structures loaded primarily in tension and for different materials and skin thickness four panels were analyzed, fabricated, and tested. This Section describes those analyses, panels, and test data.

2.1 GENERAL INTRODUCTION

The residual strength predictive method should be able to predict fracture in panels of typical aircraft structural geometry and materials. For this reason it was elected to examine lower wing structure since high, uniaxial stress occurs in this region. Skin material was 7075-T73 of two thicknesses, 0.063 and 0.193 inch, selected to produce essentially plane stress and mixed mode fracture behavior. In addition, a panel consisting of all titanium material, sized to represent typical fighter aircraft lower wing structure, was analyzed and tested using the proposed residual strength prediction technique. The reinforcing substructure for all panels consisted of angle sections which were fastened to the skin using standard, aircraft fastening techniques. For one panel configuration both an initially broken and intact central stiffener were analyzed and tested.

The analytical techniques employed in predicting the residual strength of the uniaxial loaded panels of this Section were those outlined in Reference 1 which consists of employing the Bueckner/Hayes energy approach using Dugdale plasticity assumptions combined with a flexible fastener finite element model. Failure is based on either a stiffener or skin critical failure criterion. The basis of the skin critical criterion is the tangency between the material crack growth resistance curve, or \sqrt{J}_R curve, with the crack driving force curves in terms of \sqrt{J} .

2.2 BROKEN AND INTACT STRINGER-THIN SKIN

The panel geometry selected for this analysis consists of typical lower wing construction (outboard of the engines) for a large transport type aircraft. Crack geometries were similar for two identical panels. The difference between the two was, one contained an initially broken central stringer and it was intact in the other. However, it was realized that either this situation or the through cracked skin-stringer could occur in service situations in a random manner. Therefore, the panels analyzed and tested in this part of Phase III represent those situations where a common crack length was used for comparative purposes in a broken and intact stringer situation.

2.2.1 Description of Test Panel(s)

The drawing of the test panel(s) is shown in Figure 1 and is identified as -15 assembly for the intact stringer and -23 for the broken central stringer case. The overall skin width of the 7075-T73 was 38.5 inches with a 5.5 inch spacing between rivet and angle centerlines. This spacing produced a six bay panel, symmetric about the panel centerline, i.e., three bays on either side of the center angle.

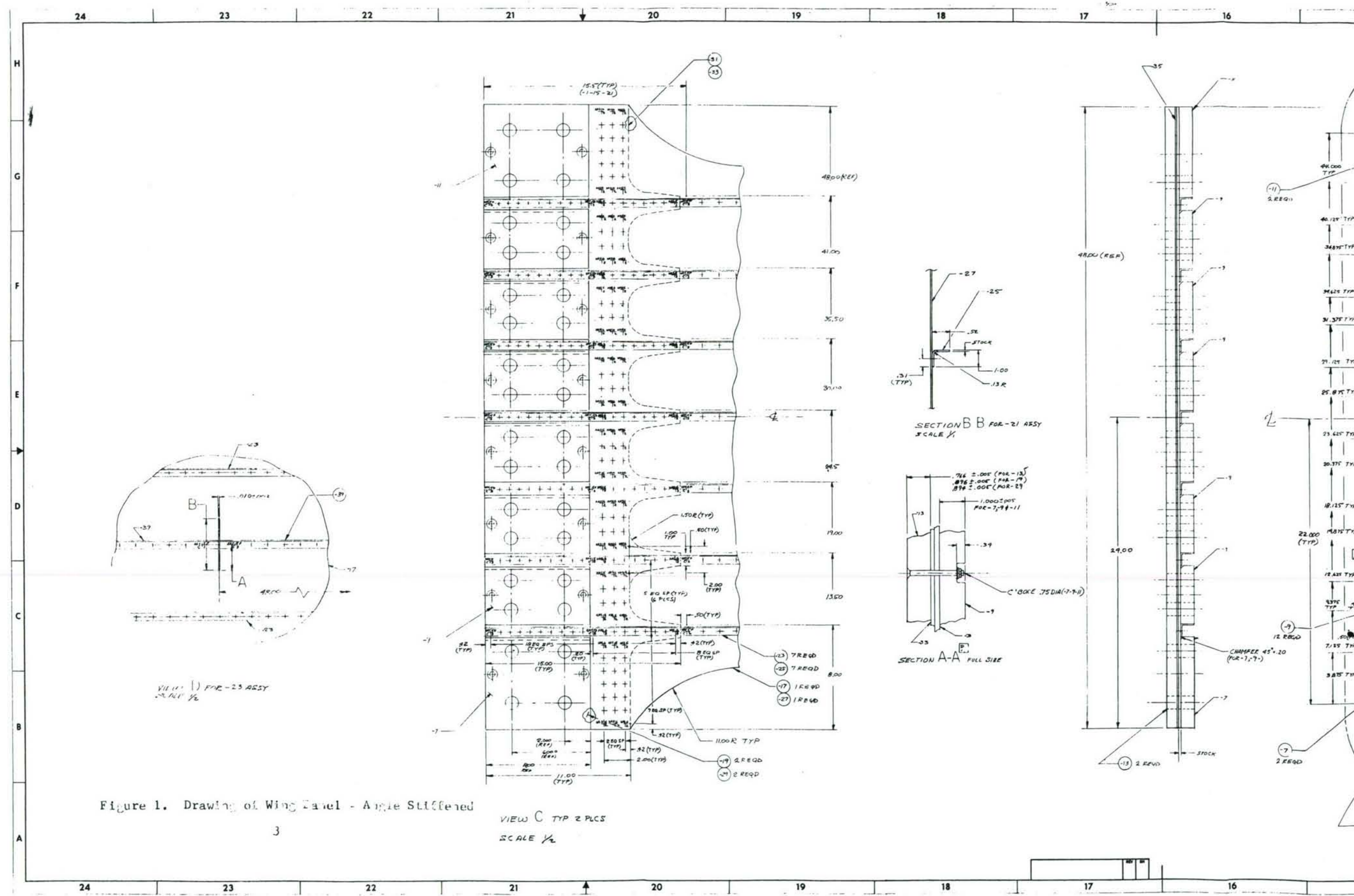
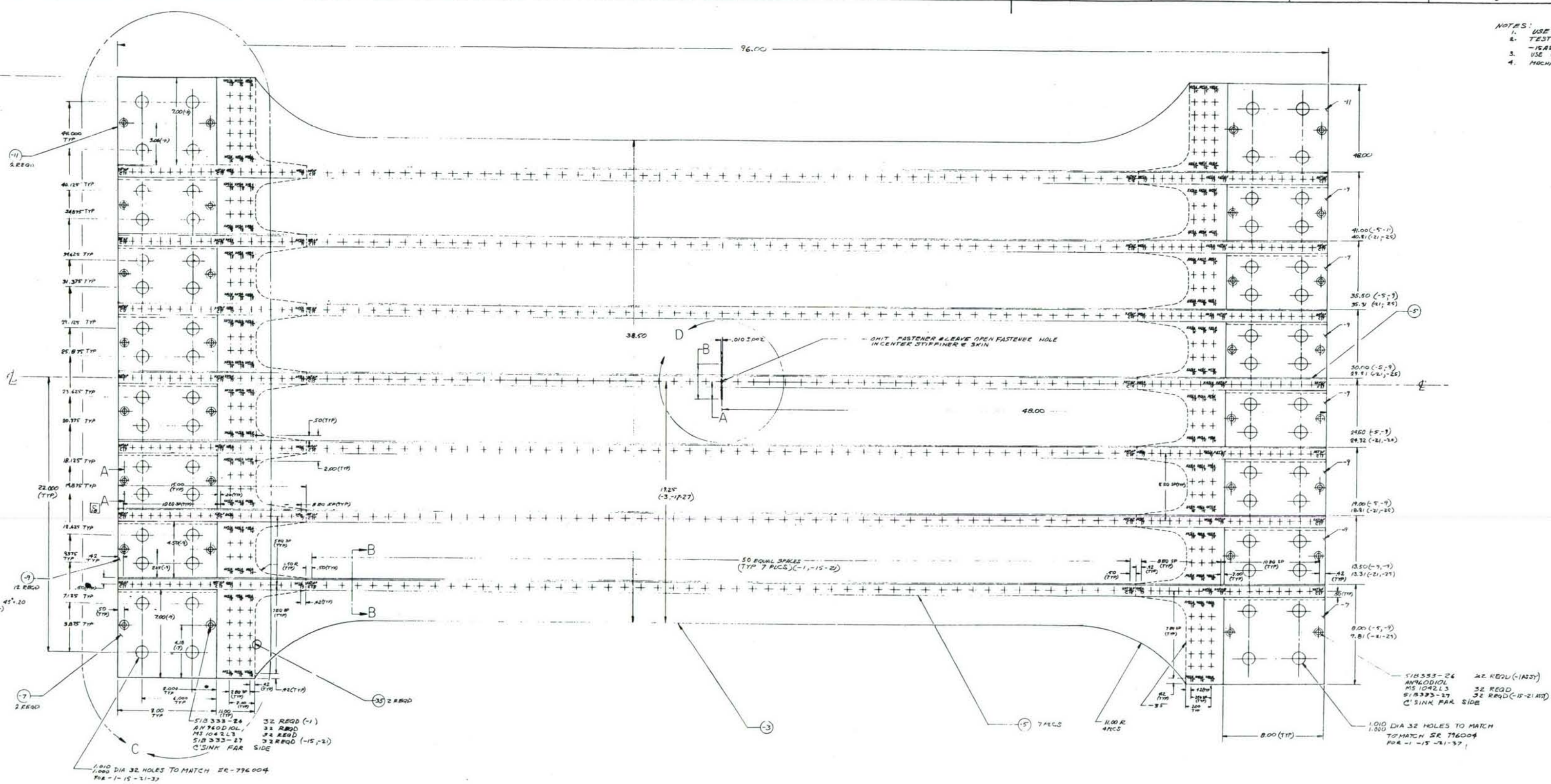
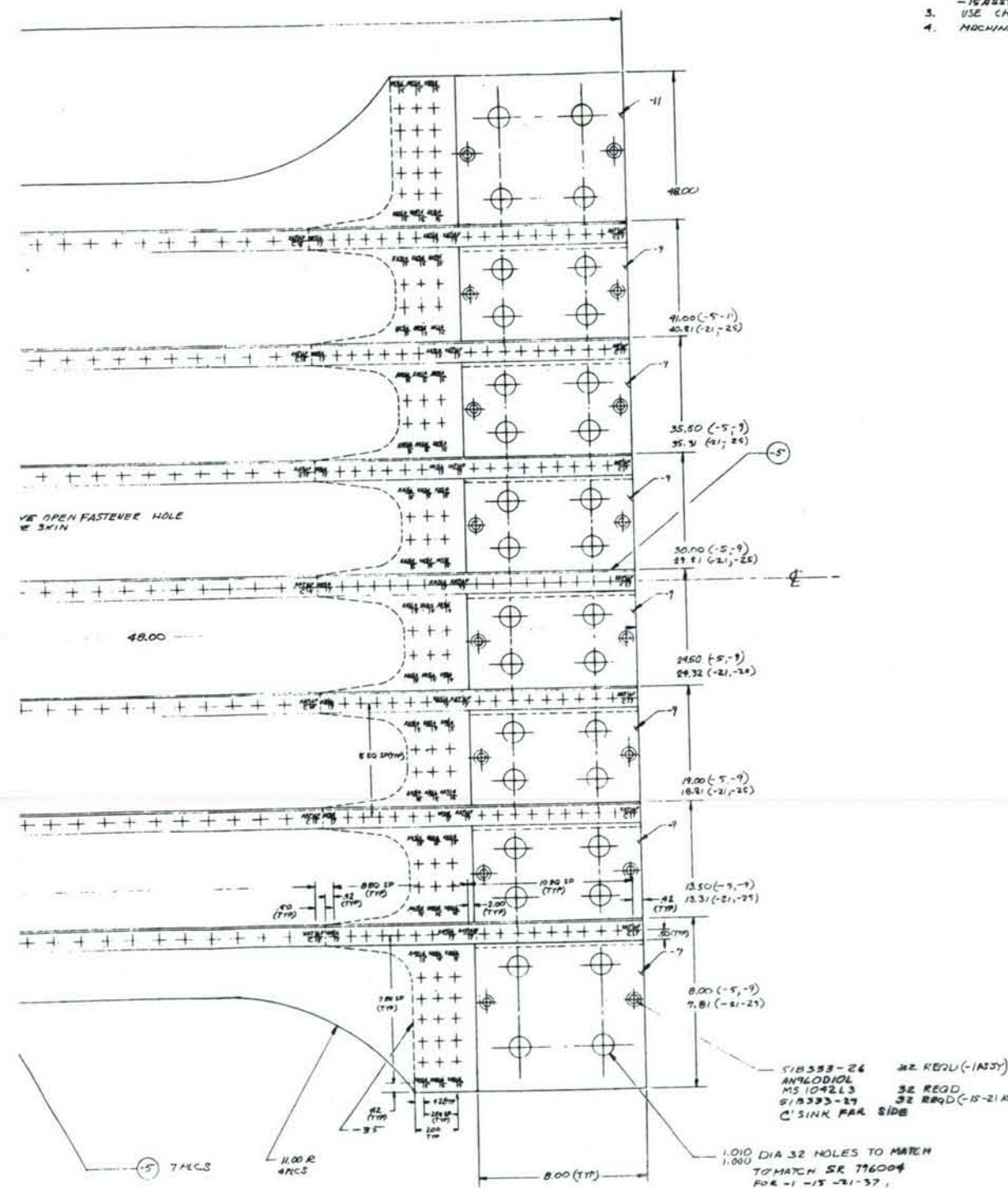


Figure 1. Drawing of Wing Panel - Angle Stiffened





NOTES:

1. USE PROCESS SPEC FM-21 . FM-21, 1M-23, MA-23, MA-23, MA-23
2. TEST MAX LOAD: -1 ASSY TO 500,000 LBS;
-1 ASSY TO 210,000 LBS; -2 ASSY TO 300,000 LBS
3. USE CHARACTERIZED SHEET FOR ALL SKINS
4. MACHINE ALL OVER. ✓

ASSY	A	B
-1	425	850
-15	2.50	5.00
-2	2.50	5.00
-23	2.50	5.00

The selected angle sections were AND 10134-1001 (7075-T6 extrusions) with the one inch leg attached by 3/16 inch diameter, flush head steel HI-LOK's (19PB-3) at 1.3 inch pitch in the test area. In that portion of the lower wing simulated by these panels, the upstanding leg would normally be attached to the upper wing through an attached shear web (chordwise). Table I lists the panel, skin and angle cross sectional thicknesses, areas, and materials (including skin material identification, see Reference 2 for code). It should be noted that the 29% stiffening ratio in Table I is representative of construction for typical, large transport outer lower wings.

Figure 1 shows that the initial starter slot had a half length of 2.50 inches and an overall length of 5.00 inches for both the -15 and -23 panels. Overall panel lengths were normally 96 inches including padded grip ends and 74 inches excluding grip ends. The padded ends were designed to produce a minimal amount of inplane bending due to loading eccentricity. Each panel contained 20 strain gages, the location of which are detailed in Section 2.2.3. A standard beam type clip gage was mounted on the skin side of both panels to record crack opening displacement at the crack and panel centerline.

2.2.2 Finite Element Modeling and Analysis

The analyses of the panels with intact (-15) and broken (-23) central angle were conducted in a manner similar to the zee stiffened panels of Phase II (Reference 1) of this study. Both elastic and elastic-plastic analyses were conducted for various crack lengths for the panel with the intact stringer. The elastic-plastic analysis was based on the assumption of a Dugdale type strip plastic zone. For the panel with the broken stringer, elastic and elastic-plastic analyses were conducted for the crack length used in the test panel. The finite element modeling, elastic, and elastic-plastic analyses of the panels are discussed in the following subsections.

2.2.2.1 Finite Element Modeling of Intact and Broken Stringer Panels

The finite element modeling is similar to that used in Phase II (see Reference 1). The panel is modeled as a two-dimensional structure. Triangular membrane elements were used to model the skin. The angle stiffeners of this panel are modeled like the zee stiffeners for the zee stiffened panels of Phase II. The connected leg of the angle stiffener is modeled as a rod element and the upstanding leg of the angle is modeled as a rectangular membrane element. The effect of asymmetry caused by the L shaped cross-section is not considered. In this case only a quarter panel need be modeled for finite element analysis due to panel symmetry. The analysis, of Phase II panels showed that in cracked, stiffened panels only four to eight fasteners above (and below) the crack surface connecting stringer to skin were effective in load shedding from skin to stringer. The other fasteners had little influence on load transfer to the stringers. The number of fasteners effective in load transfer was also found to be dependent on crack length. Taking into consideration these trends only the first nine fasteners were modeled as individual shear elements in the finite element model. The depth of the shear elements was kept the same as the diameter of the fastener. That portion of the panel beyond the nine fasteners from crack plane was assumed to be continuously attached. This assumption allows a coarser grid to be used in the

TABLE I THIN SKIN-ANGLE STIFFENED WING PANEL
AREAS AND MATERIAL IDENTIFICATION

PANEL NUMBER	MEASURED THICKNESS (Inches)		CROSS SECTIONAL AREAS (Inches ²)		SKIN MATERIAL/ AND I.D. (See Ref. 2)	PERCENTAGE OF TOTAL ANGLE AREA TO SKIN AREA
	Angle	Skin	Total Angles	Skin		
-15	.063	.0625	.700	2.40625	7075-T73/4-3	29.1%
			TOTAL PANEL CROSS SECTIONAL AREA = 3.10625			
-23*	.063	.0625	.700	2.40625	7075-T73/4-2	29.1%
			TOTAL PANEL CROSS SECTIONAL AREA = 3.10625			

*Central Stringer Broken

finite element modeling away from the crack, reducing the total number of grid points and computer run time. This is a particularly important consideration in this type of panel where four stiffeners are modeled in one quarter panel. If all the fasteners in all the stiffeners are modeled as individual shear elements, the number of grid points becomes excessive with large computer run times. The flexible fastener model was used in the analysis. The shear elements in the finite element model were proportioned to account for the flexibility of the fasteners as discussed in Section 3.1.3 of Reference 1. The finite element model of the angle stiffened panel is shown in Figure 2. The model has 710 grid points and contains 781 triangular membrane elements representing the skin. The size of the smallest triangular element used ahead of the crack tip is 0.125 inch. The computer run time for an elastic analysis with a crack length of 5.50 inches is 5 minutes. A complete Dugdale model type elastic-plastic analysis for the same crack length with eight load (or plastic zone) cases requires approximately 22 minutes.

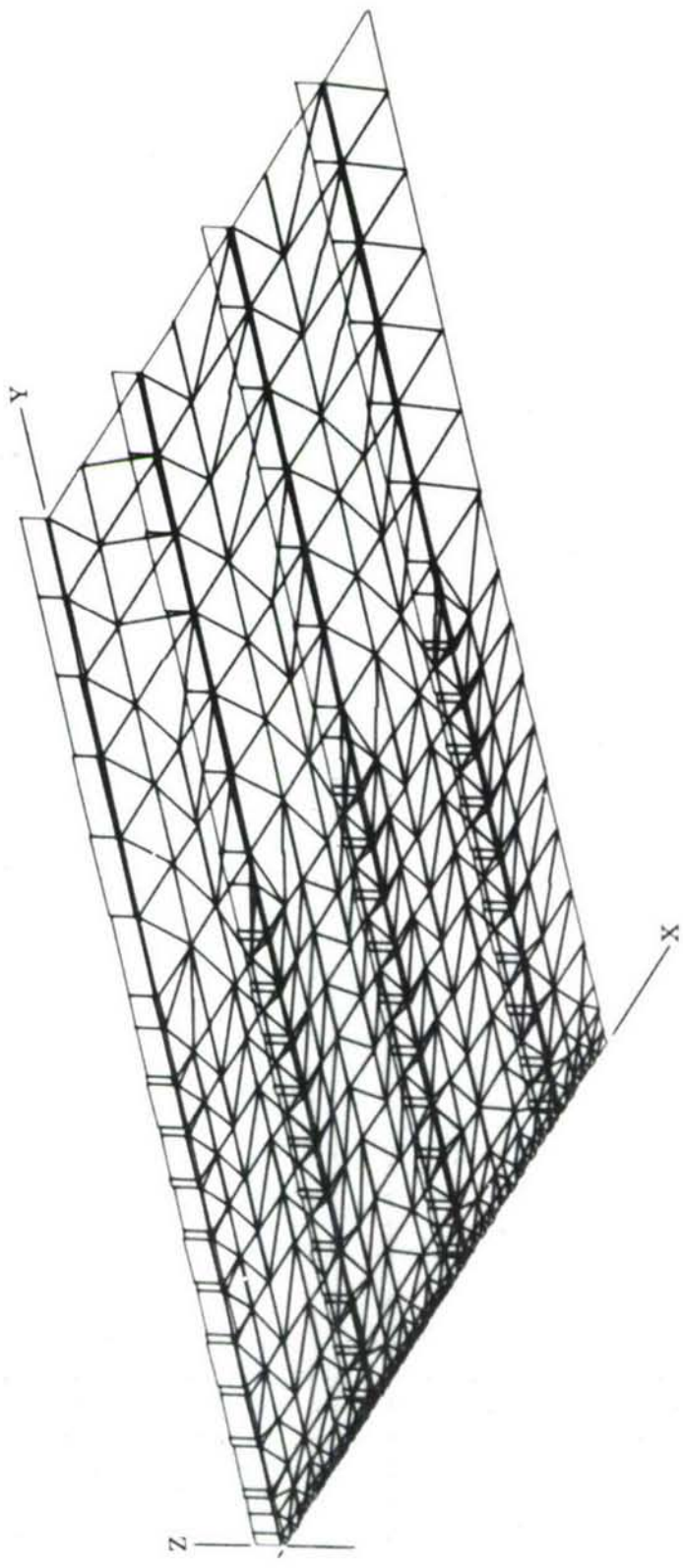


Figure 2. Basic Finite Element Model for Angle Stiffened, Lower Wing Panel

2.2.2.2 Elastic and Elastic-Plastic Analysis of Panels With Intact and Broken Stringer

An elastic analysis of the intact (-15) and broken (-23) central stringer panels was conducted for a half crack length of 2.75 inches. Two different contours were used to compute J integral values. These two contours are shown in Figure 3. The elastic square root of J (\sqrt{J}) values obtained for the two contours were within 0.5 percent. Figure 4 shows the plot of square root of J versus applied stress normalized to skin material yield strength, for these two panels. It is seen that the square root of J values for the broken central stringer case is approximately 22 percent higher than those for the intact stringer case. The crack surface openings for these two cases are plotted in Figure 5. The crack surface opening at the center line of the crack in the broken stringer case is approximately 77 percent higher than that for the intact central stringer panel. It should be noted in Figure 5, that the maximum crack surface opening for the intact stringer case occurs away from the center line of the crack, whereas for the broken stringer case it occurs at the center line of the crack.

In the elastic-plastic analysis of the -15 and -23 panels a Dugdale type strip plastic zone was assumed ahead of the crack tip. The Bueckner-Hayes approach, as discussed in Reference 1, was used for the Dugdale type elastic-plastic analysis. The variation of \sqrt{J} with p/F_{ty} for both intact (-15) and broken (-23) central stringer cases using this analysis is shown in Figure 6 for a half crack length of 2.75 inches. For the same applied stress the square root J values for the broken stringer case are higher than those for the intact stringer case. At an applied stress of 80 percent of the skin material yield the broken stringer case \sqrt{J} value is 22 percent higher than that for an intact stringer case. For both panels the elastic-plastic analysis gives square root J values higher than those given by an elastic analysis. The difference in the \sqrt{J} values between the two methods of \sqrt{J} analyses is 12 percent for an applied stress of 80 percent of the skin material yield strength. For the intact central stringer case the variation of stress in the central stringer, at the centerline of the crack and panel with applied stress is shown in Figure 7. At an applied stress of 80 percent of yield the stresses in the stringer from the elastic-plastic analysis are 20 percent higher than those given by a purely elastic analysis. These stresses have been plotted to determine if the crack length under consideration represents a stringer critical case as proposed in the analysis and discussed subsequently in Sub-Section 2.2.4.

In the residual strength prediction method it is necessary to plot a curve between the square root J and crack length for various applied loads. In order to determine these values it is necessary to perform an elastic-plastic analysis for various crack lengths. The selected half crack lengths were 1.50, 2.75, 4.0, 5.0, 5.5, and 6.5 inches for the intact stringer case (-15 panel) only. A similar analysis was not conducted for the broken stringer (-23 panel) case due to the large computer run times involved. The residual strength predicted for the intact stringer case with the square root of J curve shown in Figure 4 were used to predict the residual strength of the broken stringer case as discussed in Sub-Section 2.2.4. The

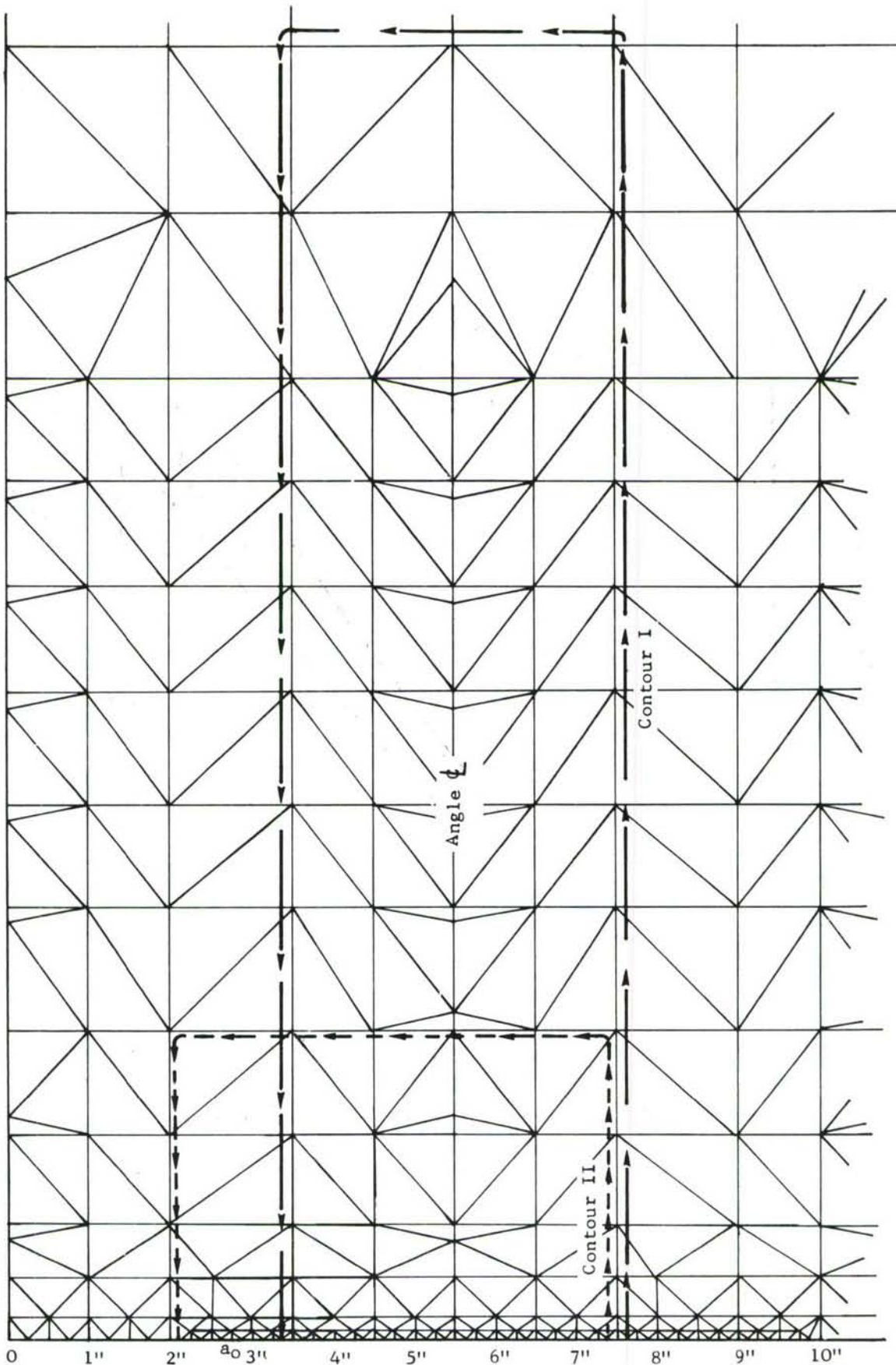


Figure 3. Contours for J Integral Calculations - Angle Stiffened, Lower Wing Panels

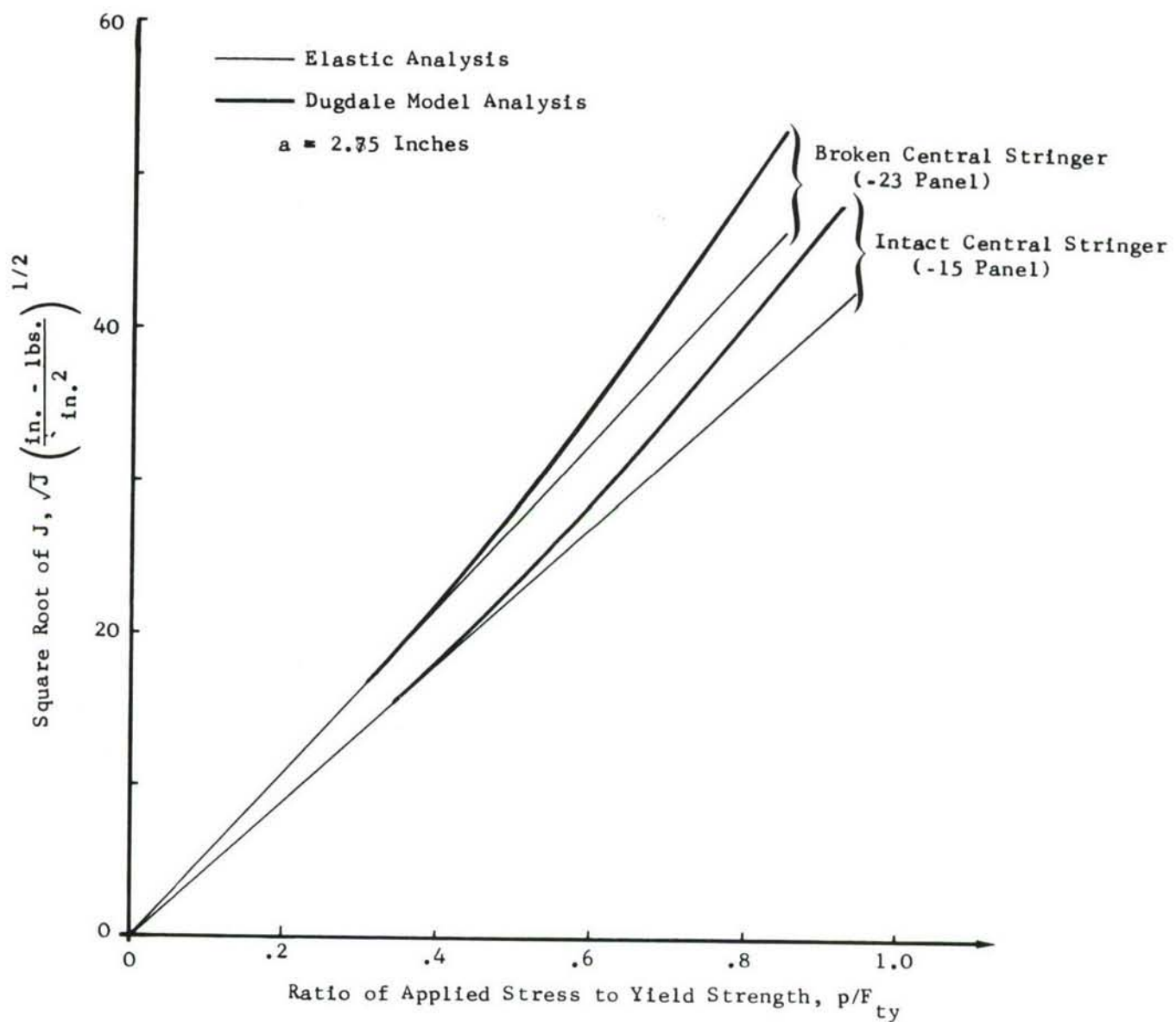


Figure 4. Comparison of Square Root of J Values for Intact and Broken Central Stringer Cases - Thin Skin

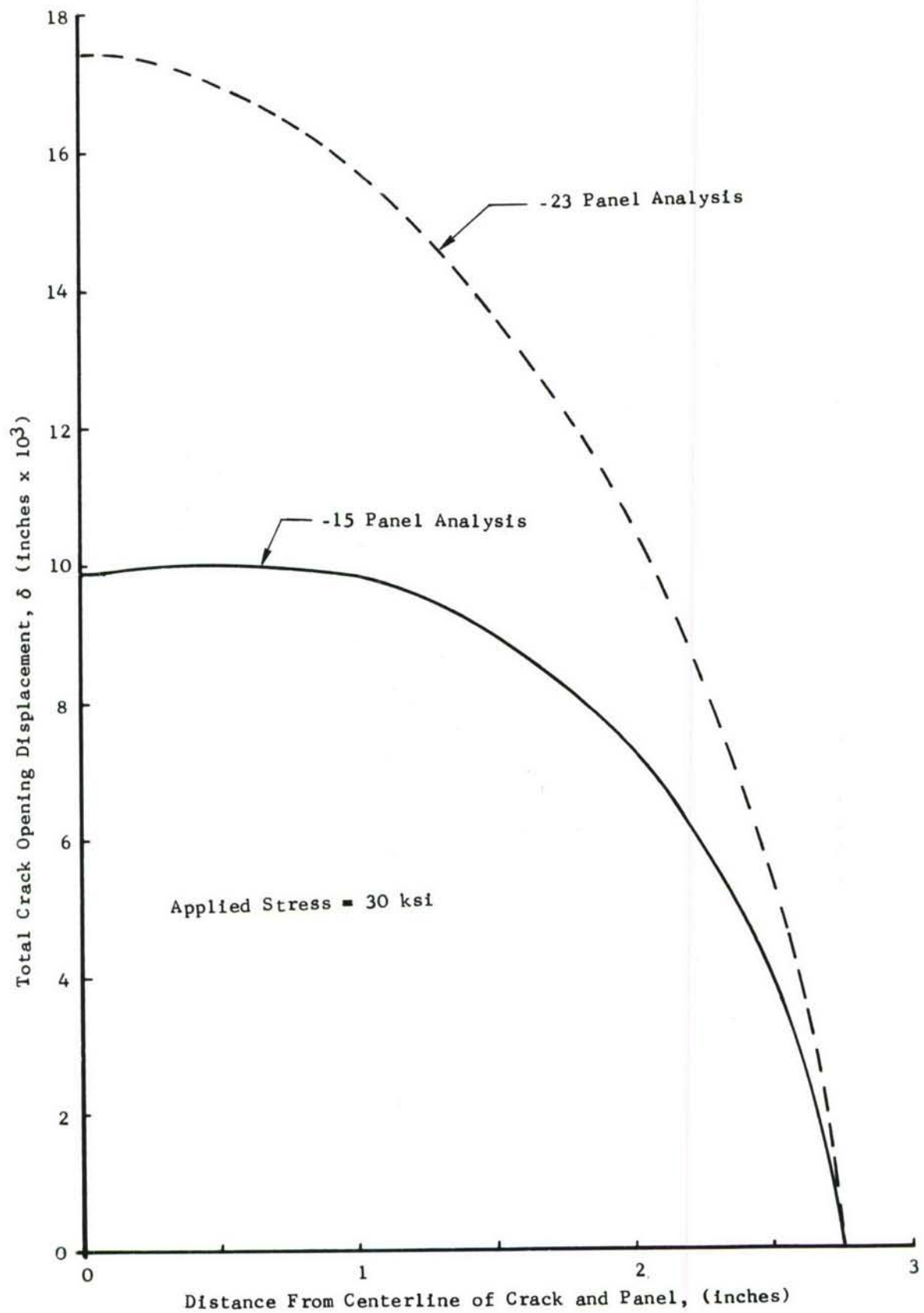


Figure 5. Crack Opening Displacement for Broken (-23) and Intact (-15) Stringers, Angle Stiffened Panels

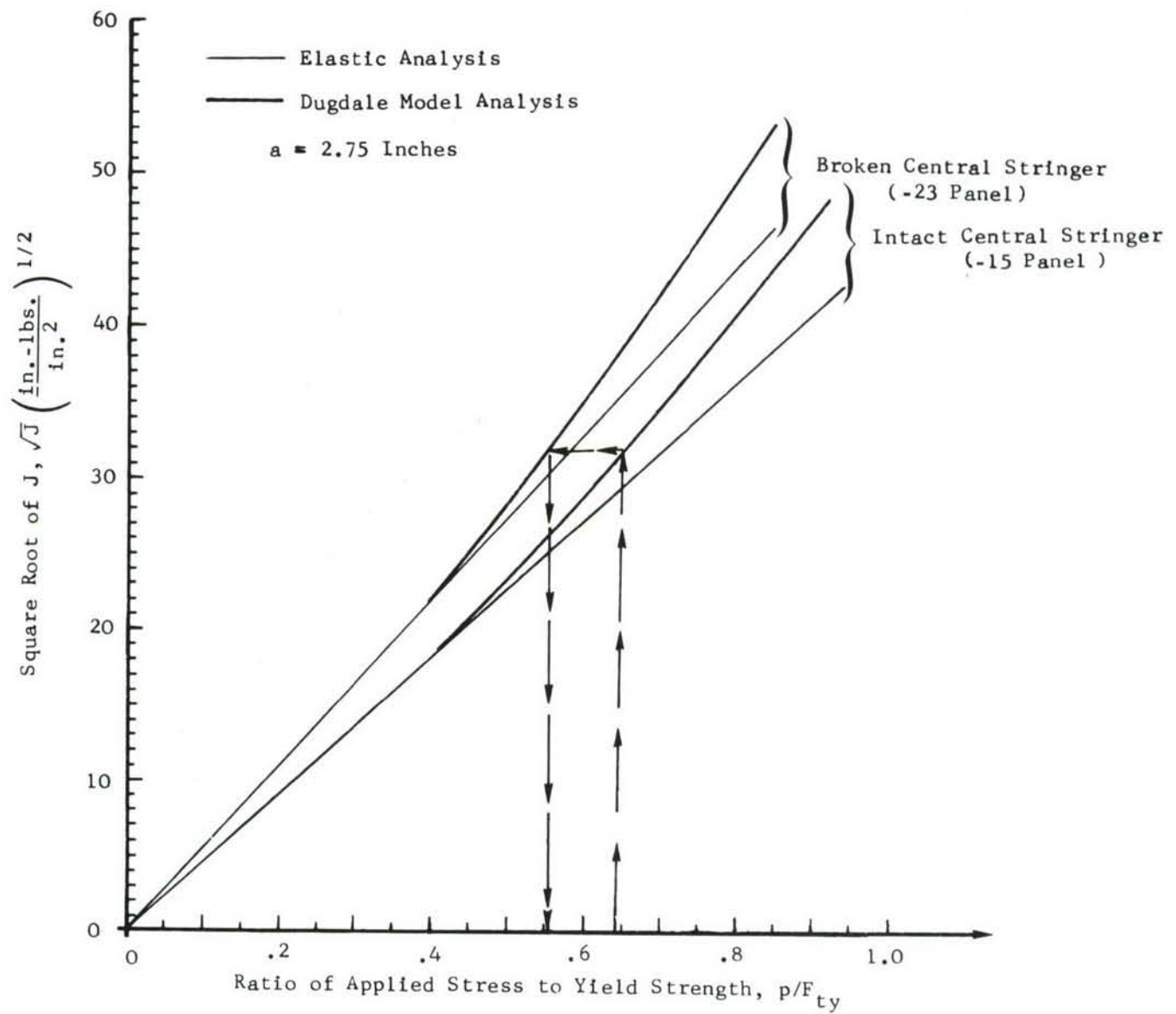


Figure 6. Prediction of Broken Stringer Panel Stress From Intact Stringer Analysis

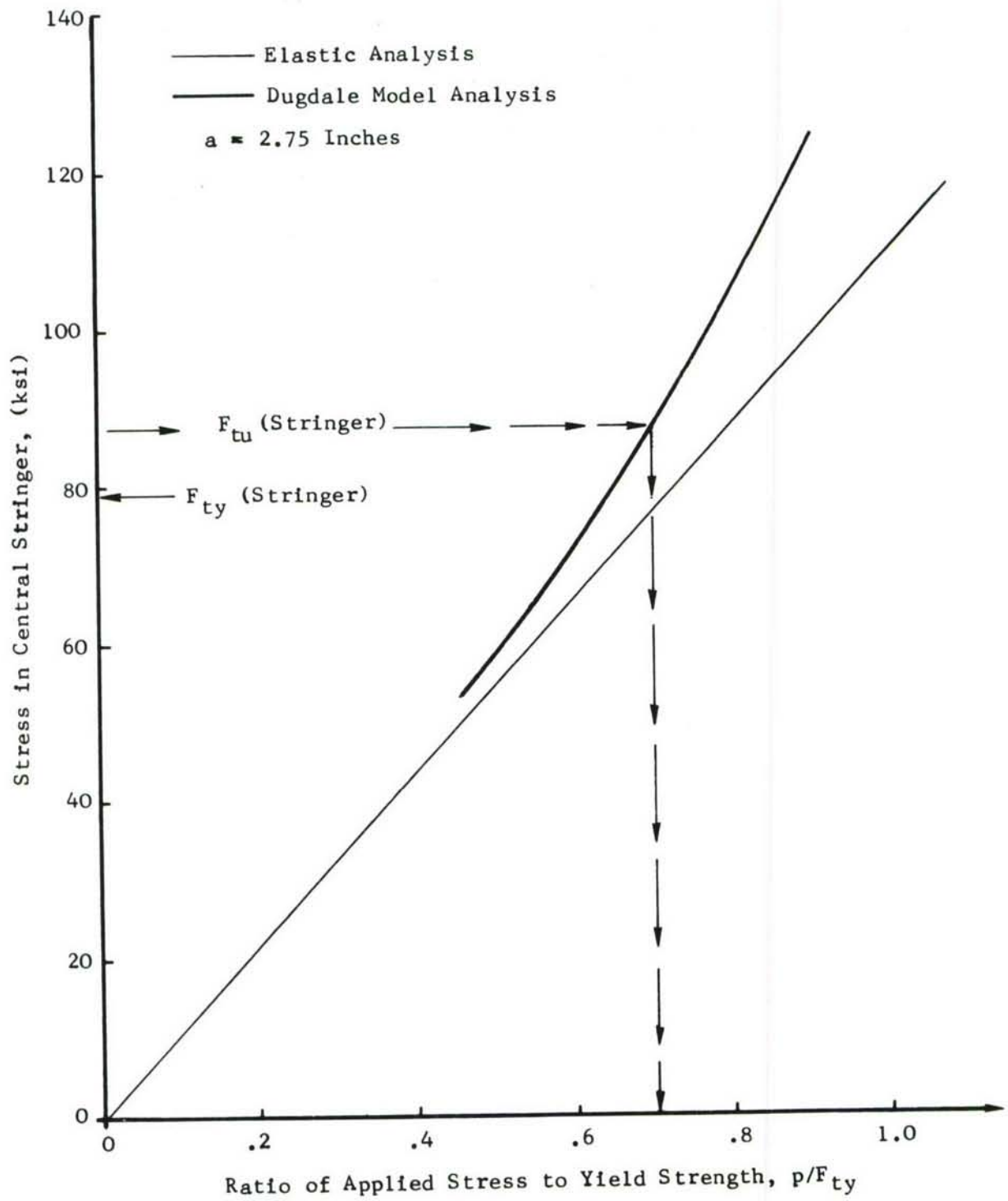


Figure 7. Stress in Central Stringer as a Function of Applied Stress Based on Elastic and Elastic-Plastic Analysis - Intact Stringer

square root J values as a function of applied stress for various crack lengths are shown in Figure 8. These values are cross plotted to show the variation of square root of J with crack length for the same applied stress in Figure 9. For the same applied stress, square root J values increase with crack length to a half crack length of about 4.0 inches. With further increase in crack length the square root J values decrease due to the influence of the adjacent stringer. Once the crack is beyond the center line of the stringer the value of square root J increases again with crack length.

2.2.3 Experimental Results and Discussion

To prevent repetition within the various sections, a complete description of overall test arrangement, data recording instrumentation and reduction technique are described in this sub-section. Following this discussion the experimental results for the intact and broken stringer cases will be presented, along with discussion of the results obtained.

2.2.3.1 Test Arrangement - General

All panels were loaded uniaxially in a 500,000 pound load frame. The overall test setup is shown in Figure 10. Loading of the test panel is accomplished through a slotted clevis attached directly to the bolted on grip ends. Load is introduced through an M.T.S. Model 406 Controller which controls the 500,000 pound cylinder. Load was recorded on three separate units; a HONEYWELL 194 chart recorder, HEWLETT-PACKARD, model 7045A, x-y recorder and on magnetic tape in conjunction with strain recording.

High speed, 16 mm (split frame) black and white motion picture coverage was used to monitor both slow stable tear and final fracture at approximately 1,000 frames per second. Load was monitored on film by placing a DC voltmeter reading output load voltage, within the field of view of the camera.

Instrumentation on all wing panels consisted of an M.T.S. clip gage excited by an ECTRON Differential DC Amplifier (Model 687). The output was recorded on an x-y plotter. This gage in all cases spanned the centerline of the crack and panel on the skin side. Knife edges were mounted on the panel with epoxy and the clip gage positioned between the two knife edges.

Recording of the twenty (20) strain gages on each panel was accomplished in two ways: first by direct reading all twenty gages employing a DATRAN Model strain gage printer during load holding procedures and second through magnetic tape recording of 12 selected gages during both load holding and increasing load testing. Three (3) gages were alternately monitored using both methods of recording to determine any error in the strain sensing systems.

The tape data recording system consisted of the strain gage signal transmitted through a balance box fed to an ASTRO-DATA Model 889 Amplifier and recorded on a 14 channel HONEYWELL Model 7600 recorder. Twelve channels were utilized for strain gage recording, one for load cell voltage and the remaining channel for voice. After each test these data were played back through a BRUSH Mark 200 recorder for data reduction of strain and load versus time.

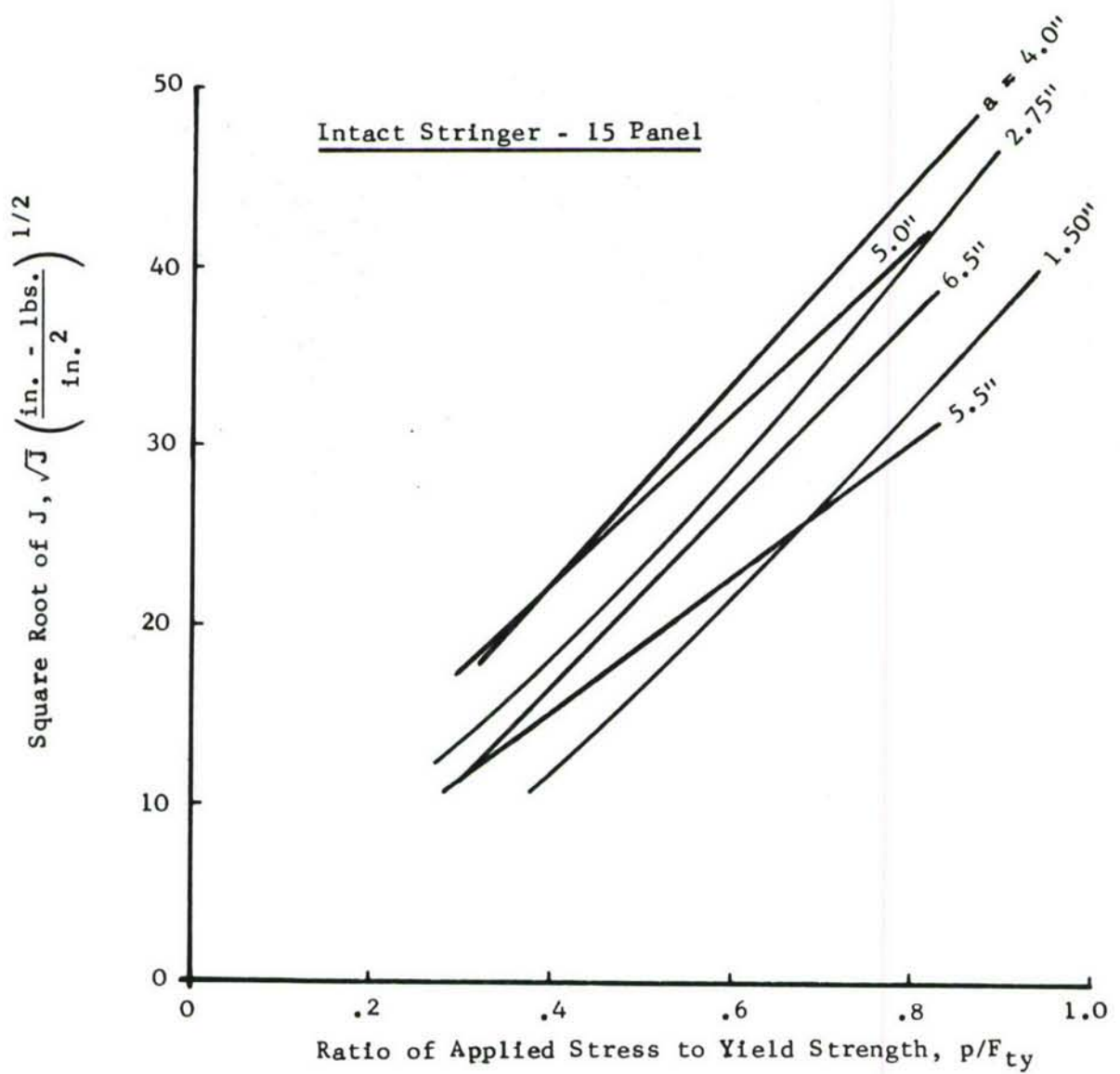


Figure 8. Square Root of J as a Function of Applied Stress for Varying Crack Lengths - Intact Stringer

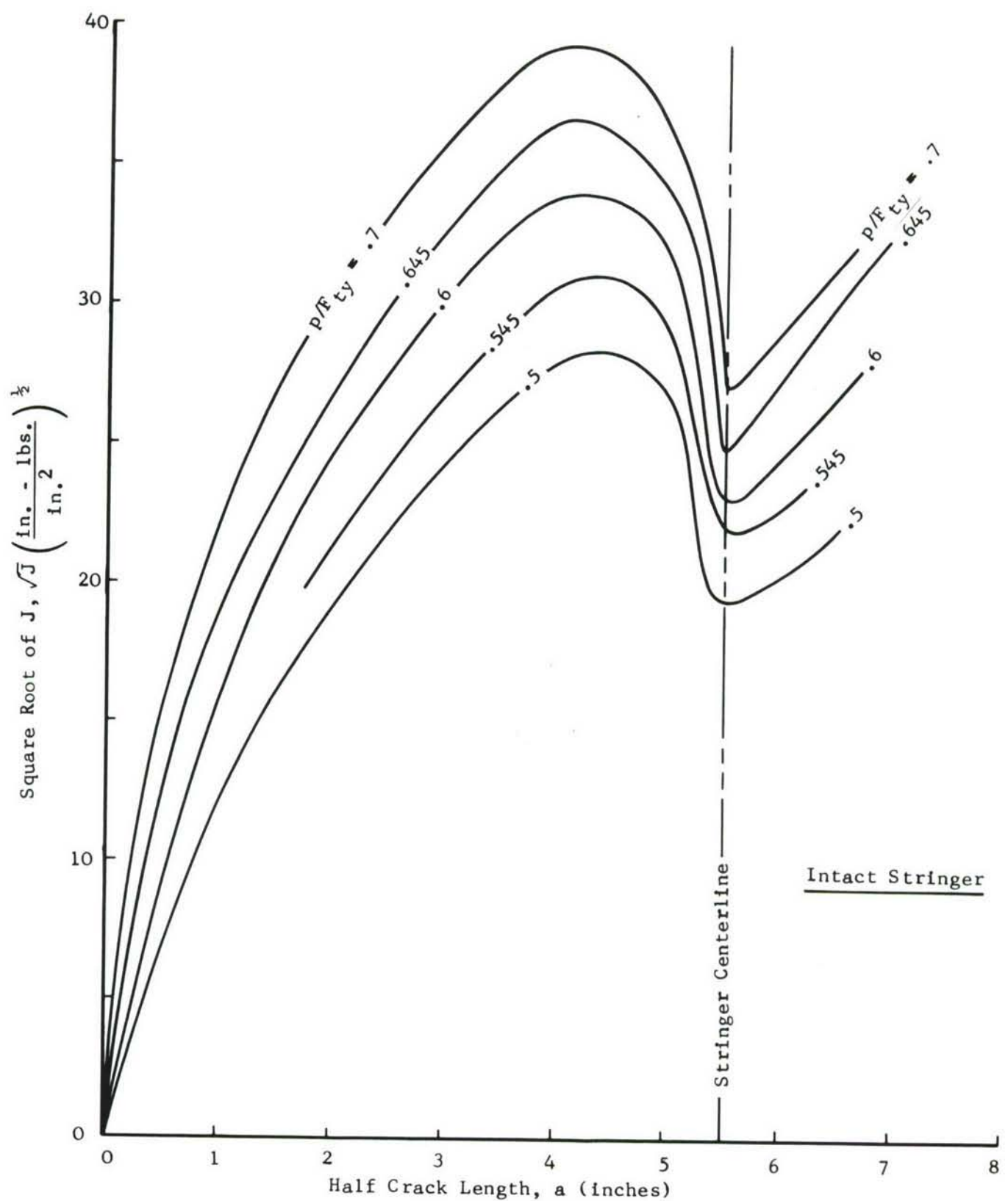


Figure 9. Square Root of J as a Function of Crack Length - Intact Stringer

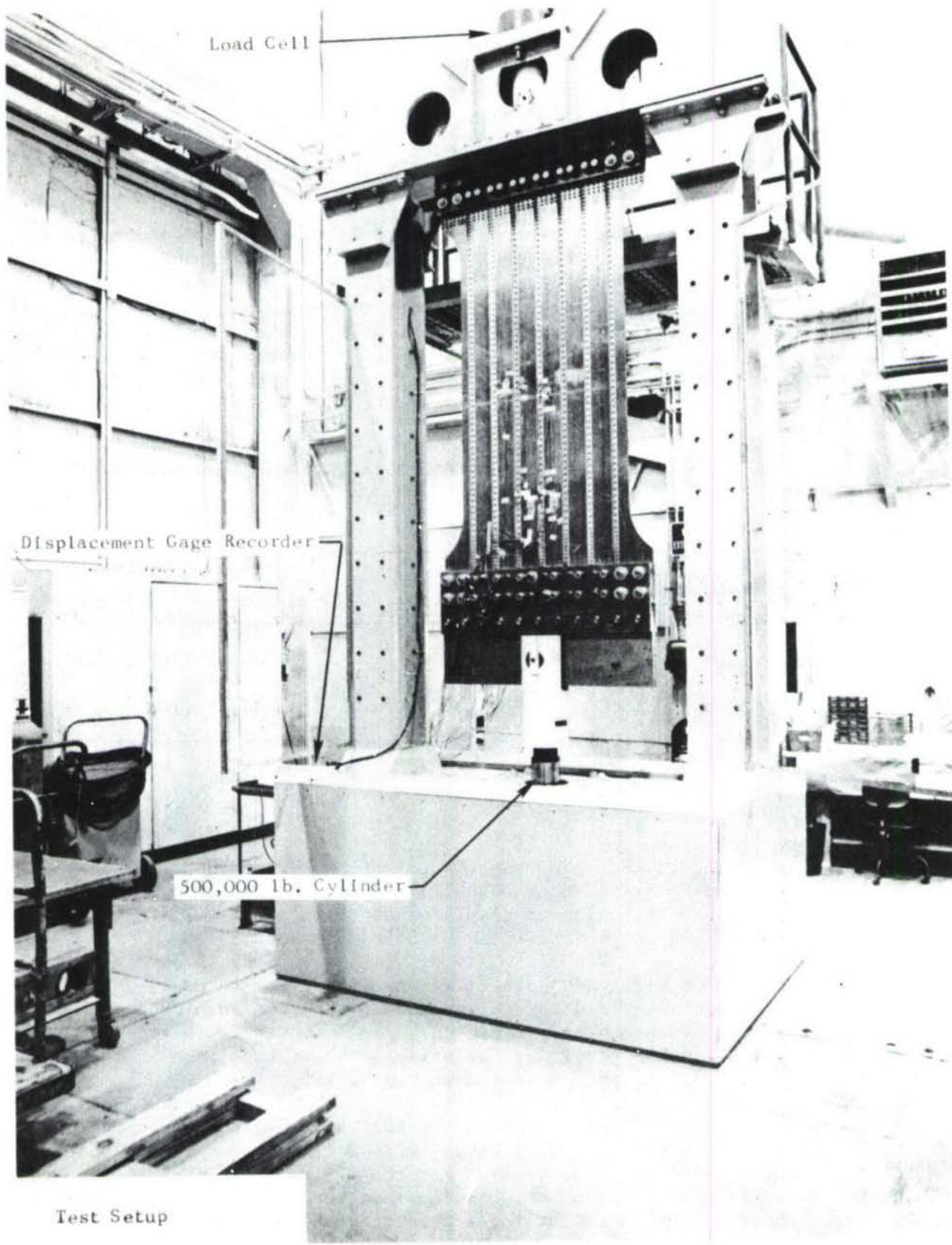


Figure 10. View of Test Panel in 500,000 Pound Load Frame

Balancing of strain gages and zero initial readings were taken with the specimen hanging "free" from the top clevis - the bottom pin was "pulled" during all initial zero readings. In-test and post fracture, zero load strain readings were taken with the loading pin in place.

2.2.3.2 Fatigue Precracking, Strain Data and Fracture of Broken and Intact Stringer Cases

In order to start from a natural crack condition in the two panels, each was fatigue precracked approximately 0.2 inches from the ends of the machined slot using tension-tension, constant amplitude, sinusoidal loading. Maximum fatigue cycling load (stress) levels were determined using the stress intensity solutions of Reference 3 and assuming a maximum stress intensity of 15 ksi $\sqrt{\text{inch}}$ in both cases, and a fatigue stress ratio of approximately 0.1. Table II summarizes the fatigue loadings and total crack lengths for these two panels. The crack lengths were measured after panel failure.

TABLE II FATIGUE PRECRACKING AND CRACK LENGTH DATA, -23 AND -15 PANELS

PANEL	FATIGUE LOADS		NO. OF CYCLES	FATIGUE CRACK LENGTH(S) (Inches)		
	MAXIMUM (kips)	MINIMUM (kips)		LEFT	RIGHT	TOTAL
-23*	7.3	0.8	63,000	2.70	2.76	5.46
-15	23.0	3.0	10,200	2.79	2.76	5.55

* Broken Central Stringer

Figures 11 and 12 show the front (skin) side view of the -23 and -15 panels in the loading frame and Figures 13 and 14, the back (angle) side of these panels. The positioning of displacement (clip) gage, strain gages initial saw slots and panel detail can be noted for each case.

After fatigue cycling and zero balancing of all strain gages and displacement gage, a strain/load survey was accomplished on each panel by loading in specific load intervals. These data are noted in Table III for the broken central stiffened panel and Table IV for the intact panel. The reference of each strain gage is shown in Figure 15.

Load versus total displacement gage output is shown in Figure 16 for the initially broken central angle panel (-23) and in Figure 17 for the initially intact stringer case (-15). For the -23 panel inplane buckling in the two bays was quite evident at very low load levels, (approximately 15 to 20 kips); whereas, the intact stringer case required approximately twice this load for crack buckling.

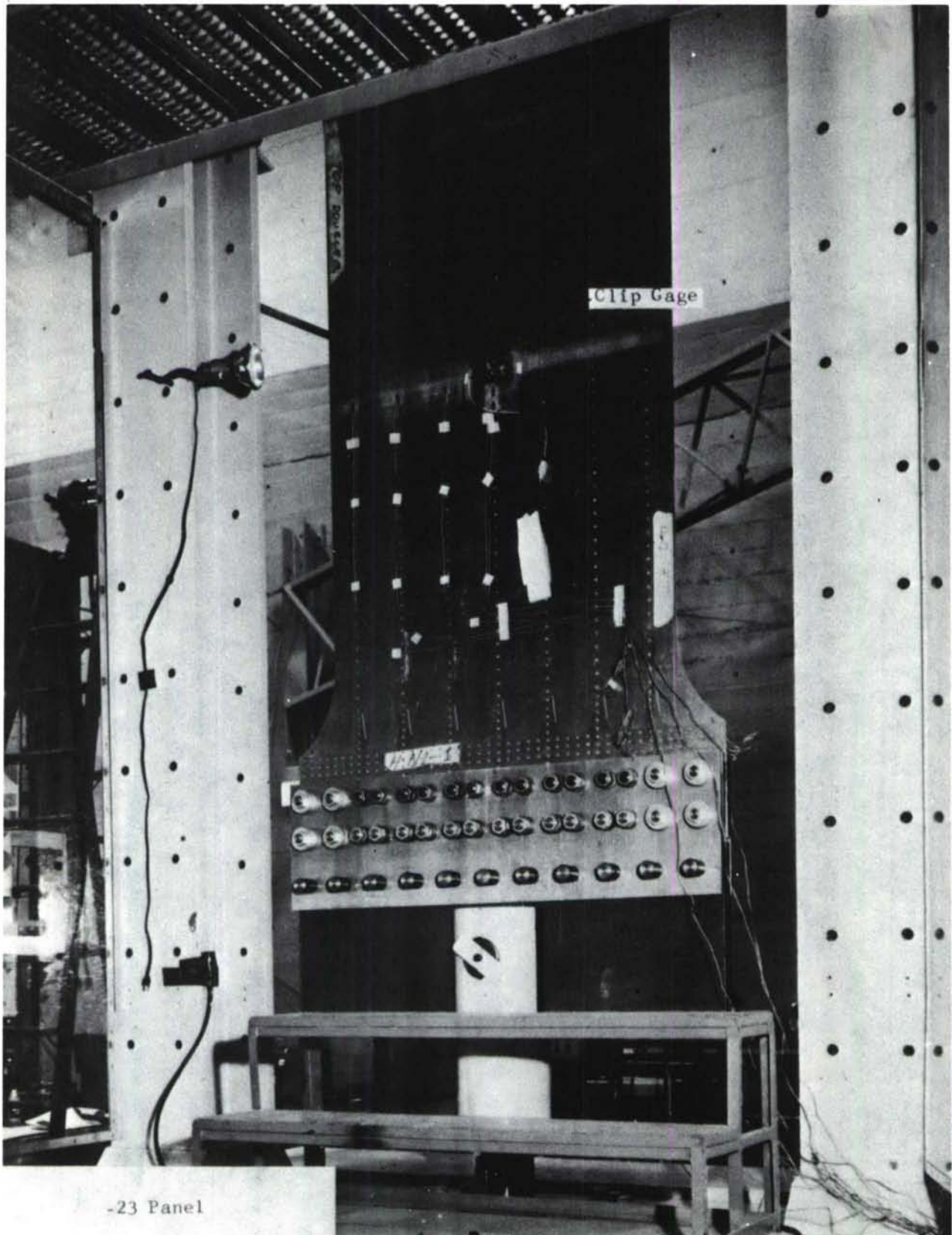


Figure 11. Overall View of Skin Side of Wing Panel Angle Stiffened,
Lower (Center Stringer Broken)

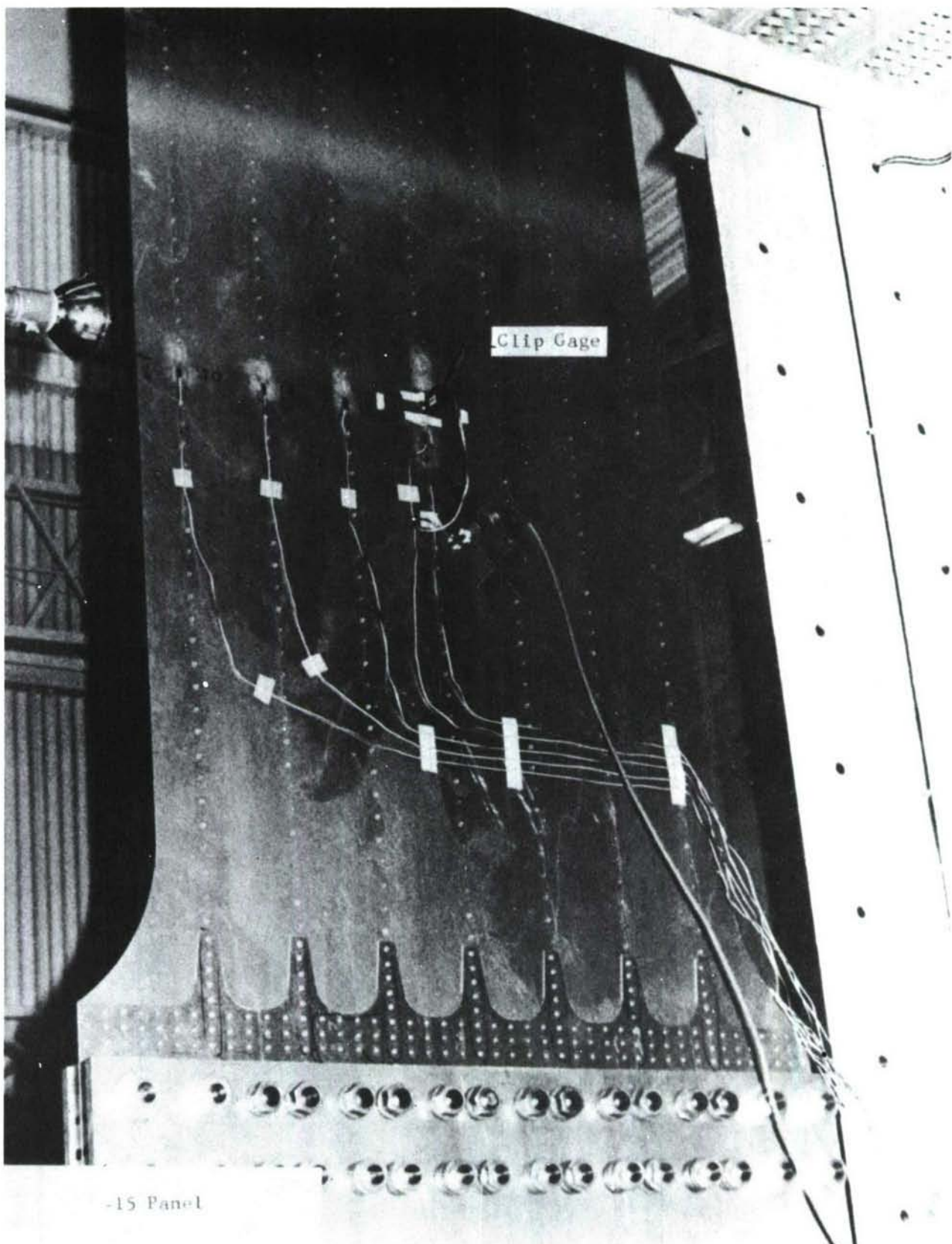
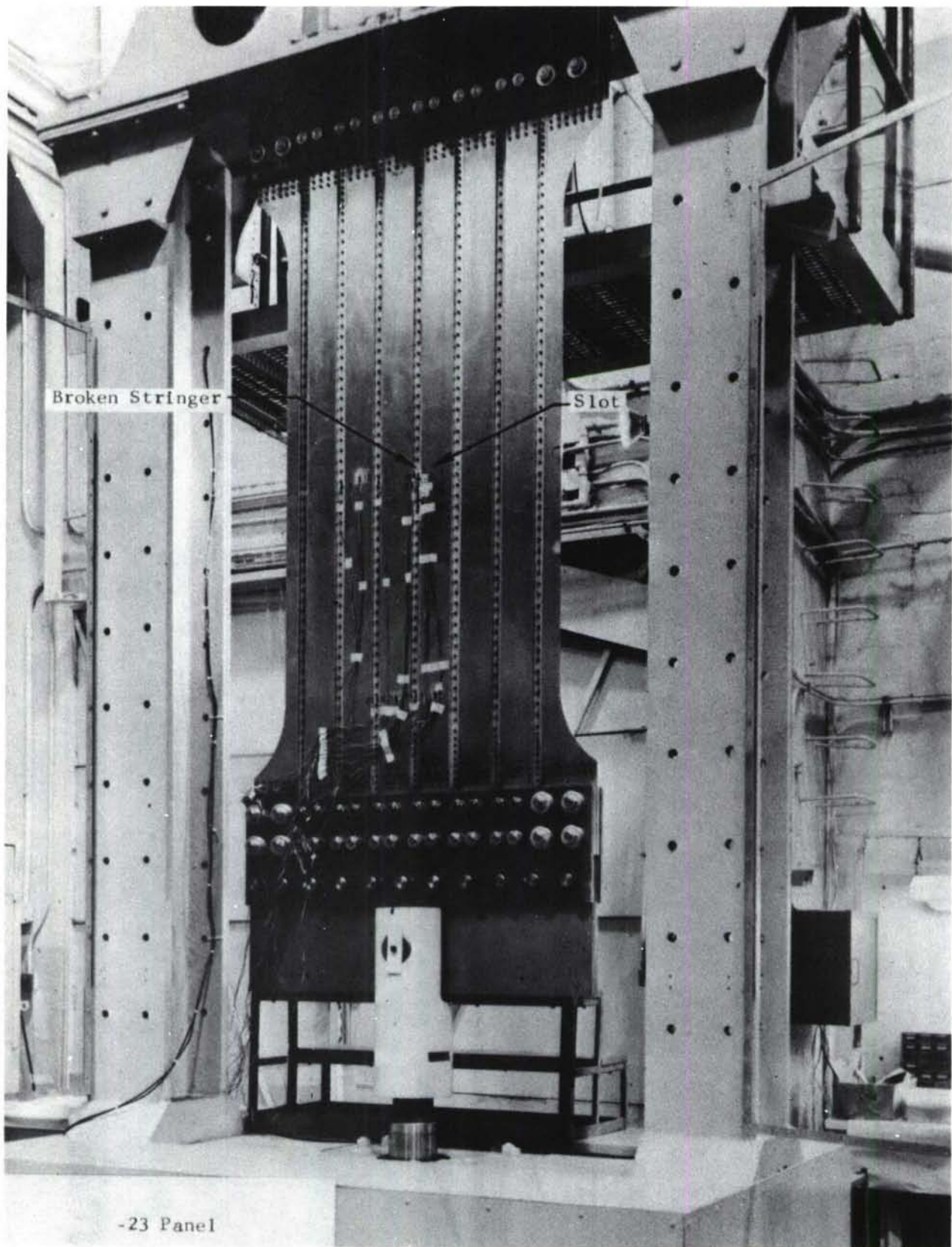


Figure 12. Overall View of Skin Side of Wing Panel Angle Stiffened,
Lower (Center Stringer Intact)



-23 Panel

Figure 13. Overall View of Angle Stiffened Side of Wing Panel Angle
Stiffened, Lower (Center Stringer Broken)

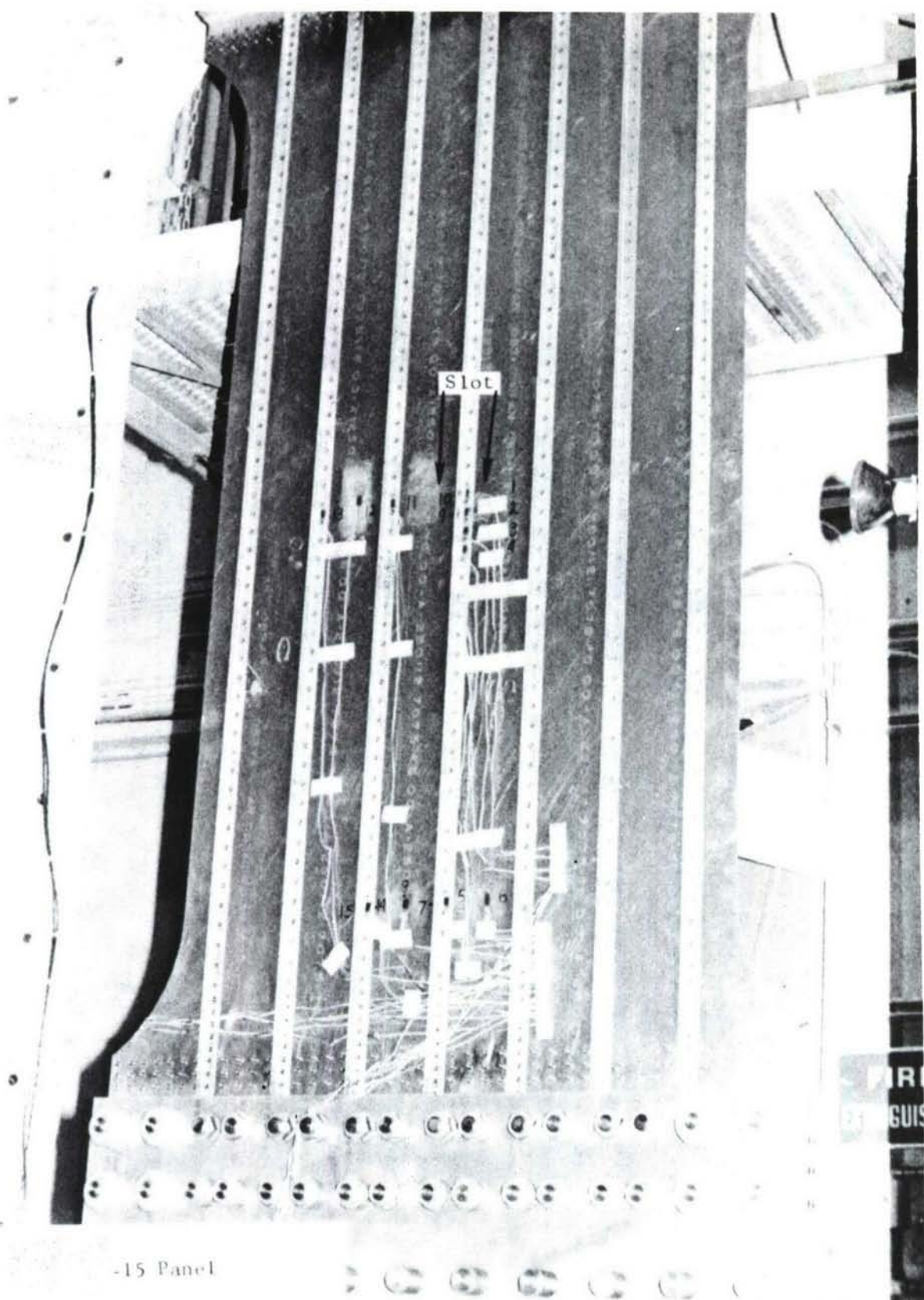


Figure 14. Overall View of Angle Stiffened Side of Wing Panel Angle
Stiffened, Lower (Center Stringer Intact)

TABLE III STRAIN GAGE DATA, -23 WING PANEL ANGLE STIFFENED, LOWER (CENTER STRINGER BROKEN)

*S.S.T. = Slow Stable Year

TABLE IV STRAIN GAGE DATA, -15 WING PANEL ANGLE STIFFENED, LOWER (CENTER STRINGER INTACT)

PANEL NUMBER	LOAD (KIPS)	GAGE LOCATION AND STRAIN X 10 ³ inches/inch (See Figure 15)														
		①	②	③	④	⑤	⑥	⑦	⑧	⑨	⑩	⑪	⑫	⑬	⑭	
-15	-014 ZERO	-004 0	.02 .321	-004 .55	0 .321	-.04 .26	0 .26	-.02 .56	-.02 .56	-.004 .385	-.004 .385	0 .783	-.02 .783	0 .70	-.02 .67	
(a = 2.775")	11.0	.641 1.213	.68 1.28	.55 .82	.32 .60	.32 .56	.32 .60	.30 .58	.30 .58	.321 .589	.321 .589	.413 .740	.413 .740	.38 .70	.36 .67	
20.0	.716 30.0	1.82	1.15	.847 1.15	.88 .82	.847 1.098	.88 .82	.847 1.098	.88 .82	.842 1.115	.842 1.115	1.052 1.406	1.052 1.406	.98 1.28	.92 1.22	
40.0	2.198 50.0	2.28	1.58	1.165 1.165	1.18 1.18	1.08 1.08	1.18 1.18	1.08 1.08	1.12 1.12	1.083 1.391	1.083 1.391	1.402 1.763	1.402 1.763	1.58 1.58	1.45 1.54	
50.0	50.0	2.662 1.092	2.76 2.20	2.00 2.40	1.498 1.822	1.52 1.85	1.38 1.65	1.45 1.75	1.40 1.423	1.40 1.68	1.40 1.674	1.402 2.107	1.822 2.167	1.58 1.88	1.432 1.84	
60.0	50.0	50.0	2.62	1.93	1.565 1.60	1.60 1.60	1.38 1.43	1.43 1.43	.02 -.02	-.02 -.02	.018 -.023	.020 -.049	-.02 -.02	.04 A	.006 -.022	
70.0	50.0	3.092 3.15	2.35 2.35	1.822 1.85	1.65 1.65	1.75 1.75	1.65 1.65	1.65 1.68	1.65 1.68	1.421 1.421	1.674 2.107	2.167 2.167	1.58 1.58	1.438 1.55	1.75 1.75	
80.0	50.0	3.65 3.65	2.75 2.75	2.20 2.20	1.95 1.95	2.05 2.05	1.98 1.98	1.95 1.95	2.20 2.25	—	2.18 2.48	2.18 2.48	1.70 1.70	1.70 1.70	1.432 1.432	
90.0	50.0	4.58 4.58	3.45 3.45	2.90 2.90	2.58 2.58	2.65 2.65	2.58 2.58	2.58 2.58	2.58 2.58	2.82 2.82	2.82 2.85	2.85 2.85	2.85 2.85	2.65 2.65	1.55 1.55	
GROSS T.E.R.	99.0	—	—	—	—	—	—	—	—	—	—	—	—	—	—	
HOLDING AFTER TEST	111.7	5.349 1.272	6.00 -0.65	3.82 -0.38	3.516 -0.38	3.62 0	3.32 -0.35	3.10 0	3.014 -0.29	3.08 -0.02	2.832 2.214	3.039 0.011	6.754 -3.314	7.655 -0.067	5.18 0.03	4.32 4.45
ZERO	116.1	6.20	3.95	3.75	3.45	3.22	3.25	2.98	2.85	2.80	2.18	4.70	4.00	6.68	2.62	2.55
FRACTURE	116.1	6.20	3.95	3.75	3.45	3.22	3.25	2.98	2.85	2.80	5.38	4.55	5.0	2.78	+5.0	+5.0
POST FAILURE	ZERO	OUT	OUT	OUT	OUT	OUT	OUT	OUT	OUT	OUT	.022	.058	OUT	OUT	OUT	OUT

* S.S.T. = Slow Start Timer

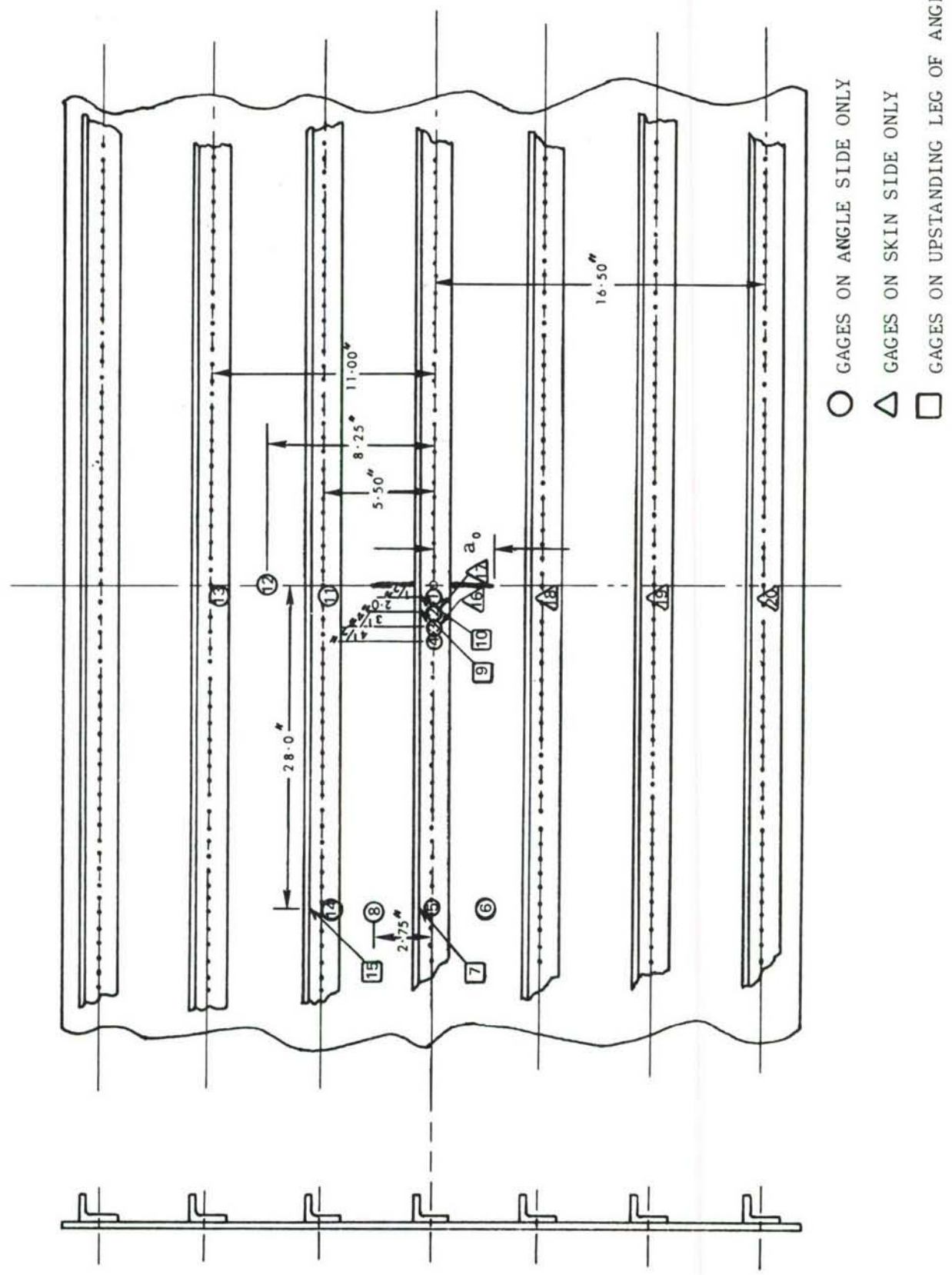


Figure 15. Strain Gage Locations, -23 and -15 Panels

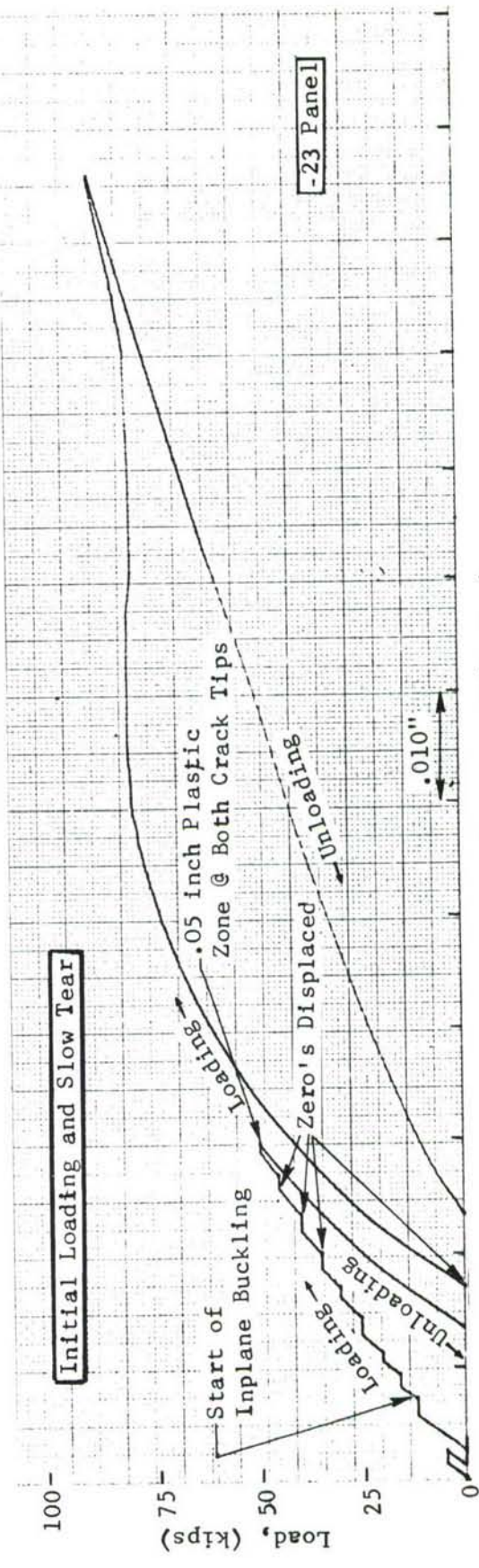
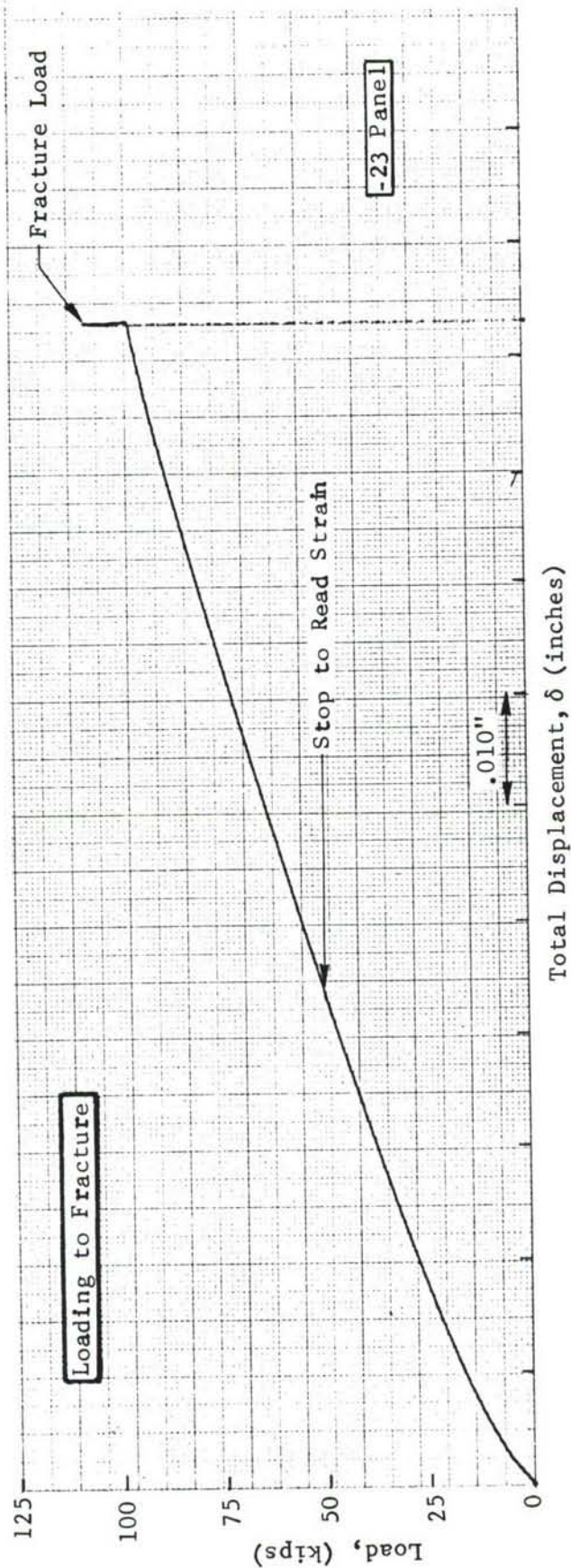


Figure 16. Load-Displacement Curves for -23 Panel Angle Stiffened, Lower (Center Stringer Broken)

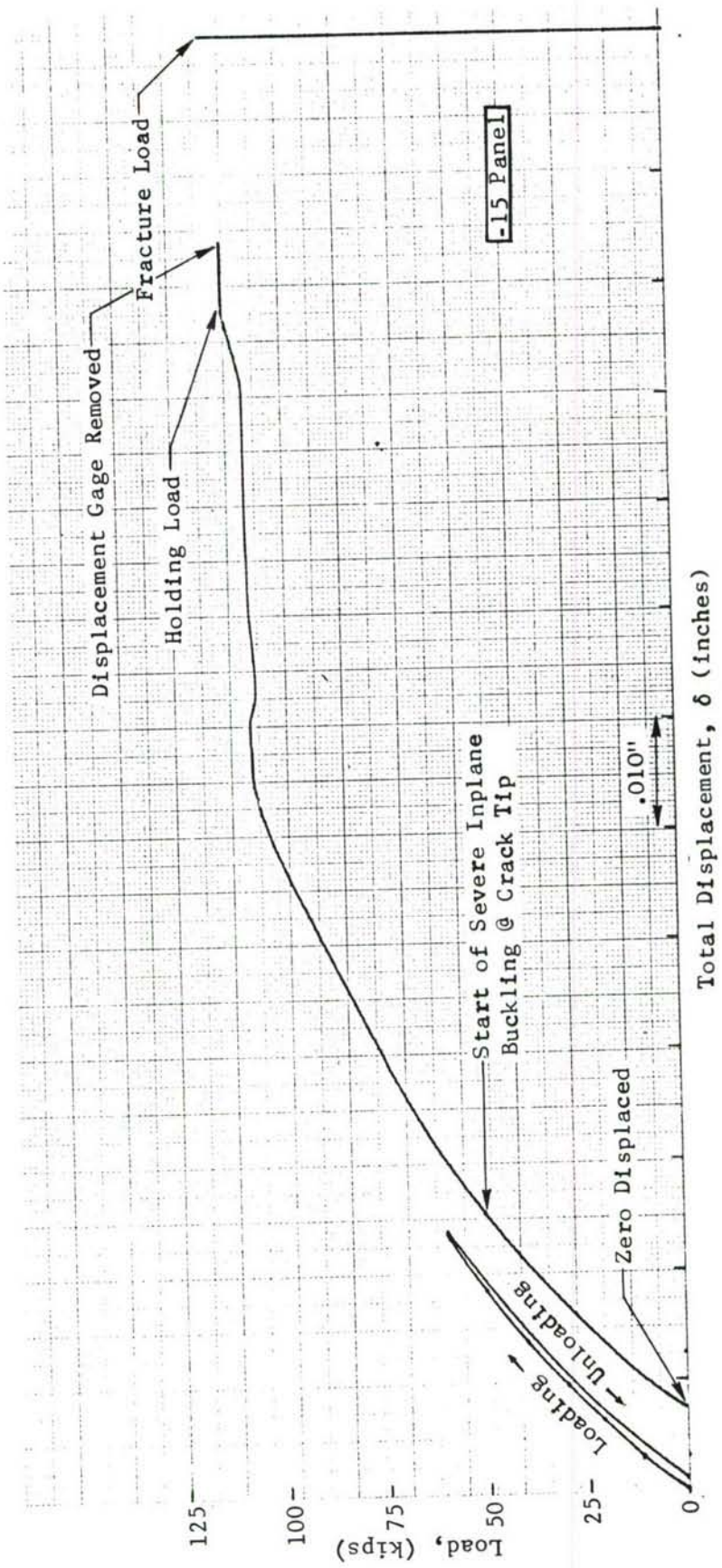


Figure 17. Load-Displacement Curves for -15 Panel Angle Stiffened, Lower (Center Stringer Intact)

Both panels were loaded in increments as noted in the data of Tables III and IV and Figures 16 and 17. Loading was stopped at the first sign of crack extension accompanying large plastic zone build-up. After unloading and measurement of the crack, the loading was re-initiated using ramp loading of 100,000 pounds per minute. Slow, stable tear occurred for both panels and the cracks arrested at the adjacent stringers. Strain readings were taken at the maximum load point where the crack(s) arrested. This load was 91 kips for the -23 panel and 111.7 kips for the -15 panel. At this point the panels were unloaded and a ramp loading of 100,000 pounds per minute was again initiated. Several load hold conditions were instituted on the way to fracture at which time strain data were recorded. Continuing loading caused fracture at 107.2 kips for the -23 panel and at 116.1 kips for the -15 panel.

Motion picture coverage was initiated at the start of slow tear and as close to fracture as possible in each case.

The displacement data for the -23 panel (Figure 16) indicates a staircase appearance due to deliberate offsetting of the x axis zero during the initial strain survey at each load hold condition. This offsetting procedure was not followed for the -15 panel, except for the final fracture trace. On this panel (Figure 17) the gage was removed from the specimen prior to fracture since it was close to being out of travel at the final load hold condition.

Figures 18 and 19 indicate the fracture surfaces for the -23 and -15 panels. Fracture occurred through the center line of fasteners in both cases. The back side or angle side of the -23 and -15 panel after fracture are shown in Figures 20 and 21. The angles fractured at the centerline fasteners along the crack path in both cases.

2.2.3.3 Comparison of Experimental and Analytical Strains

Figure 15 shows the location of strain gages on both the intact and broken central angle panel. Tabulated in Table IV are the strain gage readings for various applied loads at a crack length of 5.55 inches. Figure 22 shows the experimental and analytical variation of strain in the central stringer with increasing distance from the crack for the -15, intact stringer panel with a half crack length of 2.775 inches. Good correlation is noted between experimental strains and those obtained from the elastic analysis. The experimental data of Figure 22 is cross plotted in Figure 23 to show the variation of strain with applied stress for the -15 panel. Note that up to an applied stress of 22 ksi a good correlation is obtained between elastic analysis and experimental strains. At higher applied stresses the experimental strain in the stringer close to the crack plane is slightly lower than that given by an elastic analysis.

For the broken central stringer (angle) panel the variation of strains in the central stringer with increasing distance from crack plane is shown in Figure 24. It can be seen that the strain gage just above the crack surface (one-half inch away) is in compression under tensile loads as predicted by the analysis. Good correlation is obtained between the elastic analyses and

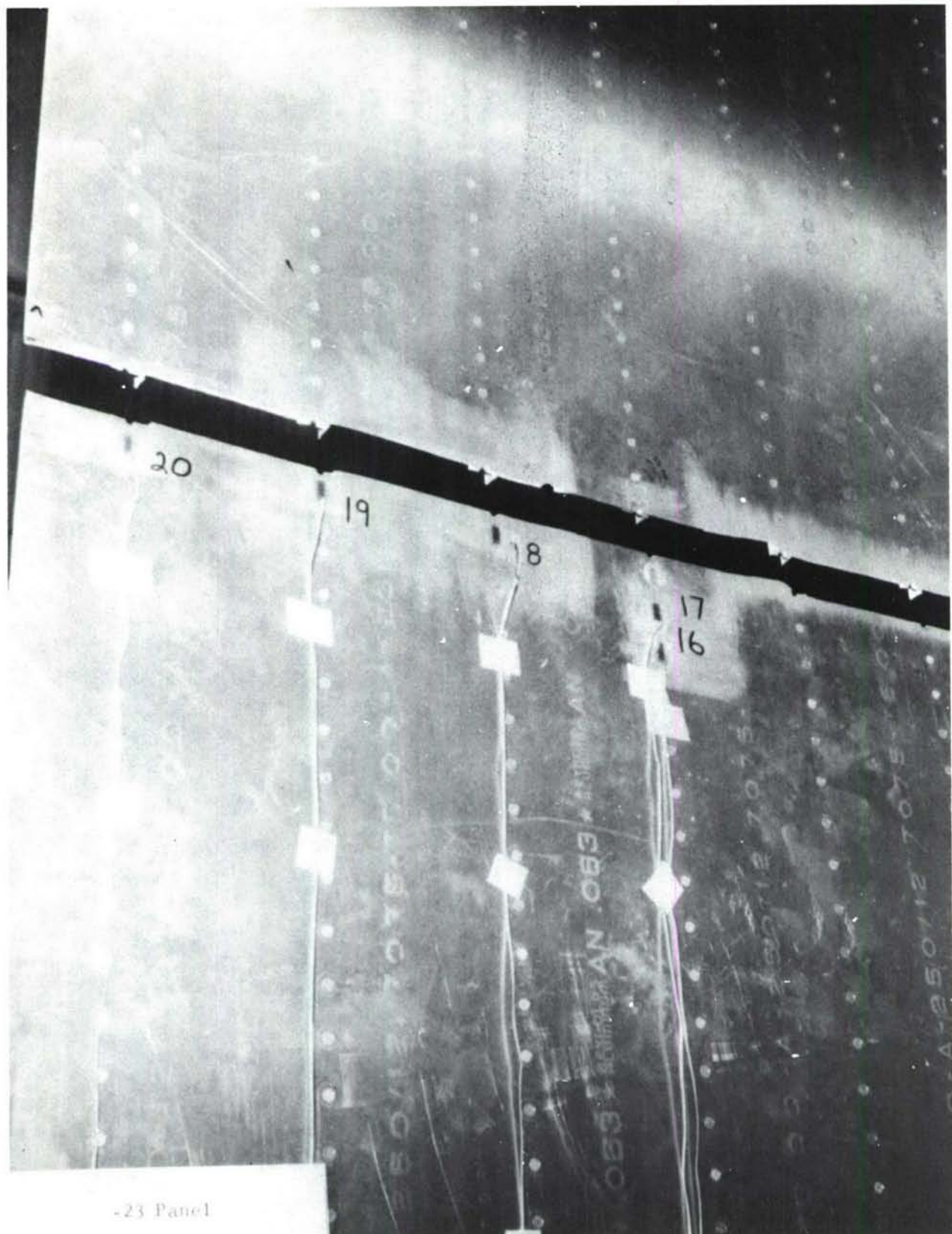


Figure 18. View of Fracture Surface from Skin Side, Wing Panel Angle Stiffened, Lower (Center Stringer Initially Broken)

-15 Panel

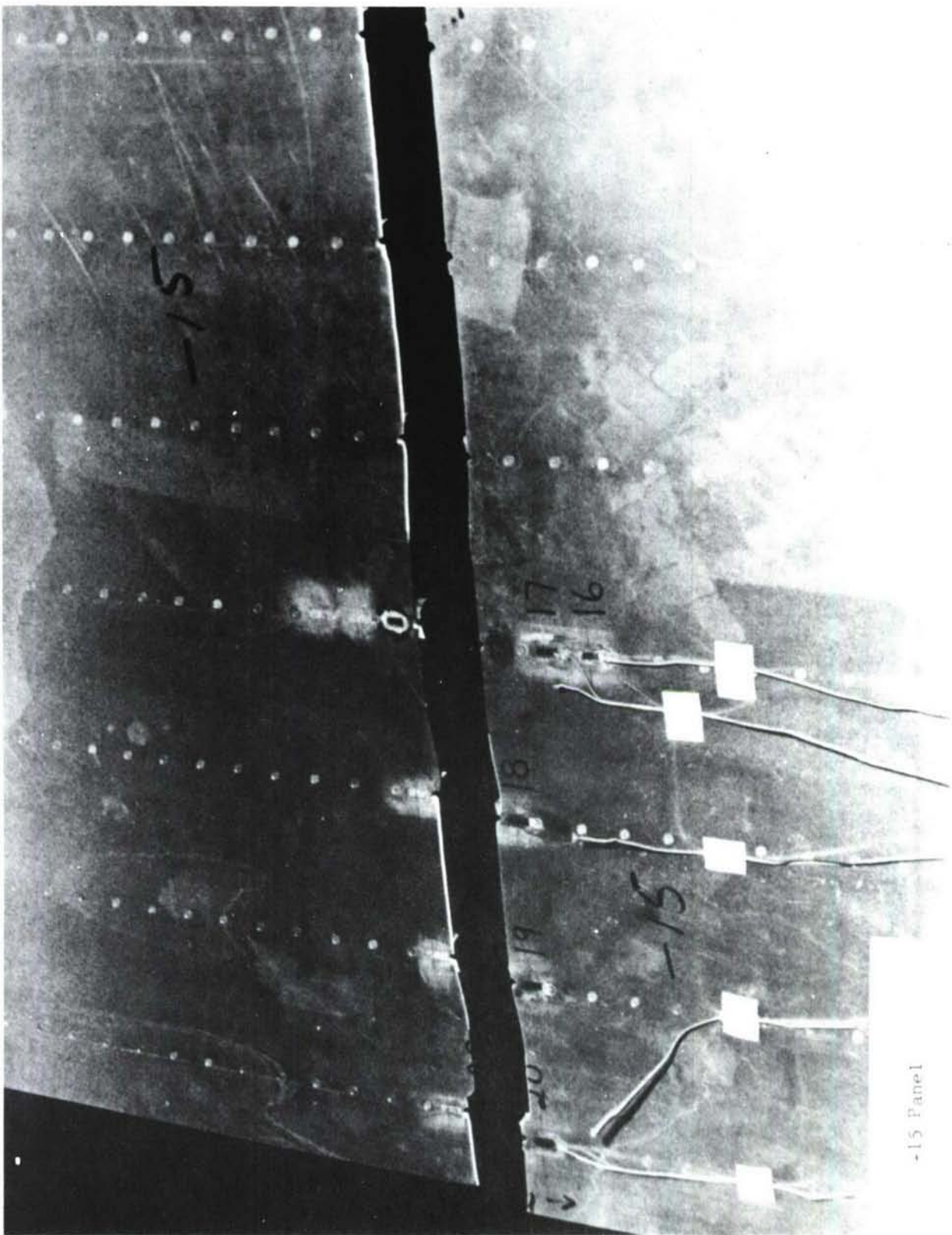


Figure 19. View of Fracture Surface from Skin Side, Wing Panel Angle Stiffened, Lower (Center Stringer Initially Intact)

-23 Panel 1



Figure 20. View of Fracture Surface from Stringer Side, Wing Panel Angle Stiffened, Lower (Center Stringer Initially Broken)

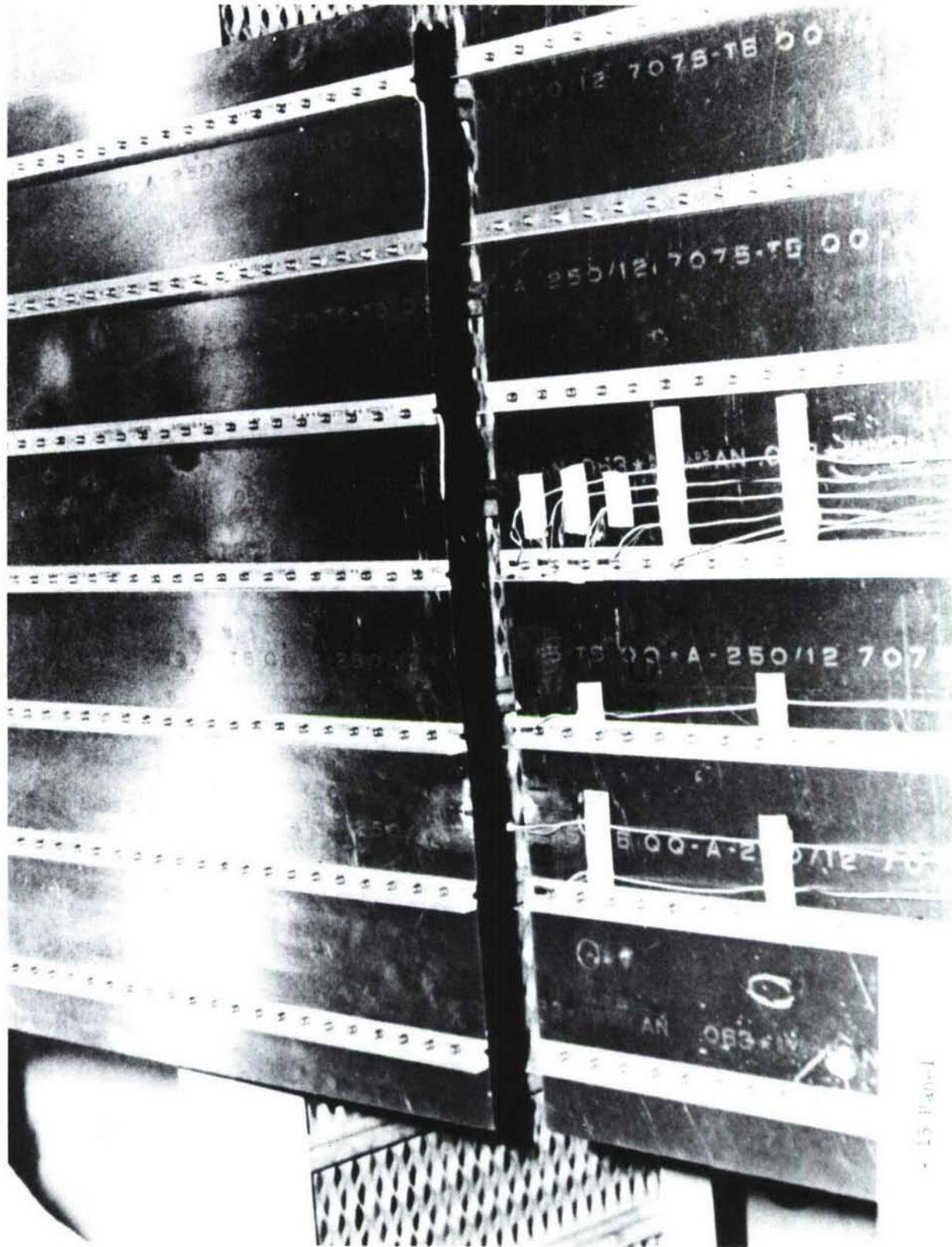


Figure 21. View of Fracture Surface from Stringer Side, Wing Panel Angle Stiffened, Lower (Center Stringer Initially Intact)

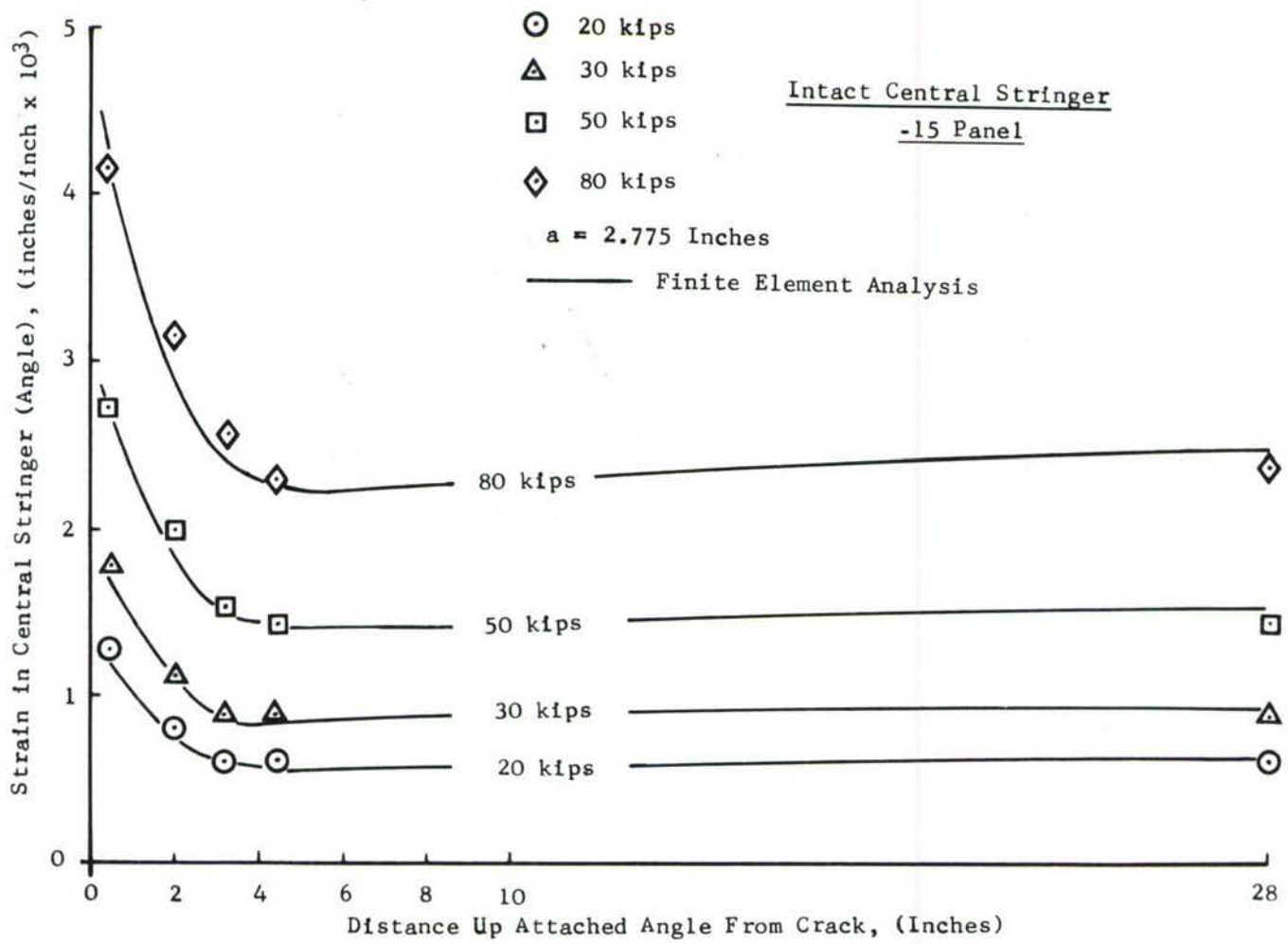


Figure 22. Strain in Central Stringer for -15 Panel, Angle Stiffened, Lower

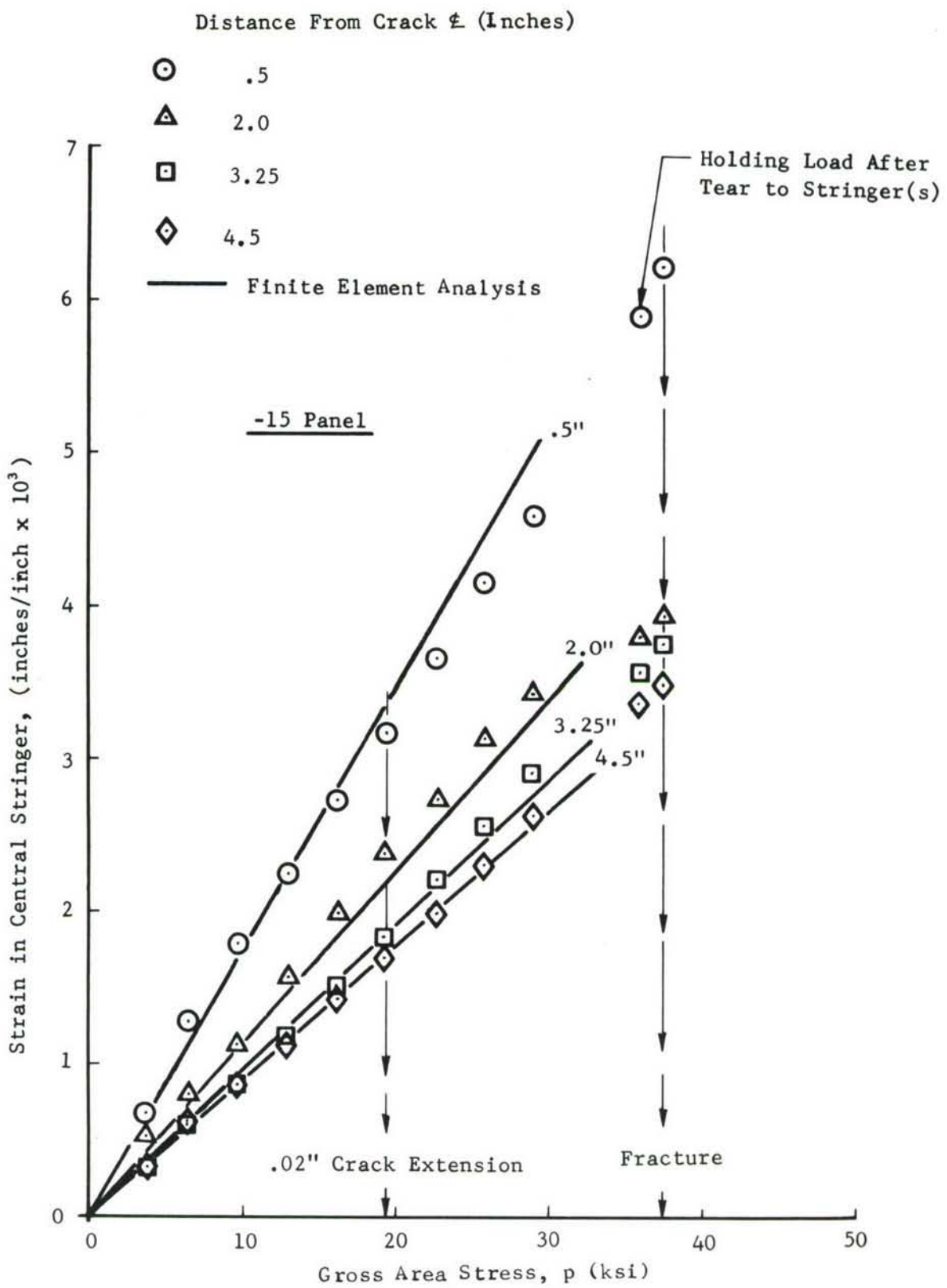


Figure 23. Strains in Central Attached Angle Away from the Crack Plane as a Function of Applied Stress for -15, Intact Angle Stiffened Panel

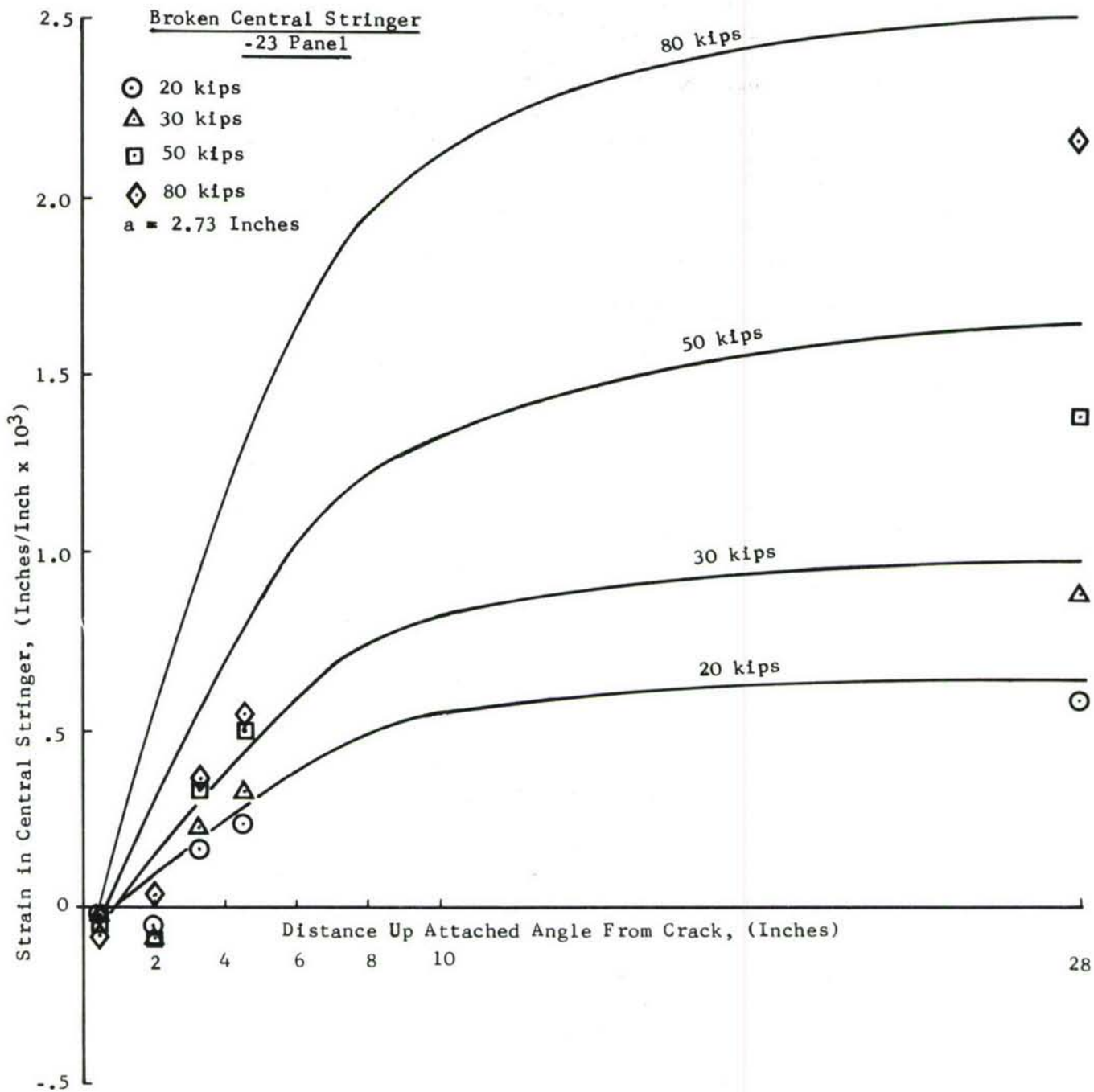


Figure 24. Strain in Central Stringer for -23 Panel, Angle Stiffened, Lower

the experimental measured strains up to an applied load of 50 kips (applied stress of 16.6 ksi), however, at higher loads the elastic strains are considerably larger. In comparing Figures 22 and 24, it can be observed that the experimental strains deviate from the elastic results at a lower applied stress for the broken stringer case. This is due to the higher stress intensity factors and larger plastic zones for the broken stringer panel (-23) compared to the intact stringer (-15) panel. A comparison of stringer strains in the -15 and -23 panels is shown in Figure 25. The stringer strains are from a location one-half inch above the crack surface. For the broken central stringer panel (-23) the strain in the center stringer is compressive for all applied loads (also see Figure 24). The stringers located 5.5 inches from the center line of the crack and panel have higher strains for the broken stringer panel compared to corresponding strains in the adjacent stringers of the -15 panel. The correlation between experimental strains and elastic analytical strains is good up to an applied stress of 20 ksi for both panels. Beyond that point plastic zone build-up and small crack extension has occurred for the -15 panel.

2.2.4 Residual Strength Prediction

The residual strength of panels with intact and broken central stringers is predicted in this section. The results are compared with those obtained from the tested panels.

2.2.4.1 Residual Strength of Panel with Intact Central Stringer

The procedure discussed in the Phase II report (Reference 1) was used to predict the residual strength of the complex aircraft structural panels of Phase III. The elastic-plastic analysis based on an assumed Dugdale type plastic zone ahead of the crack tip in conjunction with the $\sqrt{J_R}$ resistance curve of the skin material was used in the residual strength prediction for the skin critical fracture cases. On the \sqrt{J} versus crack size (a) plots for the panel, discussed in Sub-Section 2.2.2.2 (Figure 9), the $\sqrt{J_R}$ versus Δa_{PHY} material resistance curve is overlayed at the initial crack length of interest. The applied stress at which $\sqrt{J_R}$ versus Δa_{PHY} , and \sqrt{J} versus $a_{PHYSICAL}$ curves become tangential will determine the stress at which instability occurs and the crack propagates rapidly. After this point of instability, if the \sqrt{J} curve for the panel dips below the $\sqrt{J_R}$ resistance curve of the material the crack will be arrested otherwise it will propagate catastrophically. The stresses in the stringer which are obtained from the elastic-plastic analysis and the ultimate strength of the stringer material are used initially to determine if a stringer critical case prevails.

The stresses in the central stringer for the panel with the intact central stringer and a half crack length of 2.75 inches are shown in Figure 7. The ultimate strength of the stringer material (7075-T6 extrusions) was found to be 87.2 ksi from tensile test data. Using this ultimate stress value and the Dugdale type elastic-plastic analysis shown in Figure 7, the failure

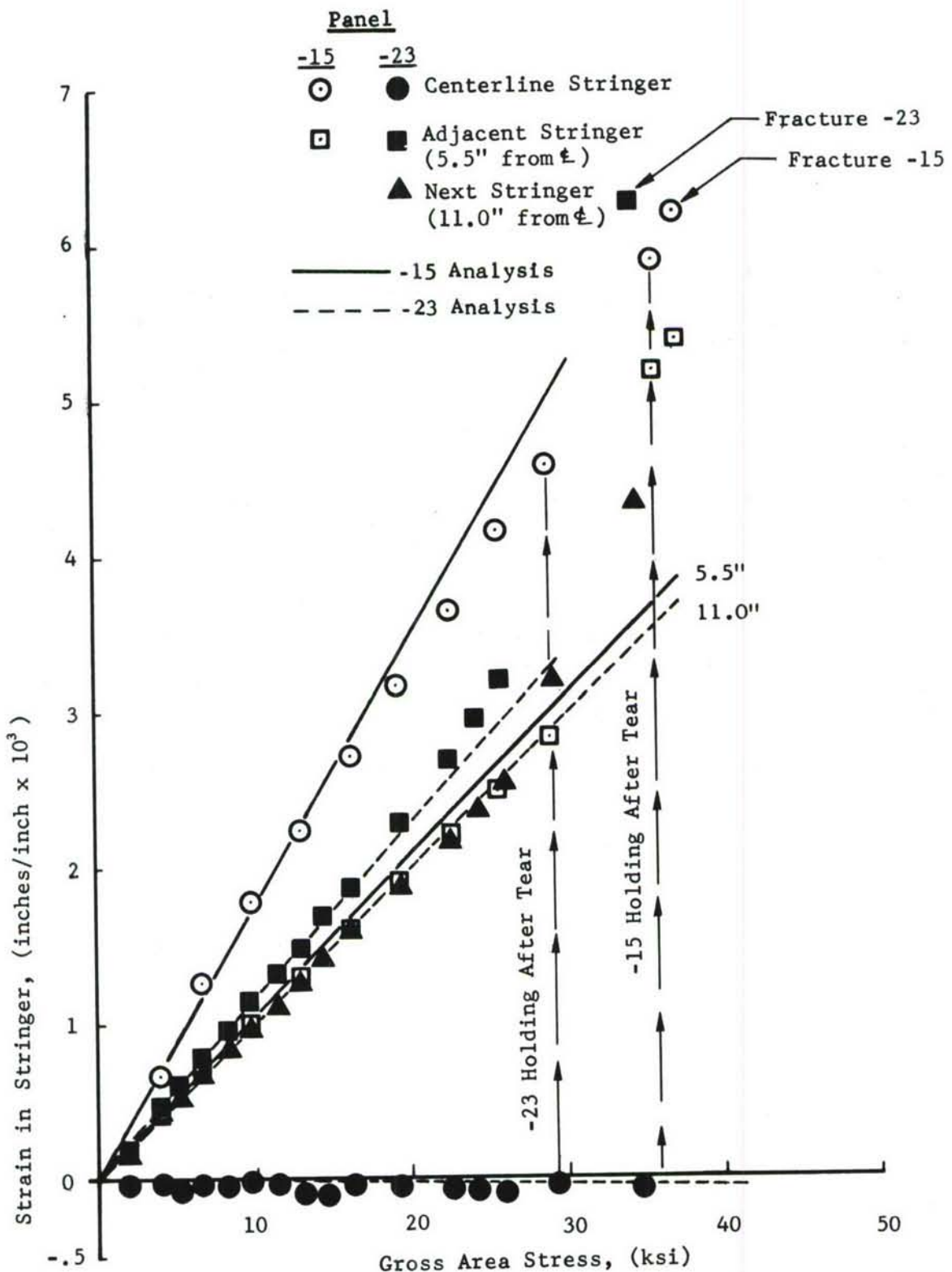


Figure 25. Strain in Central and Outer Attached Angles as a Function of Applied Stress for Broken (-23) and Intact (-15) Stiffened Panels

of the central stringer (angle) is predicted at $p/F_{ty} = 0.7$. Next consider the \sqrt{J} versus crack length plot for various applied stresses as shown in Figure 26. Superimposed on this plot is the $\sqrt{J_R}$ versus Δa_{PHY} resistance curve of the 7075-T73 skin material plotted at a physical half crack length of 2.775 inches. It is seen from this Figure that at the stringer critical stress $p/F_{ty} = 0.7$, there will be considerable slow tear in the skin and therefore the stringer stresses shown in Figure 7 will not be valid. From Figure 26, the resistance curve of the material plotted on the physical half crack length of 2.775 inches (initial half crack length in the tested panel) is tangential to the \sqrt{J} versus a curve of the panel at an applied stress of $p/F_{ty} = 0.545$. Thus the first point of crack instability occurs (after slow crack growth) at this stress and the crack starts a rapid advance. However, from Figure 26, it is noted that at a half crack length of 4.45 inches the \sqrt{J} curve for the panel drops lower than the resistance curve of the material, i.e., beyond this point the resistance of the material is higher than \sqrt{J} developed in the stressed panel, and hence the running crack will become arrested. The crack was arrested at the rivet hole in the -15 panel where the stringer is connected to the skin. The resistance curve of the skin material is now replotted at a half crack length of 5.5 inches (distance from centerline of the stringer to panel centerline), where the crack became arrested. For this crack length the \sqrt{J} curve of the panel becomes tangential to the resistance curve at an applied stress of $p/F_{ty} = 0.645$. Hence the crack instability occurs at that stress and crack starts running catastrophically. Beyond this point of instability the \sqrt{J} values in the panel are higher than the resistance curve of the skin material and therefore no possibility exists for crack arrest. The \sqrt{J} curve of the panel will continue to rise under increasing load until the influence of the next stringer on panel stress (11 inches from the centerline of the panel) is felt and the \sqrt{J} value will once again have a decreasing trend and reach a second minima at that point. From the trend of the \sqrt{J} curve in Figure 26 it is evident that at an applied stress of $p/F_{ty} = 0.645$ the \sqrt{J} value of the panel will be higher beyond a half crack length of 7.5 inches. Therefore no possibility of crack arrest is possible at the second stringer, i.e., 11 inches from the centerline of the crack, under increasing load conditions.

The panel analyzed above (-15 panel) was tested to failure. Slow tear in this panel started at a load of 60 kips which corresponds to p/F_{ty} of 0.32. At this applied load slow tear on each crack tip was about 0.02 inch (see Table IV). The first point of instability (rapid crack extension) occurred after an applied load of 60 kips and before a load of 111.7 kips. At 111.7 kips the crack had already reached the angle stiffeners and became arrested. From theory the first point of instability is at an applied stress of 0.545 F_{ty} or a load of 104 kips (see Figure 26). After the crack had torn to the angle stiffeners, the panel was able to take a load of 111.7 kips without any further slow tear. At an applied load of 111.7 kips (i.e., $p/F_{ty} = 0.58$) the slow tear analysis from Figure 26 is approximately 0.05 inches. This is less than the radius of the rivet hole.

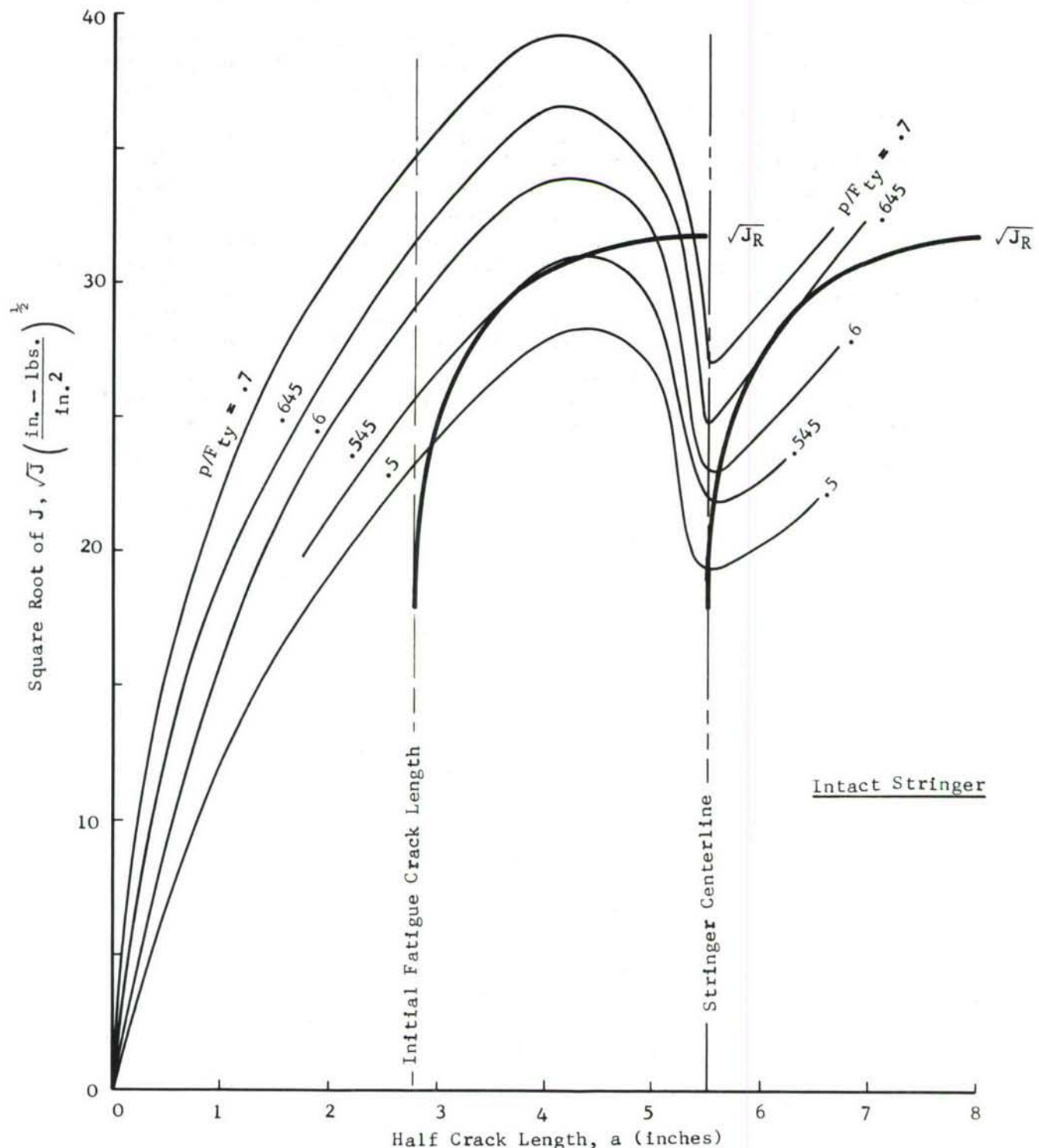


Figure 26. Residual Strength Prediction Plot for -15 Panel (Intact Stringer)

The measured failure load of the panel was 116.1 kips (see Table IV). The predicted failure is at $p/F_{ty} = 0.645$ or panel load of 123.4 kips. This predicted failure load is within 6.28 percent of the measured failure load for the -15 panel.

2.2.4.2 Residual Strength of Panel with Broken Central Stringer

For this panel the central stringer (angle) is broken and therefore represents a skin critical case. A complete elastic-plastic analysis for various crack lengths was not conducted for this panel. An elastic-plastic analysis was computed for the tested crack length of approximately 5.5 inches. The comparison of elastic-plastic analysis for the intact and broken stringer panels is shown in Figure 6. The elastic and elastic-plastic \sqrt{J} values for the broken central stringer case are higher in both analyses. Hence the \sqrt{J} versus crack length curves for various applied loads will have the same shape as shown in Figure 9 for the intact stringer case, however, the \sqrt{J} values will be higher at the same crack length and applied stress. Thus in the case of the broken stringer the first point of instability will be at some stress lower than $p/F_{ty} = 0.545$ and crack arrest will occur. The tested crack lengths for broken and intact stringer are similar and hence \sqrt{J}_R values at failure for these two panels would be expected to be similar. Using the predicted value $p/F_{ty} = 0.645$ and the elastic-plastic analysis for a half crack length of 2.75 inches (Figure 6, intact stringer) the \sqrt{J} value at failure is $31.7 \left(\frac{\text{in.-lbs.}}{\text{in.}^2} \right)^{\frac{1}{2}}$. Using this \sqrt{J} value and the elastic-plastic analysis for the broken stringer panel with a half crack length of 2.75 inches (Figure 6) the predicted failure stress is $p/F_{ty} = 0.558$. The actual failure load of the -23 panel was 107.2 kips whereas the predicted failure load corresponding to $p/F_{ty} = 0.558$ is 106.74 kips. Thus the predicted load is within 0.44 percent of the actual failure load.

2.3 TITANIUM PANEL

To determine the influence of material and toughness (through variation of resistance curve) on the residual strength of fatigue cracked panels, an all titanium panel was tested and residual strength determined. The skin material consisted of a beta mill annealed Ti-6Al-4V and formed angles of annealed Ti-6Al-6V-2Sn. The construction once again as with the previous panels represents a typical lower surface wing construction sized for a fighter type aircraft.

2.3.1 Description of Test Panel

Figure 1 indicates the drawing of the titanium test panel and is identified as a -21 assembly, however, the term titanium panel is used in the report. Overall skin width was 38.5 inches with a panel length of approximately 90 inches. Spacing between rivet and angle centerlines was 5.5 inches. This spacing was identical to that of the previous wing panels and results in a six bay panel symmetric about the panel centerline.

The titanium angles were fabricated from 0.064 inch thick, Ti-6Al-6V-2Sn (mill annealed) by passing through a heated die. The material is the same as that previously characterized in Reference 2 and no change in material properties of the attached leg were noted due to the hot forming operation. Dimensions of the angle are shown in Figure 1, (Section B-B). As with the previous aluminum wing panels the angles were attached through the one inch leg by 3/16-inch diameter, flush head steel HI-LOK's (19PB-3) at 1.3 inch pitch in the test area. Listed in Table V are the panel, skin, and angle cross sectional thicknesses, areas, and material identification. It will be noted that the stiffening ratio of this panel is within 0.2 percent of the -15 aluminum wing panel (see, e.g., Table I).

TABLE V TITANIUM SKIN-ANGLE STIFFENED WING PANEL AREAS AND MATERIAL IDENTIFICATION

MEASURED THICKNESS (Inches)		CROSS SECTIONAL AREAS (Inches ²)		SKIN MATERIAL/ AND I.D. (See Ref. 2)	PERCENTAGE OF TOTAL ANGLE AREA TO SKIN AREA
Angle	Skin	Total Angles	Skin		
.064	.058	.6524	2.233	Beta Mill Ti-6Al-4V/ TC #3	29.2%
		Total Panel Cross Sectional Area = 2.8854 in ²			

Indicated in Figure 1 is a starter slot 5.00 inches in overall length. As with the previous panels 20 strain gages were positioned as shown in Figure 27. In addition, the beam clip gage was mounted on the skin side to record crack opening displacement at the crack and panel centerline.

2.3.2 Finite Element Modeling and Analysis

The analyses of the all titanium panel was performed in a manner similar to the intact stringer, all aluminum panel (-15). Both elastic and elastic-plastic analyses were performed for various crack lengths. The finite element modeling, elastic, and elastic-plastic analyses of the panels are discussed in the following subsections.

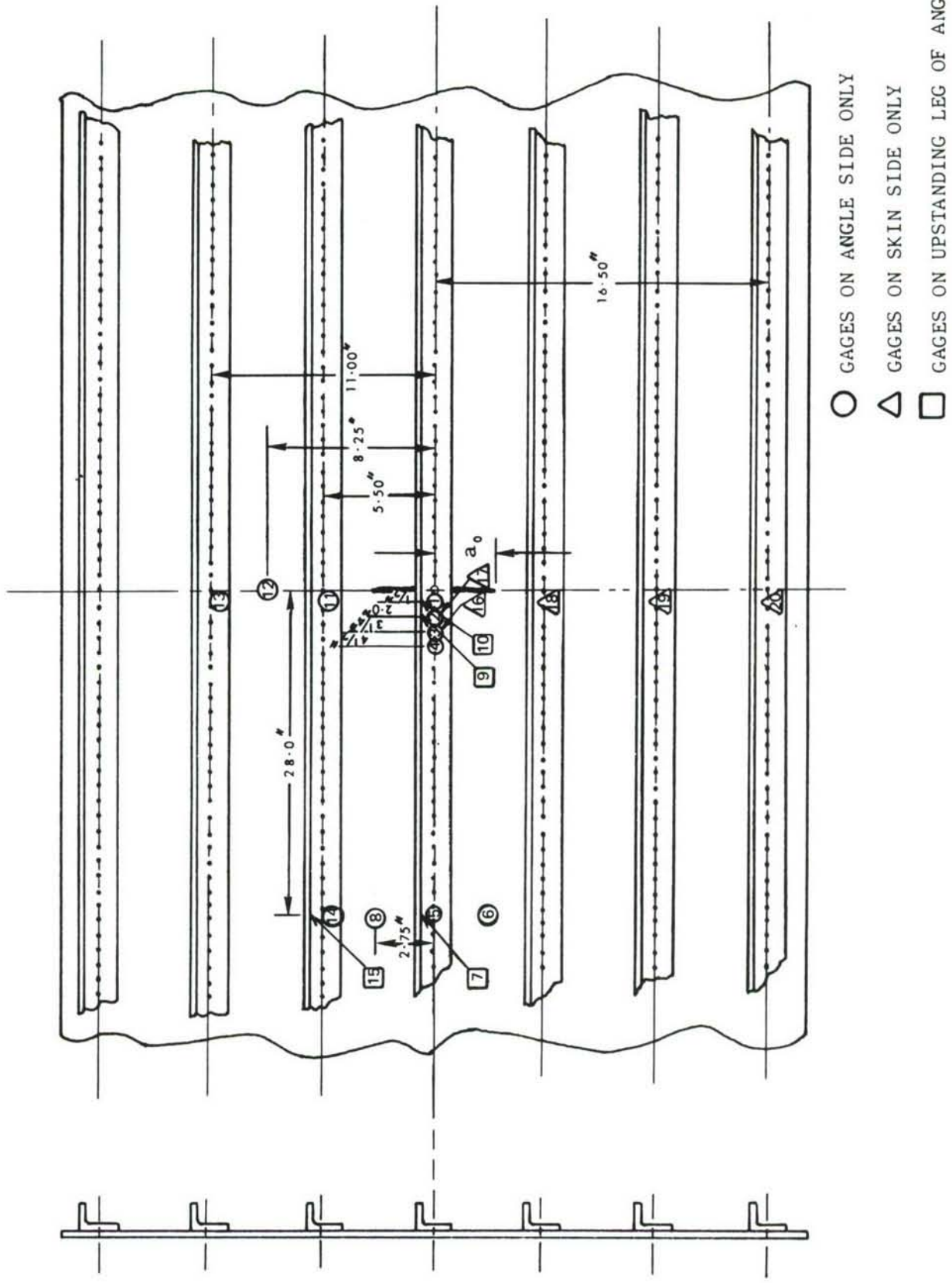


Figure 27. Strain Gage Locations - Titanium Panel

2.3.2.1 Finite Element Modeling of the Al1 Titanium Panel

The finite element model used to analyze the aluminum panel (-15) was adopted to treat the titanium panel. The size of the angles and skin thickness for this panel were different from those of the aluminum panel. The (x, y) co-ordinates of all grid points in the finite element model were kept the same as for the aluminum panel and only the z (dimension perpendicular to the plane of the panel, see Figure 2) coordinates required changing. Changes were made in the thicknesses and areas of the triangular membrane and rod elements of the finite element model to comply with the dimensions used for the titanium panel.

2.3.2.2 Elastic and Elastic-Plastic Analyses of Al1 Titanium Panel

An elastic analysis of the titanium panel with intact central stringer was performed for a half crack length of 2.875 inches. The contours shown in Figure 3 were used to evaluate J. The variation of \sqrt{J} with p/F_{ty} is shown in Figure 28.

The elastic-plastic analysis was conducted assuming a Dugdale type strip plastic zone ahead of the crack tip. The variation of \sqrt{J} with p/F_{ty} , using Dugdale type elastic-plastic analysis, is shown in Figure 28 for a half crack length of 2.875 inches. At an applied stress of 80 percent of yield the values of \sqrt{J} given by an elastic-plastic analysis are 18 percent higher than those given by an elastic analysis. To obtain \sqrt{J} versus crack length curves for various applied loads required for the residual strength prediction, five half crack lengths were selected: 1.75, 2.875, 4.75, 5.5, and 6.0 inches. The plot of \sqrt{J} versus applied stress is shown in Figure 29 for these physical crack lengths. These \sqrt{J} values have been cross plotted in Figure 30 to show the variation of \sqrt{J} with crack length for various applied loads (stress). From Figure 30 it can be seen that the \sqrt{J} values increase with crack length to a half crack length of approximately 4.75 inches and then decrease with additional crack length. The \sqrt{J} values reach a minimum value at the stringer (angle) located at 5.5 inches from the crack and panel centerline. When the crack is beyond the centerline of the stringer, the \sqrt{J} values increase again with crack length.

2.3.3 Experimental Results and Discussion

In References 1 and 2 the data necessary to evaluate crack growth resistance based on K_R versus Δa were presented for the Ti-6Al-4V Beta Mill Annealed material. However, those data were not presented based on the proposed failure criterion, i.e., $\sqrt{J_R}$ versus Δa . As a prelude to the analytical and experimental evaluation of the residual strength of this titanium panel these data will be presented in the next section. References 1 and 2 should be consulted for details of how these data were obtained and the associated heat treatment, microstructure and mechanical property data for this material.

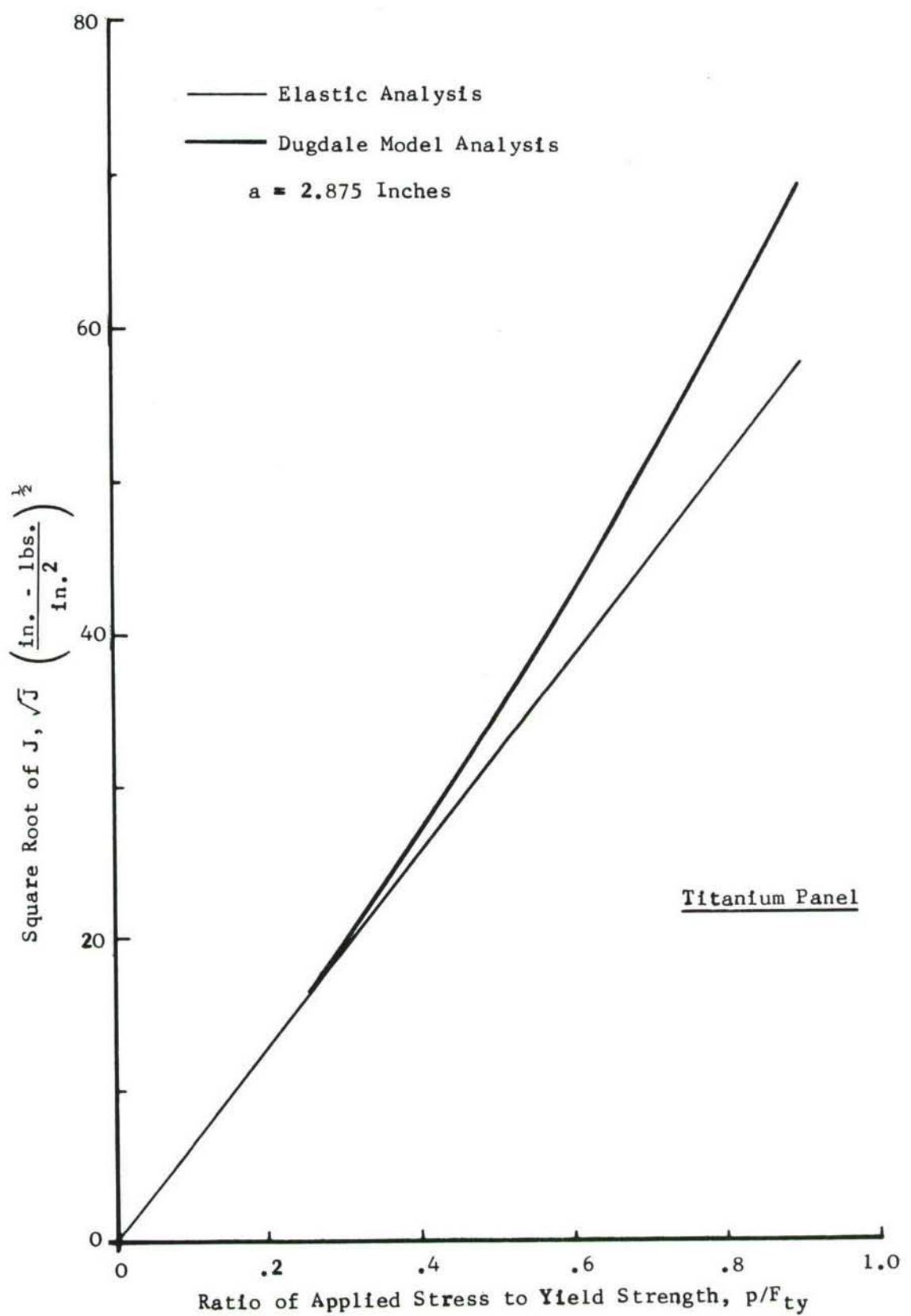


Figure 28. Elastic and Elastic Plastic Analysis of Al1 Titanium Panel

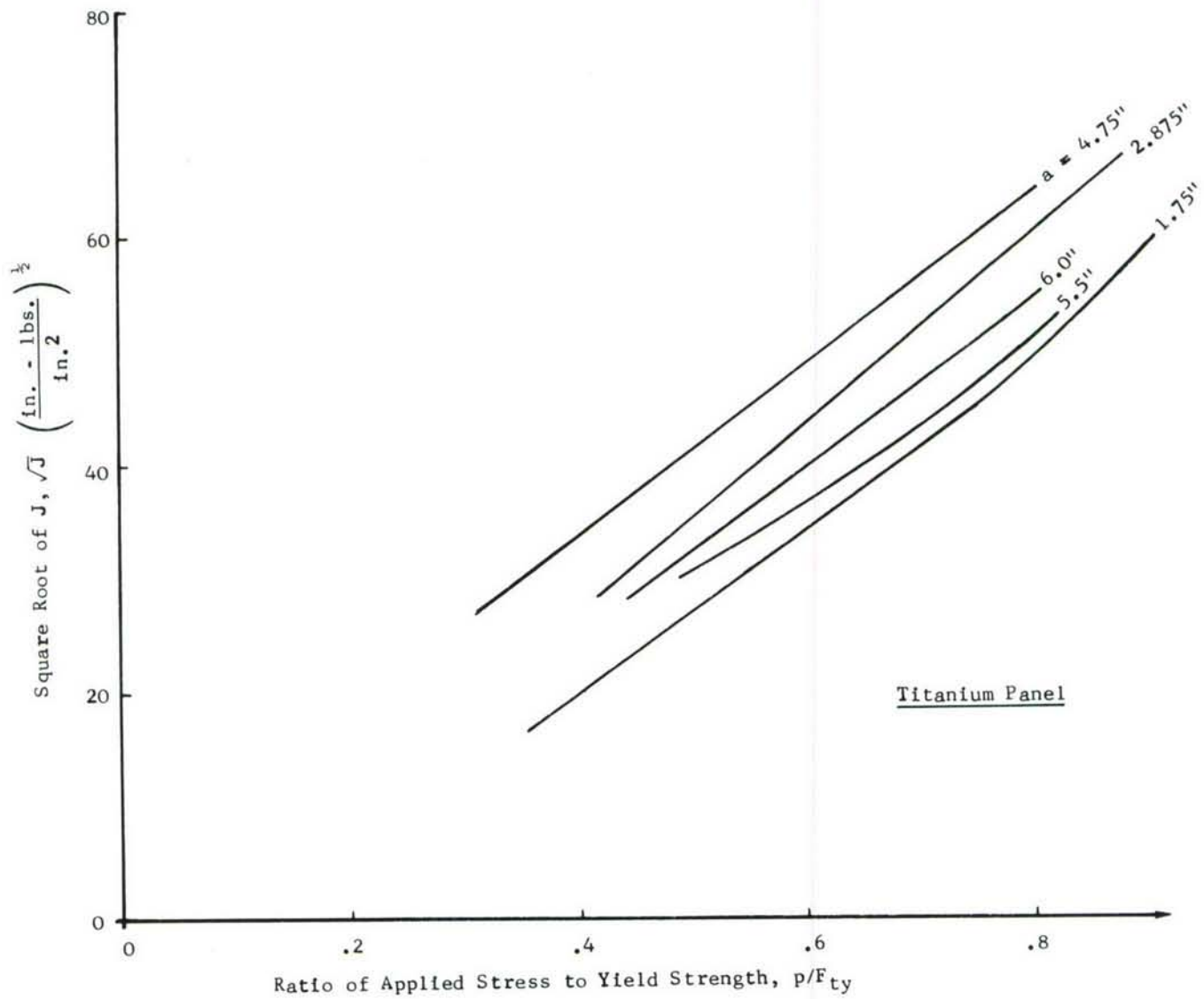


Figure 29. Square Root of J as a Function of Applied Stress for Varying Crack Lengths - All Titanium Panel

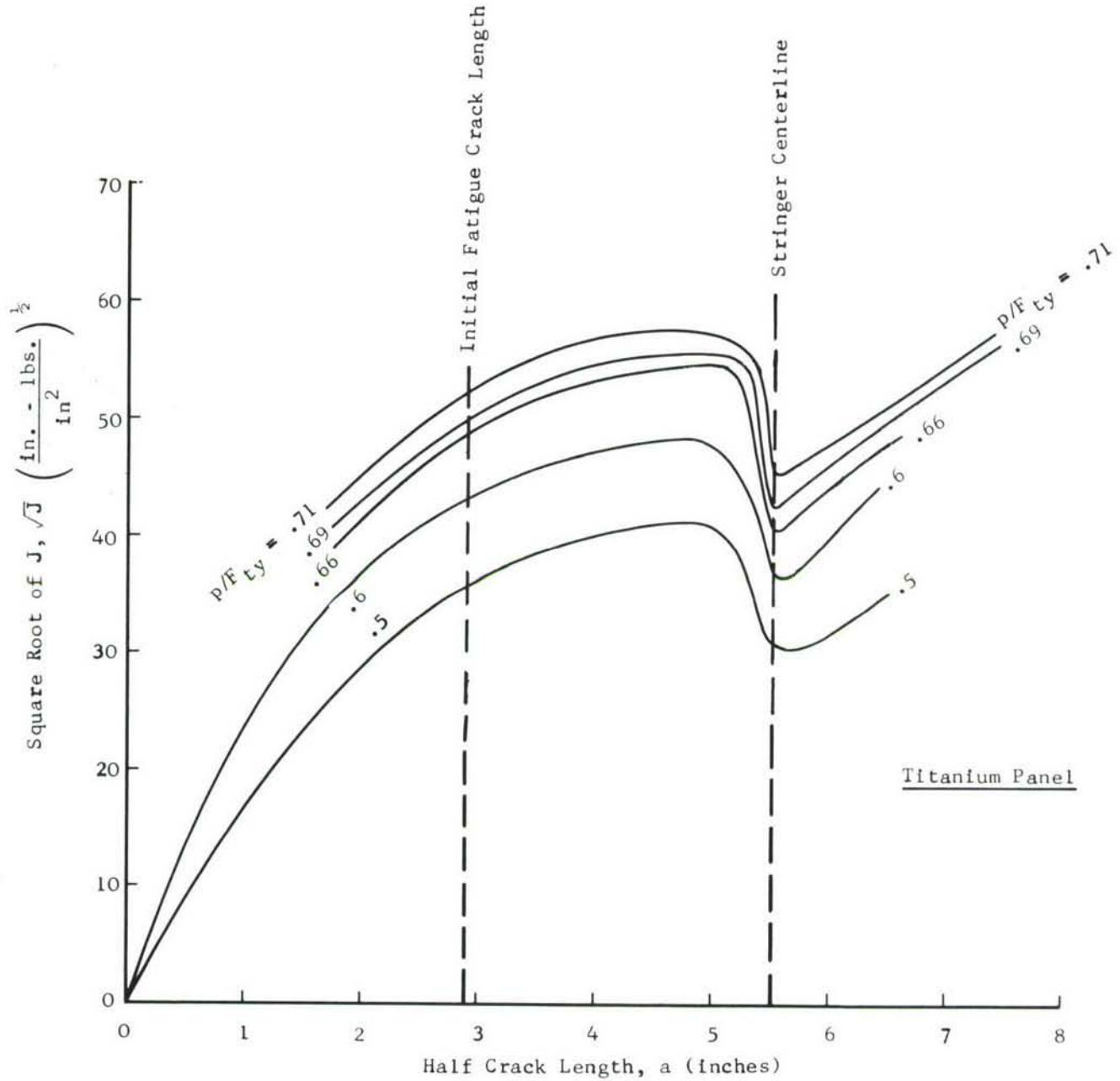


Figure 30. Square Root of J as a Function of Crack Length - Titanium Panel

2.3.3.1 $\sqrt{J_R}$ Crack Growth Resistance Data for Beta Mill Annealed Ti-6Al-4V

Two thicknesses (.053 and .187 inches) and two fracture plane orientations (LT and TL) were examined, using the crack line wedge loaded (CLWL) specimen geometry. Figure 31 indicates the $\sqrt{J_R}$ versus Δa_{PHY} values for the LT direction and Figure 32 for the TL direction in the thinner gage and Figures 33 and 34 for the thicker gage material in the LT and TL direction respectively. Consistency of data is quite evident for the thinner gages. The thicker gage material in the LT direction shows evidence of banding which is reflected from crack deviation from a plane normal to the loading axis for this material (see Reference 2 for specific discussion of this behavior).

2.3.3.2 Fatigue Precracking, Strain Data and Fracture of Titanium Panel

The titanium panel was precracked in the same manner as the previous aluminum panels. Sinusoidal, constant amplitude, tension-tension loading was employed and an initial maximum stress intensity of approximately 20 ksi $\sqrt{\text{inch}}$ and then 25 ksi $\sqrt{\text{inch}}$ selected for fatigue loading. Subsequent loading was at lower K_{max} levels to sharpen the crack. Table VI summarizes the fatigue loading and total crack length for this titanium panel. The final fatigue crack lengths were measured after fracture.

TABLE VI FATIGUE PRECRACKING AND CRACK LENGTH
DATA - TITANIUM PANEL

FATIGUE LOADS		NUMBER OF CYCLES	FATIGUE CRACK LENGTH(S)		
MAXIMUM (kips)	MINIMUM (kips)		LEFT (Inch)	RIGHT (Inch)	TOTAL (Inch)
20.0	3.0	3,000	0	0	0
33.5	11.0	18,200	.11	.08	5.19
27.0	3.0	12,050	.35	.31	5.66

Figures 35 and 36 show the front (skin) side view and angle side view of the all titanium panel.

After fatigue cycling and zero balancing of all strain gages and displacement gage a strain/load survey was taken by loading to specific load intervals. These data are noted in Table VII. Figure 27 has been repeated as Figure 37 following the strain table for convenience in locating gage positions.

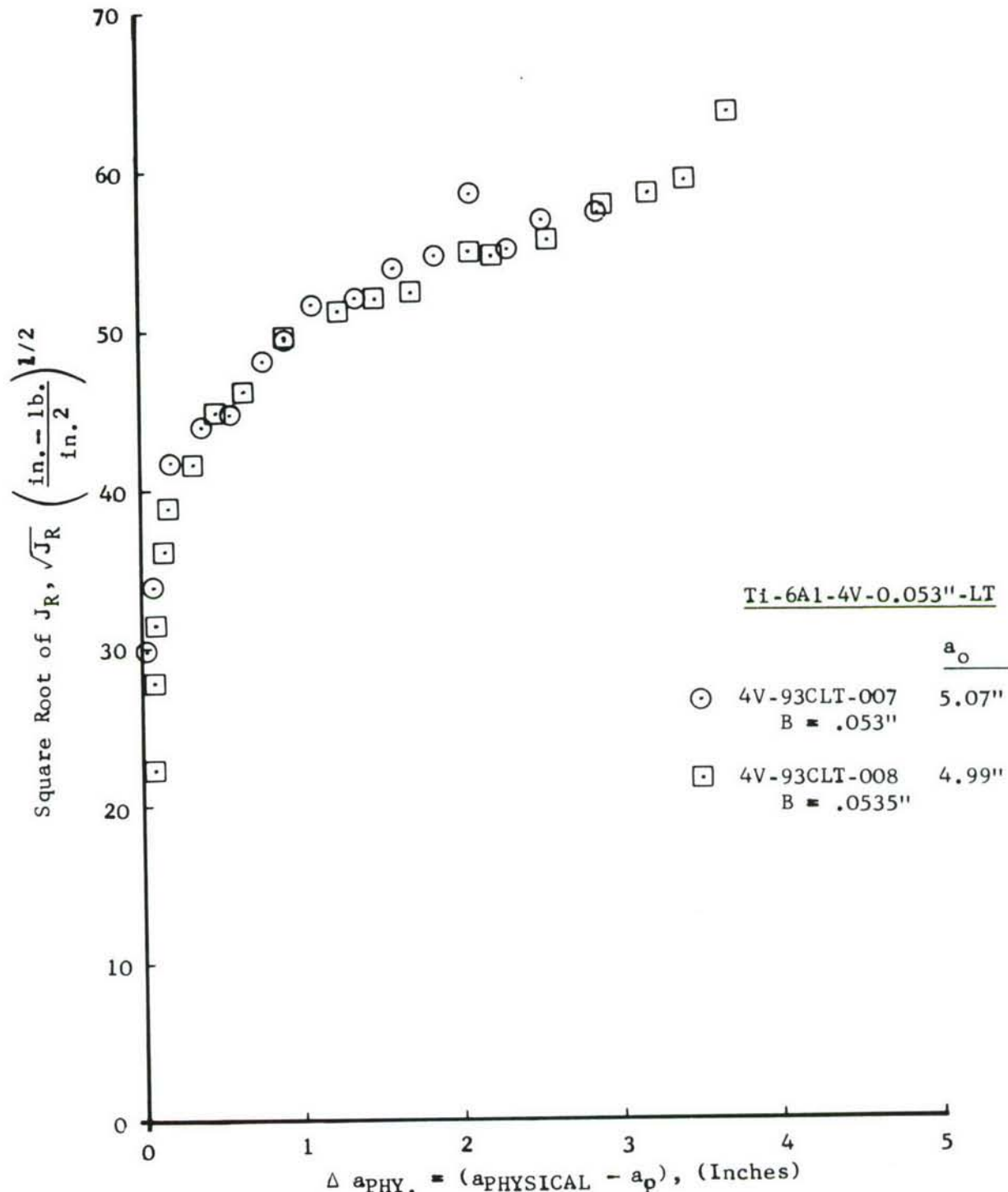


Figure 31. $\sqrt{J_R}$ Crack Growth Resistance Data - Ti-6Al-4V
(Beta Mill Annealed) - .053", LT

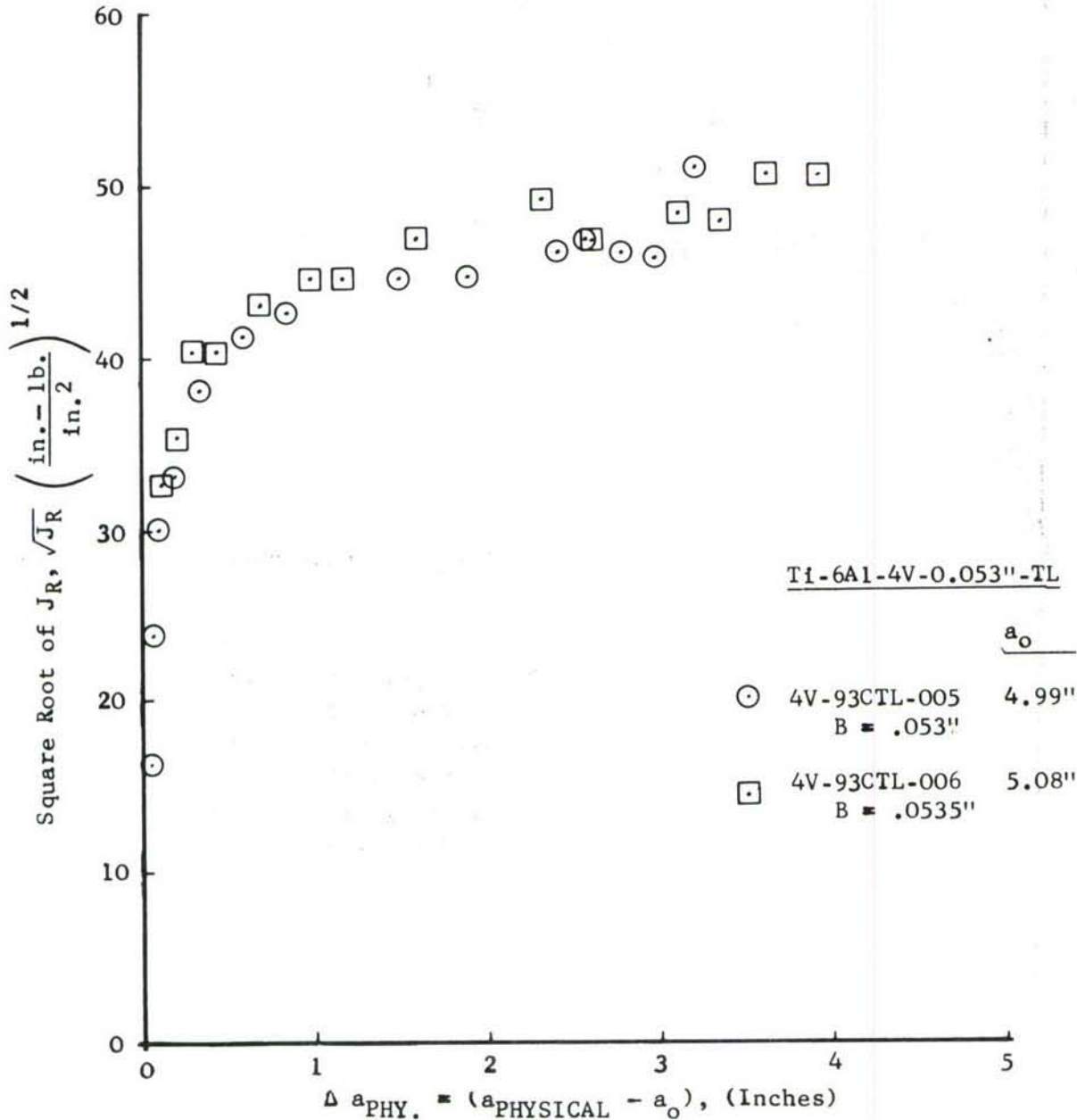


Figure 32. $\sqrt{J_R}$ Crack Growth Resistance Data - Ti-6Al-4V
(Beta Mill Annealed) - .053", TL

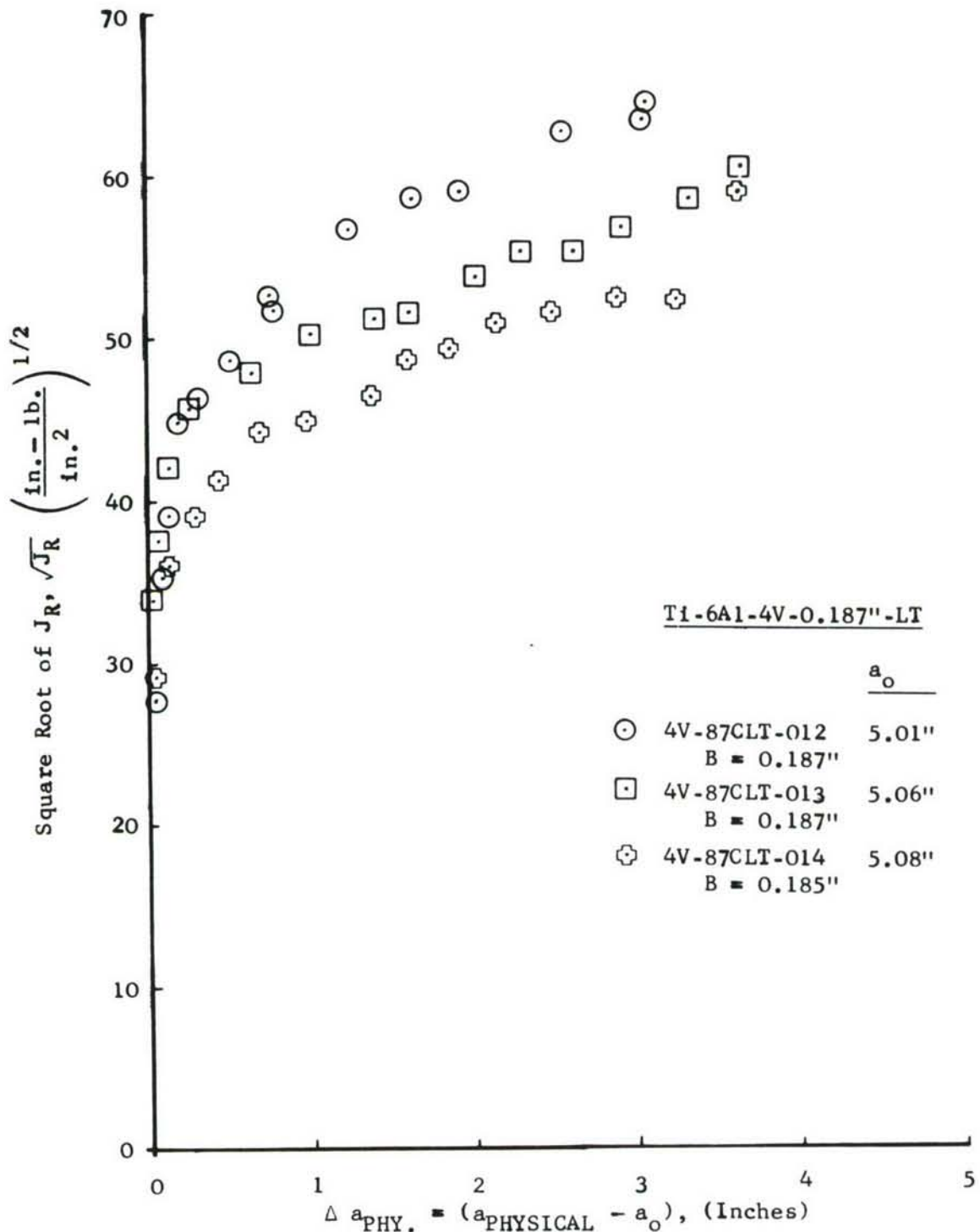


Figure 33. $\sqrt{J_R}$ Crack Growth Resistance Data - Ti-6Al-4V
(Beta Mill Annealed) - .187", LT

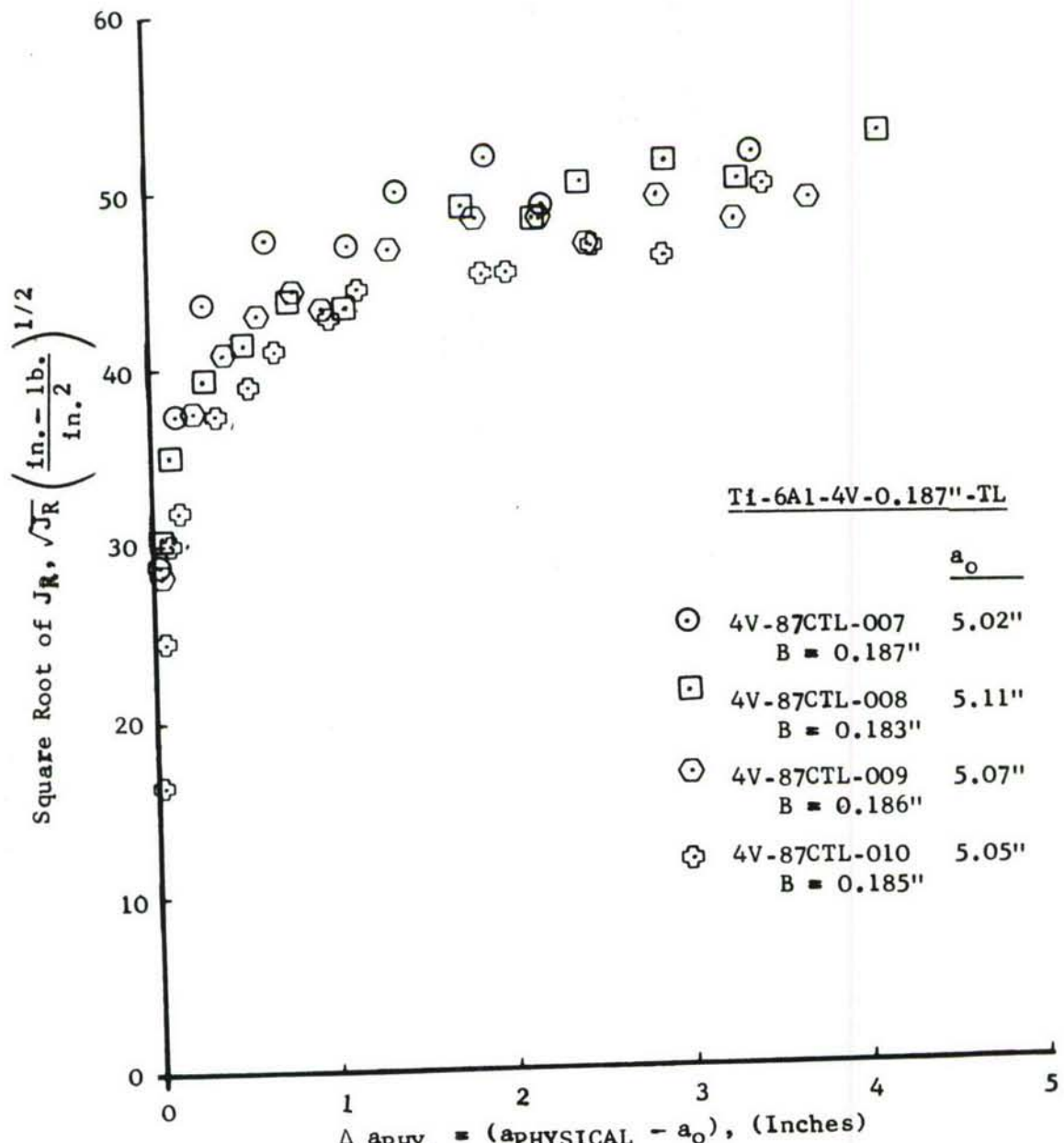
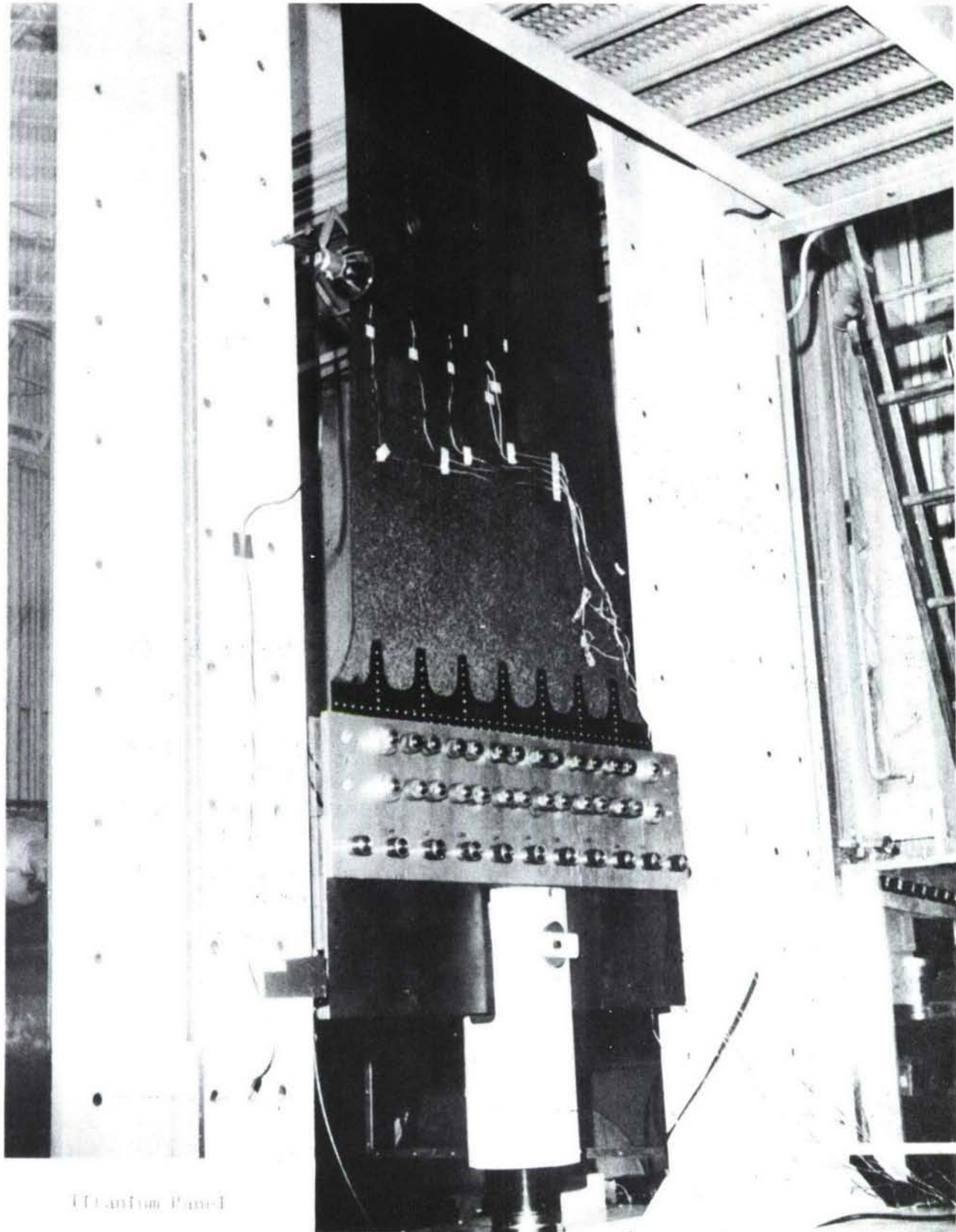


Figure 34. $\sqrt{J_R}$ Crack Growth Resistance Data - Ti-6Al-4V
(Beta Mill Annealed) - .187", TL



Titanium Panel

Figure 35. Overall View of Skin Side of Wing Panel Angle Stiffened, Lower (All Titanium Panel)



Figure 36. Overall View of Angle Stiffened Side of Wing Panel Angle Stiffened, Lower (All Titanium Panel)

TABLE VII STRAIN GAGE DATA, TITANIUM WING PANEL STIFFENED, LOWER

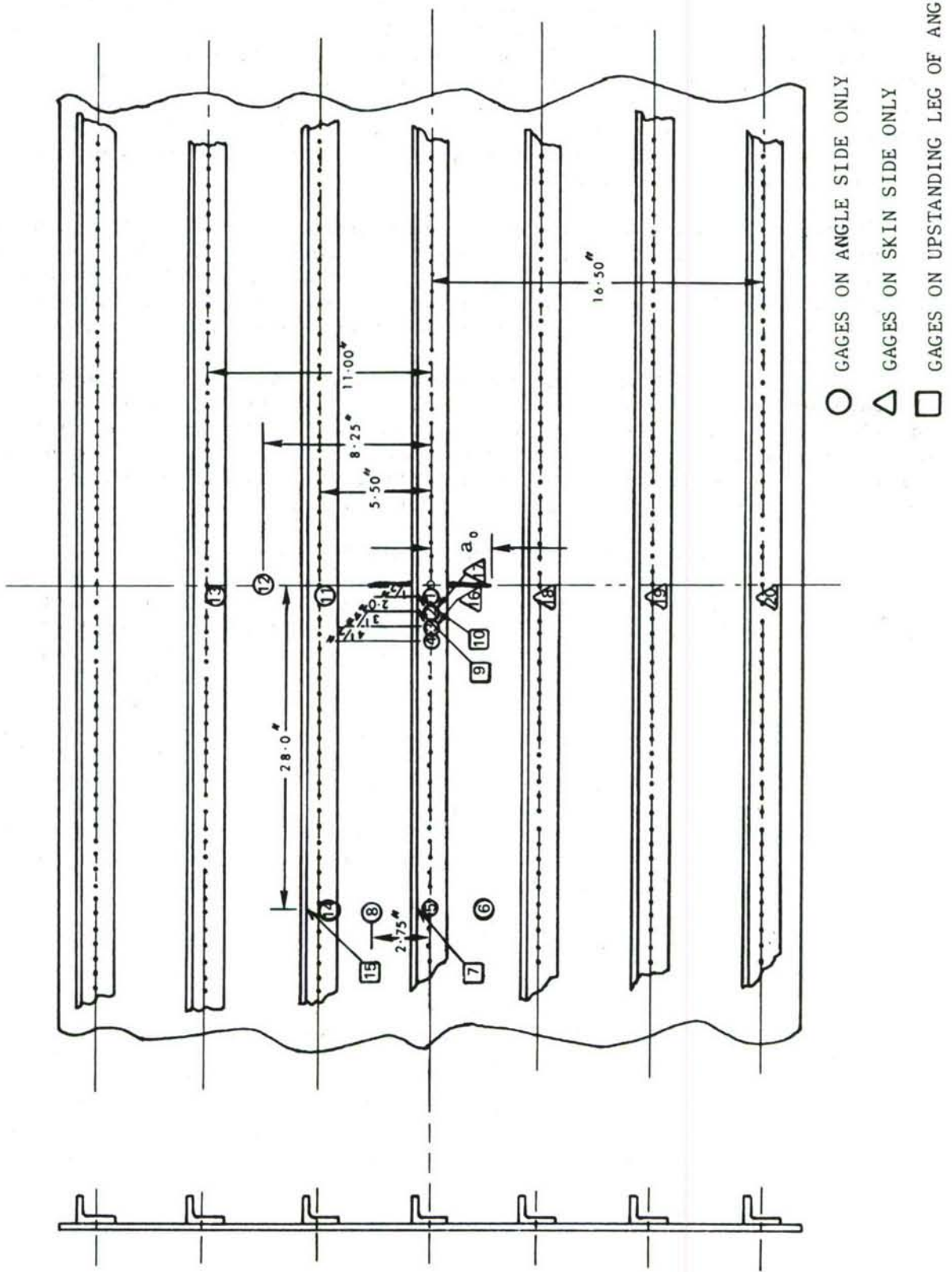


Figure 37. Strain Gage Locations - Titanium Panel

Load versus total displacement gage output is shown in Figure 38. Four distinct loadings are noted. Strain data were recorded for the last three load excursions, the first of these involved a strain survey from zero load to 80 kips. After unloading, loading was re-initiated using ramp loading of 100,000 pounds per minute until some visible crack extension took place. This extension (~ 0.10 inch) is noted on both the strain (Table VII) and displacement data (Figure 38.) at a load of 142.4 kips. At this point the load was again reduced to zero and ramp loading once again initiated after measurement of the crack extension.

During the loading to failure the crack extended slowly to the adjacent stringers at which time an attempt was made to hold the load. However, the arrest was of such short duration (< 3 seconds) compared to the loading rate (100,000 pounds/minute) that the instruction to the operator to hold the load was futile. Final fracture for this titanium panel was at 220.6 kips.

Figures 39 and 40 show the fracture surface of the titanium panel from the skin and angle sides. Due to the large grained structure for the skin material the zig-zag appearance was not unexpected. This behavior for the Beta Mill annealed condition was quite common to this material as noted in Reference 2. Fracture of the angles essentially occurred along the line of center fasteners with one exception as shown in Figure 40.

2.3.3.3 Comparison of Experimental and Analytical Strains

Figure 37 shows the location of strain gages on the titanium panel. Tabulated in Table VII are the strain gage readings for various applied loads at a crack length of 5.66 inches. Figure 41 shows the experimental and analytical variation of strain in the central stringer with increasing distance from the crack. Good correlation is noted between experimental strains and those obtained from the elastic analysis. The experimental data of Figure 41 is cross plotted in Figure 42 to show the variation of strain with applied stress for this panel. Good correlation is obtained between elastic analysis and experimental data to an applied stress of 28 ksi. At higher applied stresses the experimental strain in the stringer close to the crack plane is lower than that given by an elastic analysis. Away from the crack plane, the correlation between experimental strains and those obtained by elastic analysis is good to an applied stress of 60 ksi.

2.3.4 Residual Strength Prediction

The residual strength prediction procedure discussed in Section 2.2.4 (see also Reference 1) was used to predict the residual strength of the all titanium panel. The analytical stresses in the central stringer (angle) with a half crack length of 2.875 inches are shown in Figure 43. The ultimate strength of the stringer material (Ti-6Al-6V-2Sn) was determined through test to be 167.3 ksi. Using this ultimate strength value and the Dugdale type elastic-plastic analysis stringer stresses were determined as

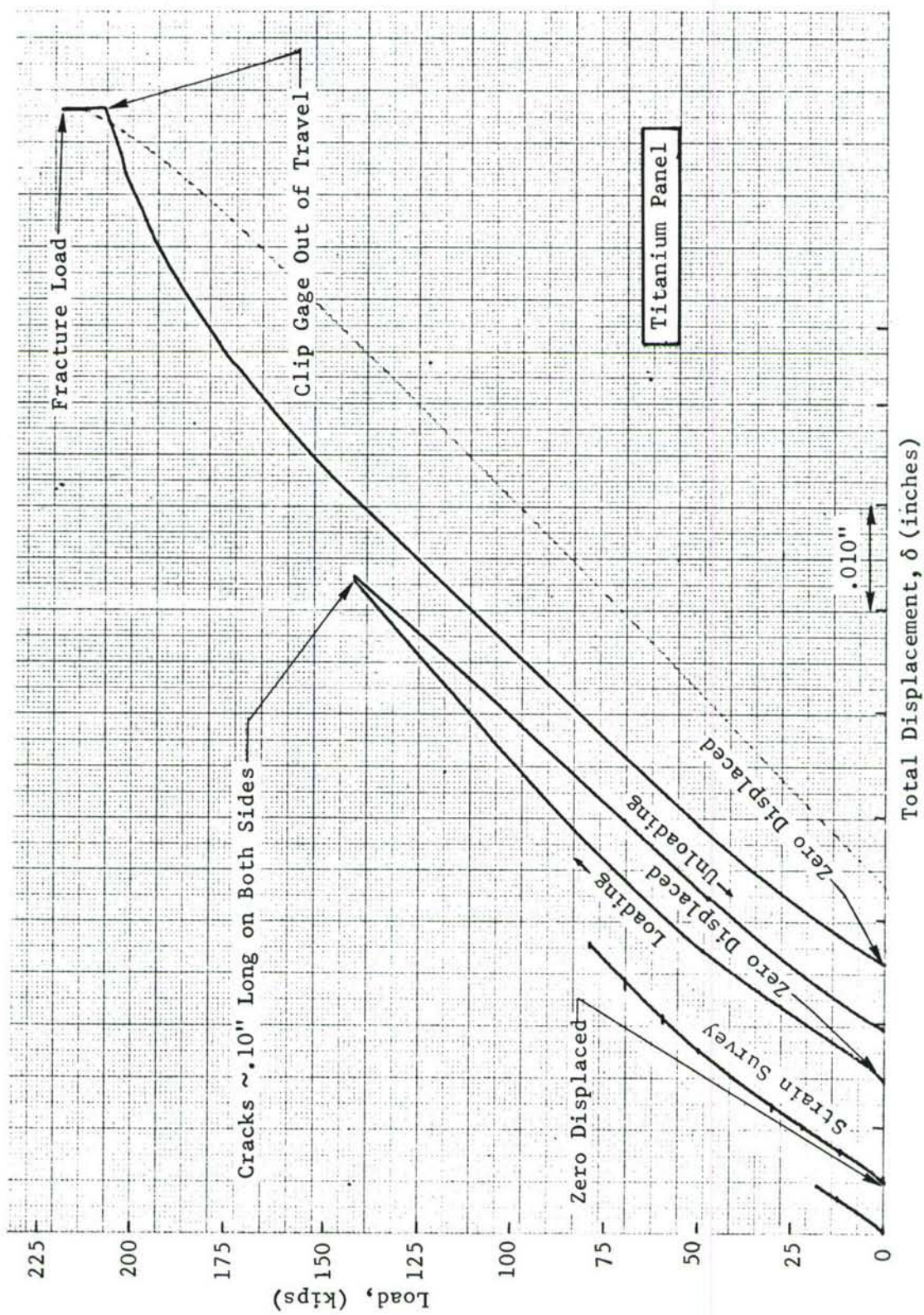


Figure 38. Load-Displacement Curves for Titanium Wing Panel Angle Stiffened, Lower

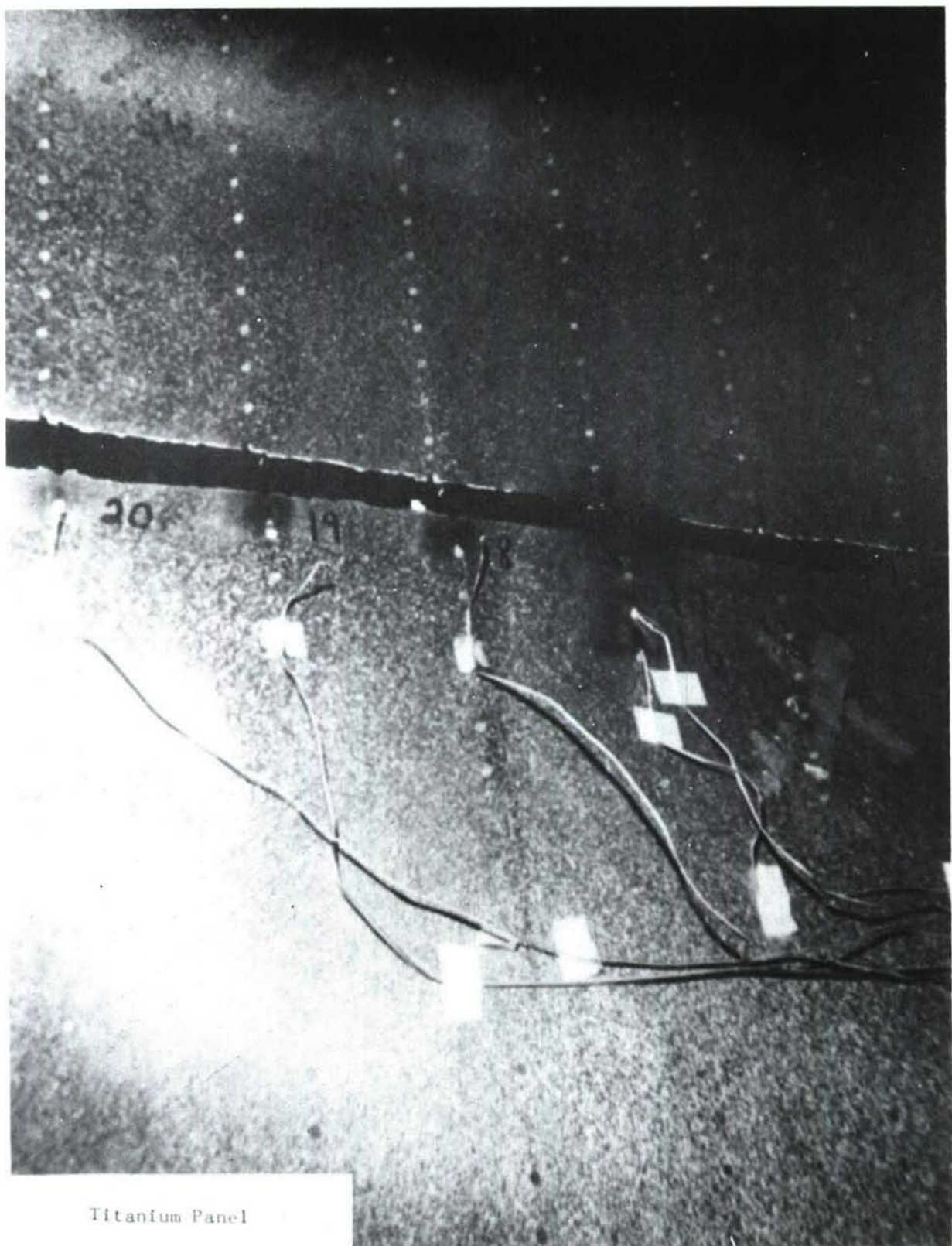
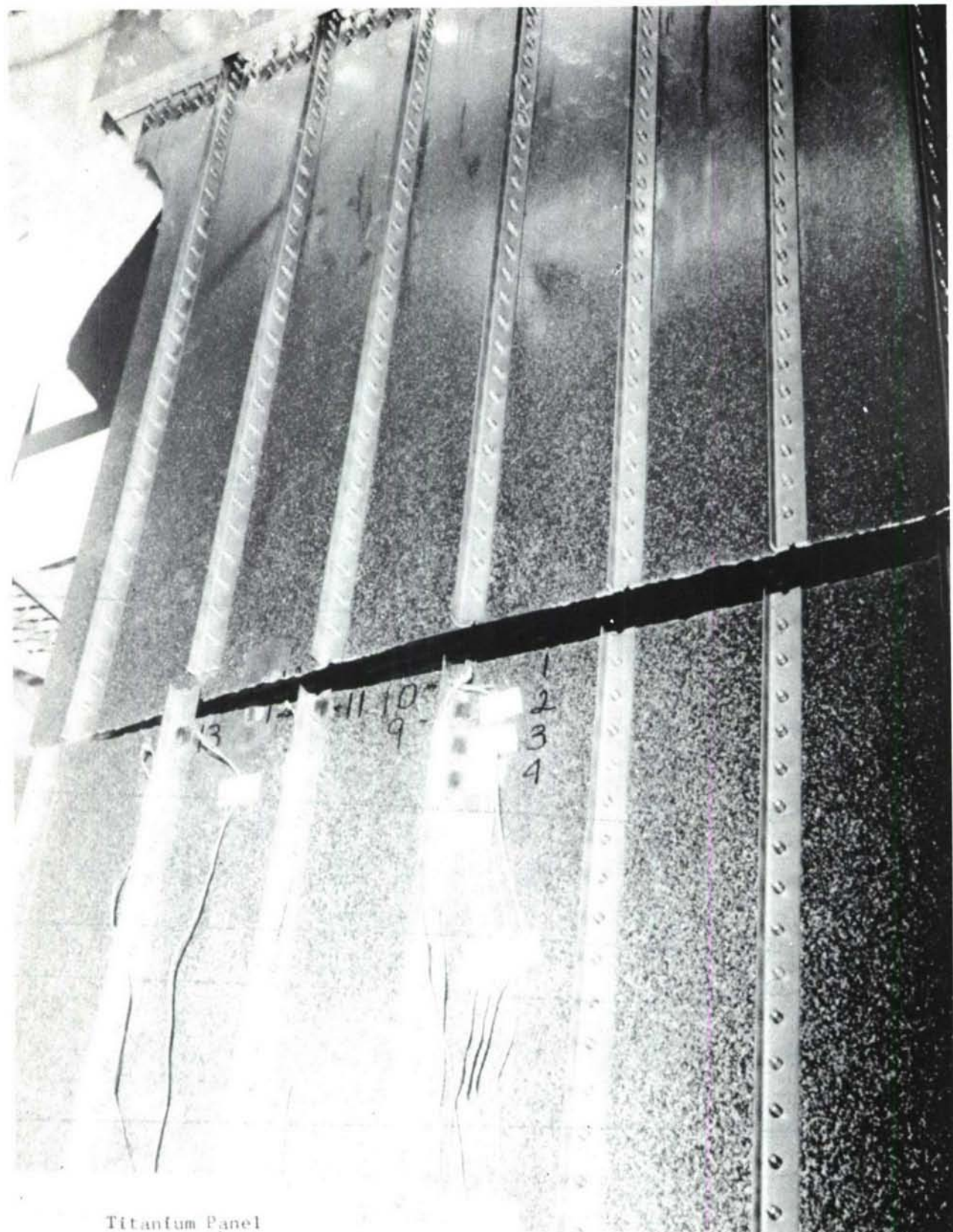


Figure 39. View of Fracture Surface From Skin Side, Wing Panel Angle Stiffened, Lower (All Titanium Panel)



Titanium Panel

Figure 40. View of Fracture Surface From Stringer Side, Wing Panel Angle Stiffened, Lower (All Titanium Panel)

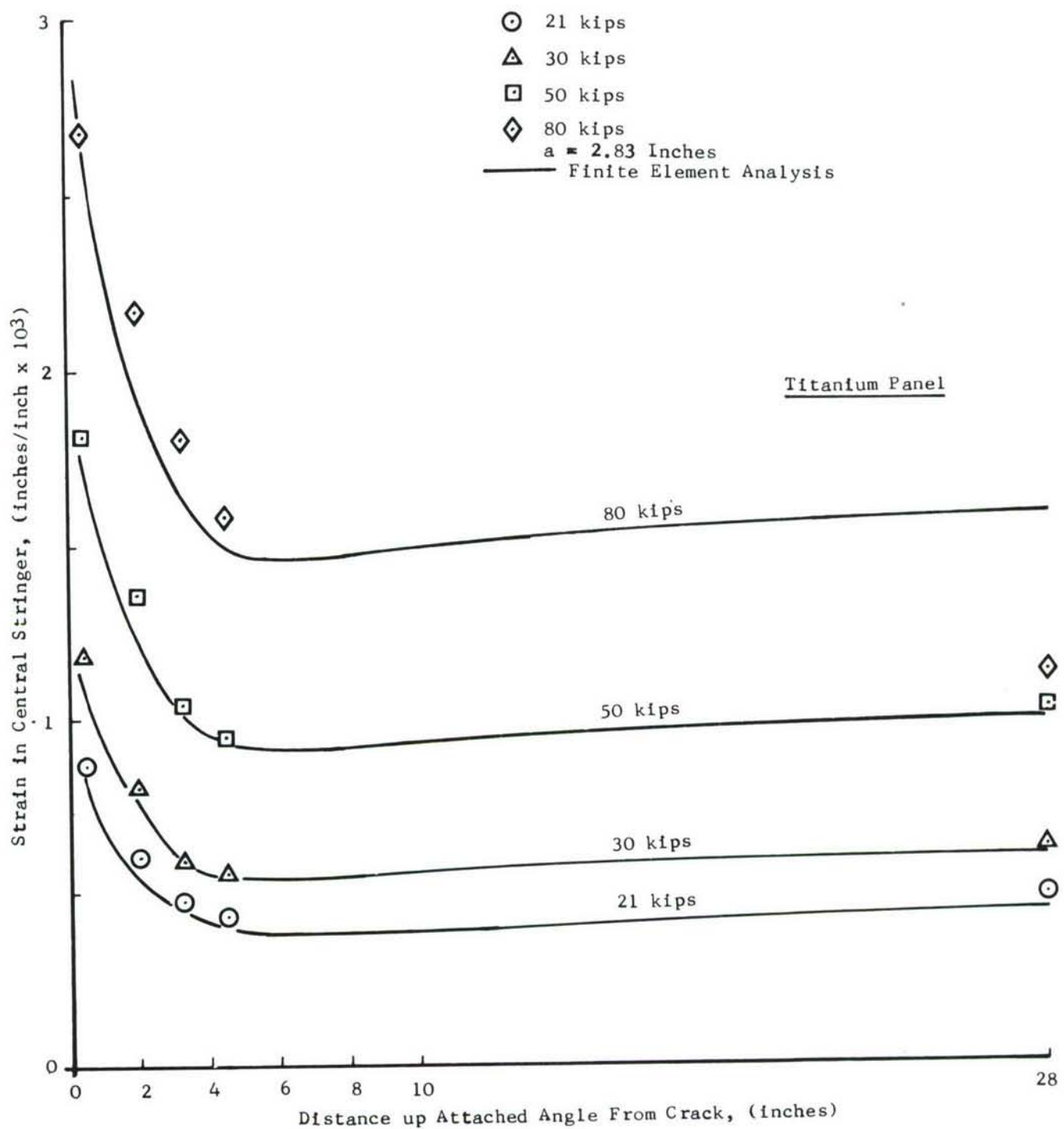


Figure 41. Strain in Central Stringer for All Titanium Panel, Angle Stiffened, Lower

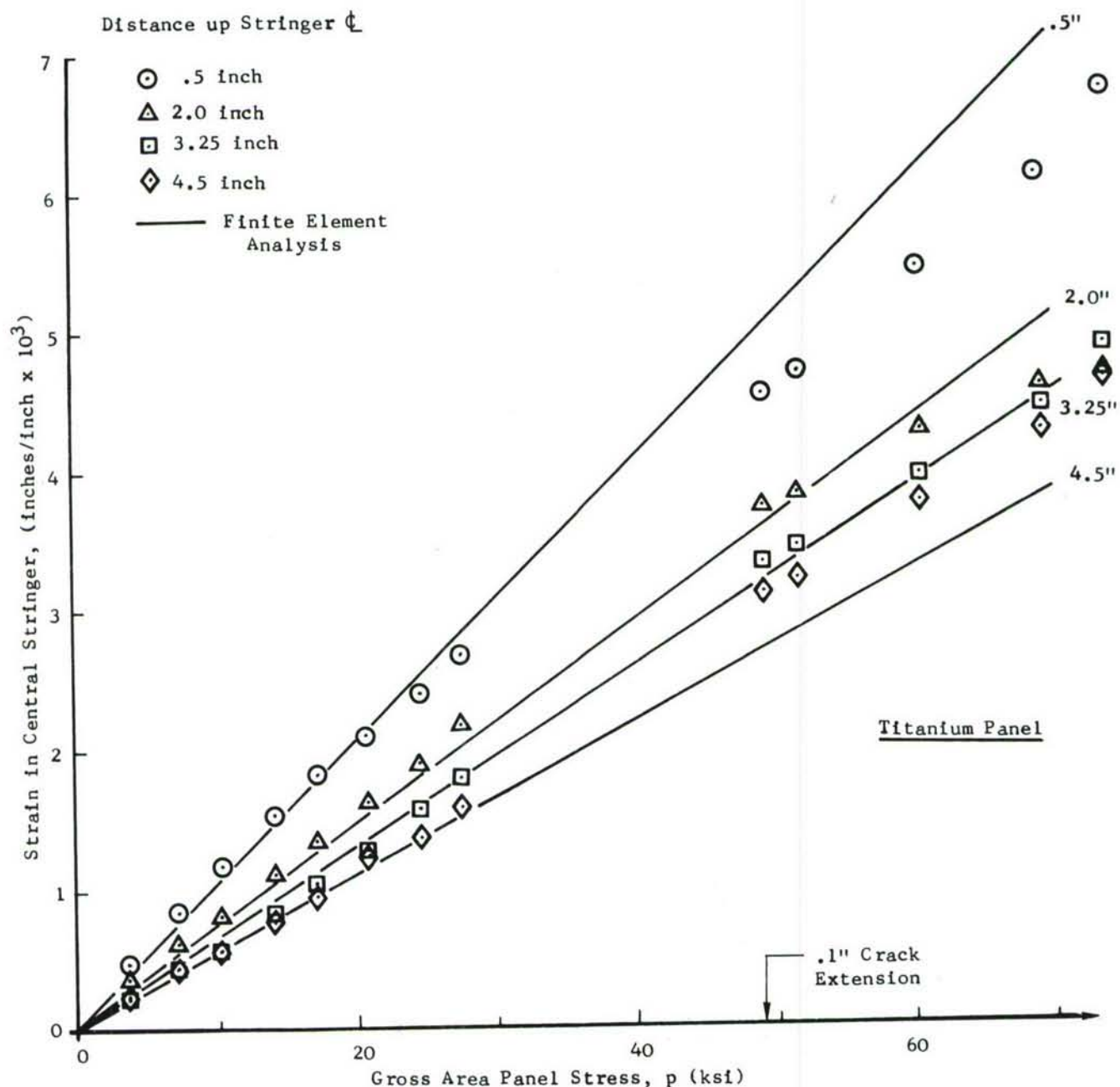


Figure 42. Strain in Central Attached Angle Away From the Crack Plane as a Function of Applied Stress for All Titanium Panel

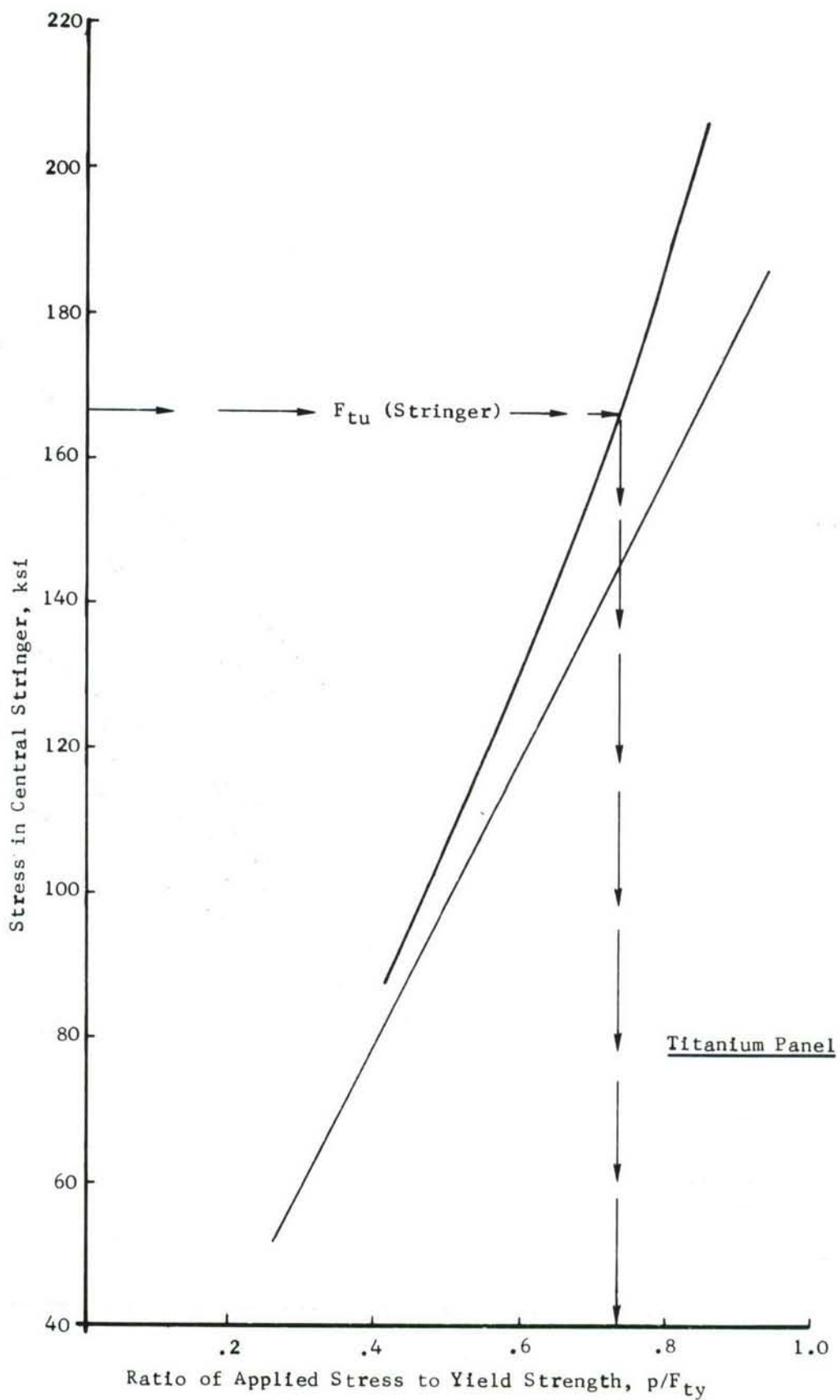


Figure 43. Elastic and Elastic-Plastic Stress in Central Stringer as a Function of Applied Stress - All Titanium Panel

shown in Figure 43. The failure of the central stringer (angle) is predicted at $p/F_{ty} = 0.735$. Now consider the \sqrt{J} versus crack length plot for various applied stresses as shown in Figure 44 for the all titanium panel. Superimposed on this plot is the $\sqrt{J_R}$ versus Δa_{PHY} resistance curve of the Beta Mill annealed Titanium-6Al-4V skin material plotted at a physical half crack length of 2.83 inches. It can be noted from this Figure at the stringer critical stress of $p/F_{ty} = 0.735$ (determined from Figure 43) there would be considerable slow tear in the skin. Therefore the stringer stresses shown in Figure 43 will not be valid at failure as the crack length would have increased considerably prior to stringer failure. From Figure 44, the resistance curve of the material plotted at the initial fatigue half crack length of 2.83 inches (initial half crack length in the tested panel), is tangential to the \sqrt{J} curve of the panel at an applied stress of $p/F_{ty} = 0.66$. Thus the first point of crack instability (rapid crack extension) occurs after an initial period of slow crack growth. However, from Figure 44 it can be noted that immediately after the point of instability the \sqrt{J} curve for the panel drops lower than the resistance curve of the material (i.e., beyond this point the resistance of the material is higher than \sqrt{J} developed in the stressed panel). Hence the running crack will be arrested. The crack will become arrested where the next stringer (angle) is connected to the skin. The resistance curve of the material is now replotted at a half crack length of 5.5 inches (distance from centerline of the stringer to panel centerline) where the crack became arrested. For this crack length the \sqrt{J} curve of the panel becomes tangent to the resistance curve at an applied stress of $p/F_{ty} = 0.69$. Hence, the second point of crack instability occurs at this stress and the crack runs catastrophically. Beyond this point of instability upon further loading the \sqrt{J} values in the panel are much higher than the resistance curve of the skin material and therefore no possibility exists for crack arrest. It may be noted that the difference in the stress at the first point of instability (i.e., $p/F_{ty} = 0.66$) and at the second point of instability (i.e., $p/F_{ty} = 0.69$) is small. Hence, under increasing applied load, the crack will only momentarily arrest.

The titanium panel analyzed above was tested to failure. The slow tear in this panel started at a load of 142.4 kips $\left(\frac{P}{F_{ty}} = 0.43\right)$. At this load the slow tear at each end was 0.1 inch (see Table VII). The first point of instability (rapid crack extension) was at a load lower than 220.6 kips $\left(\frac{P}{F_{ty}} = 0.67\right)$. The crack was arrested at the rivet hole in the adjoining stringer(s) for only a short duration and before the increasing applied load could be held constant panel failure occurred. The time lag between the first and second points of instability was less than five seconds. For this panel the predicted first point of instability is at a load of 217.67 kips $\left(\frac{P}{F_{ty}} = 0.66\right)$ and final failure of the panel occurred at a load of 227.56 kips $\left(\frac{P}{F_{ty}} = 0.69\right)$. This load is 3.15 percent higher than the measured failure load of 220.6 kips.

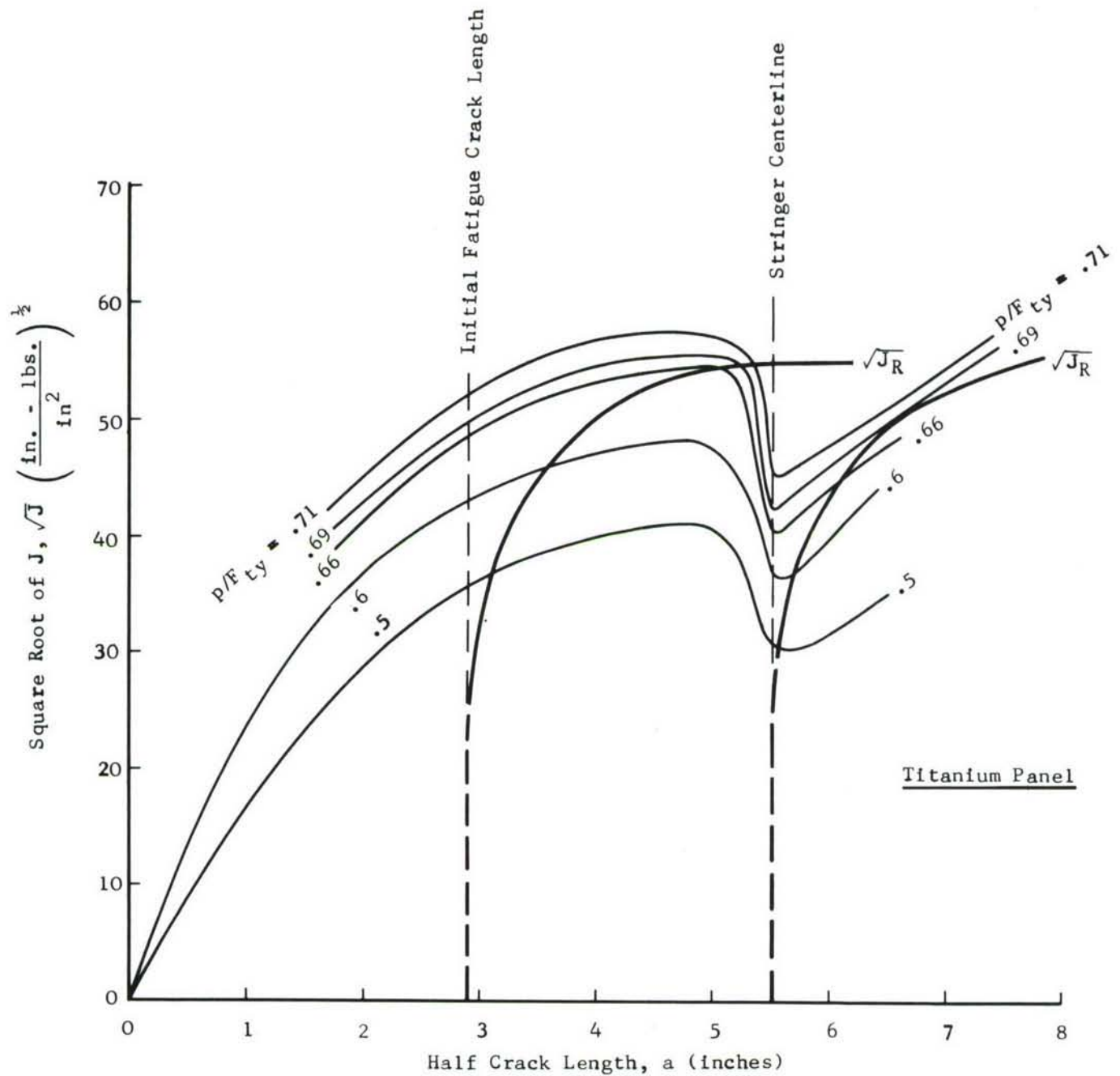


Figure 44. Residual Strength Prediction Plot for All Titanium Panel

2.4 INTACT STRINGER - THICK SKIN

The intent of testing this "thick skin" panel was to determine the effect of mixed mode fracture behavior on residual strength prediction. The material and thickness selected for this panel was chosen so that a mixed mode slow tear behavior would result. Due to the increased skin gage a rather low percentage stiffening occurred but the overall objective of a mixed mode slow tear was accomplished.

2.4.1 Description of Test Panel

Figure 1 gives the detailed geometry of this "thick skinned" test panel. It is designated as a -1 Assembly with a test section width of 38.5 inches. The 7075-T73 skin material had symmetrical angle sections (AND10133-1002, 7075-T6 extrusions) attached through the leg by 3/16-inch diameter, flush head steel HI-LOKS at 1.3-inch pitch. A bay width of 5.5 inches resulted in a six bay panel symmetric about the panel centerline.

Table VIII lists the panel, skin, and angle cross-sectional thickness, areas and material identification. At a 17 percent stiffening ratio this panel would be considered to be a lightly stiffened panel.

TABLE VIII THICK SKIN (-1) - ANGLE STIFFENED WING PANEL AREAS AND MATERIAL IDENTIFICATION

MEASURED THICKNESS (Inches)		CROSS SECTIONAL AREAS (Inches ²)		SKIN MATERIAL/ AND I.D. (See Ref. 2)	PERCENTAGE OF TOTAL ANGLE AREA TO SKIN AREA
Angle	Skin	Total Angles	Skin		
.094	.193	1.281	7.4305	7075-T73/ 5-2	17.2
		Total Panel Cross Sectional Area = 8.7115 in. ²			

The initial starter slot half length was 4.25 inches or an overall length of 8.50 inches. Twenty strain gages were positioned as shown in Figure 45. As with the other wing panels a beam type clip gage was mounted on the skin side to record crack opening displacement at the crack and panel centerline.

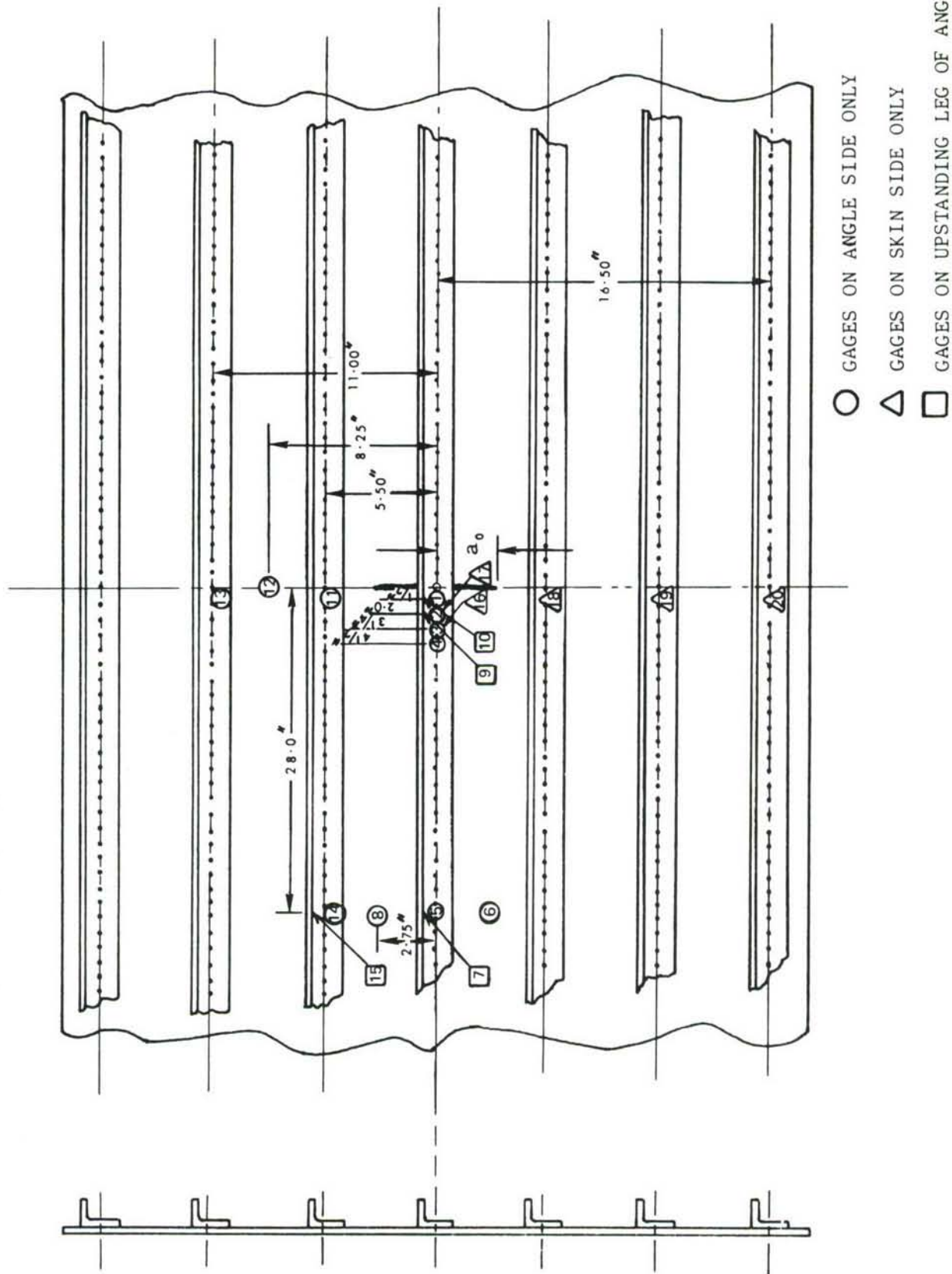


Figure 45. Strain Gage Locations - Thick Skin (-1) Panel

2.4.2 Finite Element Modeling and Analysis

The finite element model employed to analyze the -15 panel was adopted for use in this thick skin panel. Changes were required in both skin thickness and stiffener areas to correspond to the actual skin thickness and stiffener areas of this (-1) panel. The (x, y) co-ordinates of all grid points in the finite element model of the -1 panel were the same as previously employed for the -15 panel. The z co-ordinates of grid points connecting rod and membrane elements (representing stiffeners) were changed to correspond to the skin thickness and stiffener dimensions of the -1 panel.

An elastic analysis was conducted at a half crack length of 4.5 inches. The contours shown in Figure 3 were used to evaluate J. The variation of \sqrt{J} with p/F_{ty} is shown in Figure 46.

The elastic-plastic analysis of this panel was performed assuming a Dugdale type strip plastic zone ahead of the crack tip. The variation of \sqrt{J} with p/F_{ty} is shown in Figure 46 for a half crack length of 4.5 inches. At an applied stress of 80 percent of skin material yield, the \sqrt{J} value given by an elastic analysis is 7 percent lower than that given by assuming a Dugdale model analysis. An elastic-plastic analysis for various assumed crack lengths was not performed on this panel. The stresses in the central stringer of the panel for elastic and elastic-plastic analyses are shown in Figure 47.

2.4.3 Experimental Results and Discussion

This -1 Assembly was the first panel fabricated and tested in the wing panel configuration. During one of the unloading sequences the specimen was inadvertently placed into compression loading which was sufficient to produce a permanent set in the angle sections in the test area. This resulted in a situation which adversely affected the resulting residual strength prediction. However, the strain and fracture data will be presented here with additional discussion to follow.

2.4.3.1 Fatigue Precracking, Strain Data and Fracture of Thick Skin Panel

Fatigue precracking of the -1 Assembly was accomplished in a manner similar to the previous wing panels. Sinusoidal, constant amplitude, tension-tension loading was employed at a maximum stress intensity level of 15 ksi $\sqrt{\text{inch}}$. Table IX summarizes the fatigue loading and final crack lengths for this thick, 7075-T73 panel.

Figures 48 and 49 indicate skin and angle side views of the -1 Assembly in the 500 kip test machine prior to testing.

After fatigue cycling and zero balancing of all strain gages and displacement gage a strain/load survey was taken by loading to specific load intervals. Gages 1, 3, and 6 were monitored on tape as well as by direct strain readings to compare strain data for the two systems. These data are given in Table X. It can be seen from these data that as with the comparison of strain data for the two strain recording systems in Reference 1 the correlation between the two is quite good. After the tear to the adjacent angles the panel was

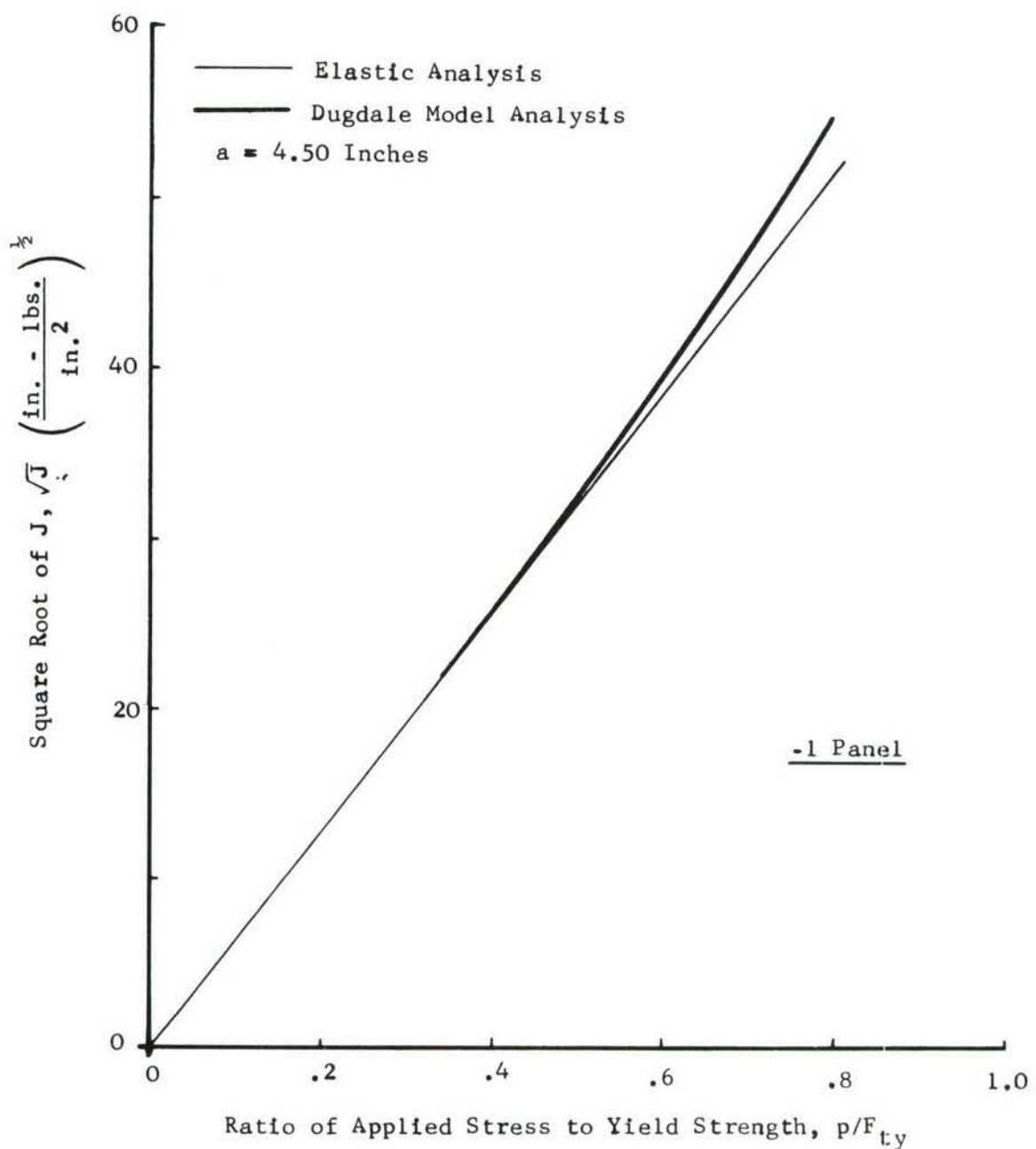


Figure 46. Elastic and Elastic-Plastic \sqrt{J} Values for Thick Skin, -1 Panel as a Function of Applied Stress

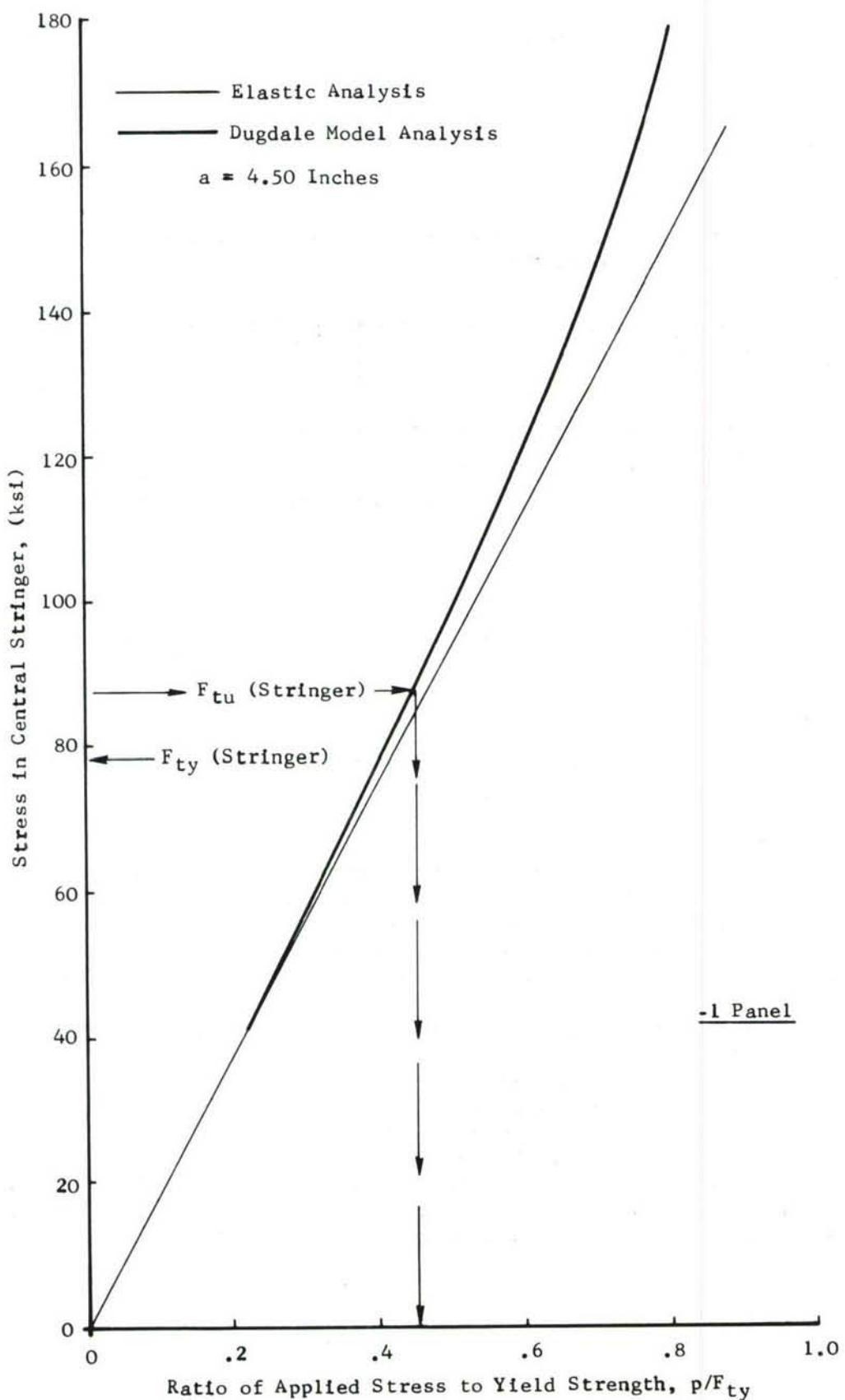


Figure 47. Elastic and Elastic-Plastic Stress in Central Stringer as a Function of Applied Stress -1 Panel

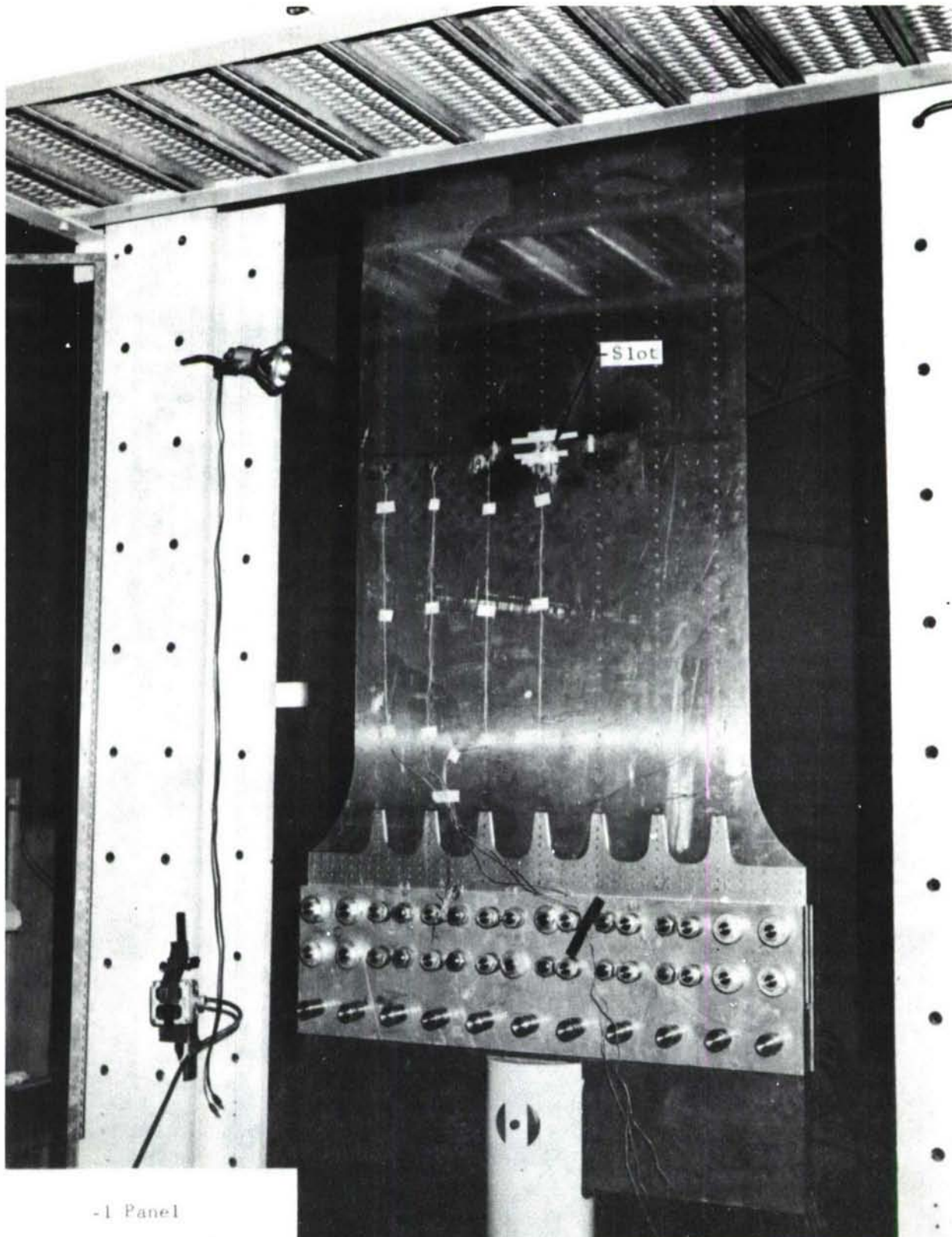
inadvertently placed in compression. The magnitude of the permanent set placed in the panel can be seen from the strain data at zero load (after tear to angles - Table X) where the strain at gage number 10 is quite large. Gage 10 is located on the upstanding leg of the angle near the crack, see e.g., Figure 45. Starting from zero load the initial strain survey went from zero to 140 kips.

TABLE IX FATIGUE PRECRACKING AND CRACK LENGTH DATA - THICK SKIN PANEL

FATIGUE LOADS		NUMBER OF CYCLES	FATIGUE CRACK LENGTH(S)		
MAXIMUM (kips)	MINIMUM (kips)		LEFT (Inch)	RIGHT (Inch)	TOTAL (Inch)
44.0	4.4	11,350	4.34	4.50	8.84

Load versus total displacement at the crack centerline are shown in Figure 50 for the load survey and slow tear and the final fracture in Figure 51. It can be seen that for the loading survey to 140 kips the zero on the deflection scale was stepped to aid in data reduction. On the loading segment which resulted in tear to the adjacent angles (see third curve of Figure 50), two significant steps can be noted. They resemble the pop-in behavior of unreinforced panels of 7075-T73 aluminum of this thickness. After crack arrest the load was held at 251.1 kips, strain readings recorded and the panel unloaded to zero. At this point the panel was inadvertently placed into compression at which point noticeable "straining" of the angles in the panel centerline occurred. The permanent set which occurred during this sequence is quite apparent from the initial part of the load-displacement trace to failure in Figure 51. The reverse curvature is common to center cracked panels which have undergone prior inplane buckling near the crack. Upon further loading fracture occurred from this -1 Assembly at 337.8 kips.

Figure 52 shows the angle side of the panel after fracture. In Figure 53 the close up of the fracture surface indicates that with the exception of two of the seven angles fracture occurred at the first line of fastener away from the crack line. In addition the permanent set due to the compression load is quite evident in the central and adjacent angles. The broken piece of angle indicates the severity of the permanent set which occurred in this panel. It can also be seen that during the tearing to the angles both mixed mode and shear crack progression occurred until the crack arrested at the fastener hole(s). Upon additional loading to fracture shear crack progression predominates.



-1 Panel

Figure 48. Overall View of Skin Side of Wing Panel Angle Stiffened, Lower (Thick Skin)

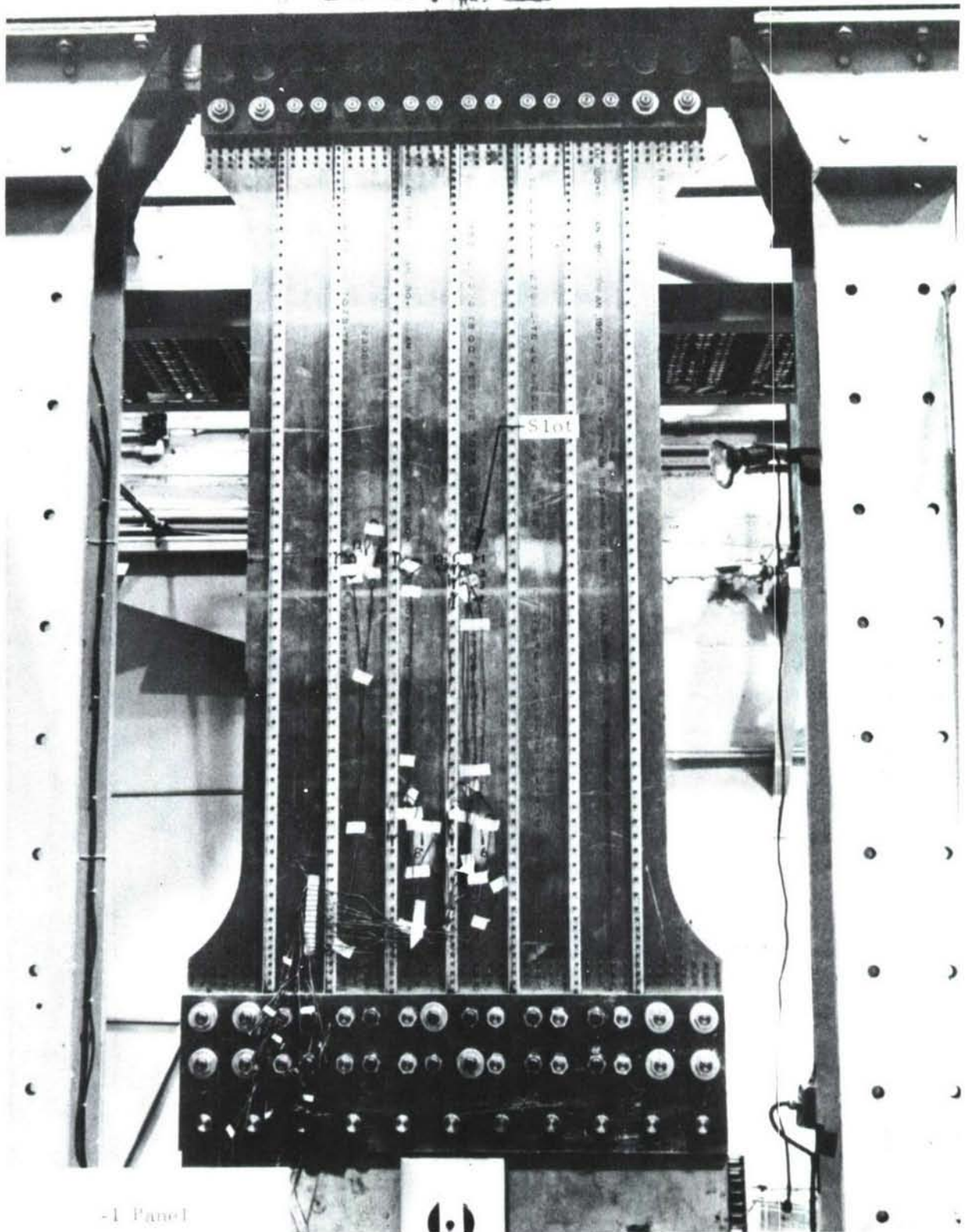


Figure 49. Overall View of Angle Stiffened Side of Wing Panel Angle Stiffened, Lower (Thick Skin)

TABLE X STRAIN GAGE DATA, -1 THICK SKIN WING PANEL ANGLE STIFFENED, LOWER

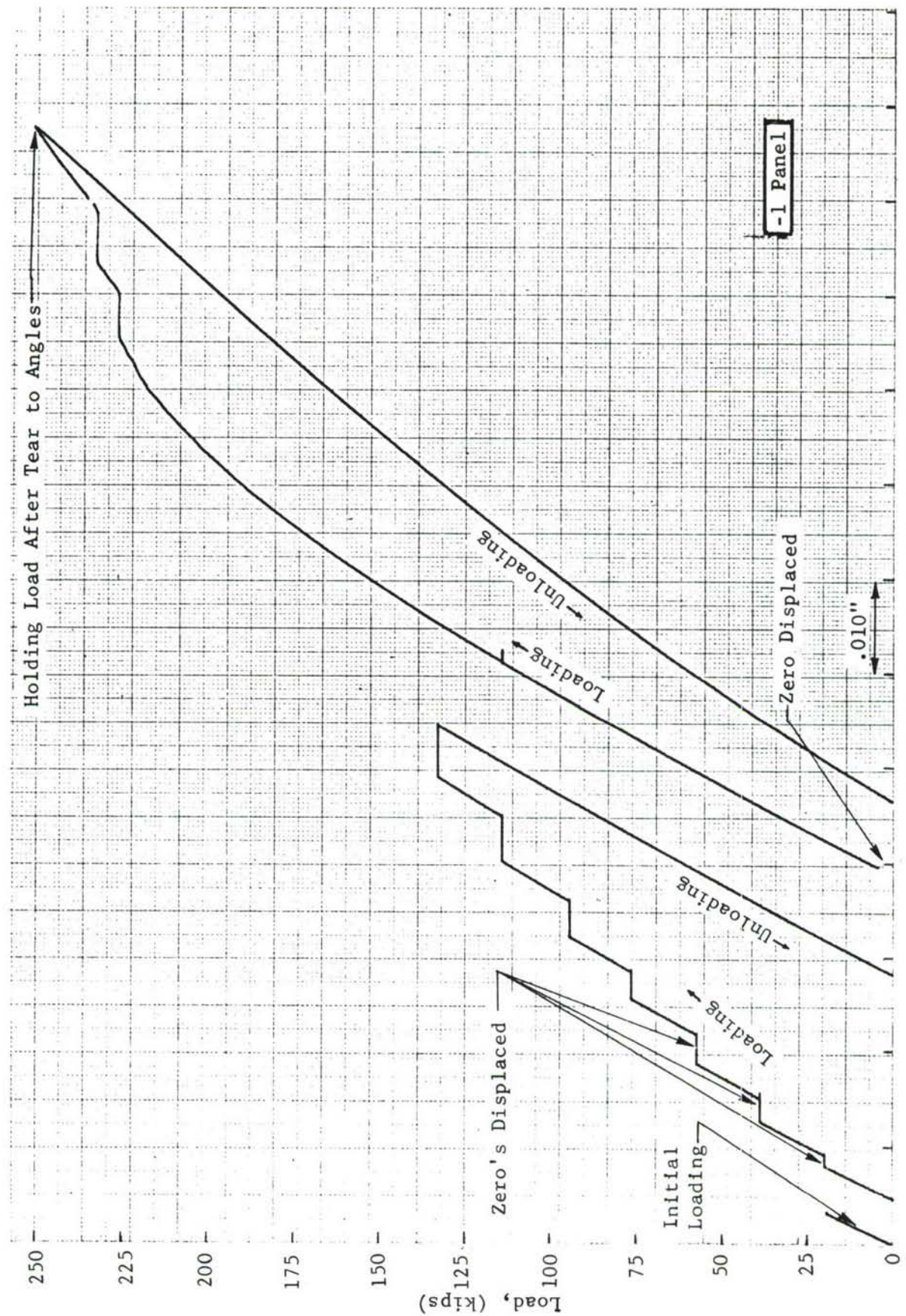


Figure 50. Load-Displacement Curves for Thick Skin - 7075-T73 Wing Panel Angle Stiffened, Lower -1 Panel

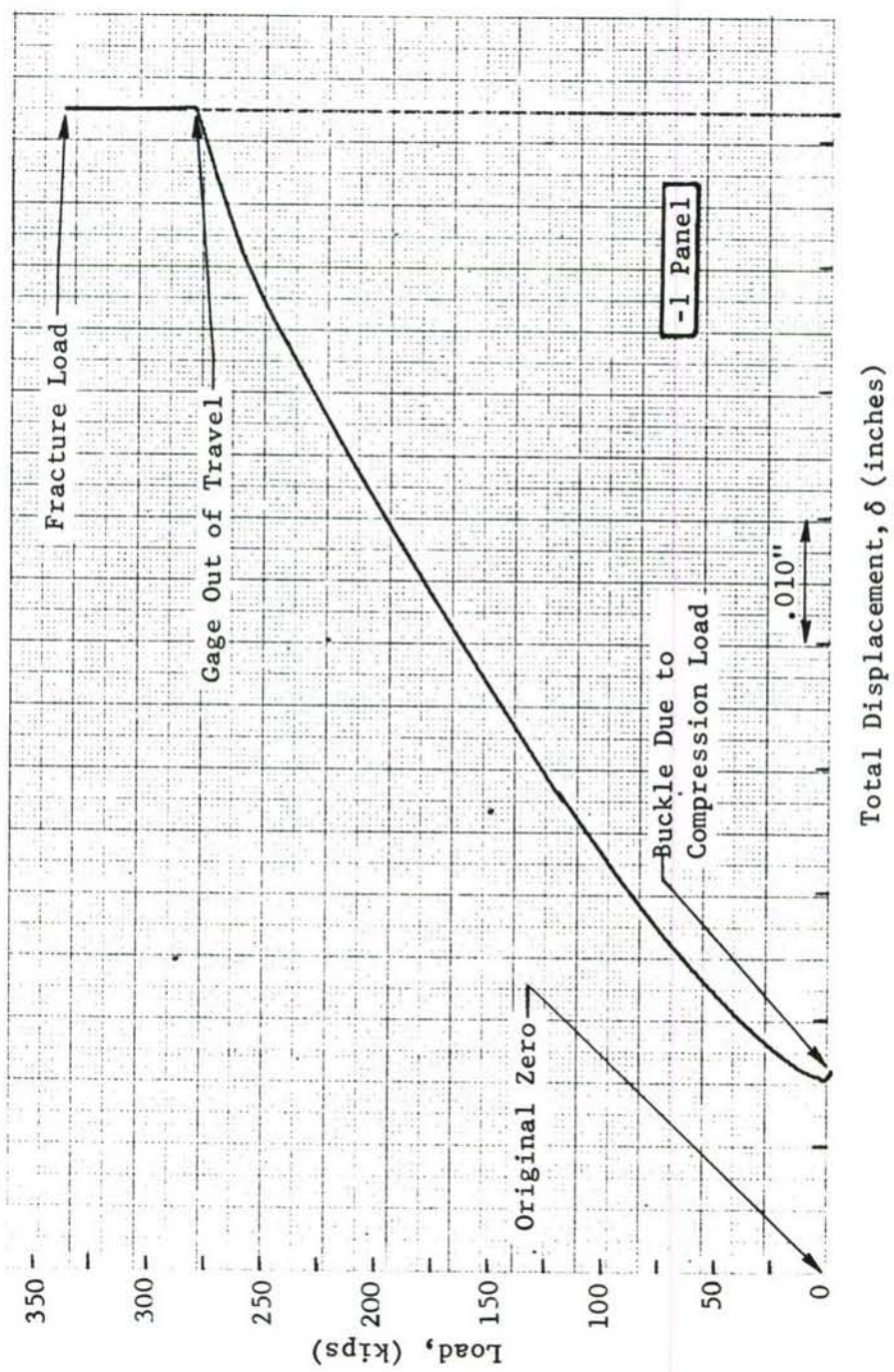


Figure 51. Load-Displacement Curves to Fracture for Thick Skin - 7075-T73
Wing Panel Angle Stiffened, Lower panel -1

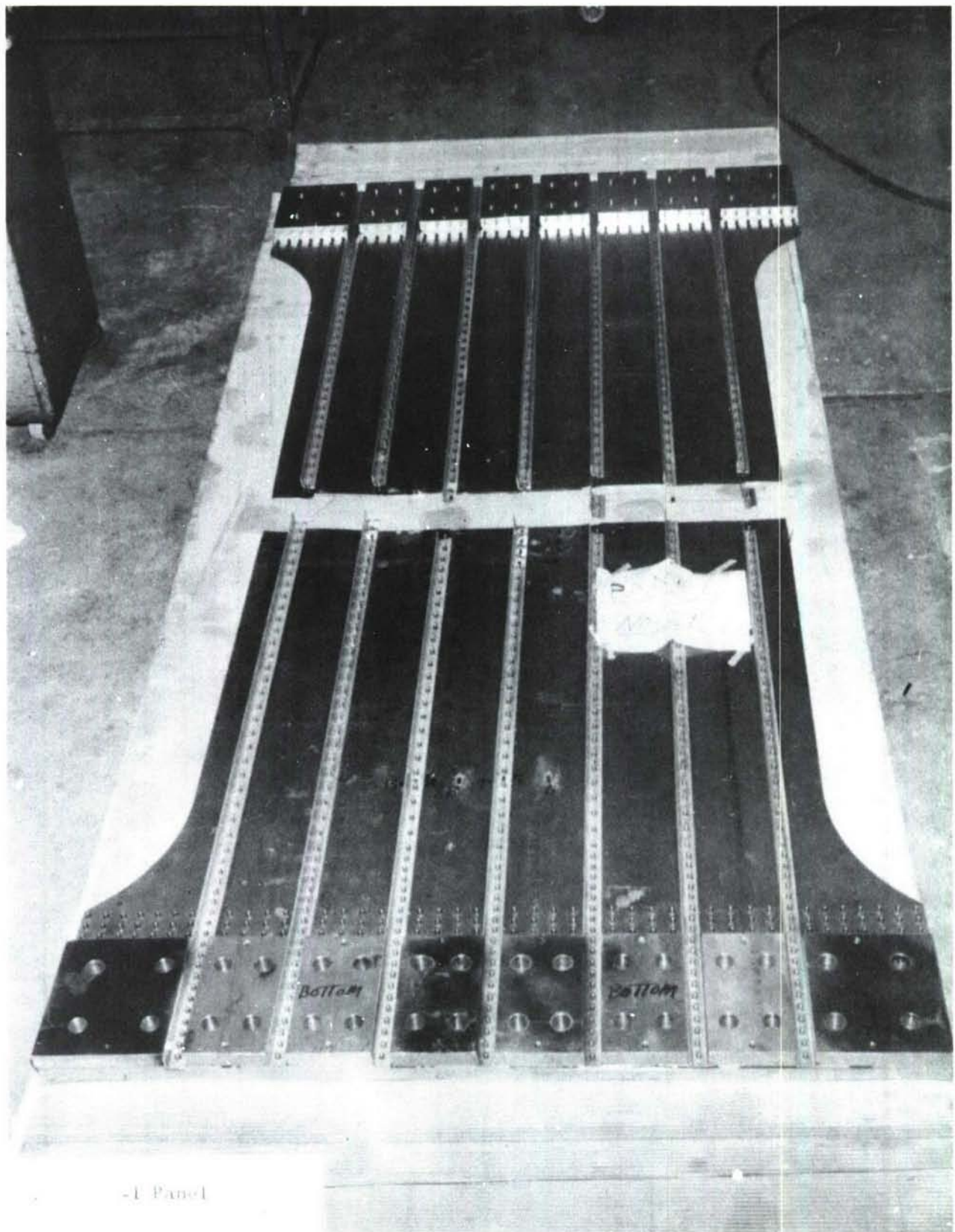


Figure 52. View of Panel Fracture From Stringer Side, Wing Panel Angle Stiffened, Lower (Thick Skin)

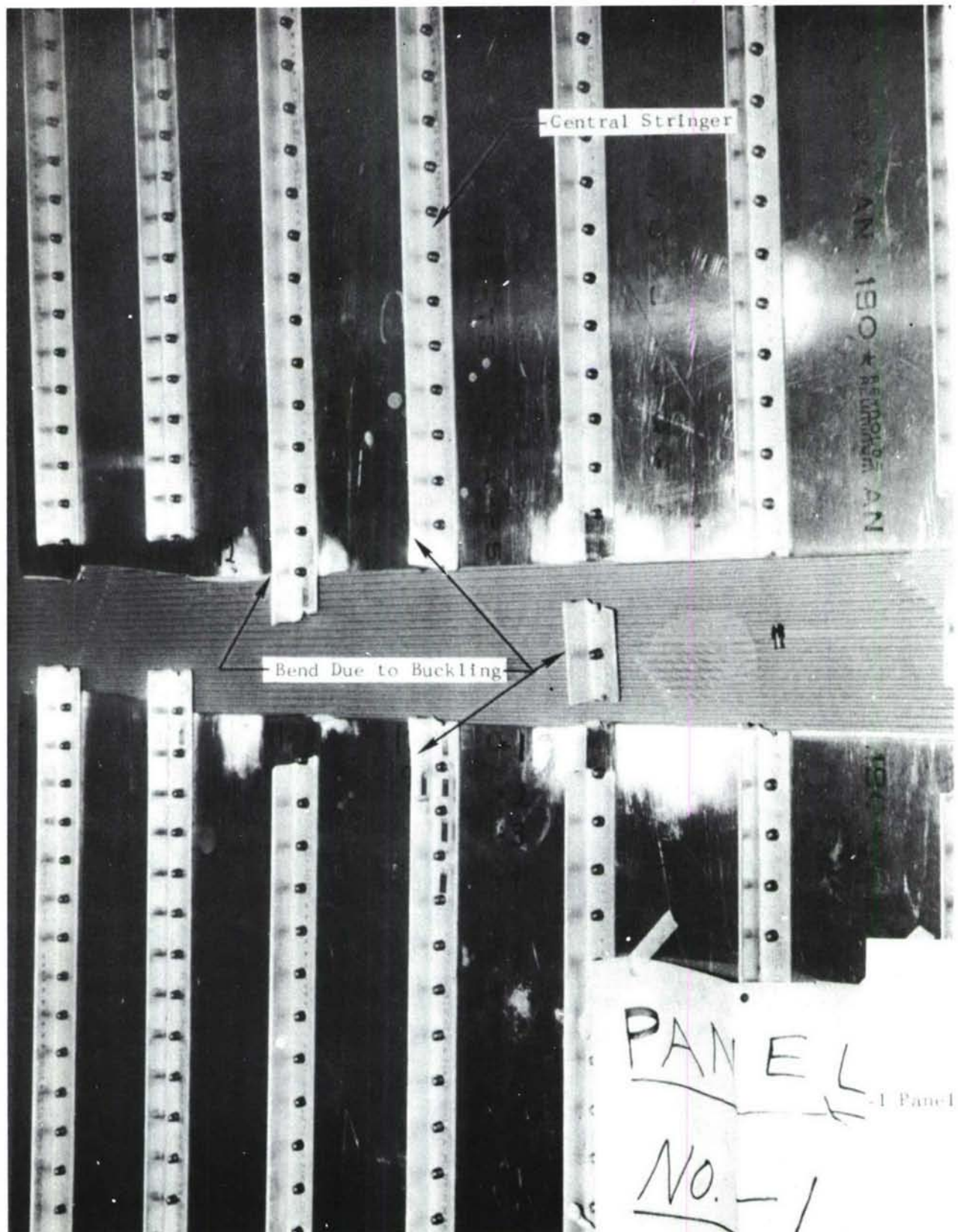


Figure 53. Close-up View of Fractured Angles, Wing Panel Angle Stiffened, Lower (Thick Skin)

2.4.3.2 Comparison of Experimental and Analytical Strains

Figure 54 shows the location of strain gages on the -1 panel. Tabulated in Table X are the strain gage readings for various applied loads at a fatigue crack length of 8.84 inches. Figure 55 shows the experimental and analytical variation of strain in the central stringer with increasing distance up the central angle from the crack at a half crack length of 4.42 inches. Good correlation is noted between experimental data and the elastic, finite element analysis. The experimental data of Figure 55 has been cross plotted in Figure 56 to show the variation of strain with applied stress. Good correlation is obtained between the experimental strain data and the elastic analysis to an applied stress of approximately 18 ksi. For higher stresses the strains in the central stringer near the plane of the crack are lower than the elastic strains. Similar behavior was observed for the titanium panel.

2.4.4 Residual Strength Prediction

The elastic-plastic analysis of this panel was not performed for various crack lengths. Hence, curves between \sqrt{J} and several physical crack lengths for various applied loads could not be plotted. It may be noted that the structural arrangement of the thick skin, -1 panel and the thin skin -15 panel are the same. Thus a plot of the trend in \sqrt{J} versus a for the -1 panel will be similar to that for the -15 panel (Figure 9), however, in this case the \sqrt{J} values will be different for the same applied stress and crack length. For a half crack length of 4.45 inches the \sqrt{J} values for the -1 panel were determined to be between 17 to 19 percent higher than those for the -15 panel. Thus for the residual strength prediction of the -1 panel it was assumed that the \sqrt{J} values, for the various crack lengths and applied stress, were 18 percent higher than those for the -15 panel. Based on this assumption, \sqrt{J} versus a curves for the -1 panel have been plotted in Figure 57 using an 18 percent increase to the curves of Figure 9. These curves were then used to determine the skin critical behavior in the panel.

The stresses in the central stringer for the -1 panel are shown in Figure 47. The ultimate strength of the stringer material (7075-T6 extrusions) was determined by test to be 87.2 ksi. Using this ultimate stress value and the Dugdale type elastic-plastic analysis shown in Figure 47, the failure of the central stringer angle is predicted at an applied stress ratio of $p/F_{ty} = 0.455$. The \sqrt{J} versus crack length plots for various applied stresses are shown in Figure 57. Superimposed on this plot is the \sqrt{J}_R versus Δa_{PHY} resistance curve of the 0.195 inch thick 7075-T73 (LT) skin material plotted at a physical half crack length of 4.42 inches. It can be seen that at the stringer critical stress $p/F_{ty} = 0.455$, there will be slow tear in the panel equal to approximately 0.8 inch at each end of the crack. Hence the stringer stresses obtained by a Dugdale analysis for a half crack length of 4.42 inches will not be valid for this panel. From Figure 57 it is seen that at an applied stress ratio $p/F_{ty} = 0.5$ the crack will slow tear to the rivet hole connecting the adjacent stiffener to skin, or a point very close to the angle centerline. It may be noted that no instability of the crack occurs before the crack slow tears to the hole due to the \sqrt{J} curves falling below the \sqrt{J}_R curve. The \sqrt{J}_R curve was replotted at the half crack

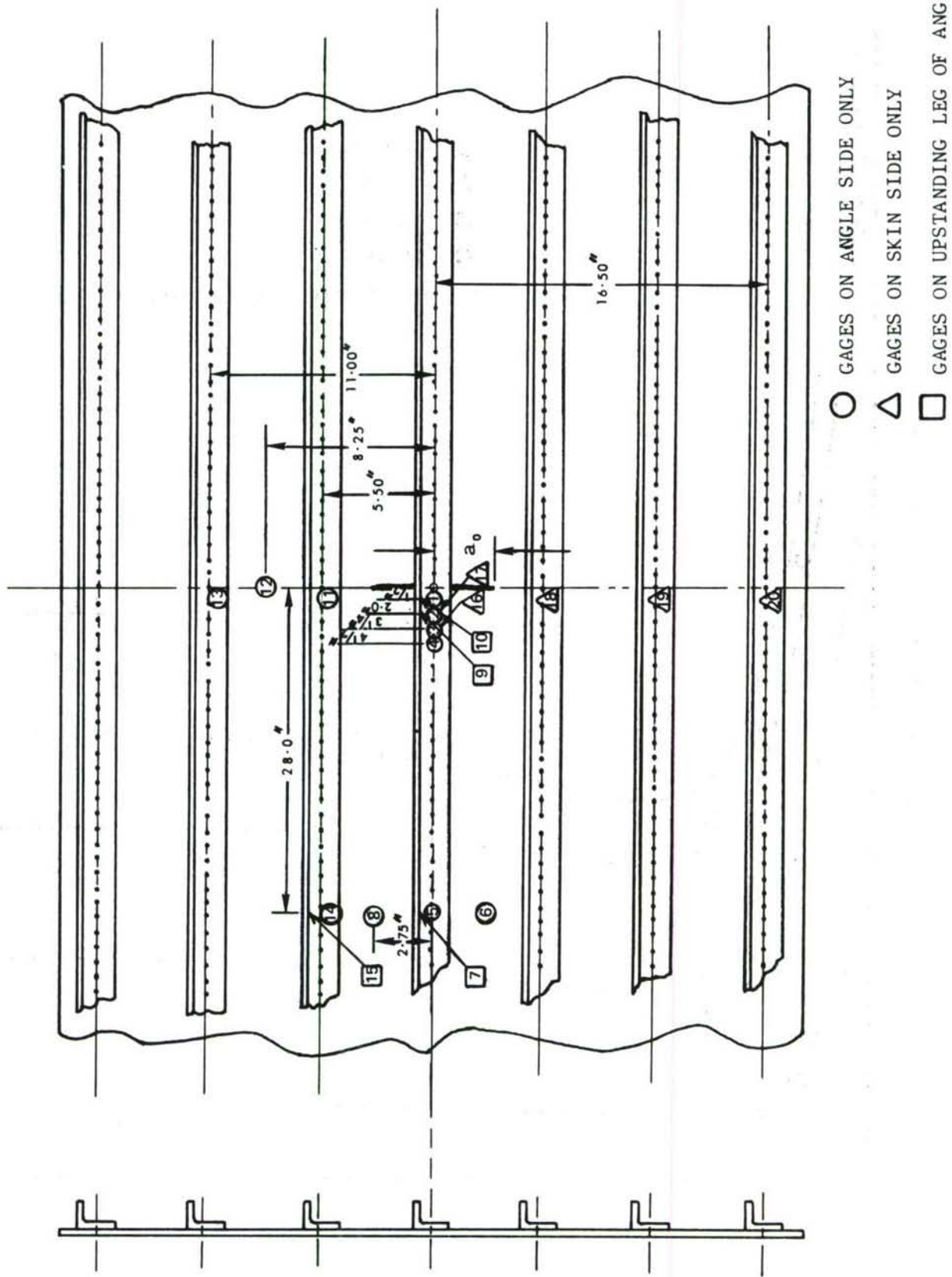


Figure 54. Strain Gage Locations - Thick Skin (-1) Panel

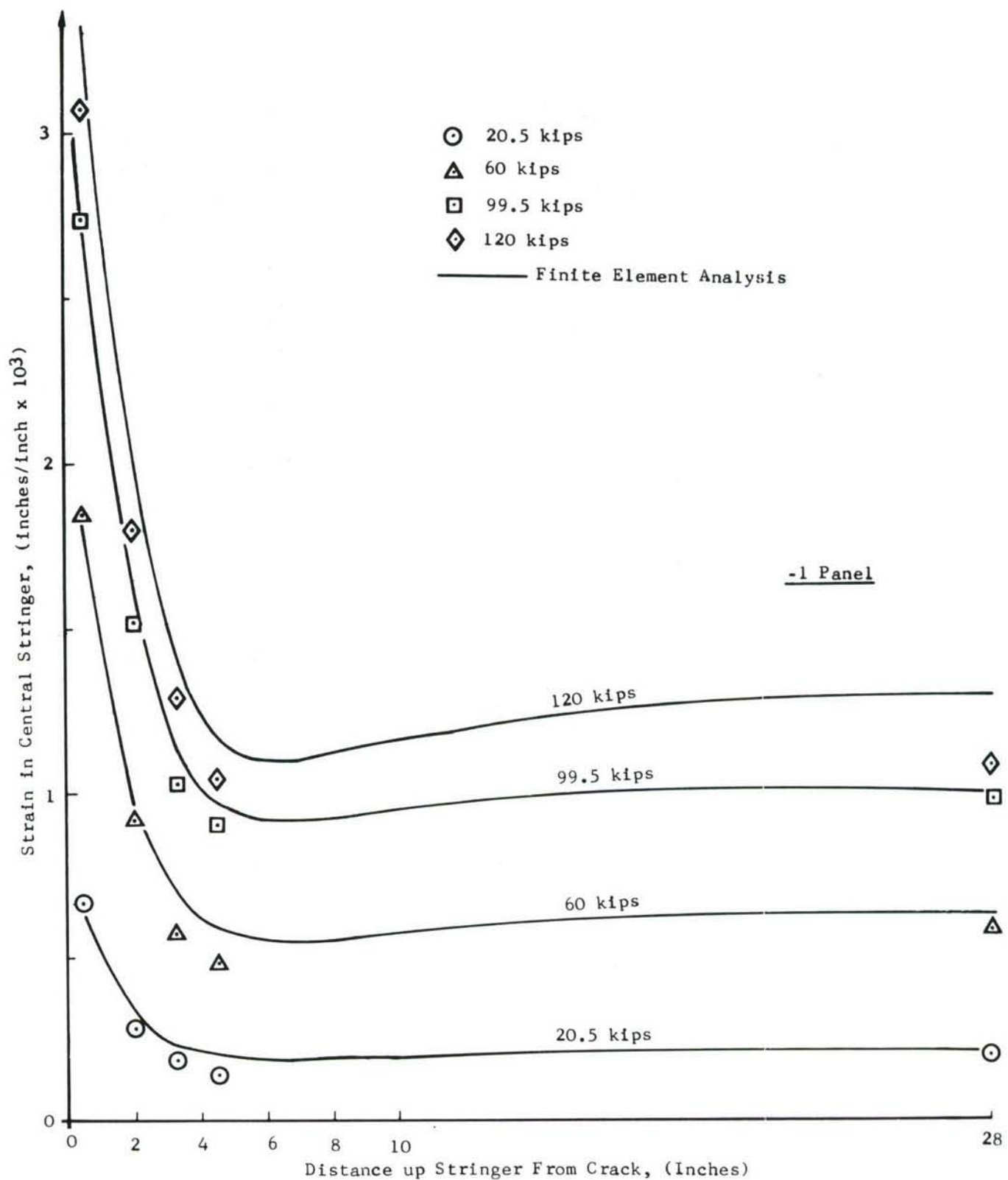


Figure 55. Strain in Central Stringer for Thick Skin, -1 Panel,
Angle Stiffened, Lower

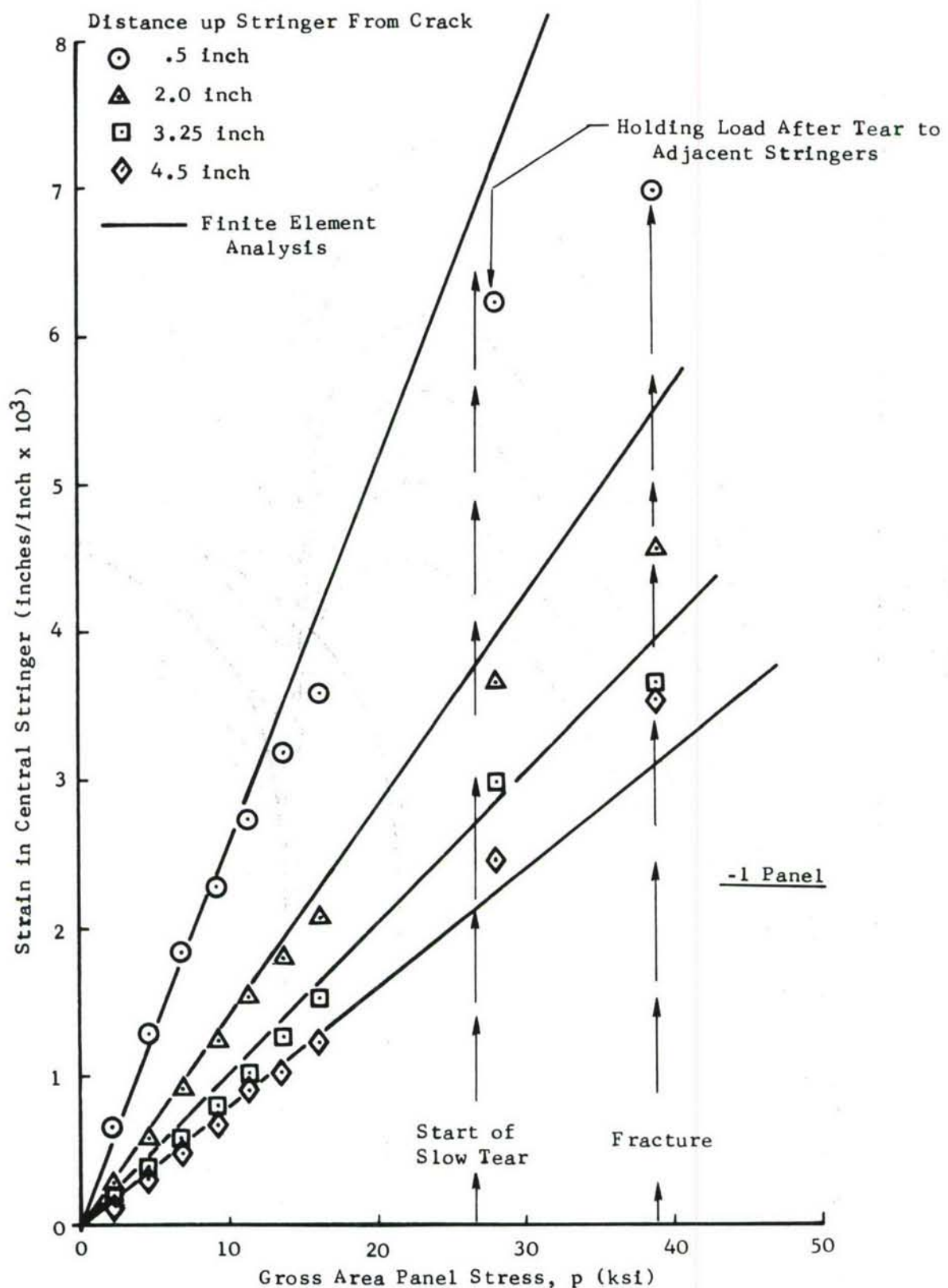
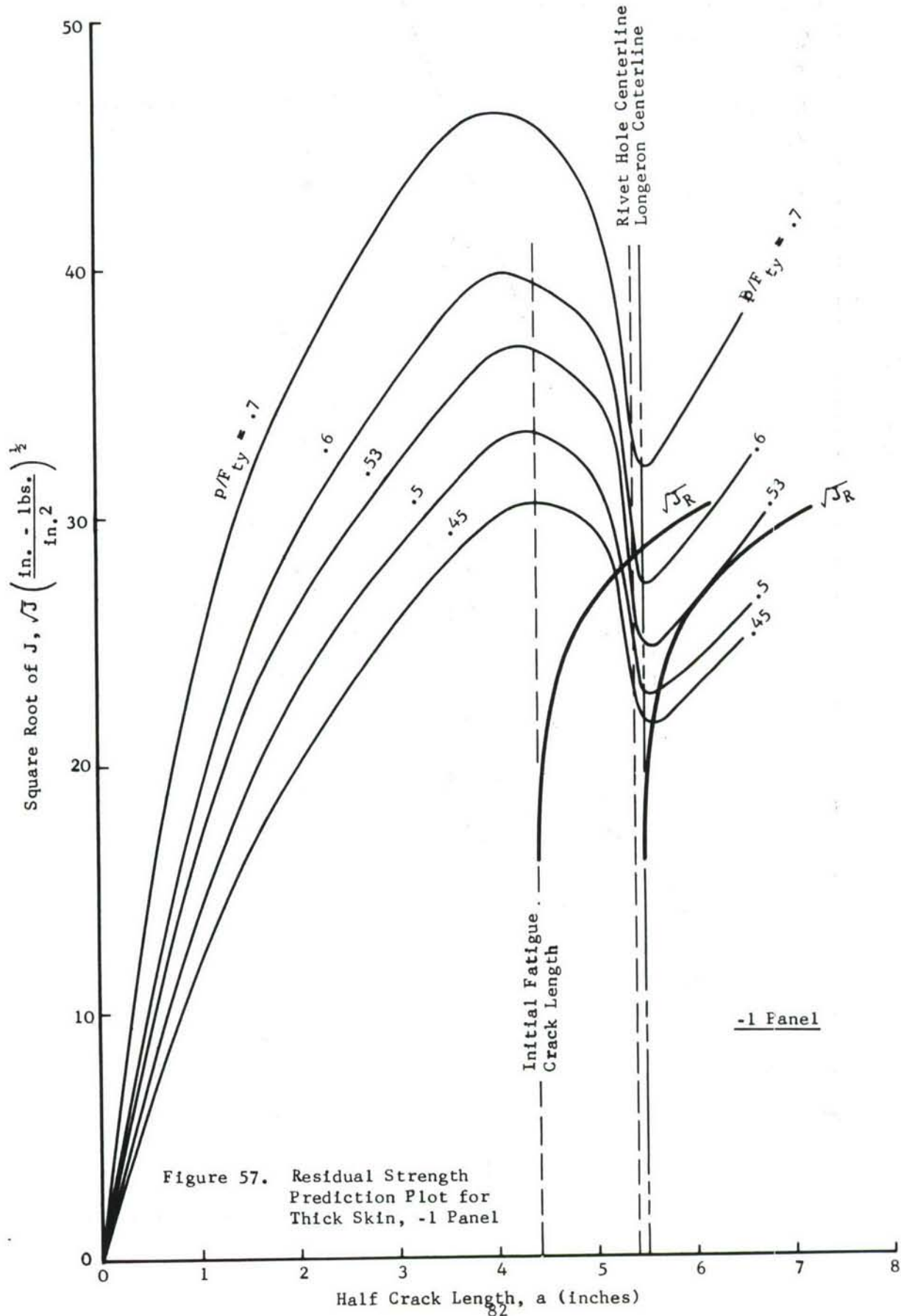


Figure 56. Strain in Central Stringer as a Function of Applied Stress -1 Panel



length of 5.5 inches or at the centerline of the stringer. For this crack length \sqrt{J} curve of the panel becomes tangential to the resistance curve at an applied stress ratio of $p/F_{ty} = 0.55$. Hence the instability should occur at this stress and the crack will start running catastrophically.

The panel analyzed above was tested to failure. Upon loading the crack tore to the rivet hole(s) at a load of 241 kips or $p/F_{ty} = 0.411$ (predicted $p/F_{ty} = 0.50$). After the slow tear to the rivet hole, the panel was inadvertently placed into compression loading which was sufficient to produce a permanent set in the angle sections in the test area. Due to this action the central stringer was able to take a much higher load. The final failure of the panel occurred at an applied load of 337.8 kips. This corresponds to a predicted failure load of ($p/F_{ty} = 0.55$) 322.456 kips. The predicted failure-load is within 4.7 percent of the measured failure-load. However, it must be noted that the \sqrt{J} versus σ curves for this panel shown in Figure 57 were not obtained by rigorous analysis and therefore represent approximate values. Thus, this predicted failure-load can be only approximate. It should be noted that the failure of this panel cannot be analyzed by the proposed technique due to the compression buckling which occurred in the test machine.

III STIFFENED BIAXIALLY LOADED PANELS

In Section II the case of uniaxially loaded panels were examined which would typically represent sections of lower aircraft wings. It is known that in most fuselage structure more complex loading conditions predominate and multi-axial loading prevails. In light of these anticipated loading conditions it was believed necessary to simulate and demonstrate the prediction technique for some form of multi-axial loading. The first decision involved choice of loading and the second the representative structure.

Choice of loading was biaxial and the structure was representative of the upper fuselage of a large transport/bomber type aircraft. The number of panels tested (two) permitted only a cursory examination of the problem of biaxial loading on residual strength. However, trends were observed and some tentative evaluation of the proposed analysis was possible. This evaluation will be discussed in subsequent subsections.

3.1 GENERAL INTRODUCTION

The influence of biaxial loading on the crack propagation and fracture strength of a cracked structure has attracted considerable attention in recent years. The biaxial loading represents a realistic state of stress in a structure. The majority of stress analysis of cracked structures available in the literature deal with uniaxially loaded cases with a loading direction perpendicular to the plane of the crack. Research has been limited in the area of biaxial loading on unstiffened panels. If elastic analysis is considered, the influence of biaxial loading is known to be slight. However, the influence of biaxial loading may not be negligible if plastic deformation is considered. In Reference 4, the influence of biaxial loading on plastic stress intensity factors was examined (plastic stress intensity factors are related to J). It was revealed that the plastic stress intensity factors are reduced by applying a positive biaxial load, i.e., the load applied in two directions is tensile. On the other hand, if the biaxial load ratio is negative (i.e., the load parallel to the crack plane is compressive) the plastic stress intensity factors increase. The magnitude of the influence of biaxial loading was shown to be dependent on the strain hardening coefficient of the material.

The influence of the biaxial loading on cracked, stiffened panels was studied in Reference 3. This data showed that the elastic stress intensity factors increased due to the application of positive biaxial loads (i.e., the loads normal and perpendicular to the cracked plane being tensile); and that the influence of biaxial loading was not negligible. This behavior is contrary to the observation in the case of unstiffened sheets. In the present study the influence of biaxial loading on stiffened sheets has been considered using both elastic and elastic-plastic analysis. The analytical results have been compared with experimental data and the influence of biaxial loading on load transfer effects has also been examined.

3.2 DESCRIPTION OF TEST PANEL(S)

Two identical test specimens were fabricated from the drawing of Figure 58. The skin material was 0.063 inch 2024-T3 sheet, zee frames were 0.063-inch thick 2024-T3; and the hat section longerons were formed from 7075-T6 nominally 0.083-inch thick. In the test area the longerons were fastened to the skin by rivets. It can be noted from Figure 58 that a -1 and -11 assembly are mentioned. The test panel identification is 2-2 and 2-3 to reflect the skin material identification code. Between frames the four bay test area contained a centrally located initial slot in the skin of 4.0-inch half length and 8.0-inch overall length.

Table XI lists the materials, cross sectional areas, and other pertinent information for these two panels.

TABLE XI FRAME-LONGERON STIFFENED PANEL AREAS AND MATERIAL IDENTIFICATION

PANEL NUMBER	MEASURED THICKNESS (Inches)			TOTAL CROSS SECTIONAL AREAS (Inches ²)			SKIN MATERIAL/ AND I.D. (See Ref. 2)	PERCENT-AGE OF TOTAL LONGERON AREA TO SKIN
	Frame	Long-eron	Skin	Frame	Long-eron	Skin		
2-2	.063	.083	.0635	.94	2.3535	2.540	2024-T3/ 2-2	92.7
				Total Panel Cross Sectional Area = 4.8935				
2-3	.063	.083	.0635	.94	2.3535	2.540	2024-T3/ 2-3	92.7
				Total Panel Cross Sectional Area = 4.8935				

A description of the loading arrangement will follow in Section 3.4. Twenty strain gages were placed at various locations on the skin, longeron(s), and frame(s). A standard beam type clip gage was mounted on the skin side of both panels to record crack opening displacement at the crack and panel centerline.

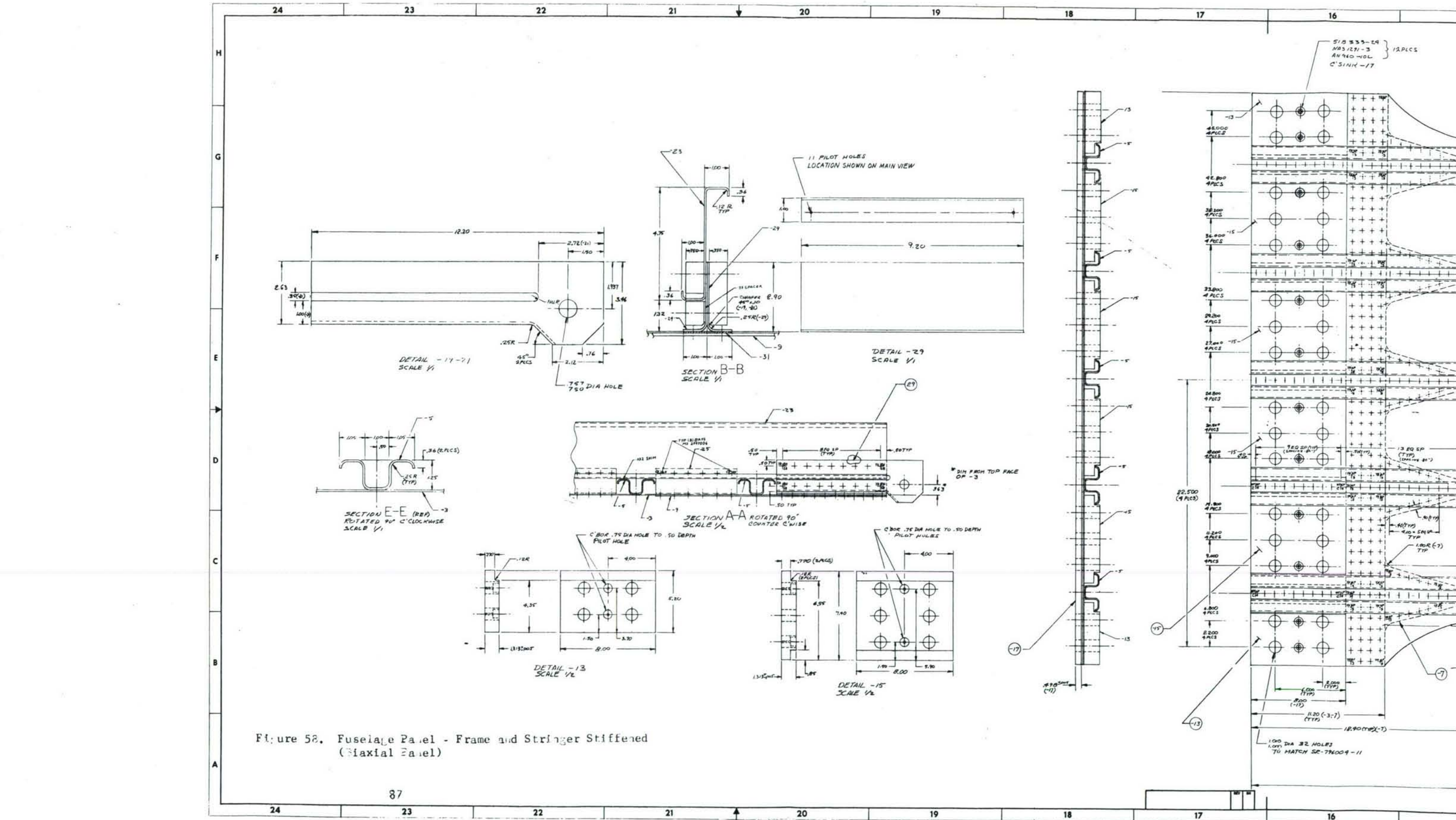


Figure 58. Fuselage Panel - Frame and Stringer Stiffened (Biaxial Panel)

16

15

1

1

51B 533-29 }
NAB 1291-3 } 12 PLES
AN 960-40L }
2' SINK -17

SECTION A-A

SECTION B-B

DIA .30

ASSY	A	B
-1	4.00	8.00
-11	4.00	8.00

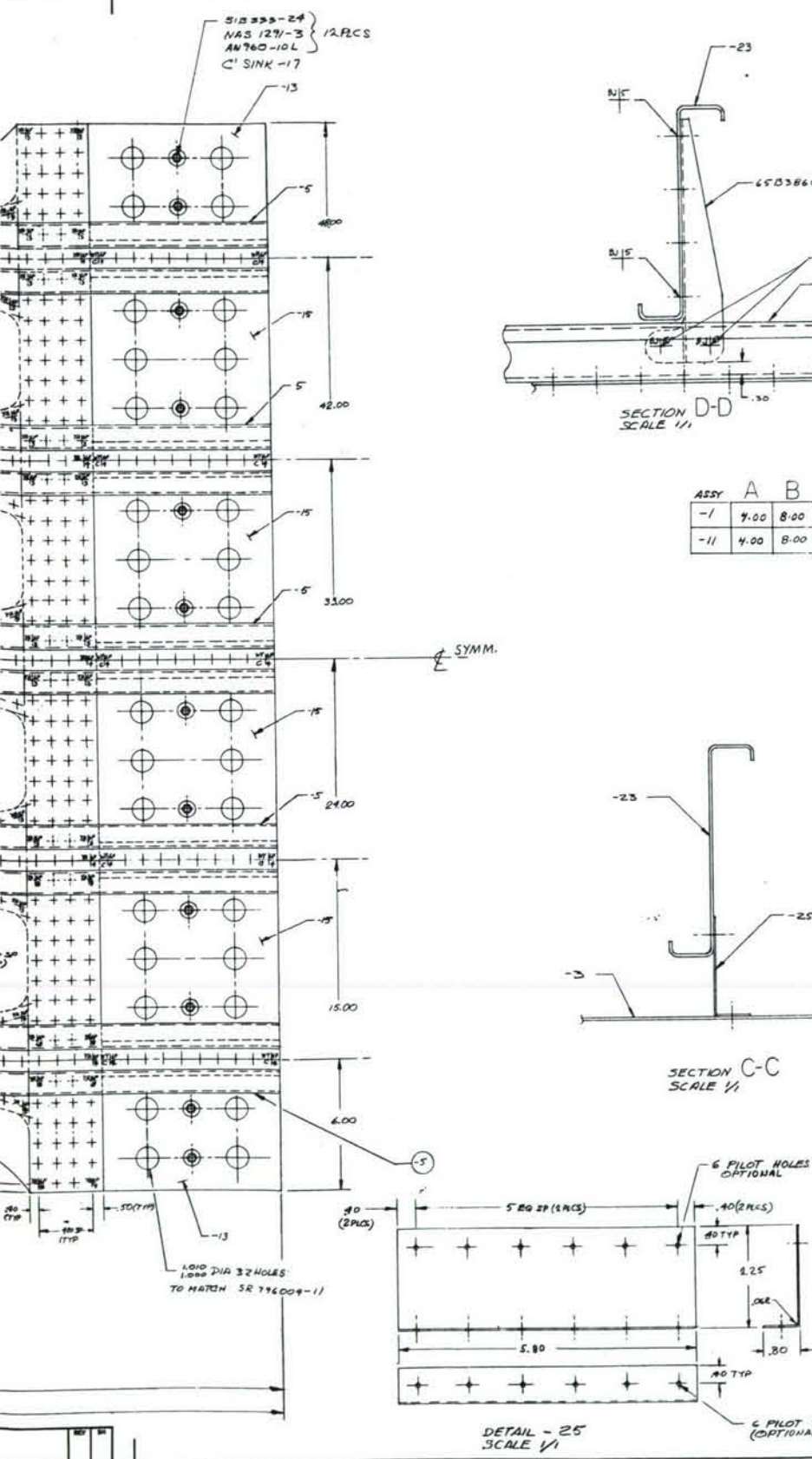
A technical drawing of a U-shaped metal bracket. The bracket has a vertical leg on the left and a vertical leg on the right, which meet at a central horizontal section. A horizontal line extends from the top of the left vertical leg to the left, with the label "-23" positioned above it. Another horizontal line extends from the bottom of the left vertical leg to the left, with the label "-3" positioned below it. A third horizontal line extends from the top of the right vertical leg to the right, with the label "-25" positioned above it.

SECTION C-C
SCALE 1/

The technical drawing illustrates a bracket assembly. It features a central horizontal slot with a width of 5.80 inches. Above this slot, there is a top flange with a total width of 10.75 inches. The top flange has a thickness of .40 inches and includes six pilot holes. The distance between the centers of these holes is .40 inches. Below the top flange, there is a bottom flange with a thickness of .30 inches. The overall height of the bracket is 2.25 inches. A note indicates that the top flange is optional.

DETAIL - 25
SCALE $\frac{1}{16}$

6 PILOT HOLES
(OPTIONAL)



NOTES:

- 1. USE PROCESS SPECS FHN-1, FHN-6-2, FHN-21,
MAY-23, MAY-22, MAY-23, MA-1-24
- USE SPECIFIED MATERIAL
- MACHINE ALL OVER $\frac{1}{16}$
- 4) HEAT TREAT TO T62 TEMPER PER HT-
- 5. .40 ED FOR $\frac{1}{4}$ IN. FASTENERS
- 6. .50 ED FOR $\frac{1}{4}$ IN. FASTENERS

<i>ASSY</i>	A	B
-1	4.00	8.00
-11	4.00	8.00

SECTION C
SCALE 1/1

The technical drawing illustrates a structural connection with the following dimensions and features:

- Horizontal distance from the left edge to the first hole: 5 EQ SP (2 PCS)
- Horizontal distance between the first and second holes: .40 (2 PCS)
- Vertical distance between the top and bottom rows of holes: .40 TYP
- Total vertical height of the hole pattern: 1.25
- Bottom horizontal distance from the left edge to the last hole: S.80
- Bottom horizontal distance from the left edge to the rightmost hole: .30
- Bottom horizontal distance from the center of the bottom row to the rightmost hole: .40 TYP
- Annotation "6 PILOT HOLES OPTIONAL" is located at the top right.

DETAIL - 25
SCALE 1/1

3.3 FINITE ELEMENT MODEL AND ANALYSIS

The analysis of the biaxially loaded panel was conducted using two different biaxial load ratios. The finite element modeling, elastic, and elastic-plastic analyses of the panel are discussed in the following subsections.

3.3.1 Finite Element Modeling of Biaxially Loaded Panels

The finite element modeling used is similar to that used in the analysis of the Phase II panels (Reference 1). The panel is essentially modeled as a two-dimensional structure. Triangular membrane elements were used to model the skin. The longerons of this panel are modeled like the stiffeners of the wing channel panel of Phase II (Section 3.1 of Reference 1). The connected leg of the longeron is modeled as a rod element and the two upstanding portions of the longeron (web portions) are combined to represent rectangular membrane elements. The thickness of the membrane elements is equal to the combined thickness of the two outstanding portions (web elements). The two flange portions and lips are combined to represent one rod element. The frame is modeled in a similar way as the longeron. The connected portion is modeled as a rod element and the outstanding leg as a membrane element. The flange and lip portion of the frame were combined to represent one rod element.

The portion of the shear clip connected to the skin was modeled as a rod element and that portion connected to the frame was modeled as a membrane element. The rivets connecting the skin to the shear clips were modeled using the flexible fastener model. The first nine rivets from the crack plane, connecting the skin to the longeron, were modeled as individual shear elements. These shear elements were proportioned to represent a flexible fastener model. The portion of the panel beyond the first nine rivets was assumed to be connected by continuous shear elements as for the angle stiffened panels (refer to Subsection 2.2.2.1). The shear elements were proportioned to account for fastener flexibility. Only one quarter of the panel was modeled for finite element analysis. The finite element model of the biaxial panel is shown in Figure 59.

3.3.2 Elastic and Elastic-Plastic Analysis of the Biaxial Panel

The elastic and elastic-plastic analysis of the biaxially loaded panel was performed to study the influence of biaxial loading on load transfer to stringers, crack openings, and J values. The elastic and elastic-plastic analysis of this panel is discussed in the following subsections.

3.3.2.1 Elastic Analysis of Biaxial Panel

The elastic analysis of the biaxial panel was performed for various crack lengths ($a = 4.5, 5.75, 8.00, 9.00, 11.0$ inches) with a uniaxial to biaxial ratio of 1:0 (i.e., no biaxial load applied). Two different contours were used to evaluate \sqrt{J} for a half crack length of 4.5 inches. These contours are shown in Figure 60. The \sqrt{J} values determined for these two contours were within one percent of each other. Thus for other crack lengths only Contour I (Figure 60) was used to evaluate the square root of J values.

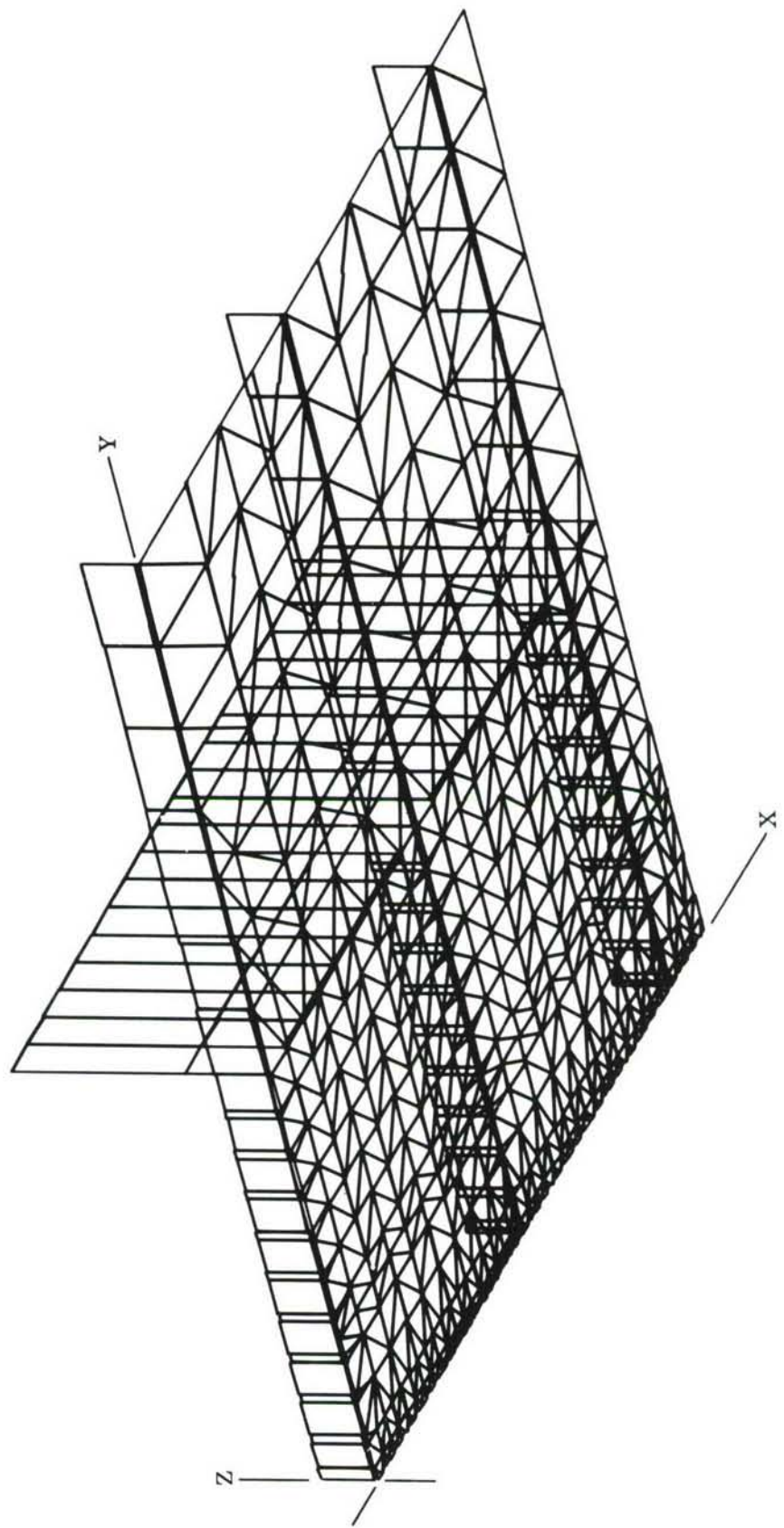


Figure 59. Finite Element Model of Biaxial Panel(s)

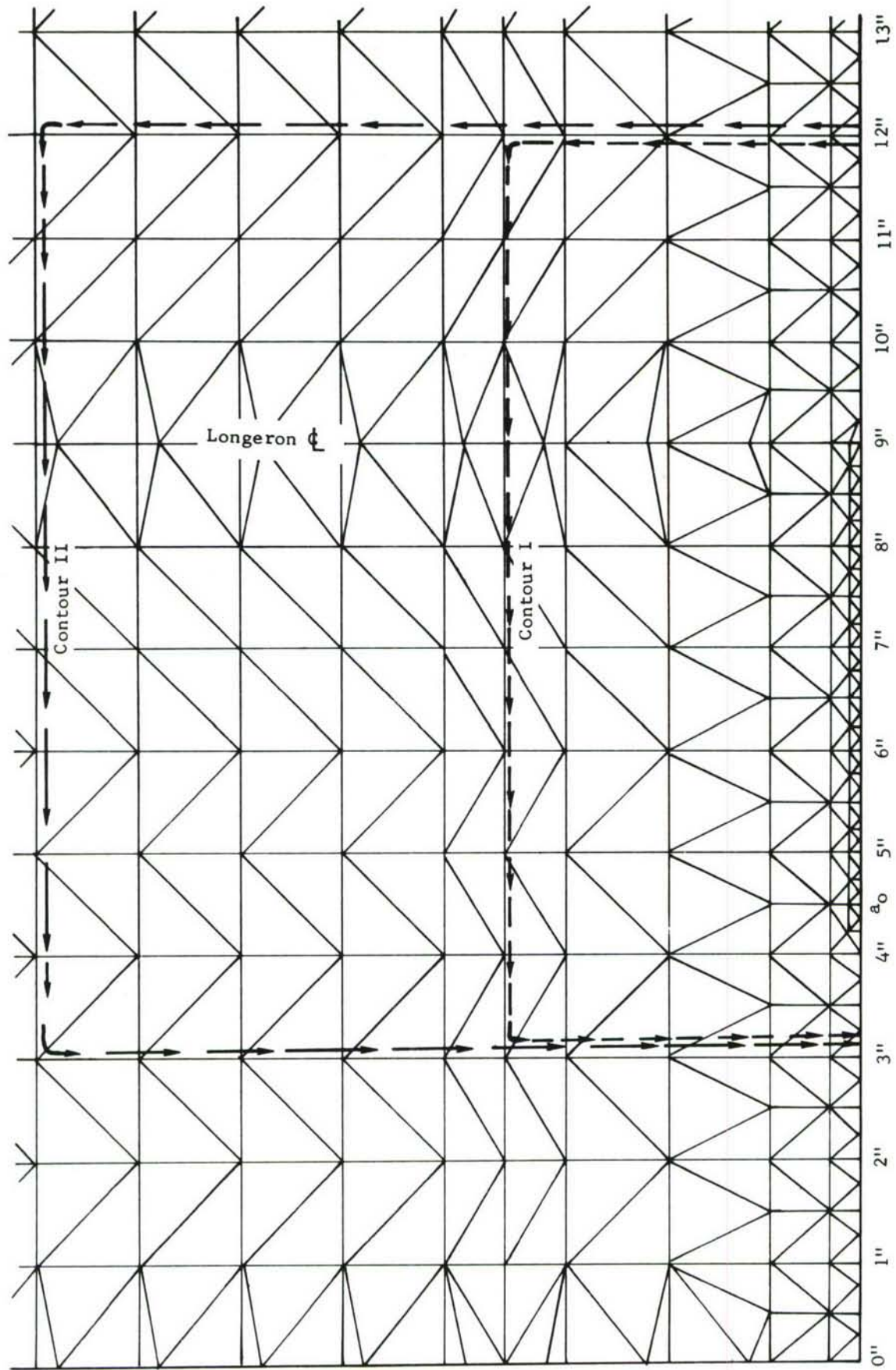


Figure 60. Contours Used to Evaluate J for Biaxial Panels

Values of square root J obtained for various crack lengths with the 1:0 biaxial ratio are shown in Figure 61. The \sqrt{J} value increases with crack length. When the crack tip is in the vicinity of the next stringer (longeron) the values decrease. Once the crack tip is beyond the centerline of the longeron, the square root J values increase again. The stresses in the central stringer (longeron) for various crack lengths are indicated in Figure 62. For the same applied stress, the stress in the central stringer increases with crack length.

An elastic analysis of the biaxial panel was also performed at a biaxial load ratio of 1:1 for a half crack length of 4.5 inches. For this crack length, the plot of \sqrt{J} versus applied stress is shown in Figure 63, for a biaxial ratio of 1:1 and also 1:0 (no biaxial load applied). The biaxial load ratio 1:1 here refers to ratio of total load applied in y direction to load applied in x direction. It is surprising to note that for the same stress applied in the uniaxial or y direction (p) the square root J value increases due to the application of a biaxial load. The values due to the application of a biaxial load being 13 percent higher than those due to a uniaxial load only. This behavior is contrary to that observed in unstiffened panels where it is known that the effect of biaxial tensile load with the same sign as the uniaxial load, is to reduce the crack opening displacement and stress intensity factors (Reference 4). For unstiffened panels the effect of biaxial load on elastic analysis is known to be of a second order of magnitude (Reference 5). As J is related to the stress intensity factor, this increase of square root of J with application of biaxial load for stiffened panels indicates that the stress intensity factor ahead of the crack tip increases due to biaxial load. Similar increases in stress intensity factors due to biaxial loads for stiffened panels were observed in Reference 3. This is due to the fact that biaxial load causes less load transfer to the central stringer and consequently larger crack surface openings or displacements. The crack surface openings are related to the stress intensity factors and hence, the stress intensity factors increase due to the application of a biaxial load in a stiffened panel. Figure 64 shows the plot of stress in the central stringer (longeron), at the plane of the crack, for biaxial load ratios of 1:1 and 1:0. The application of a 1:1 biaxial load causes a 15 percent reduction in stringer or longeron stress. The crack surface openings as a function of distance from the center of the crack (along the crack line), for uniaxial load (biaxial load equals zero) and biaxial load ratio 1:1 are shown in Figure 65. The crack surface openings or displacements at the center of crack increase 14 percent over the uniaxial load case (biaxial ratio 1:0) when a 1:1 biaxial load ratio is applied. Thus for a stiffened panel the elastic analysis indicates that the effect of biaxial load is to increase crack opening and J and reduce load transfer to the central stringer. The influence for this panel geometry was determined to be between 13 to 15 percent.

The stresses in the stringers (longerons) located at 9 inches and 18 inches from the centerline of the panel and crack are shown in Figure 66. The stresses in the stringer, 9 inches from the centerline of the crack are reduced by 23 percent and the stresses in the stringer 18 inches away are reduced by 4 percent due to a biaxial load ratio of 1:1.

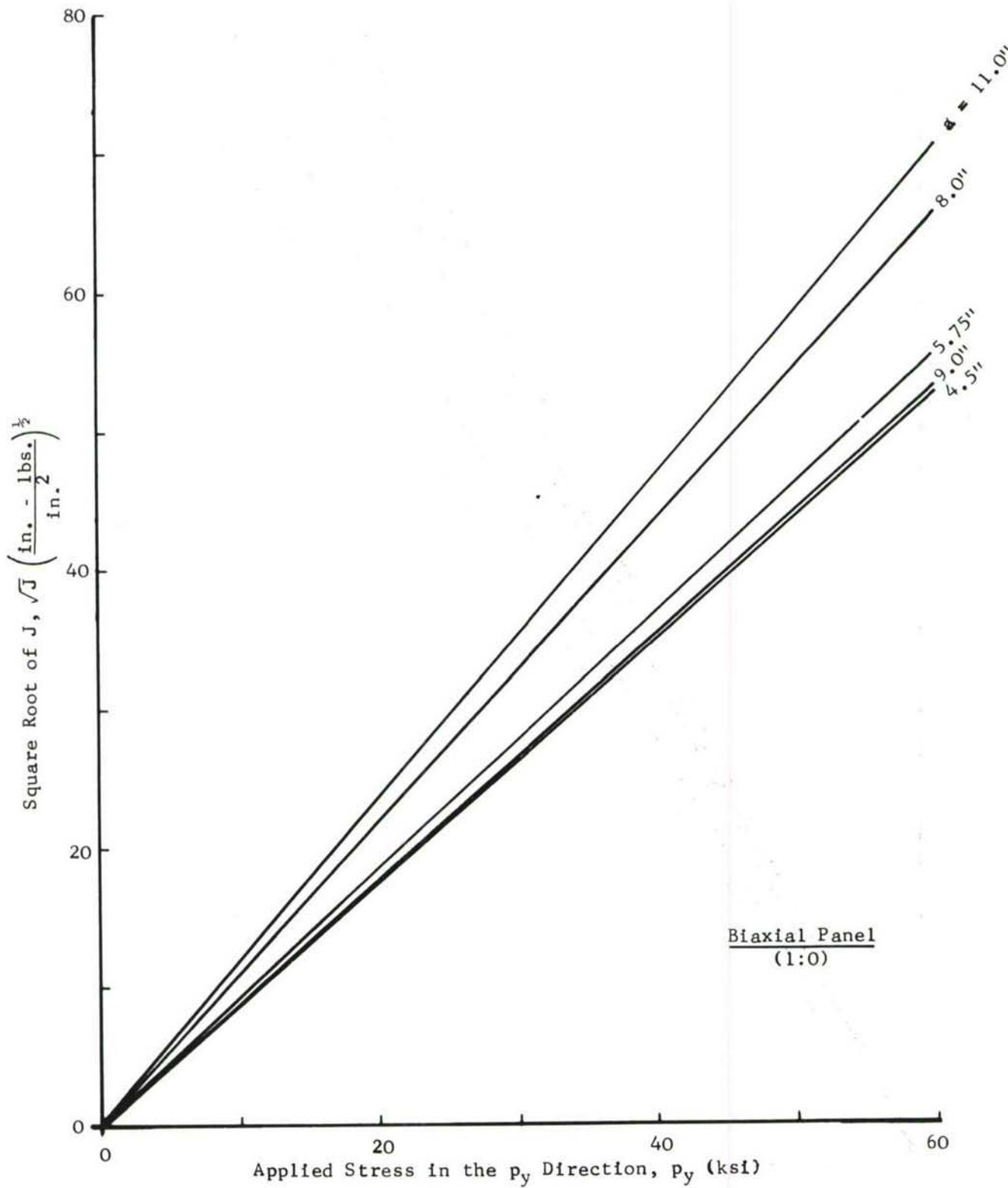


Figure 61. Square Root of J for Varying Crack Lengths as a Function of Applied Stress - Biaxial Panel

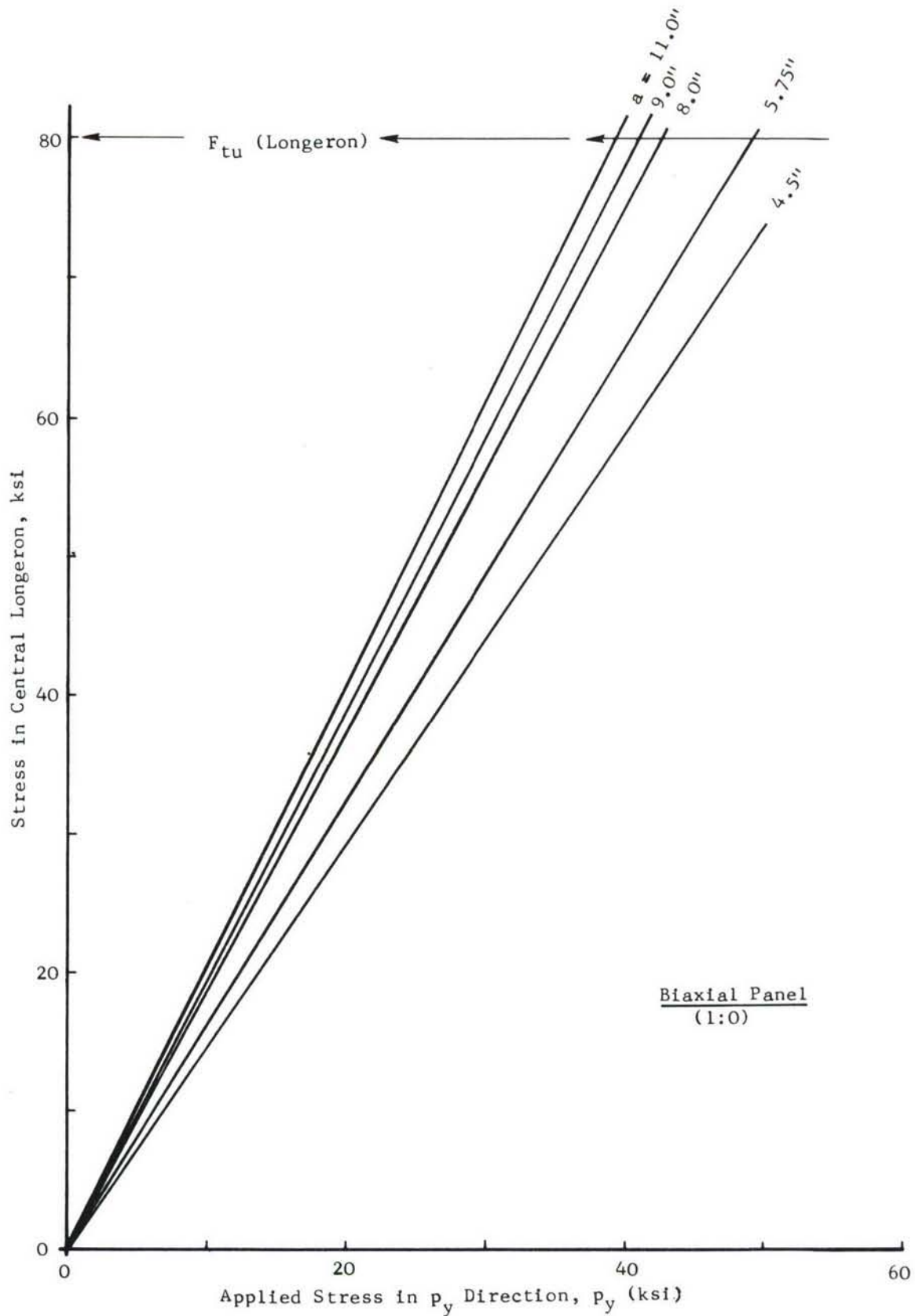


Figure 62. Stress in the Central Longeron as a Function of Gross Area Panel Stress for Varying Crack Length - Biaxial Panel

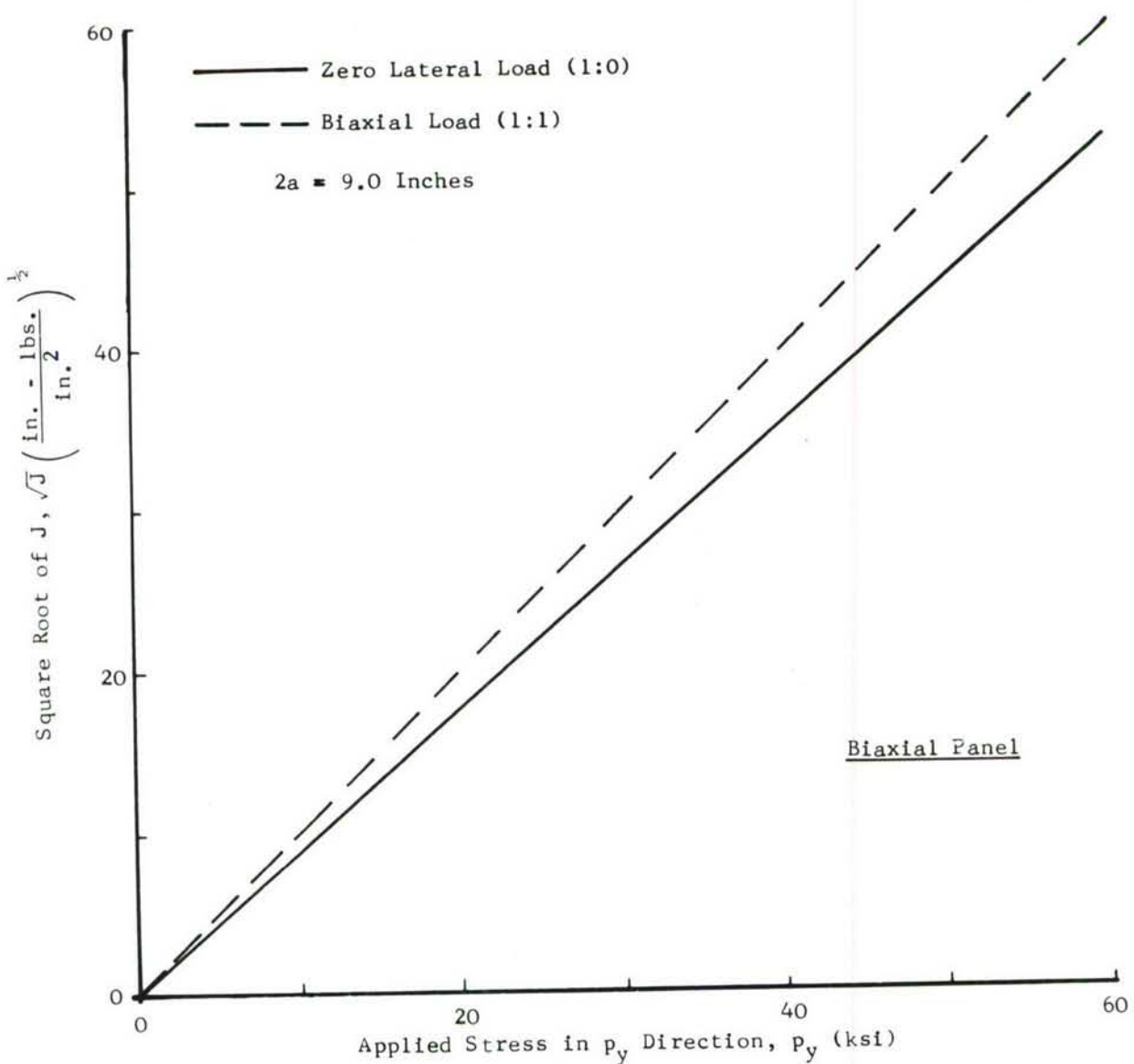


Figure 63. Elastic \sqrt{J} Values as a Function of Applied Stress for Two Biaxial Load Ratios

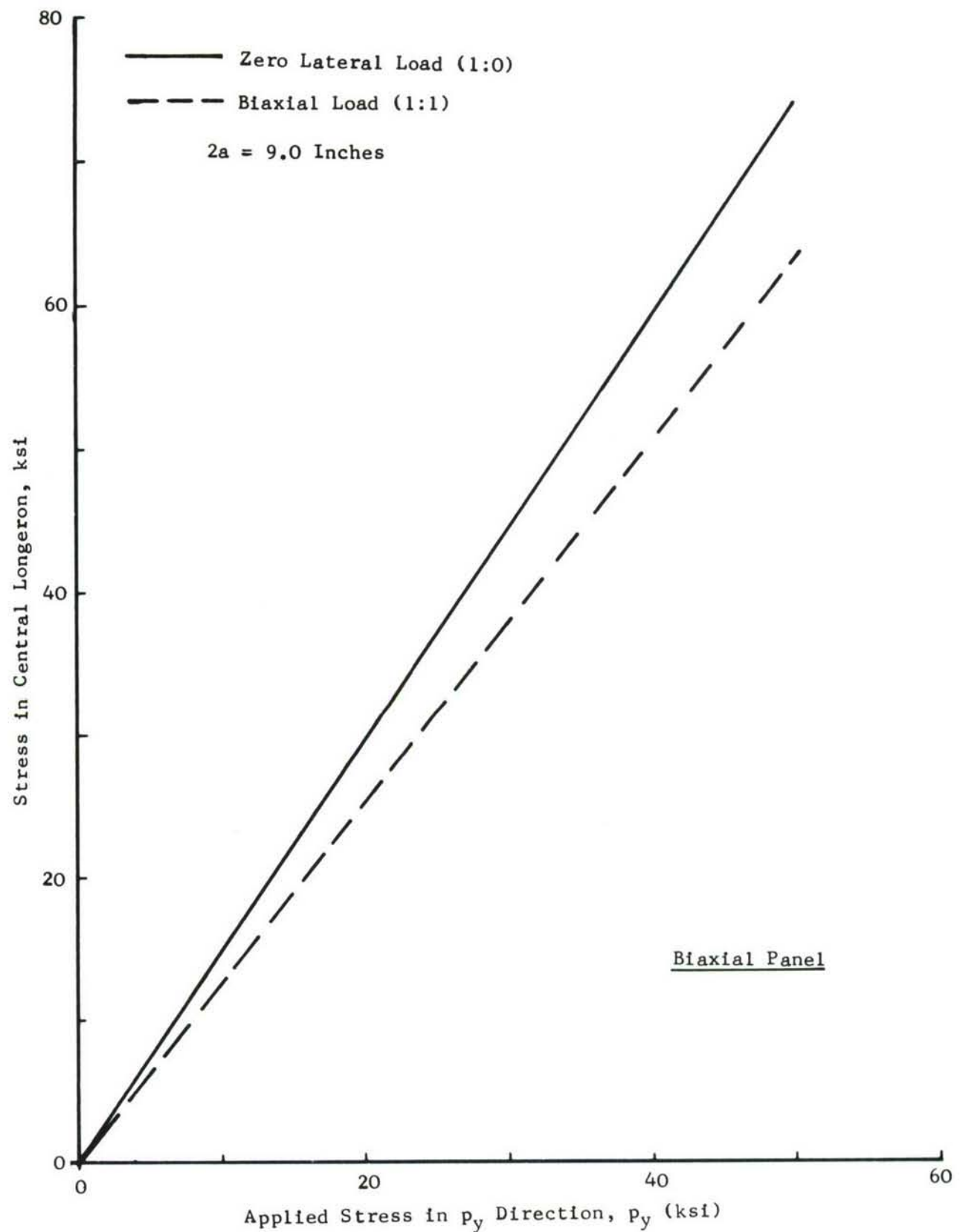


Figure 64. Stress in the Central Longeron as a Function of Applied Stress for Two Biaxial Load Ratios

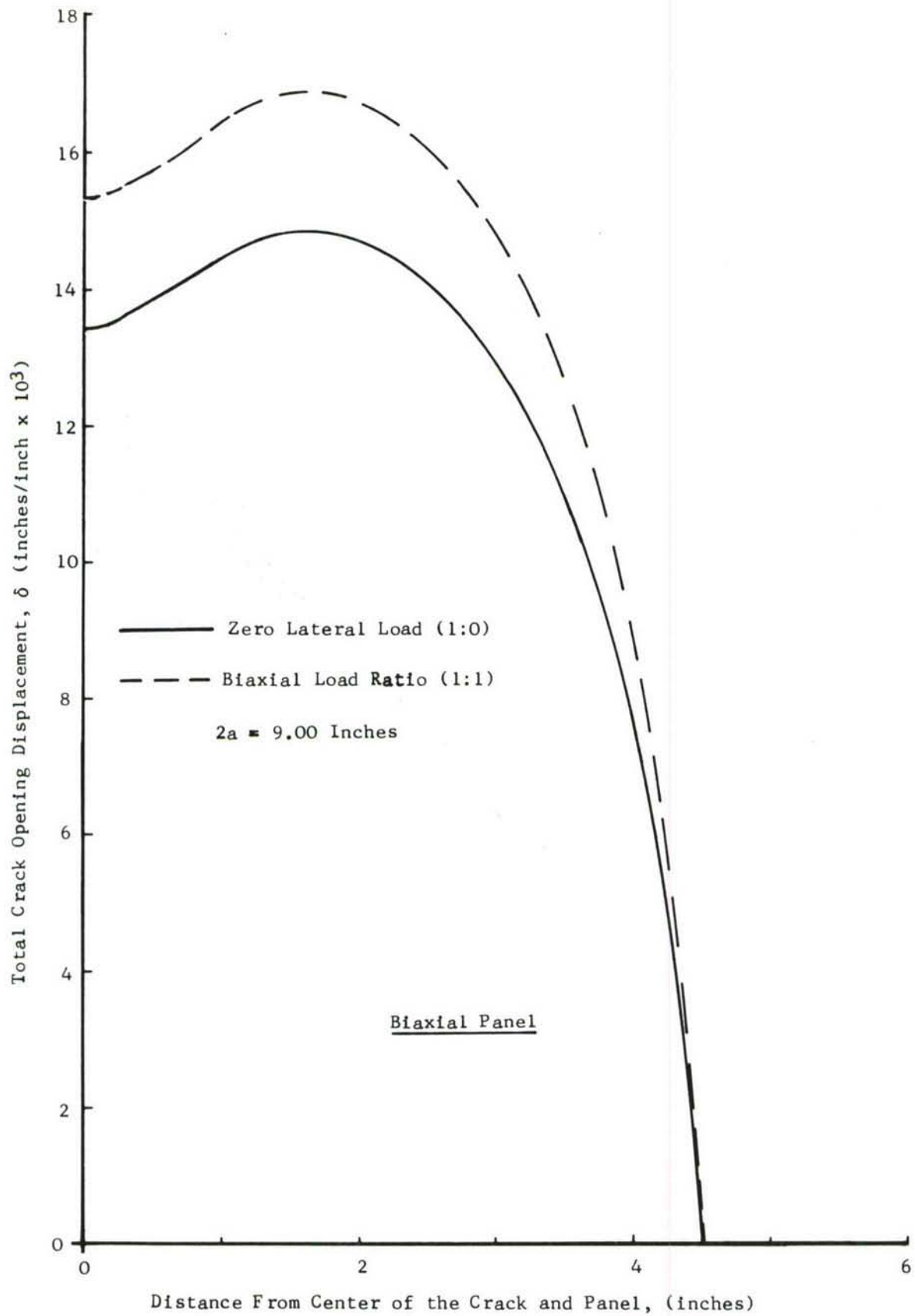


Figure 65. Total Crack Surface Displacements as a Function of Distance Along the Crack for Two Biaxial Load Ratios

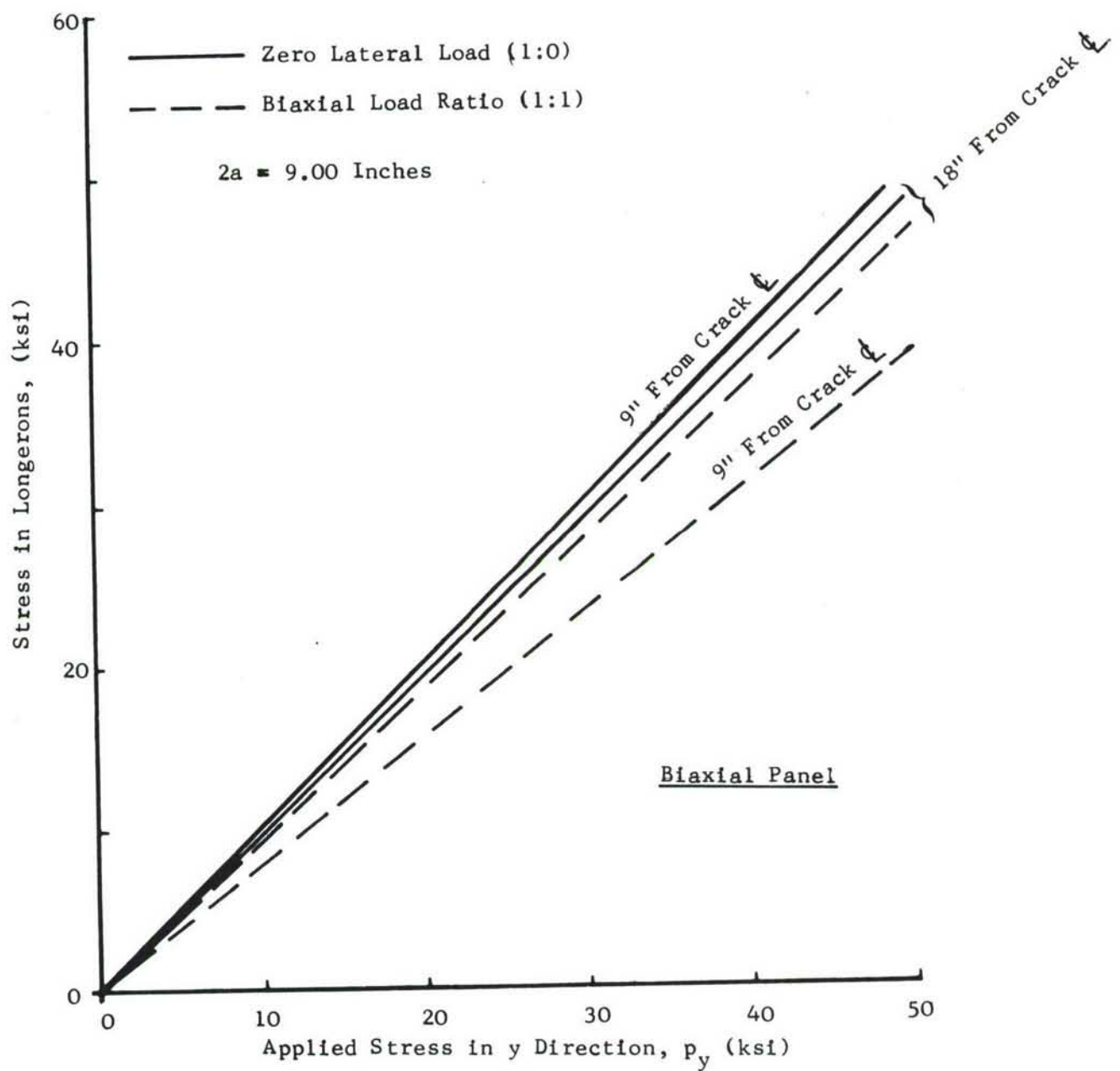


Figure 66. Stresses in Adjacent Longerons for Two Biaxial Load Ratios

3.3.2.2 Elastic-Plastic Analysis of Biaxial Panel

The elastic-plastic analysis of the biaxially loaded panel based on Dugdale type strip plastic zone could not be performed under biaxial loading due to the fact that the Dugdale model is only applicable to uniaxial load cases. The application of a biaxial stress will change the state of the stress and hence the plastic zone ahead of the crack tip. The size of the Dugdale plastic zone is determined by removing stress singularities ahead of the crack. The effect of biaxial loading on stress singularities is of second order and hence the influence of biaxial loading on a Dugdale type plastic zone will be very small. Thus a Dugdale analysis in biaxial loading will not give a realistic representation of plasticity ahead of the crack tip. Considering these factors it was felt more appropriate to perform the elastic-plastic analysis of the biaxial panel based on Prandtl-Reuss material behavior. The elastic-plastic analysis based on Prandtl-Reuss material behavior for various load increments involves considerable computer time. Thus, it was decided to perform an elastic-plastic analysis assuming Prandtl-Reuss material behavior for only one crack length. The length selected was 8.50 inches or the crack length of the tested panels with biaxial load ratios of 1:0, 1:1/3, 1:2/3, and 1:1. The corresponding applied load increments were 10, 20, 30, 40, and 45 ksi. The \sqrt{J} integral values were computed using Contour I shown in Figure 60. The variation of \sqrt{J} with applied stress for a half crack length of 4.25 inches and various biaxial ratios is shown in Figure 67. For the same applied load normal to the crack (p) the \sqrt{J} values increase as the load in the x direction is increased, i.e., biaxial load ratio is increased. This behavior is similar to that observed for the elastic analysis. The stress at which nonlinear effects are observed decreases as the biaxial load ratio increases. The variation of stress in the central stringer, at the plane of the crack, as a function of applied stress, for various biaxial load ratios is shown in Figure 68. Here again the behavior is similar to the elastic analysis where the stress in the central stringer decreases as the biaxial load ratio increases, i.e., load in the x direction is increased.

The influence of biaxial loading on the plastic zone size ahead of the crack tip is shown in Figure 69. It is seen that at an applied stress (normal to the crack) of 40 ksi, the plastic zone size decreases with the increase in the biaxial load (the applied load in x direction being of same sign as the load normal to the crack). Similar reduction in the size of the plastic zone due to application of biaxial load was also observed in the analysis of Reference 4.

3.4 EXPERIMENTAL RESULTS AND DISCUSSION

The details of load application, strain gage location, strain surveys, etc., were common to both the 2-2 and 2-3 panels and a general description of each will follow. All instrumentation employed to record and analyze data, i.e., load, COD, strain were identical to that used for the uniaxially loaded wing panels. A description of this test and data reduction arrangement is given in Section 2.2.3.1 and will not be repeated here.

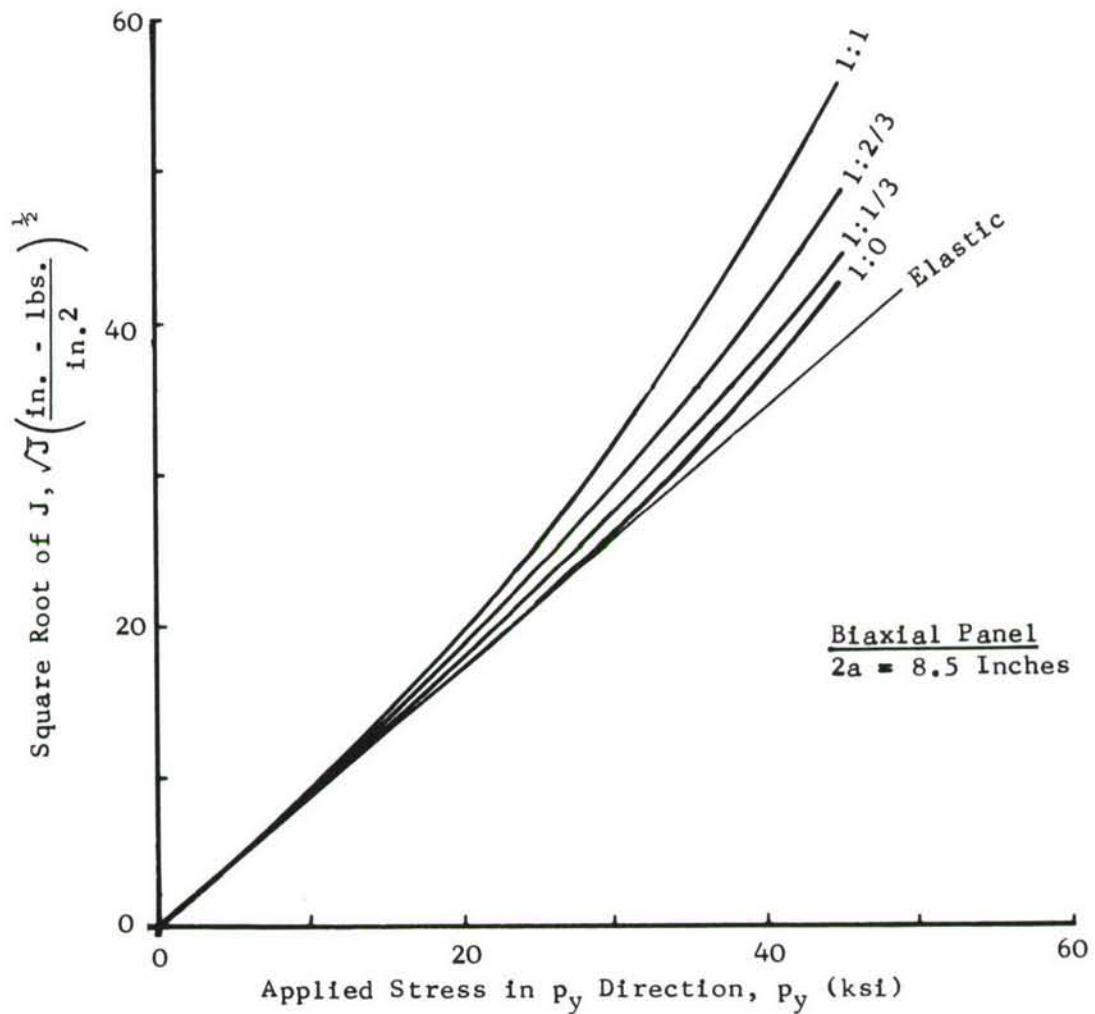


Figure 67. Square Root of J for Varying Biaxial Load Ratios Using Prandtl-Reuss Material Assumptions

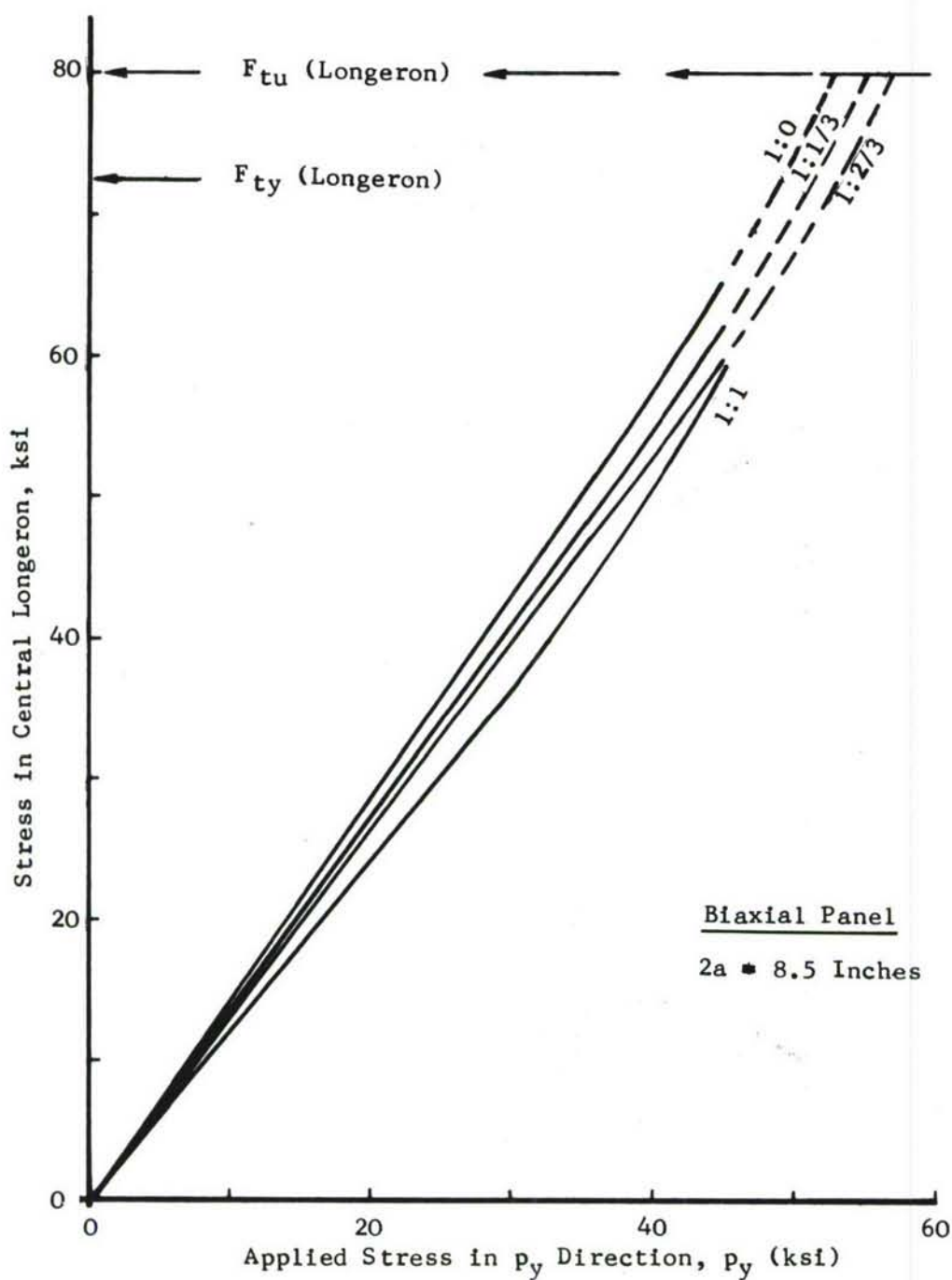


Figure 68. Stress in Central Longeron for Varying Biaxial Load Ratios Using Prandtl-Reuss Material Assumptions

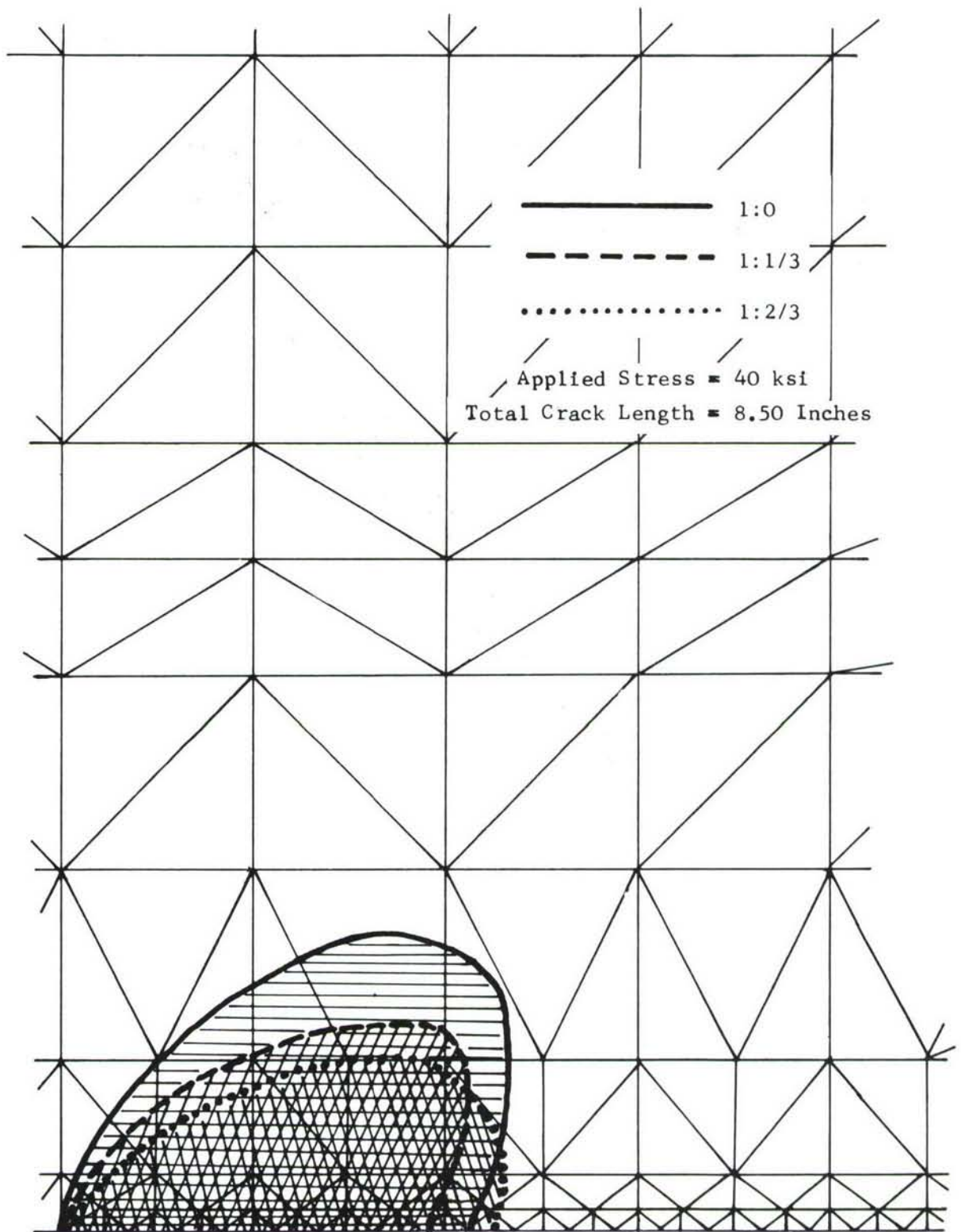


Figure 69. Plastic Zone Sizes for Three Biaxial Load Ratios Using Prandtl-Reuss Material Assumptions

The lateral loading was applied through two (2), ten-inch hydraulic cylinders each capable of providing a 120,000 pound load through a whiffle-tree arrangement connected to the frames/skin (see Section B-B of Figure 58) on both sides of the panel. A view of the overall structural test setup is shown in Figures 70 and 71 in which the support frame for the lateral load cylinders and whiffle-tree can be seen in the 500,000 pound load frame. A four channel EDISON load maintainer was used to control load for these side cylinders.

It will be noted that in the loading arrangement shown in Figure 70 that some panel bending is unavoidable since the lateral (side) loading is fixed and not free to move in a vertical direction when load is applied along the panel length. As with the previous wing panels care was taken to minimize inplane bending by padding at the grip ends. It will be noted in the discussions of the test data for the individual panels that the lateral constraint presented a rotational bending problem only at the highest lateral side loads.

3.4.1. Fatigue Precracking, Strain Data and Fracture of Biaxial Loaded Panels

To start from a natural crack condition in the two panels each was fatigue precracked approximately one quarter inch from the ends of the machined slot using tension-tension, sinusoidal loading. An approximation of the stress intensity for this panel was made using the solutions of Reference 3. Assuming a maximum, cyclic stress intensity of 12 ksi $\sqrt{\text{inch}}$ in both cases. It was subsequently determined that the stress intensity was conservative and a change was made to higher load levels. The fatigue stress ratio was maintained at between 0.1 and 0.25 to restrain local crack bending at lower load levels. Table XII summarizes the fatigue loadings and total crack lengths for the two biaxial panels. Measurement of final fatigue crack length was accomplished after panel failure.

TABLE XII FATIGUE PRECRACKING AND CRACK LENGTH DATA, 2-2 AND 2-3 BIAXIAL PANELS

PANEL	FATIGUE LOADS		NUMBER OF CYCLES	FATIGUE CRACK LENGTH (Inches)		
	MAXIMUM (kips)	MINIMUM (kips)		LEFT	RIGHT	TOTAL
2-2	19.5	2.0	31,000	-	-	-
	24.0	2.4	44,000	.06	.09	8.15
	28.0	7.0	11,800	.20	.20	8.40
2-3	28.0	7.0	22,000	.26	.24	8.50

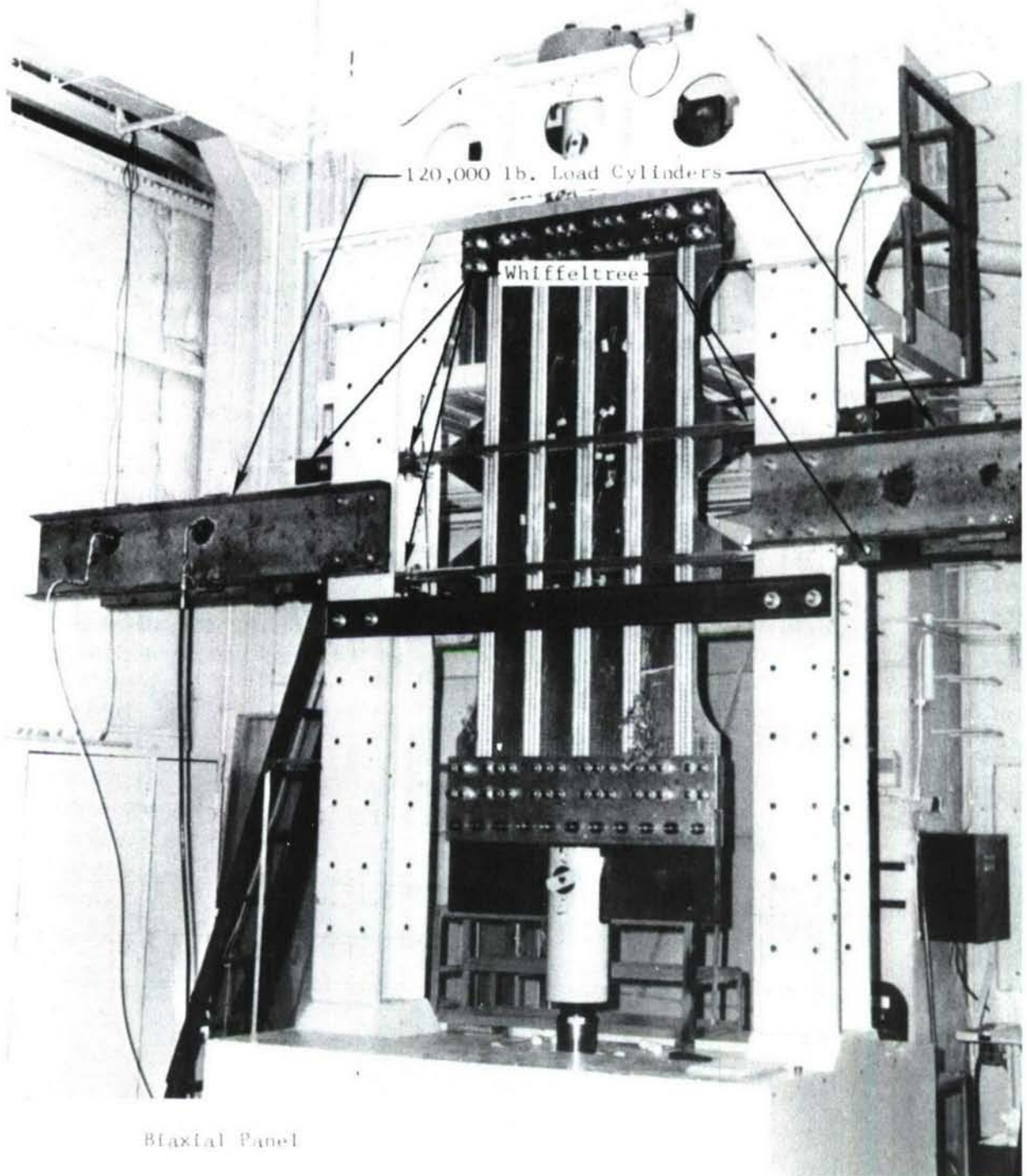


Figure 70. Stiffener-Side View of Loading Arrangement for Biaxial Panels

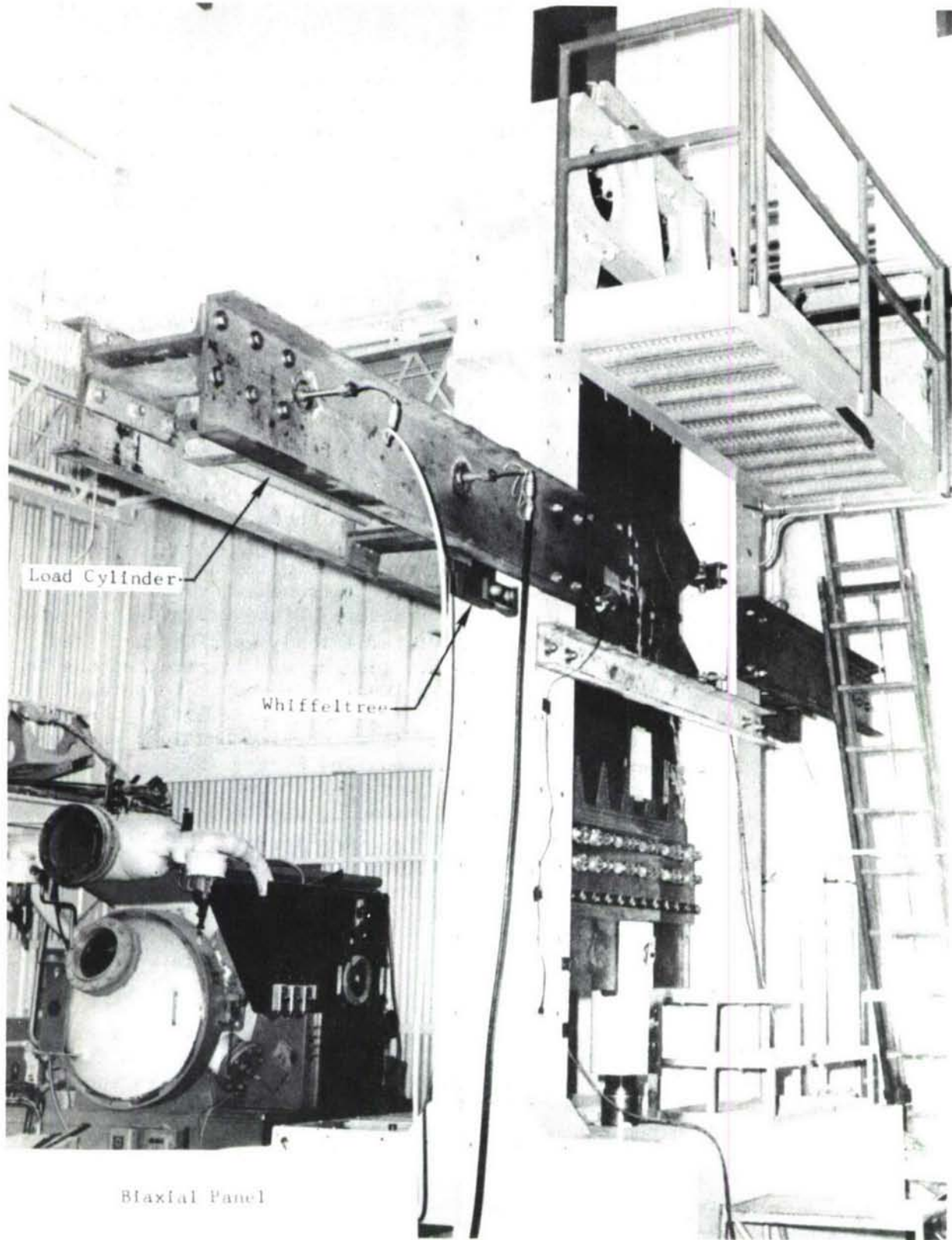


Figure 71. Side View of Lateral Loading Arrangement for Biaxial Panels

Figures 72 and 73 show the front (skin) side view of the biaxial panel in the test machine. It will be noted that the diamond shaped doublers are used to aid in transmitting load to the skin from the whiffeltree(s). The test section is that area shown in Figure 73 between frames. Also visible is the starter slot in the skin in Figure 72. The positioning of the displacement gage points and most strain gage locations can be noted on both views.

After fatigue cycling and zero balancing of all strain gages and displacement gage with the panel in a free hanging position a series of strain/load survey was accomplished on each panel by loading to specific values of biaxial ratio. The biaxial ratio here is defined as ratio of lateral (frame) or side load to axial (lengthwise) load. Care was taken to perform this survey within the elastic range for each panel. The results of these surveys and strains during the fracture and slow tear portion of the loading cycle are given in Table XIII for the 2-2 panel and Table XIV for the 2-3 panel. The reference location of each strain gage is shown in Figure 74 located between Tables XIII and XIV.

Load versus total displacement gage output are shown in Figures 75 and 76 for the 2-2 panel and in Figure 77 for the 2-3 panel. It is of interest to note the increase in crack opening displacement with increasing lateral load under constant axial load (see Figure 75). This behavior was predicted by the analytical results. The loading to fracture of the 2-2 panel was of ramp loading (100,000 lbs./min.) to 60 kip lateral load, keeping that load constant and increasing axial load. However, loading was interrupted due to an equipment malfunction during the fracture loading process. This resulted in a stable tear to an overall crack length of 11.28 inches (5.67 inches on the left side and 5.61 inches on the right side) at which time the load was removed and a subsequent loading exercise was attempted (see Figure 75). At this crack length the panel was once again ramp loaded at 100,000 pounds per minute in both axial and lateral load. The lateral loading was stopped at 60 kips and the axial load increased at the same rate. Failure occurred in this 2-2 panel at 195.1 kips.

After the initial strain survey in the 2-3 panel (see Table XIV) the panel was loaded at 100,000 pounds per minute to a lateral and axial load of 120,000 pounds. At that point axial loading was increased to failure at 181 kips.

Motion picture coverage was initiated during the slow tear and fracture process for both biaxially loaded panels. In both cases the tear to fracture and fracture were recorded. The failure sequence for each panel is shown in Figures 78 and 79. It is obvious that the 2-2 panel (Figure 78) failed in the test section and through the longeron/skin area. However, examination of the failure sequence in Figure 79 for the 2-3 panel indicates that fracture initiated in the area of the attached doubler near the frame section (see Frame No. 9). The resulting failure of this panel was explosive. The design of the frame/skin lateral loading attachments, etc., was placed at approximately 130 kips (with no margin of safety) therefore a failure in this area could have been avoided by employing a lesser lateral load. However, in this phase of the program, with two identical specimens an order of difference in lateral loading between the two specimens was the logical scheduled test plan. Therefore, a constant 60 kip and 120 kip side load were selected as the fracture conditions prior to test.

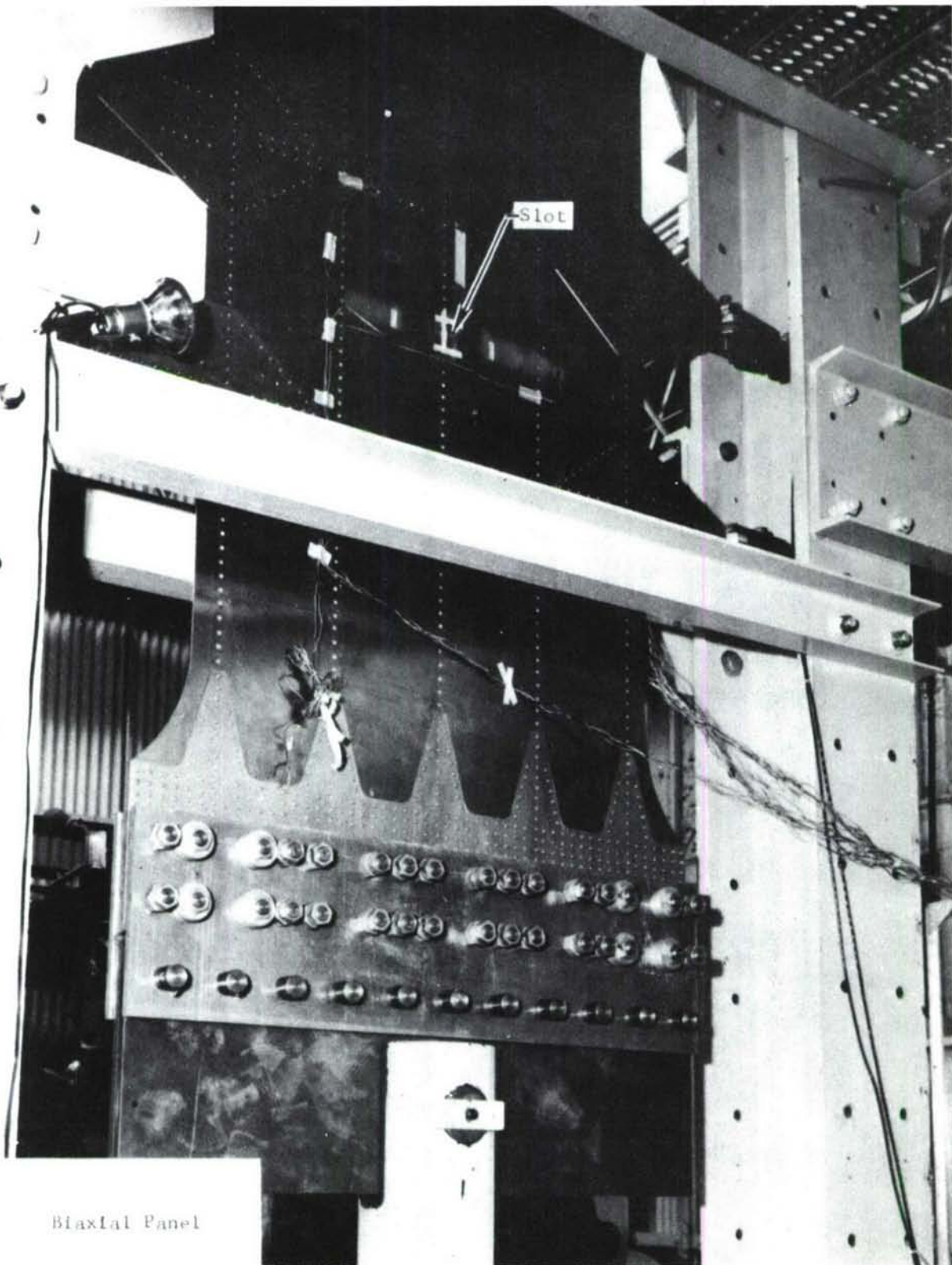


Figure 72. Skin-Side View of Biaxial Test Panel

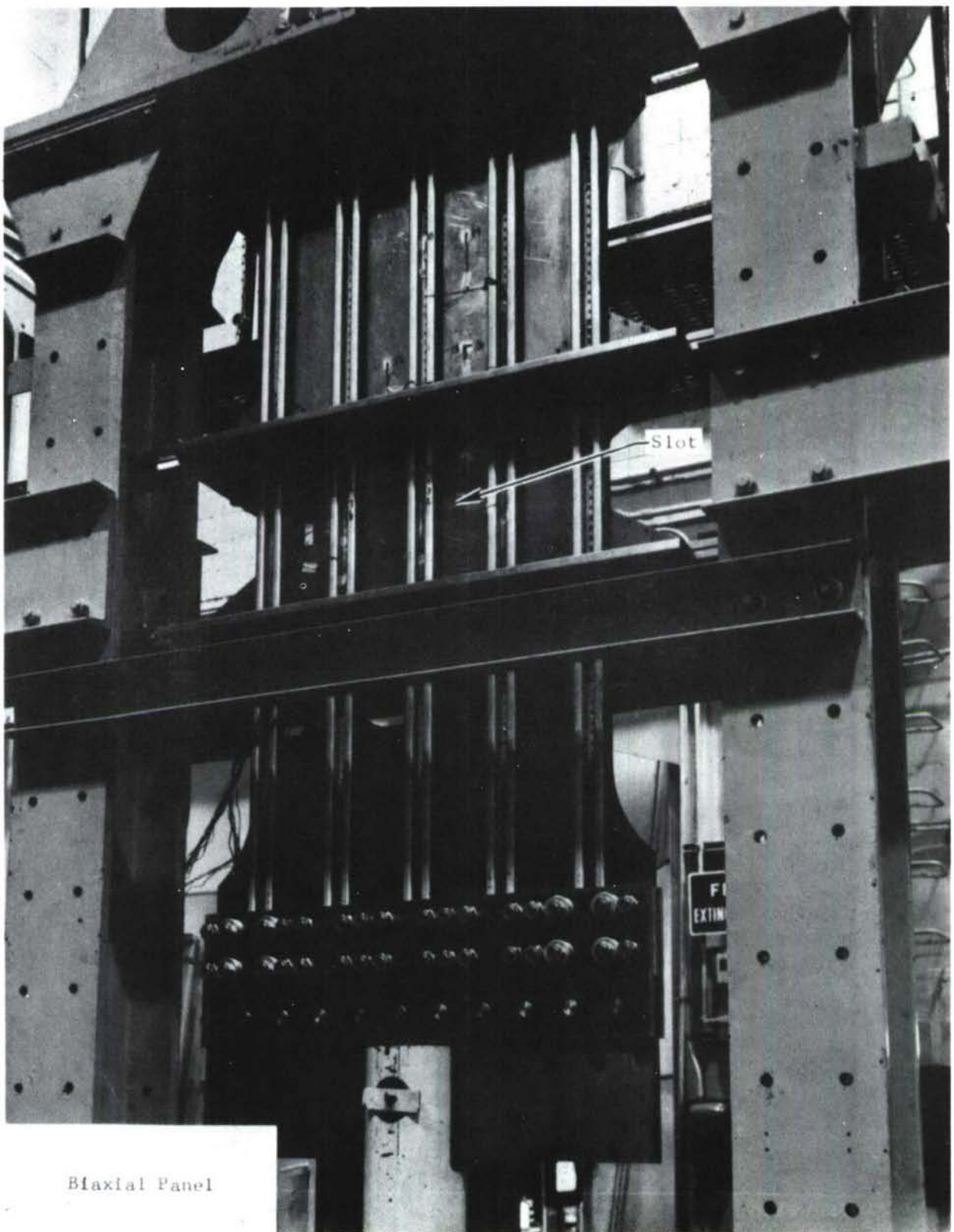


Figure 73. Longerons and Frame Side View of Biaxial Test Panel

TABLE XIII STRAIN GAGE DATA, 2-2 BIAXIAL PANEL

PANEL	LOAD P_x (kips)	LATERAL RATIO P_y/P_x	GAGE LOCATION AND STRAIN $\times 10^3$ INCHES/INCH																			
			1	2	3	4	5	6	7	8	9	10	11	12	13	14	15	16	17	18	19	Δ
2-2 ($2\alpha = 8.40^\circ$)	ZERO	ZERO	.002	.006	.003	.006	N	.008	N	.003	-.003*	.0070	-.001	.004	0	-.001	.002	0	-.004	.003	.003	
12	0	0	.0035	.214	.129	.098	N	.098	N	-.018	-.033*	-.039	-.006	-.024	.080	-.029	.076	-.026	.074	.063	-.042	
S-12	12	12	1.0	.006	.464	.280	O	.220	O	.214	O	-.003	-.027*	-.088	-.011	-.050	.180	-.057	.183	-.053	.174	-.167
S-12	12	12	1.0	.449	.465	.240	T	.170	T	.184	T	.120	-.197*	.197	.042	.286	.151	.139	.149	.196	-.098	
S-12	12	6	.5	.274	.473	.264	T	.193	T	.197	T	.044	-.101*	.041	.017	.153	.174	.039	.165	.105	.168	
S-12	12	6	.53	.281	.722	.421	R	.314	R	.311	R	.021	-.080*	.009	.010	.125	.271	.003	.270	.070	.233	.315
S-12	12	6	.67	.461	.711	.395	R	.300	R	.300	R	.097	-.179*	.146	.036	.263	.245	.107	.252	.168	.210	.327
S-12	12	18	1.0	.662	.692	.363	R	.257	R	.280	R	.198	-.307*	.288	.059	.425	.209	.238	.227	.280	.185	.296
S-12	12	18	0	.080	.706	.432	E	.336	E	.314	E	-.049	-.051*	-.122	-.011	-.014	.281	-.074	.283	-.041	.254	.208
S-12	24	0	0	-.026	.98.9	.599	C	.465	C	.436	C	-.081	-.032*	-.192	-.020	-.072	.384	-.111	.399	-.099	.364	.377
S-12	24	12	.5	.459	.966	.566	D	.418	D	.417	D	.073	-.167*	.084	.029	.240	.346	.069	.360	.134	.317	.001
S-12	24	18	.75	.667	.931	.554	R	.390	R	.398	R	.176	-.291*	.237	.055	.405	.306	.203	.333	.245	.288	.133
S-12	24	24	1.0	.863	.899	.519	R	.352	R	.377	R	.285	-.423*	.378	.079	.571	.264	.346	.306	.394	.263	.473
S-12	30	30	1.0	1.035	1.092	.691	D	.453	D	.482	D	.370	-.532*	.456	.099	.706	.326	.449	.394	.421	.346	.432
S-12	36	36	1.0	1.187	1.248	.847	D	.542	D	.576	D	.456	-.650*	.433	.116	.839	.385	.550	.479	.483	.427	.388
S-12	36	24	.67	.874	1.276	.907	E	.596	E	.597	E	.276	-.437*	.275	.071	.572	.454	.312	.521	.462	.400	.224
S-12	36	18	.5	.670	1.300	.942	D	.634	D	.612	D	.166	-.350*	.128	.045	.406	.499	.171	.546	.205	.487	.726
S-12	36	18	.017	-.059	.053	.014	O	0	O	0	O	.014	-.032*	.005	.005	.055	.099	.010	.006	.041	-.005	.016
S-12	36	18	.33	.211	.721	.48	O	0	O	0	O	0	-.011*	-.02	-.02	.02	-.001	.001	0	0	0	0
S-12	36	18	.57	.432	.765	.45	O	.72	O	.72	O	.32	-.230	-.33	.34	.02	.07	.279	-.021	.282	.019	.251
S-12	36	18	1.0	.624	.687	.42	O	.30	O	.28	O	.314	-.31	.34	.12	.02	.23	.247	.101	.260	.139	.224
S-12	36	18	1.0	.66	.70	.42	O	.28	O	.25	O	.295	-.30	.32	.06	.42	.206	.237	.233	.249	.193	.352
S-12	36	18	1.0	.604	.700	.42	O	.28	O	.25	O	.295	-.30	.32	.06	.42	.206	.237	.233	.249	.193	.352
S-12	36	18	0	.02	.72	.48	O	.37	O	.32	O	.32	-.036	.036	.036	.0	.05	.286	-.092	.271	.221	.278
S-12	36	18	0	-.036	-.014	0	O	0	O	0	O	.02	-.013*	-.02	0	.02	-.008	-.009	-.022	-.004	-.009	-.011
S-12	36	18	0	-.062	-.03	0	O	0	O	0	O	.02	-.111*	-.02	0	0	-.02	-.008	-.023	-.024	-.029	-.053
S-12	36	18	0	-.046	-.018	0	O	0	O	0	O	.093	-.70	.74	-.13	.217	.32	.101	.572	.312	.521	.376
S-12	36	18	0	-.068	-.012	1.50	O	1.02	O	.78	O	.660	-.66	.69	.14	.239*	.66	.206	.119	.572	.141	.524
S-12	36	18	0	-.068	-.012	1.48	O	1.00	O	.68	O	.58	-.595	.66	.69	.14	.238*	.67	.16	.05	.32	.522
S-12	36	18	0	-.068	-.012	1.314	O	1.00	O	.68	O	.58	-.595	.66	.69	.14	.238*	.67	.16	.05	.32	.522
S-12	36	18	0	-.068	-.012	1.201	O	1.00	O	.68	O	.58	-.595	.66	.69	.14	.238*	.67	.16	.05	.32	.522
S-12	36	18	0	-.068	-.012	1.125	O	1.00	O	.68	O	.58	-.595	.66	.69	.14	.238*	.67	.16	.05	.32	.522
S-12	36	18	0	-.068	-.012	1.044	O	1.05	O	.78	O	.68	-.690	.60	.67	.14	.238*	.67	.16	.05	.32	.522
S-12	36	18	0	-.068	-.012	1.086	O	1.04	O	.98	O	.84	-.951	.96	.94	.78	.238*	.70	.20	.140	.592	.805
S-12	36	18	0	-.068	-.012	1.044	O	1.04	O	.98	O	.84	-.951	.96	.94	.78	.238*	.70	.20	.140	.592	.805
S-12	36	18	0	-.068	-.012	1.044	O	1.04	O	.98	O	.84	-.951	.96	.94	.78	.238*	.70	.20	.140	.592	.805
SLOW TEAR	182.5	60	.33	.12	.505	.452	O	.02	O	.365	O	.358	-.346	.48	.377	.23	.15	.200	.150	.167	.167	.167
SLOW TEAR	182.5	60	.33	.12	.512	.458	O	.02	O	.365	O	.358	-.346	.48	.377	.23	.15	.200	.150	.167	.167	.167
ZER0	195.1	60	.31	.248	6.10	5.08	O	4.70	O	4.40	O	4.00	-.365	.402	.46	.377	.23	.15	.200	.150	.167	.167
ZER0	195.1	60	.31	.248	6.10	5.08	O	4.70	O	4.40	O	4.00	-.365	.402	.46	.377	.23	.15	.200	.150	.167	.167
ZER0	195.1	60	.31	.248	6.10	5.08	O	4.70	O	4.40	O	4.00	-.365	.402	.46	.377	.23	.15	.200	.150	.167	.167
ZER0	195.1	60	.31	.248	6.10	5.08	O	4.70	O	4.40	O	4.00	-.365	.402	.46	.377	.23	.15	.200	.150	.167	.167
ZER0	195.1	60	.31	.248	6.10	5.08	O	4.70	O	4.40	O	4.00	-.365	.402	.46	.377	.23	.15	.200	.150	.167	.167
ZER0	195.1	60	.31	.248	6.10	5.08	O	4.70	O	4.40	O	4.00	-.365	.402	.46	.377	.23	.15	.200	.150	.167	.167
ZER0	195.1	60	.31	.248	6.10	5.08	O	4.70	O	4.40	O	4.00	-.365	.402	.46	.377	.23	.15	.200	.150	.167	.167
ZER0	195.1	60	.31	.248	6.10	5.08	O	4.70	O	4.40	O	4.00	-.365	.402	.46	.377	.23	.15	.200	.150	.167	.167
ZER0	195.1	60	.31	.248	6.10	5.08	O	4.70	O	4.40	O	4.00	-.365	.402	.46	.377	.23	.15	.200	.150	.167	.167
ZER0	195.1	60	.31	.248	6.10	5.08	O	4.70	O	4.40	O	4.00	-.365	.402	.46	.377	.23	.15	.200	.150	.167	.167
ZER0	195.1	60	.31	.248	6.10	5.08	O	4.70	O	4.40	O	4.00	-.365	.402	.46	.377	.23	.15	.200	.150	.167	.167
ZER0	195.1	60	.31	.248	6.10	5.08	O	4.70	O	4.40	O	4.00	-.365	.402	.46	.377	.23	.15	.200	.150	.167	.167
ZER0	195.1	60	.31	.248	6.10	5.08	O	4.70	O	4.40	O	4.00	-.365	.402	.46	.377	.23	.15	.200	.150	.167	.167
ZER0	195.1	60	.31	.248	6.10	5.08	O	4.70	O	4.40	O	4.00	-.365	.402	.46	.377	.23	.15	.200	.150	.167	.167
ZER0	195.1	60	.31	.248	6.10	5.08	O	4.70	O	4.40	O	4.00	-.365	.402	.46	.377	.23	.15	.200	.150	.167	.167
ZER0	195.1	60	.31	.248	6.10	5.08	O	4.70	O	4.40	O	4.00	-.365	.402	.46	.377	.23	.15	.200	.150	.167	.167
ZER0	195.1	60	.31	.248	6.10	5.08	O	4.70	O	4.40	O	4.00	-.365	.402	.46	.377	.23	.15	.200	.150	.167	.167
ZER0	195.1	60	.31	.248	6.10	5.08	O	4.70	O	4.40	O	4.00	-.365	.402	.46	.377	.23	.15	.200	.150	.167	.167
ZER0	195.1	60	.31	.248	6.10	5.08	O	4.70	O	4.40	O	4.00	-.365	.402	.46	.377	.23	.15	.200	.150	.167	.167
ZER0	195.1	60	.31	.248	6.10	5.08	O	4.70	O	4.40	O	4.00	-.365	.402	.46	.377	.23	.15	.200	.150	.167	.167
ZER0	195.1	60	.31	.248	6.10	5.08	O	4.70	O	4.40	O	4.00	-.365	.402	.46	.377	.23	.15	.200	.150	.167	.167
ZER0	195.1	60	.31	.248	6.10	5.08	O	4.70	O	4.40	O	4.00	-.365	.402	.46	.377	.23	.15	.200	.150	.167	.167
ZER0	195.1	60	.31	.248	6.10	5.08	O	4.70	O	4.40	O	4.00	-.365	.402	.46	.377</td						

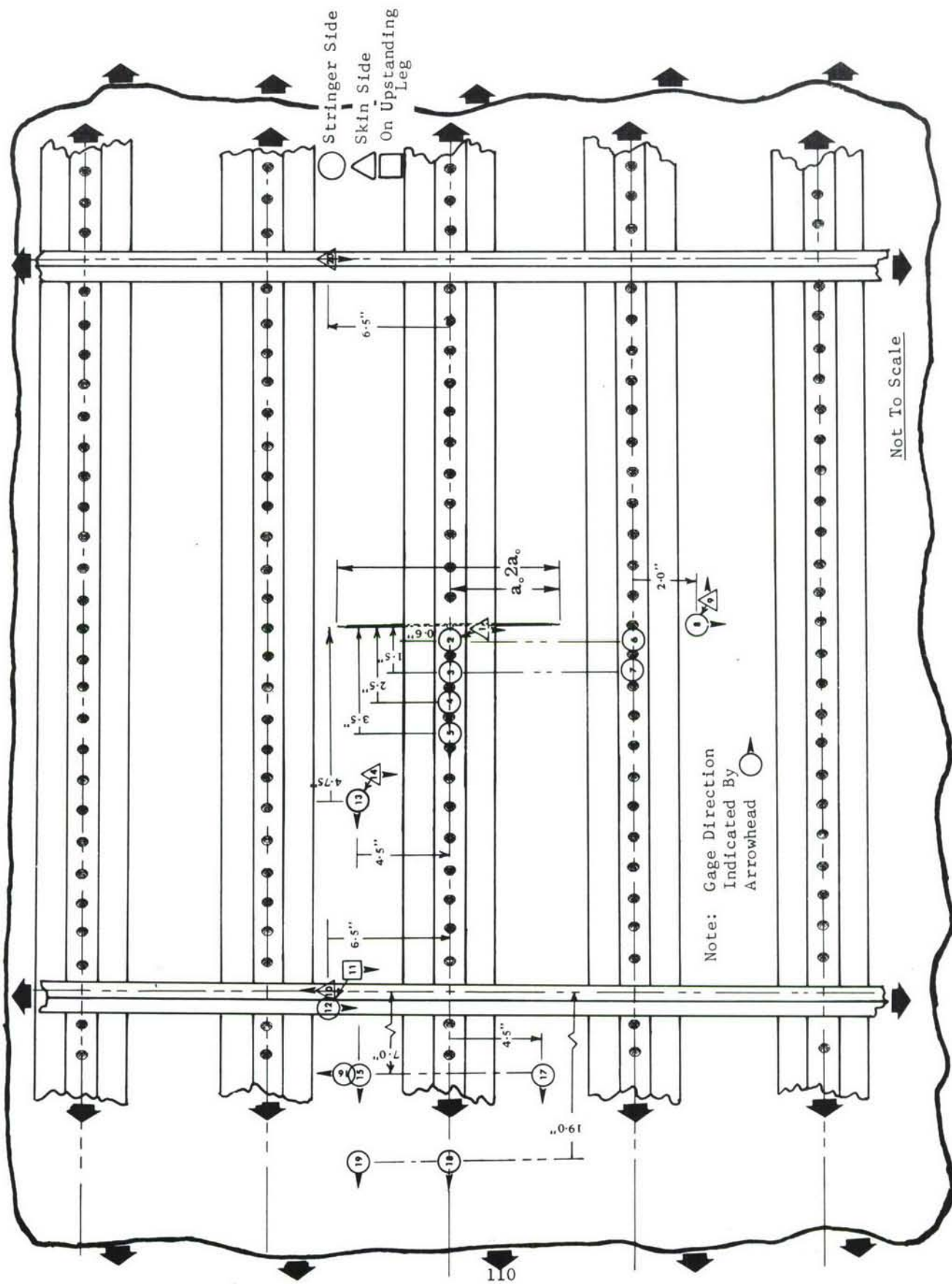


Figure 74. Strain Gage Locations - Biaxial Panels

TABLE XIV STRAIN GAGE DATA, 2-3 BIAXIAL PANEL

PANEL	LOAD Axial P _X (kip)	LATERAL P _Y (kip)	BIAXIAL RATIO LATERAL/ (kip)Axial	GAGE LOCATION AND STRAIN X 10 ³ INCHES/INCH																
				①	②	③	④	⑤	⑥	⑦	⑧	⑨	⑩	⑪	⑫	⑬	⑭	⑮	⑯	Δ _A
2-3 (2a = 8.5")	6	0	.002	.214	.098	0	.098	N	.003	-.069	-.001	.004	0	-.001	.004	0	-.004	.003	.001	.003
STRAIN	12	0	.006	.464	.280	.220	.214	T	-.018	-.011	-.040	-.006	-.024	.080	-.089	.076	-.026	.074	-.077	-.063
SURVEY	12	12	1.6	.449	.465	.240	.173	T	-.039	-.029	-.089	-.011	-.050	.180	-.057	.183	-.036	.174	.195	.167
	12	6	.5	.274	.472	.264	.193		.197	.064	.099	.017	.153	.174	.039	.165	.105	.132	.195	.182
	18	6	.33	.281	.722	.421	.316	R	.311	.021	.078	.008	.010	.125	.271	.003	.270	.070	.233	.314
	18	12	.67	.461	.711	.395	.289		.300	.097	.177	.145	.036	.263	.245	.107	.252	.168	.210	.327
	18	18	1.0	.662	.692	.363	.258	E	.280	.198	.305	.289	.059	.425	.209	.238	.227	.280	.185	.338
	18	0	0	.080	.077	.432	.336	C	.314	-.049	-.017	-.123	-.011	.014	.281	-.074	.283	-.064	.308	.264
	24	0	0	.026	.969	.599	.465		.436	-.081	-.054	-.193	-.020	-.072	.369	-.121	.399	-.099	.364	.432
	24	12	.5	.459	.964	.566	.418	O	.417	0	.078	.165	.083	.029	.260	.346	.069	.360	.134	.317
	24	18	.75	.667	.933	.554	.390	R	.398	.176	.289	.236	.055	.405	.306	.203	.333	.245	.288	.400
	24	24	1.0	.863	.899	.519	.352		.377	.285	.421	.377	.079	.571	.264	.346	.306	.354	.473	.411
	30	30	1.0	1.035	1.092	.691	.453	D	.481	D	.370	.530	.455	.100	.706	.326	.449	.394	.421	.346
	36	36	1.0	1.187	1.248	.847	.542	E	.576	E	.456	.648	.532	.116	.839	.385	.550	.479	.483	.427
	36	24	.67	.874	1.276	.907	.596		.597	D	.276	.435	.274	.071	.572	.454	.312	.521	.312	.461
	36	18	.5	.669	1.299	.842	.634		.612	D	.166	.303	.127	-.045	.406	.499	.171	.546	.205	.487
TAPE DATA	ZERO	ZERO	ZERO	.02	.02	.02	.02	0	0	0	.02	0	0	.02	.02	.02	.02	.02	.02	.02
ONLY	29.3	0	0	.08	1.18	.86	.70	.56	.60	.62	-.08	.58	-.20	-.02	-.12	-.12	-.12	-.12	-.12	-.12
	29.3	15	.51	.50	1.08	.80	.60	.46	.52	.54	.28	.54	.14	.06	.28	.28	.28	.28	.28	.28
	29.3	30	1.02	.88	1.02	.68	.54	.40	.45	.48	.62	.42	.40	.06	.70	.70	.70	.70	.70	.70
	29.8	0	.03	1.50	1.16	.98	.85	.78	.80	.85	-.15	.68	-.32	-.07	-.17	-.17	-.17	-.17	-.17	-.17
	39.8	42	1.055	1.116	1.28	.90	.73	.60	.60	.62	.82	.58	.54	.10	1.00	1.00	1.00	1.00	1.00	1.00
	51.2	54	1.055	1.45	1.60	1.16	.96	.80	.80	.82	.98	.80	.66	.13	1.32	1.32	1.32	1.32	1.32	1.32
	57	60	1.053	1.56	1.76	1.28	1.06	.90	.90	.92	1.06	.92	.70	.14	1.48	1.48	1.48	1.48	1.48	1.48
	73.8	80	1.05	2.06	2.16	1.63	1.38	1.15	1.17	1.18	1.40	1.22	.93	2.20	2.20	2.20	2.20	2.20	2.20	2.20
	84	90	1.07	2.26	2.40	1.86	1.56	1.33	1.34	1.35	1.50	1.42	1.00	.23	2.34	2.34	2.34	2.34	2.34	2.34
	120	120	1.0	—	—	2.48	2.20	1.93	—	1.92	1.90	2.02	1.16	.26	3.03	3.03	3.03	3.03	3.03	3.03
	150	120	.8	—	—	3.30	2.90	2.63	—	2.60	1.78	2.82	1.06	.28	3.20	3.20	3.20	3.20	3.20	3.20
	180	120	.67	—	—	4.23	3.73	3.53	—	3.52	1.73	3.83	.90	.30	3.16	3.16	3.16	3.16	3.16	3.16
FAILURE	181	120	.66	—	—	4.68	4.22	4.26	—	4.72	2.08	8.80	.96	.30	3.26	3.26	3.26	3.26	3.26	3.26
POST FRACTURE	ZERO	ZERO	.10	.26	.70	.26	.88	.30	OUT	1.28	OUT	-.54	.02	.48	—	—	—	—	—	—

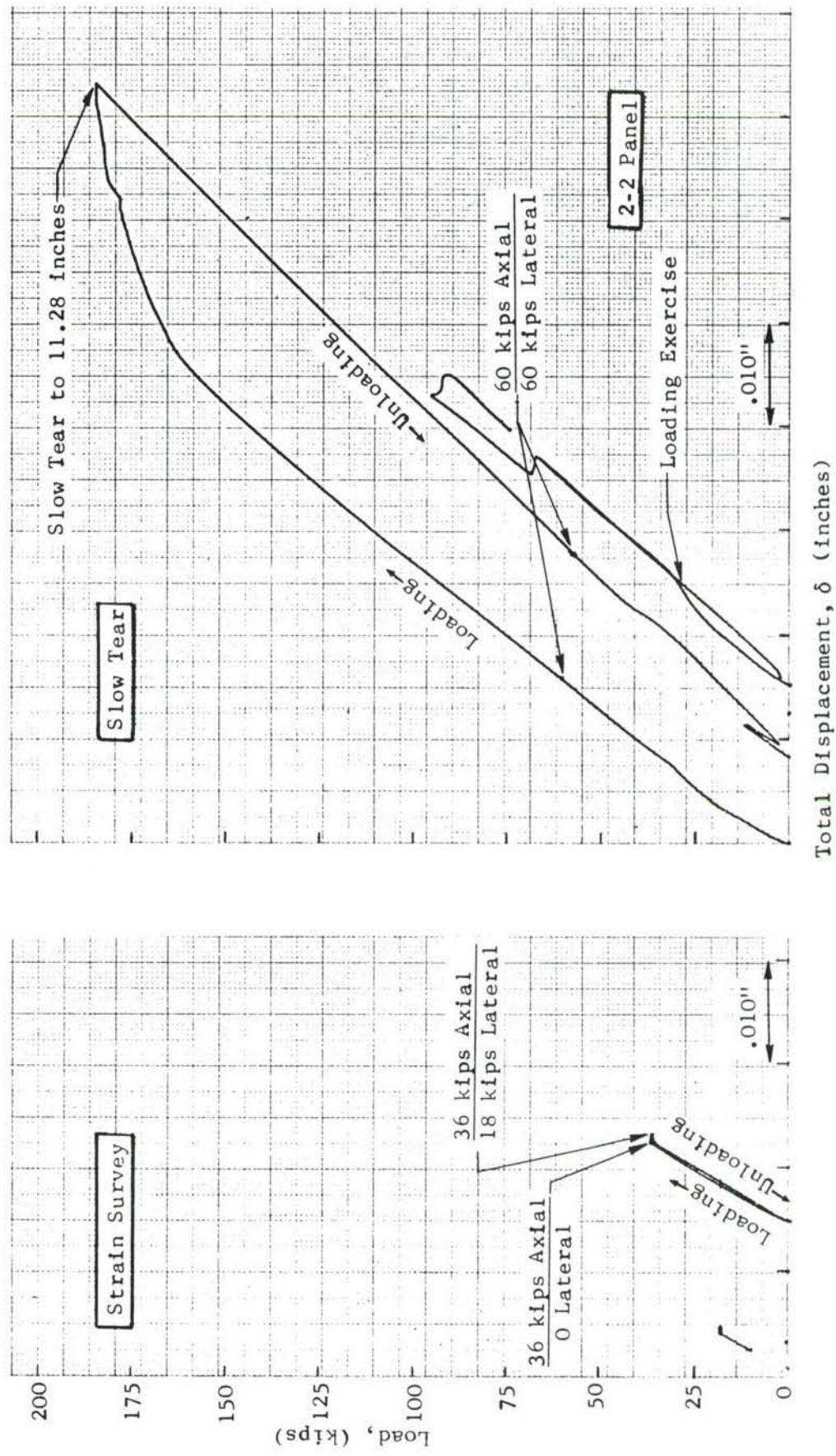


Figure 75. Load-Displacement Curves for Biaxial Panel 2-2 During Strain Survey and Slow Tear

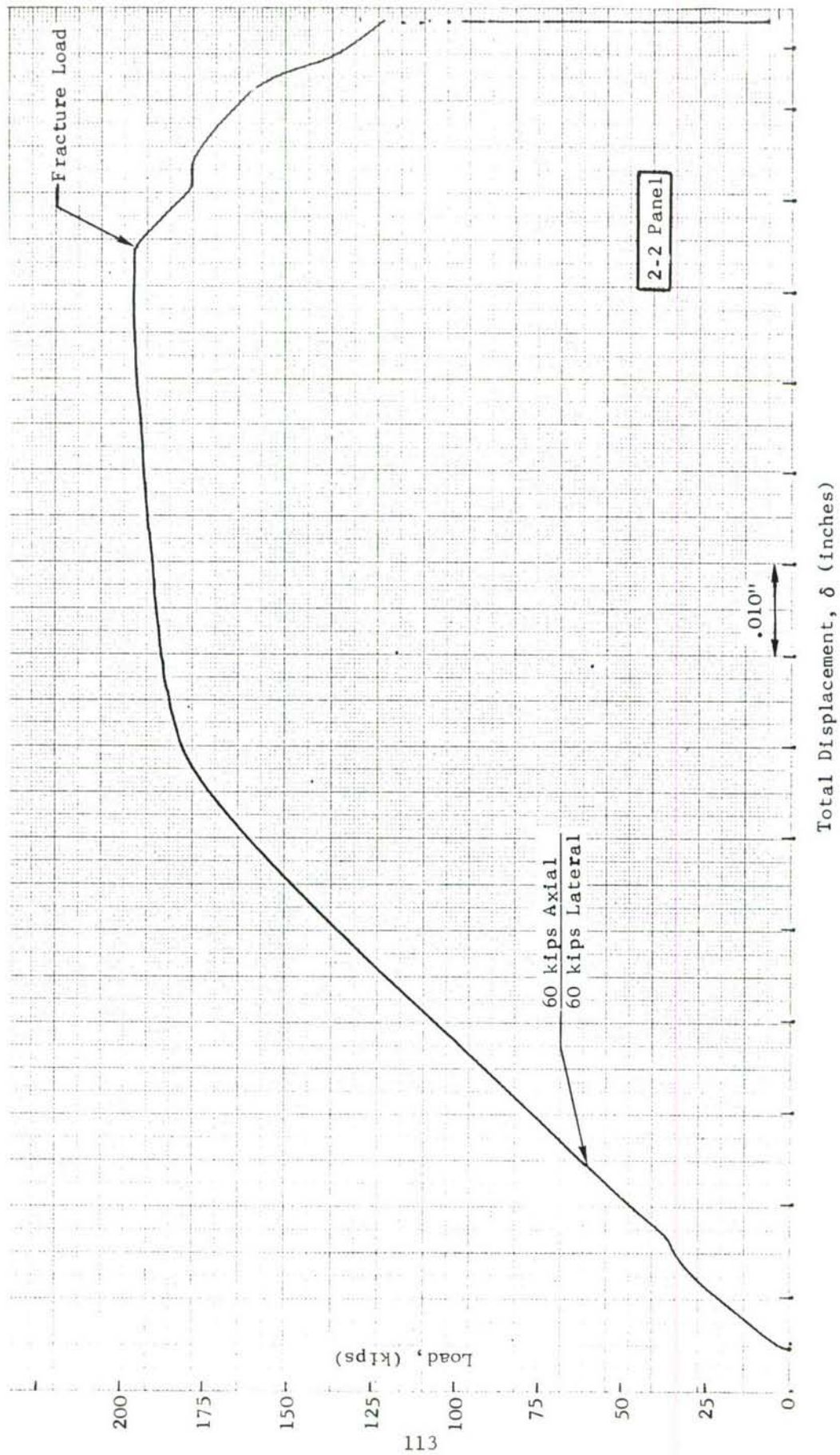


Figure 76. Load-Displacement Curve for Biaxial Panel 2-2 to Fracture After Slow Tear

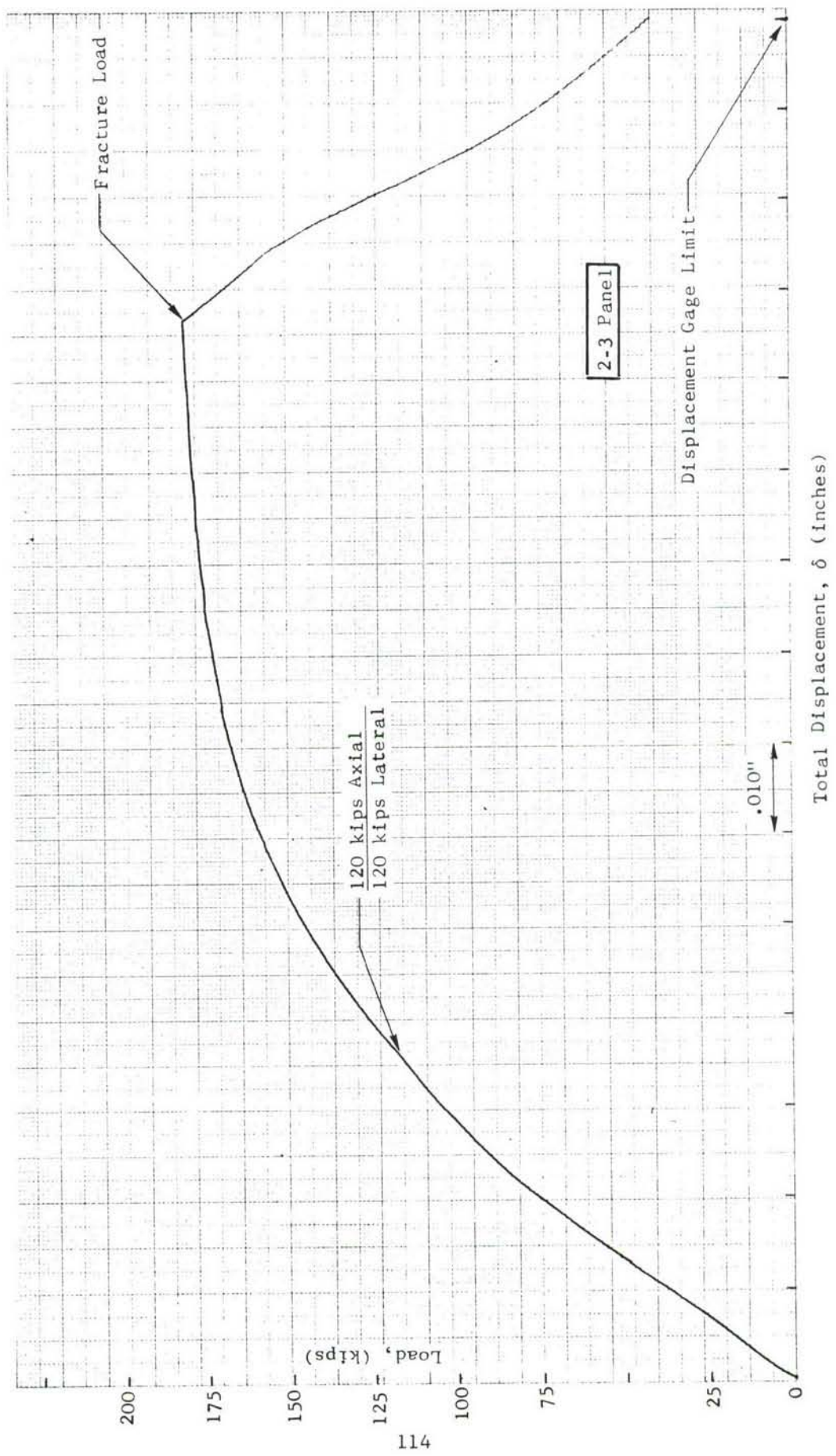


Figure 77. Load-Displacement Curve for Biaxial Panel 2-3 to Fracture

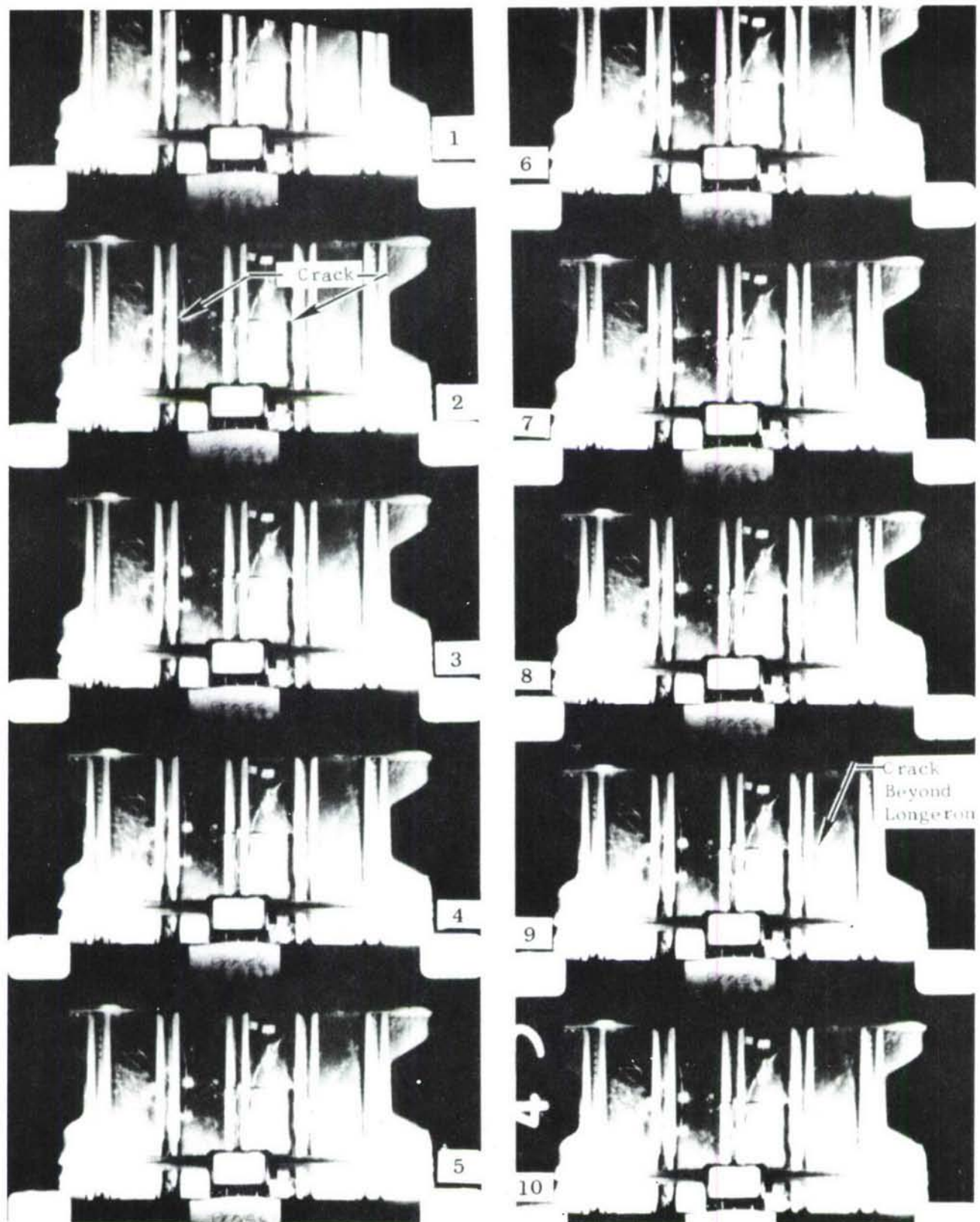


Figure 78. Fracture Sequence for 2-2 Biaxially Loaded Panel (60 kips Lateral Load)

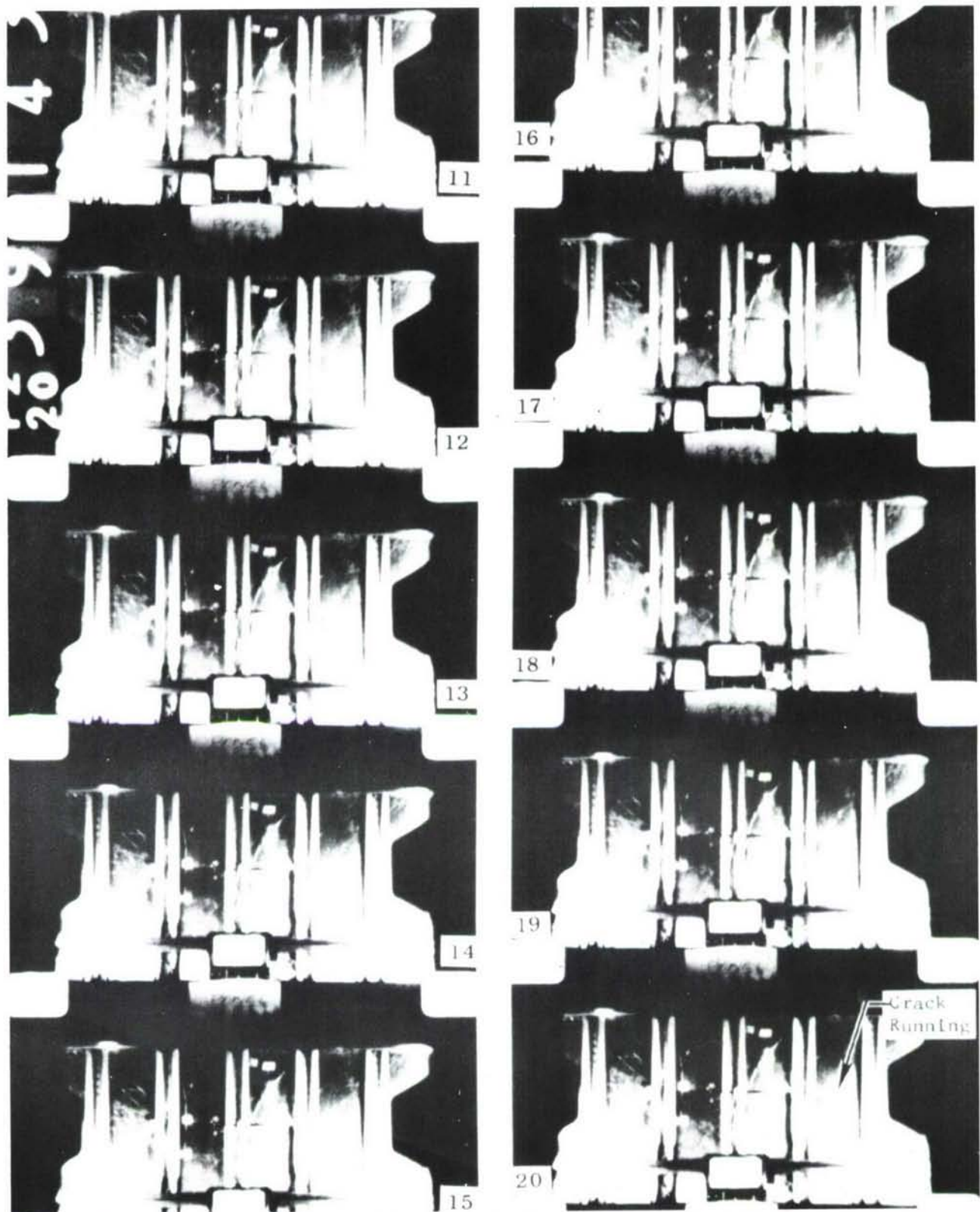


Figure 78. Fracture Sequence for 2-2 Biaxially Loaded Panel (60 kips Lateral Load) (Continued)

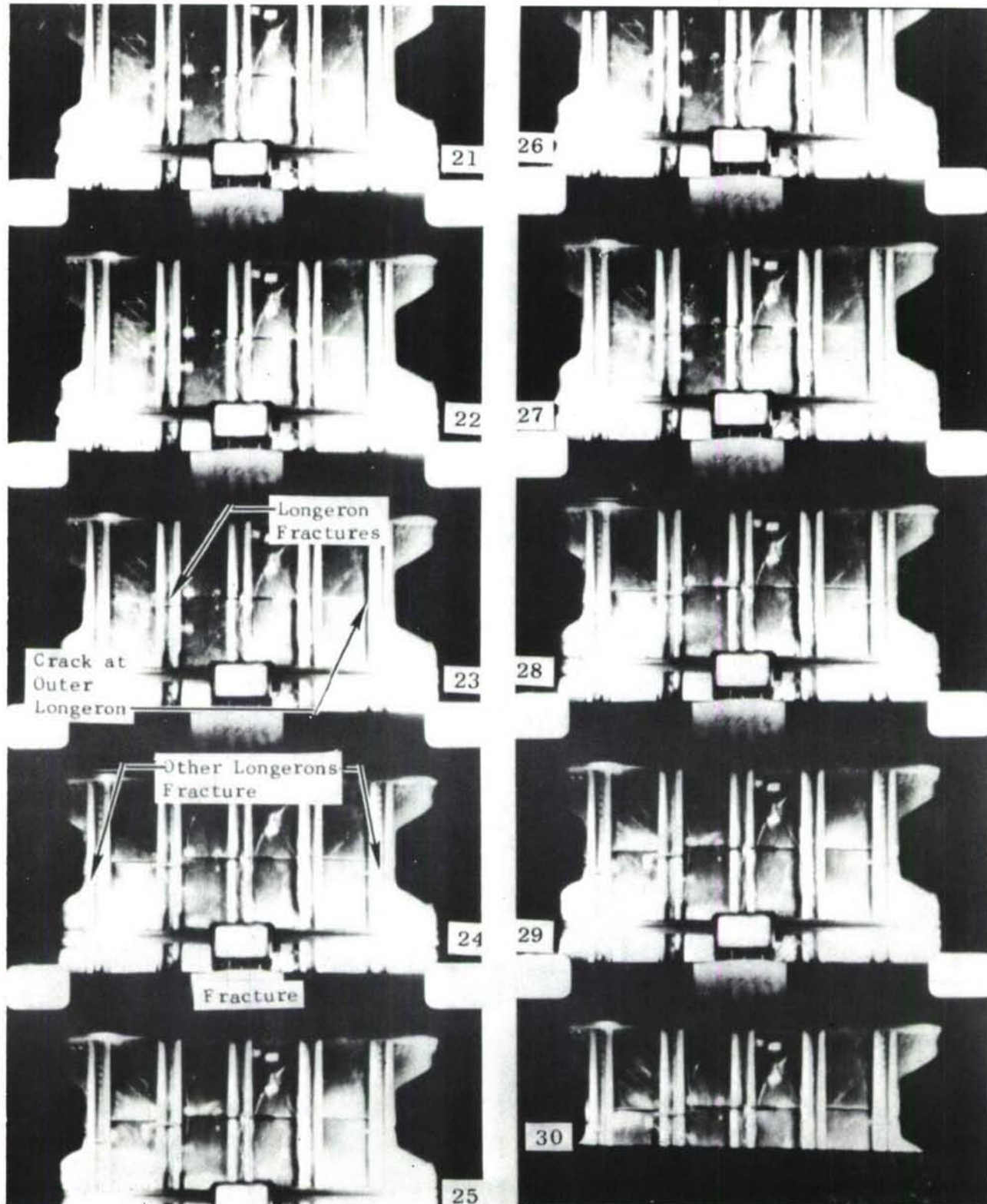


Figure 78. Fracture Sequence for 2-2 Biaxially Loaded Panel (60 kips Lateral Load) (Continued)



Figure 79. Fracture Sequence for 2-3 Biaxially Loaded Panel (120 kips Lateral Load)



Figure 79. Fracture Sequence for 2-3 Biaxially Loaded Panel (120 kips Lateral Load) (Continued)

Fracture surfaces of the 2-2 panel (60 kip lateral load at fracture) are shown in Figure 80 for the skin side and in Figure 81 for the longeron/frame side. At fracture the crack ran to (and through) the fastener holes in the adjacent longerons. The frames remained intact and four of the longerons fractured along the crack path. In the longeron which did not fail in the test section shearing of rivets was quite prevalent (see Figure 81).

Figures 82 and 83 show the fracture surfaces of the skin and angle side for the 2-3 panel (120 kip lateral load at failure). As indicated in the failure sequence for the 2-3 panel in Figure 79 the path was jagged and failure progressed from one doubler across the panel to the unzipping in the longeron area on the opposite side of the panel.

3.4.2 Comparison of Experimental and Analytical Data

Figure 74 shows the location of strain gages for the biaxial panels. Tabulated in Tables XIII and XIV are the strain gage readings for various applied loads. Figure 84 shows the variation of strain in the central stringer with applied stress for various biaxial stress ratios. The strains in the stringer at 1.5 and 2.5 inches from the crack plane show good correlation with analytical results for biaxial ratios of 1:0, 1:0.5 and 1:1. However the strain at 0.6 inch from the crack plane differs considerably from the analytical results. Figure 85 shows the variation of strain in the central stringer (longeron) and the stringer 9 inches away from the centerline of the crack, with applied stress for a constant lateral load (P_x) of 60 kips. This constant lateral load of 60 kips results in different biaxial load ratios, depending on the applied load normal to the crack surface. The experimental strains are shown for an initial crack length of 8.4 inches and "post tear" crack length of 11.28 inches. Analytical strains for a crack length of 8.5 inches are also noted in Figure 85. The correlation between experimental and analytical strains in the stringer (longeron) located 9 inches from the centerline of the crack, is good. The strains in the central stringer show a good agreement with analytical results at all but low applied stresses. The analytical strains for a crack length of 11.28 inches were not calculated so no comparison could be made.

Figure 86 shows the variation of strains in the frame members for three biaxial stress ratios, 1:0, 1:0.5 and 1:1. Analytical strains obtained from the finite element analysis are also noted. For zero biaxial load the strains in the flange and upstanding leg (web) show a good agreement with analytical results. However, strains in the attached leg show a considerable variation from the analytical results. At other biaxial load ratios, the strains in the flange portion of the frame show good agreement with the analytical data but strains in the attached and outstanding legs (web) differ considerably from the analytical results. This discrepancy between analytical and experimental attached leg strains is perhaps due to the simplified attachment model combined with the method of load application used in the finite element analysis. In the finite element model individual rivets connecting the frame to the skin were not modeled but were represented by shear elements having a width of one inch. It was also assumed that at the side of the panel the biaxial (lateral) load was uniformly distributed over a width of 13 inches.

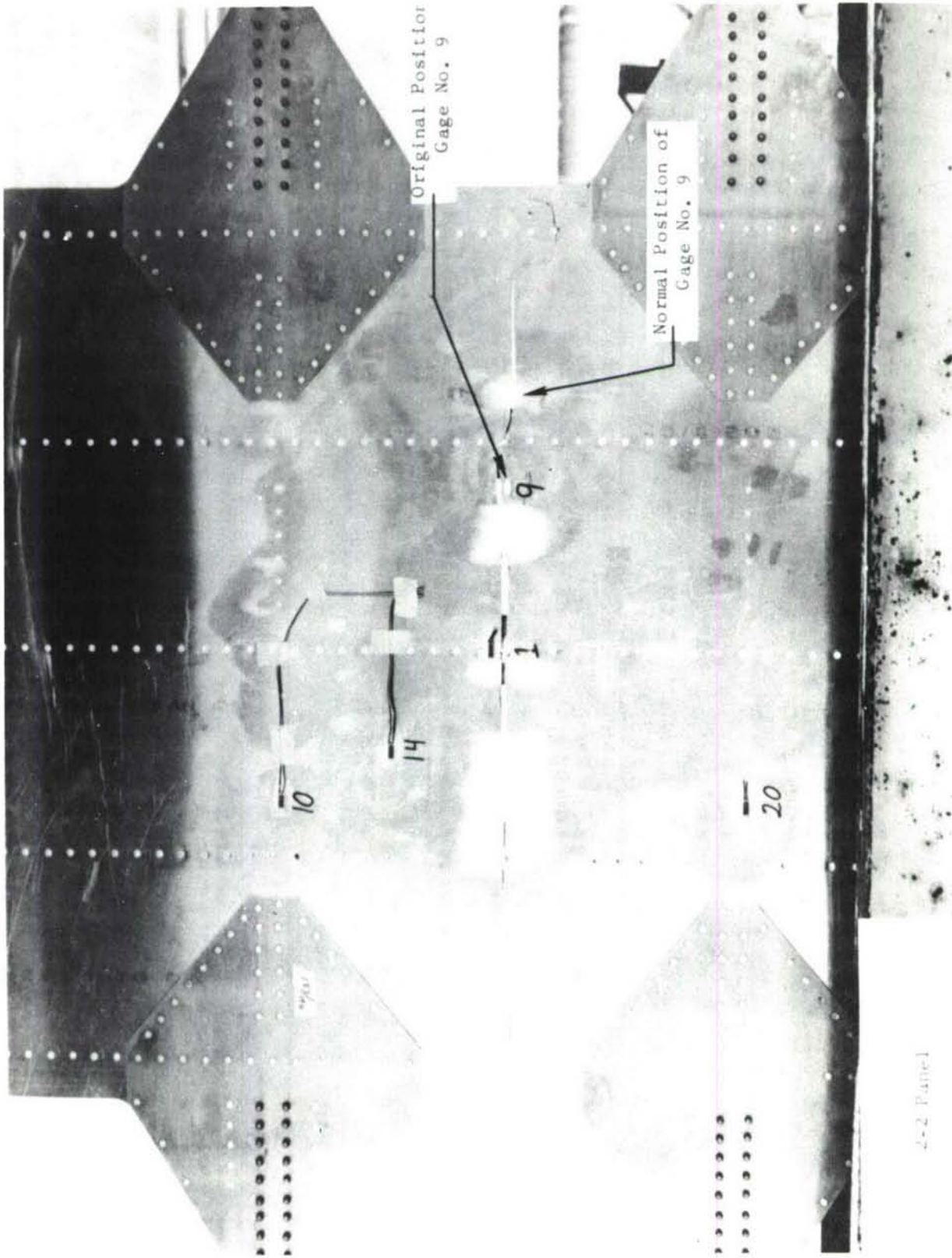


Figure 80. View of Fracture Surface from Skin Side, 2-2 Biaxially Loaded Panel

2-2 Panel

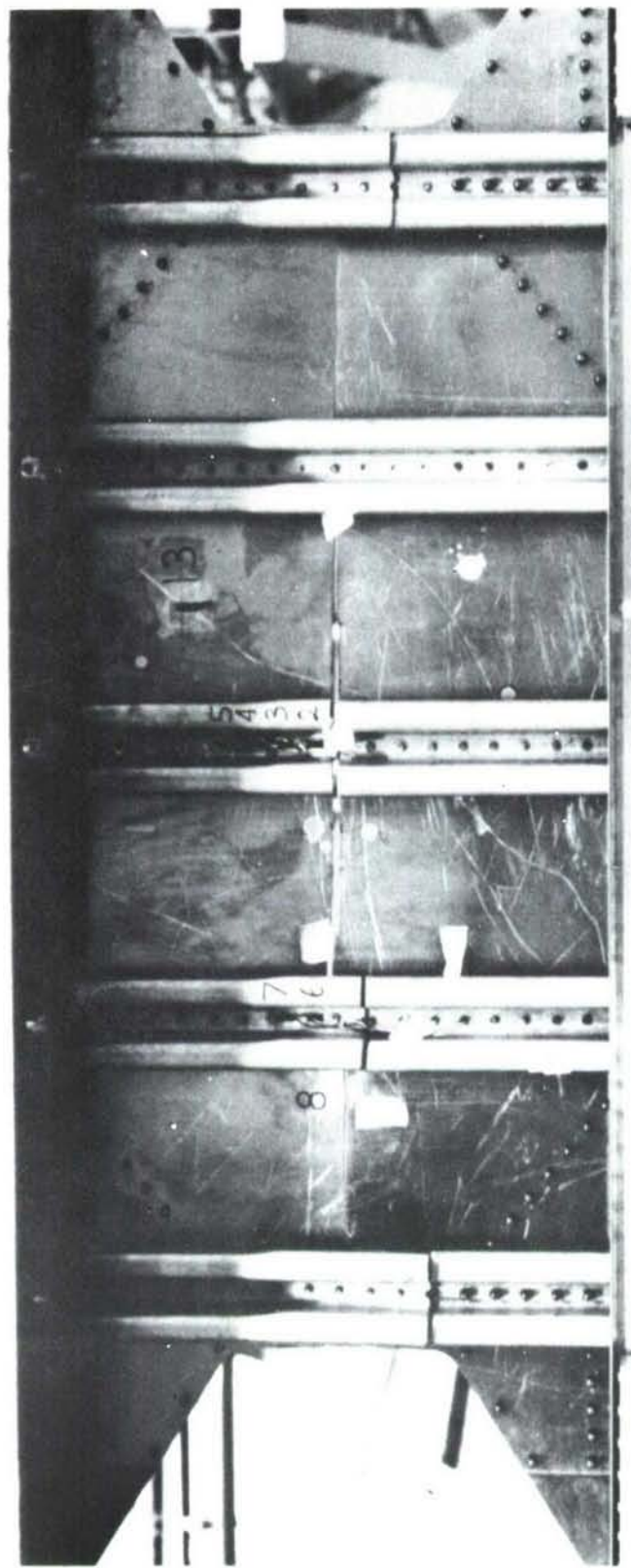
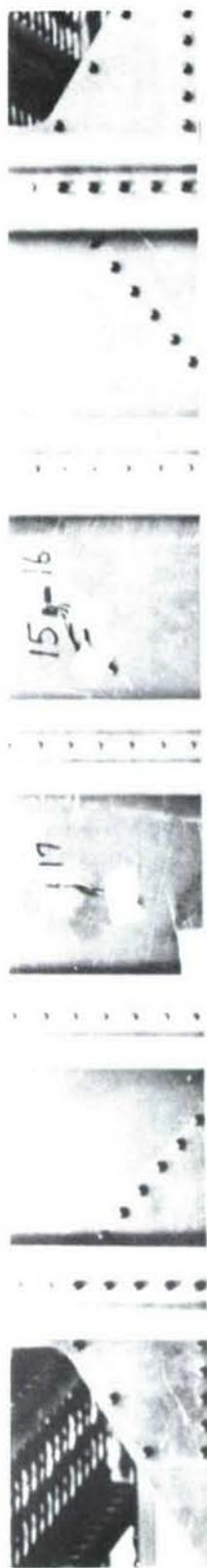


Figure 81. View of Fracture Surface from Longeron/Frame Side, 2-2 Biaxially Loaded Panel

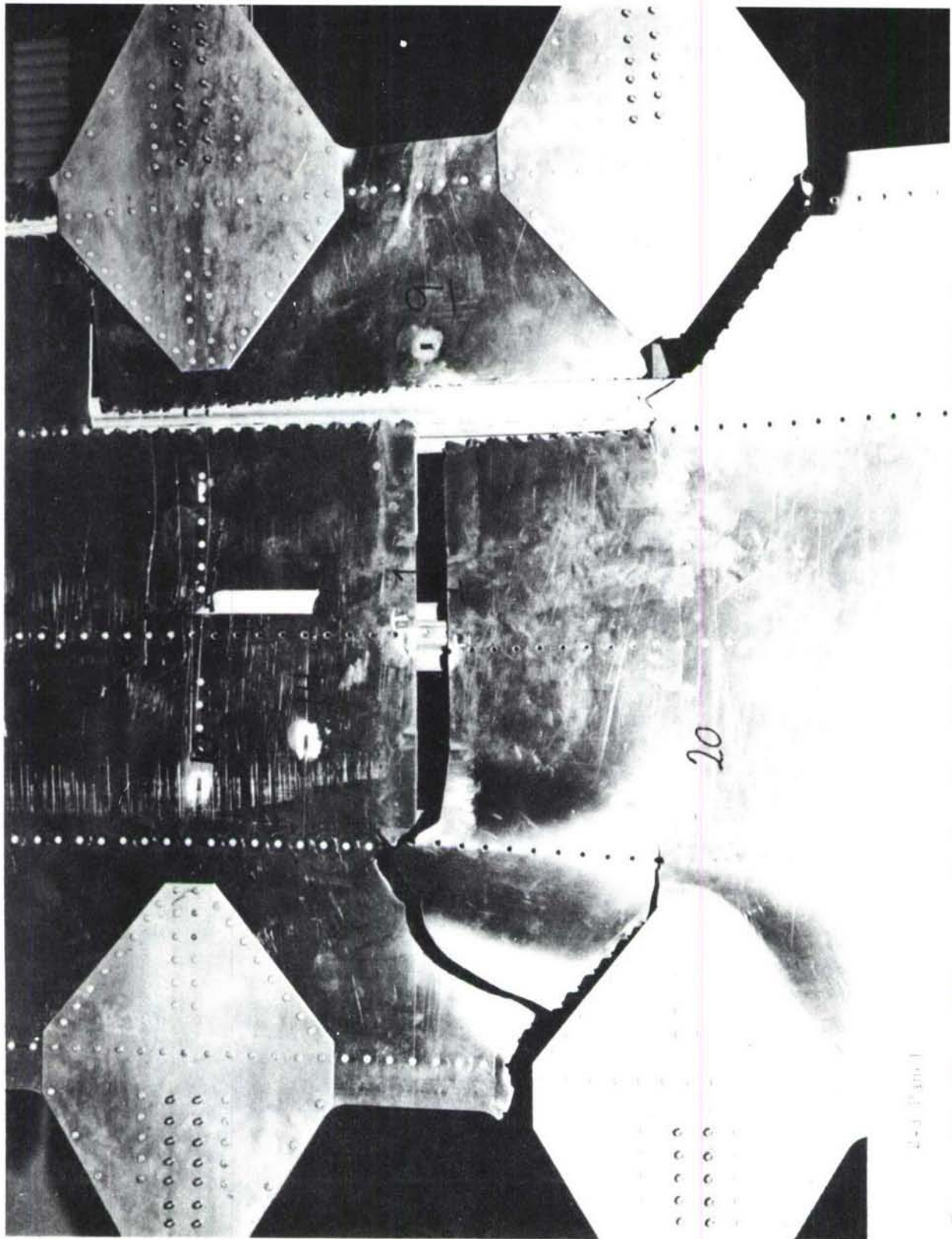


Figure 82. View of Fracture Surface from Skin Side, 2-3 Biaxially Loaded Panel

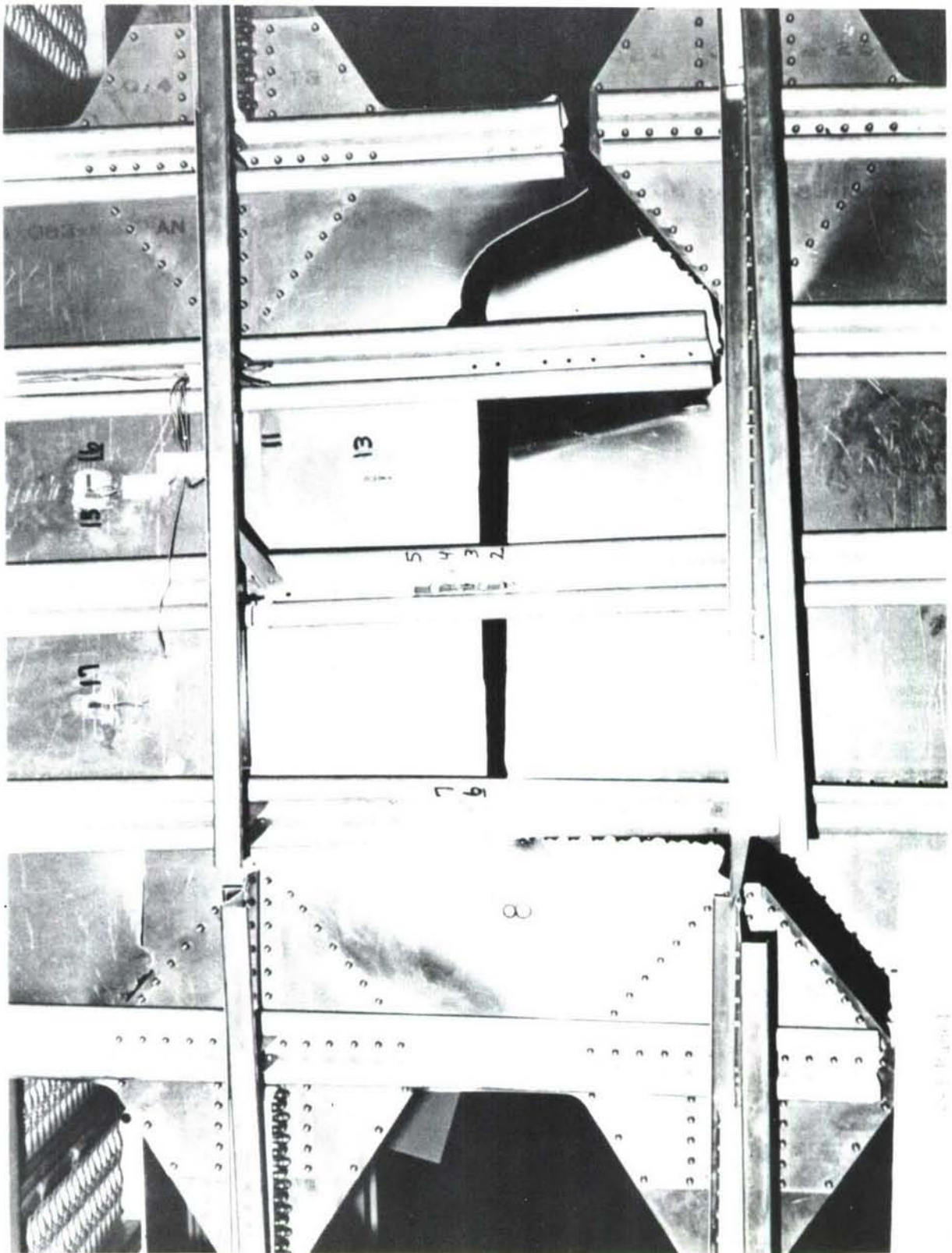


Figure 83. View of Fracture Surface from Longeron/Frame Side, 2-3 Biaxially Loaded Panel

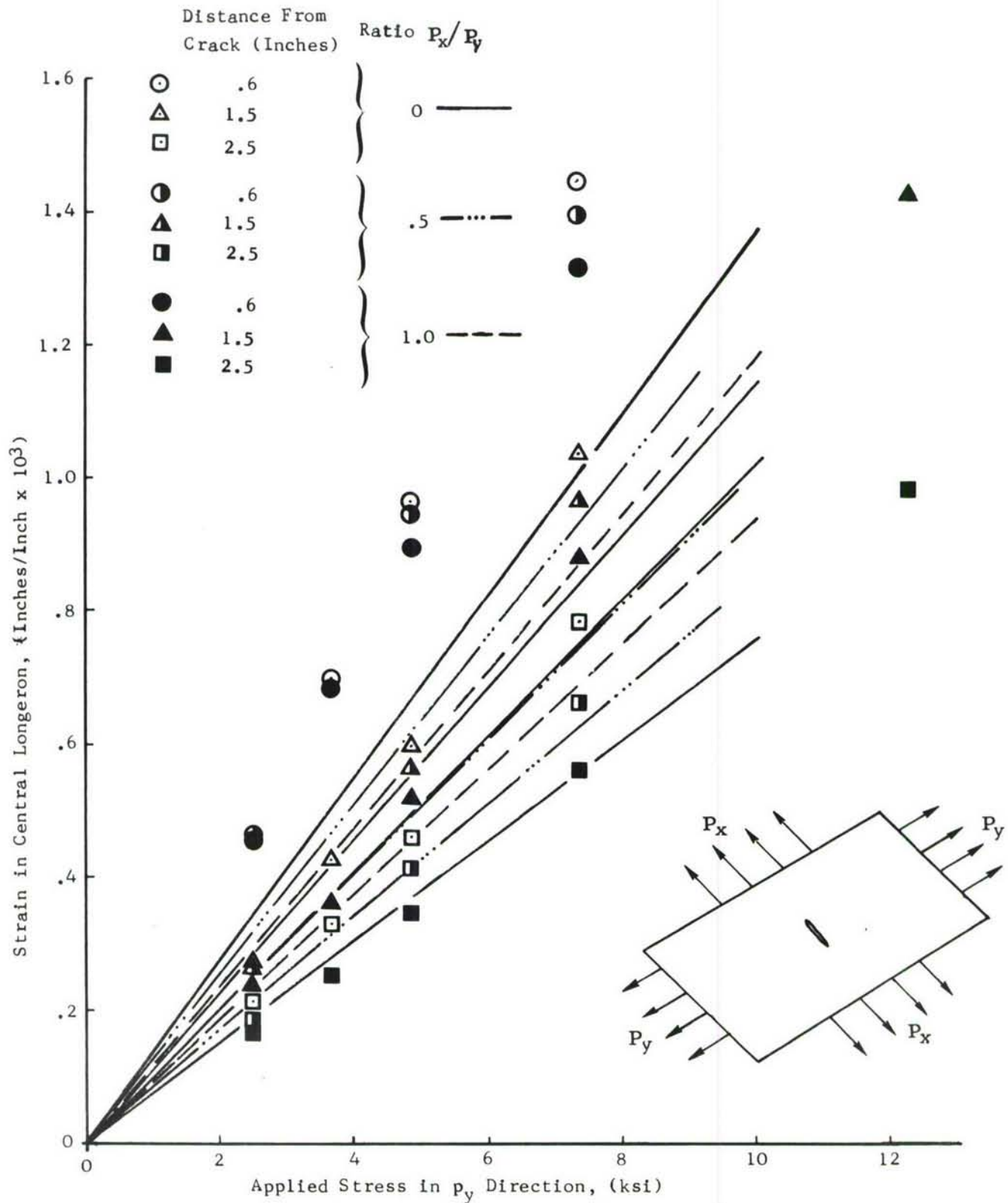


Figure 84. Strain in Central Longeron Away From the Crack at Three Biaxial Load Ratios

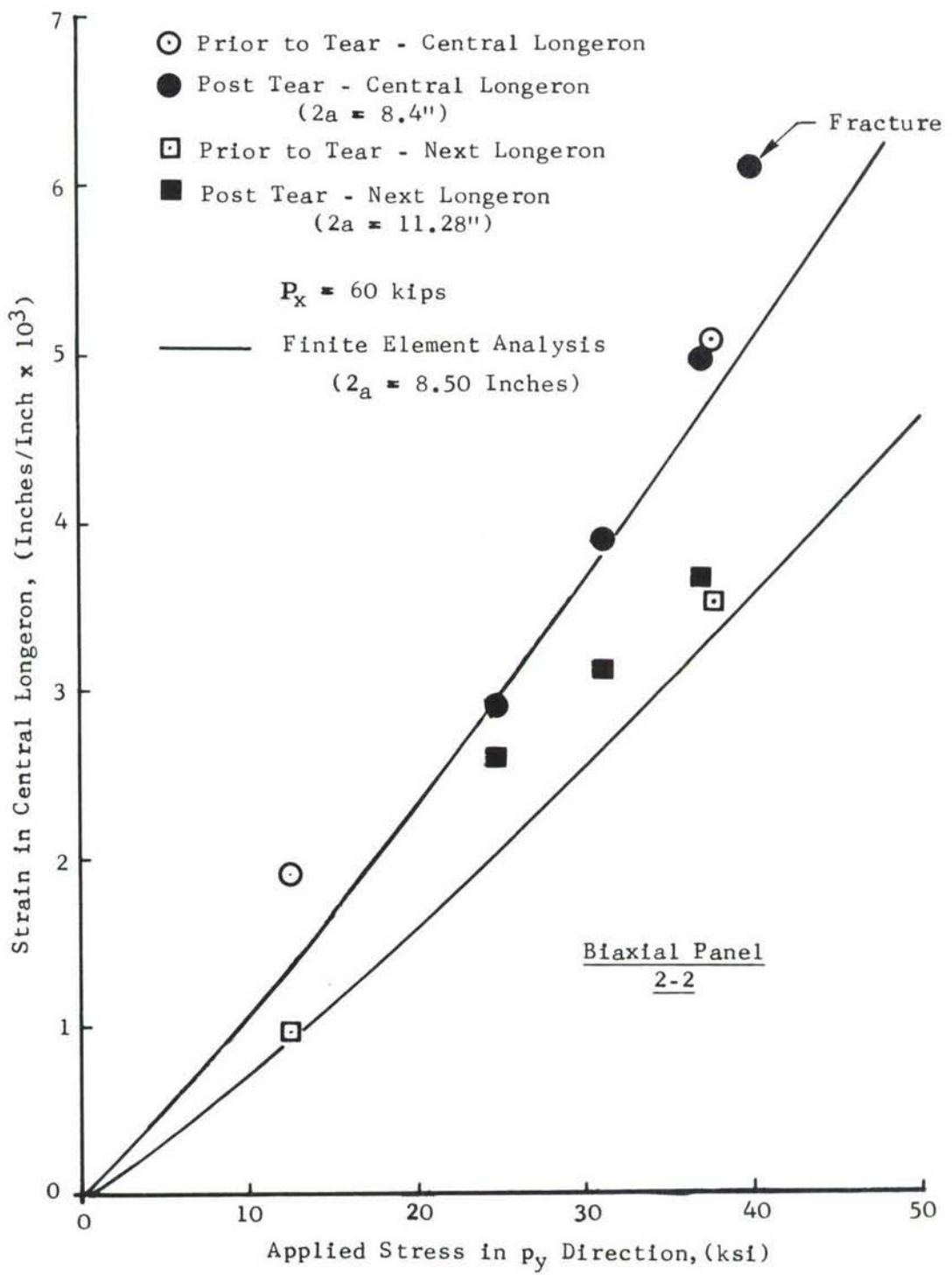


Figure 85. Strain in Longeron(s) at 0.6 Inches Away from the Crack,
Biaxial Panel 2-2

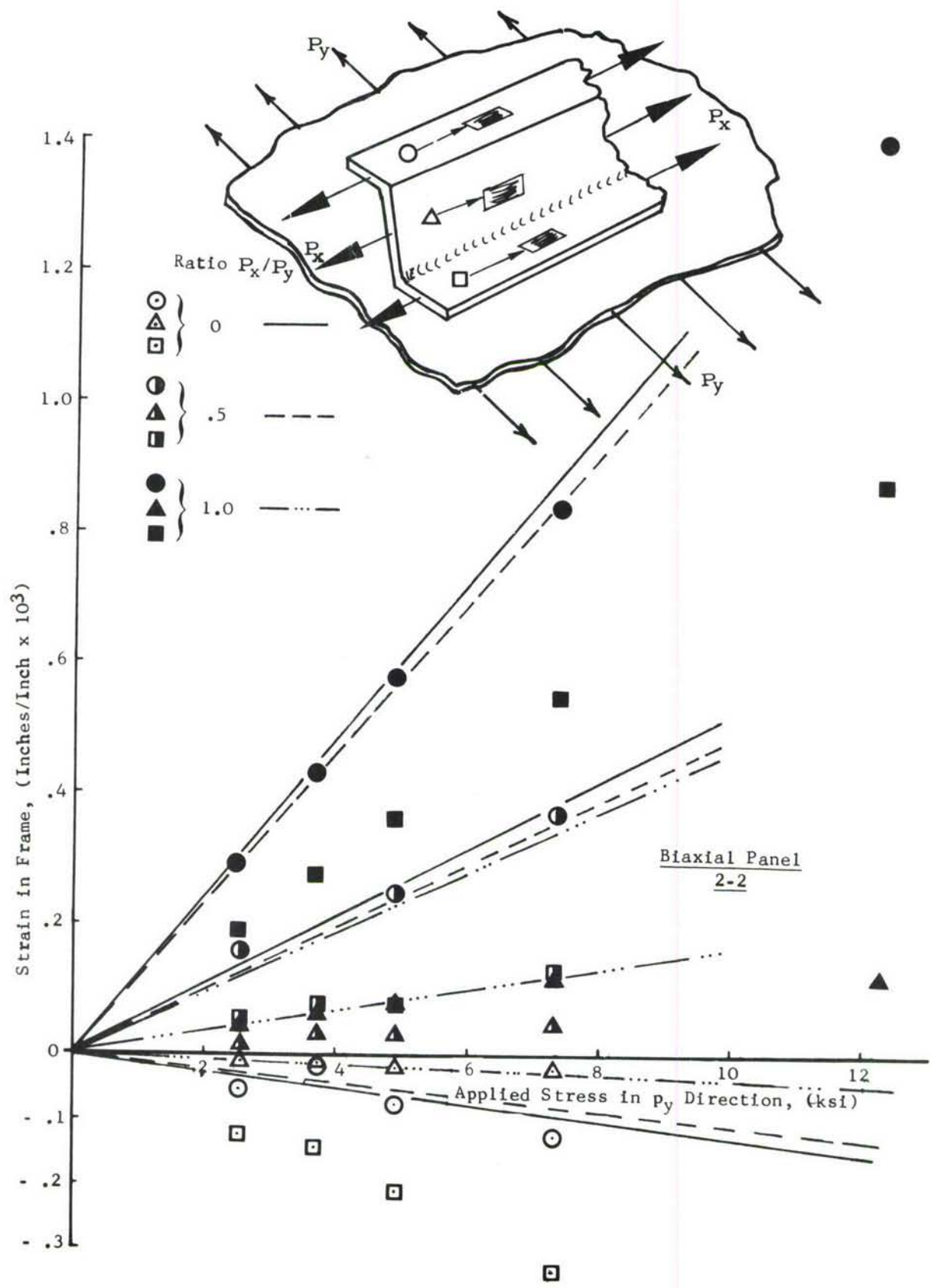


Figure 86. Strain in Frame Member as a Function of Applied Stress for Three Biaxial Load Ratios

Figure 87 shows the experimentally observed crack surface openings at the center of crack (and panel) as a function of applied stress for zero biaxial load and a biaxial load ratio of 1:1. Also indicated in Figure 87 are the analytically derived crack openings. The agreement between analytical and experimental data is excellent. The application of a biaxial (lateral) load increases the crack openings as was observed both analytically and experimentally for these panels.

3.5 RESIDUAL STRENGTH PREDICTION

For uniaxially loaded panels the residual strength prediction was based on a Dugdale type elastic-plastic analysis and $\sqrt{J_R}$ resistance curve of the material. The $\sqrt{J_R}$ resistance curve of the material was obtained from tests on the crack line wedge loaded specimen. There are no biaxial loads applied in obtaining $\sqrt{J_R}$ resistance curve. The influence of biaxial loading on the resistance curves of a material has not been studied. It was not feasible to study this influence in this program, hence it was decided to use the $\sqrt{J_R}$ resistance curve of the material without biaxial effects. As discussed earlier, Dugdale type elastic-plastic analysis could not be performed for biaxially loaded panels and the realistic analysis of this panel should be based on Prandtl-Reuss material behavior. In order to obtain \sqrt{J} versus crack length curves for various applied loads, the elastic-plastic analysis, assuming Prandtl-Reuss material behavior, would have to be performed for various crack lengths and applied loads. This would require extremely large computer run times with prohibitive cost. In the present study an elastic-plastic analysis was performed for only one crack length and elastic analysis was performed for various crack lengths. In order to obtain \sqrt{J} versus a curves, certain approximations were made. It was assumed that for a fixed applied stress, the percentage increase in \sqrt{J} due to biaxial load and Prandtl-Reuss material behavior over elastic values was the same for all crack lengths. From Figure 67, the \sqrt{J} value for 1:1/3 biaxial load is 10 percent higher than that for the elastic 1:0 load, at an applied stress of 40 ksi. Thus it is assumed that the \sqrt{J} values for 1:1/3 biaxial load will be 10 percent higher than those \sqrt{J} values based on an elastic analysis for all crack lengths at an applied stress of 40 ksi. The percentage increase in \sqrt{J} value for other applied stresses will be different. With this assumption \sqrt{J} versus a curves for various applied stresses are shown in Figure 88 for a biaxial load ratio of 1:1/3.

The stresses in the central stringer of the biaxial panel for various applied stresses based on Prandtl-Reuss material behavior are shown in Figure 68. The ultimate stress for the stringer material from tensile test data was found to be 80 ksi. Using this ultimate stress and the stringer stress for a biaxial load ratio of 1:1/3 the failure stress is predicted at an applied stress of 56.5 ksi. In Figure 88 the resistance curve of the skin material (2024-T3, 0.063" (LT)) has been plotted at a half crack length of 4.25 inches. There is considerable slow tear at an applied stress of 40 ksi. Thus the stringer stresses shown in Figure 68 will not be valid. Also from Figure 88 it is seen that there is no point of instability within the portion of $\sqrt{J_R}$ resistance curve of the material obtained from the CLWL tests.

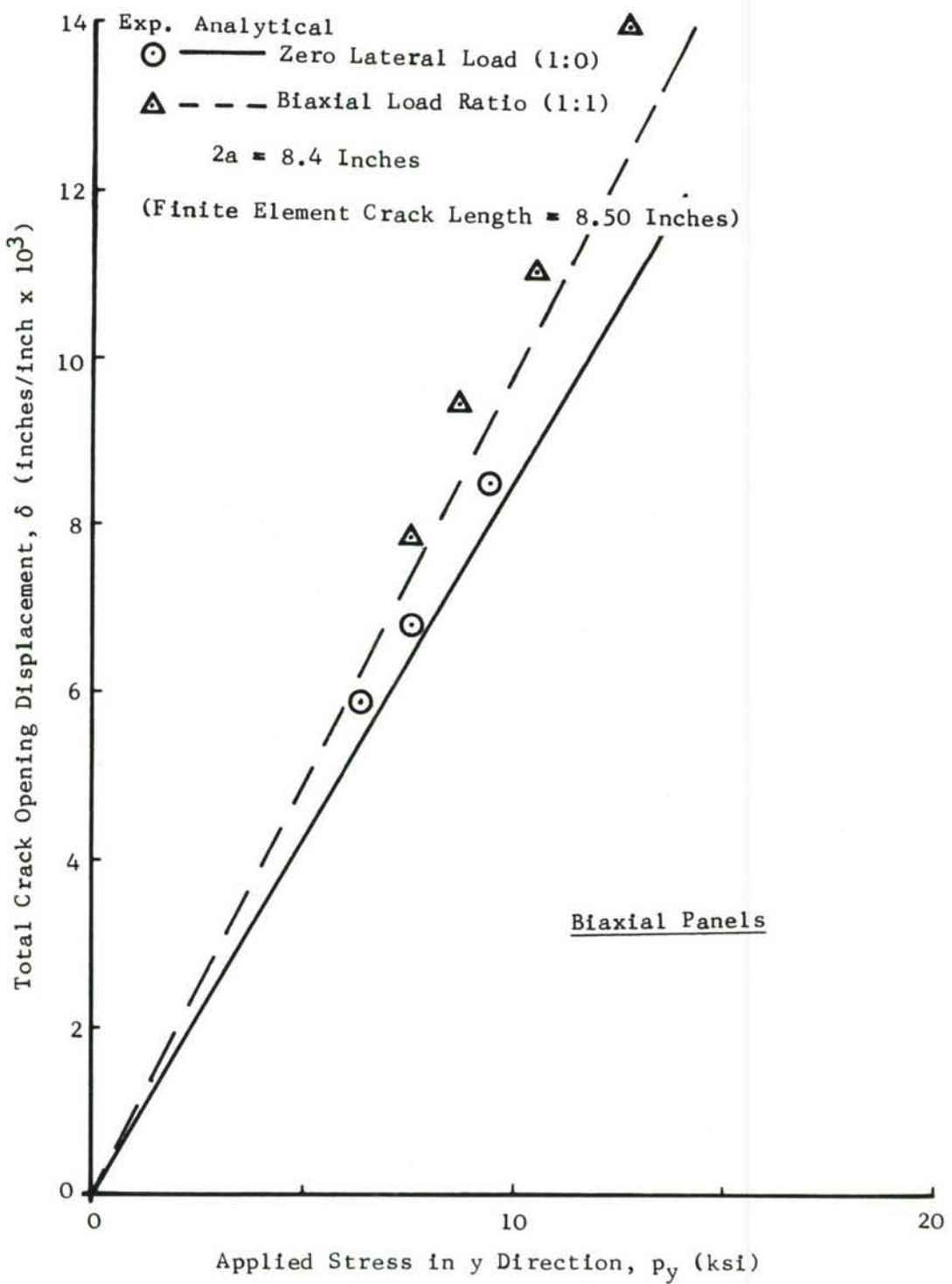


Figure 87. Total Crack Opening Displacements for Two Biaxial Load Ratios as a Function of Applied Stress

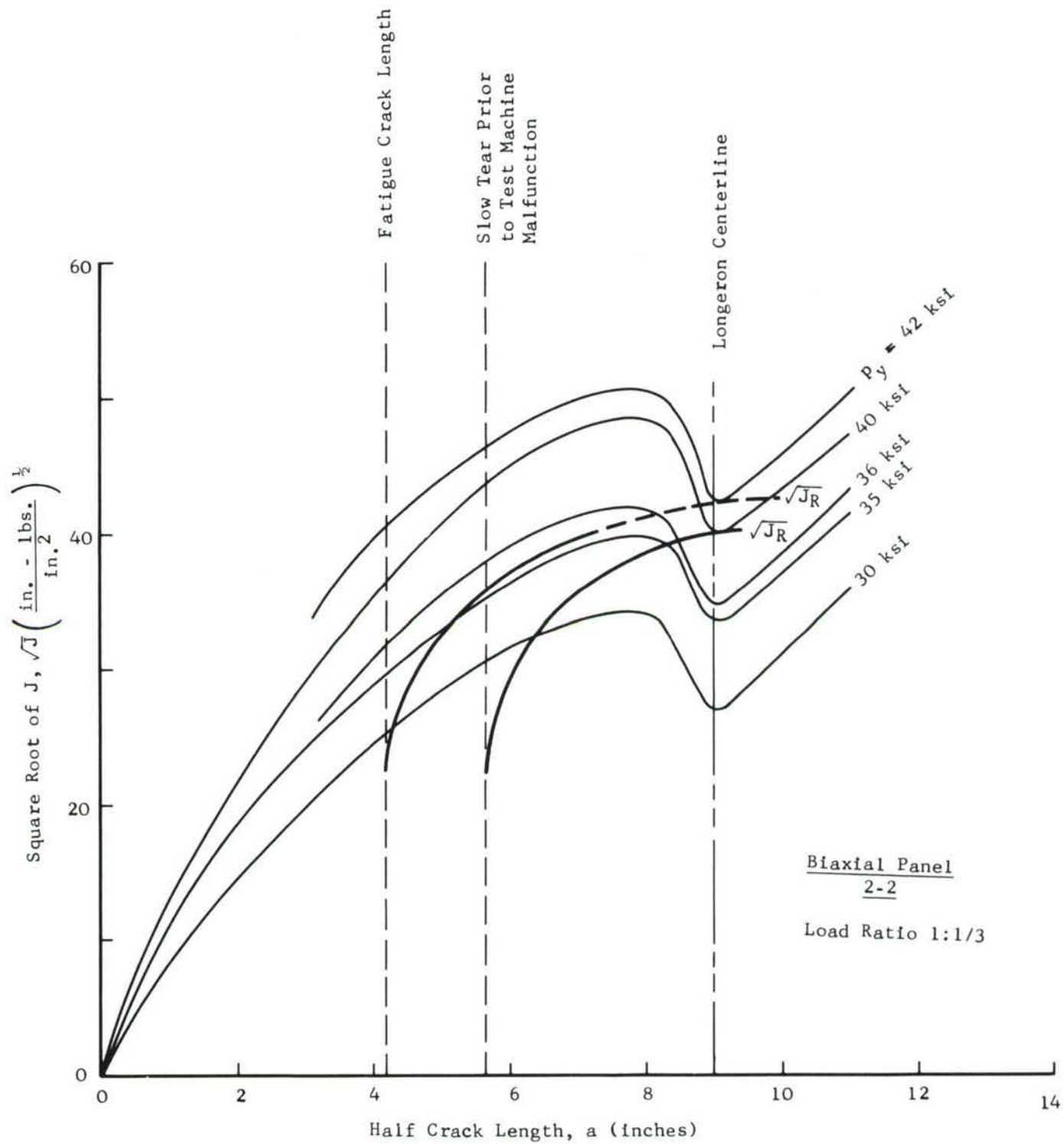


Figure 88. Square Root of J Versus Crack Length Curve for Biaxial Panel

However, if the resistance curve of the material is extrapolated the point of instability occurs at an applied stress of 42 ksi. The 2-2 panel slowly tore to a half crack length of approximately 5.63 inches and then it was unloaded. The 2-2 panel was tested again after a delay period due to equipment malfunction with this same crack length. The failure load of the panel was 195.1 kips (see Table XIII) and there was no crack arrest in the panel. In Figure 88, replotted the resistance curve ($\sqrt{J_R}$) of the material at a half crack length of 5.63 inches shows that the point of instability occurs at an applied stress of 40 ksi and \sqrt{J} values of the panel are higher than the resistance curve of the material. Hence, there should be no crack arrest in this 2-2 panel at this crack length. The predicted failure load corresponding to a stress of 40 ksi is 195.740. This is within less than one percent of the actual failure load. It must be emphasized that the \sqrt{J} versus a curves in Figure 88 are only approximate and the $\sqrt{J_R}$ curve is based on uniaxial data and hence the predicted load is only an approximation.

The approximated square root of \sqrt{J} versus a curves for the biaxial load of 1:2/3 were not plotted. Referring to Figure 67, it can be seen that for a 1:2/3 biaxial load ratio the \sqrt{J} values differ considerably from the elastic values and hence the assumptions made in obtaining the \sqrt{J} versus a curves in biaxial load ratio 1:1/3 cannot be justified. In the 2-3 panel, tested at a biaxial load ratio of 1:2/3, the crack tore to the rivet hole at the adjoining stringer and was arrested. With subsequent increase in load, the central stringer fractured and the failure started at the doublers through which biaxial load was applied to the skin. Figure 62 shows the stresses in the central stringer based on elastic analysis and zero biaxial load. Using the measured ultimate stress of the stringer material (80 ksi) and the stress in the stringer for a half crack length of 9 inches (crack length at which the crack was arrested at the longeron rivet hole) the failure of the stringer is predicted as 40.7 ksi. Due to biaxial loading the stresses in the stringer will be smaller than those shown for zero biaxial load. If an elastic-plastic analysis is considered the stresses will be larger than those shown in Figure 62. Thus, the stresses given in Figure 62 may be taken as a rough approximation of the stresses in the stringer for the 2-3 panel. The predicted "approximate" failure load is 40.7 ksi and the actual failure load of the 2-3 panel was 37 ksi.

In order to predict the failure load more accurately an elastic-plastic analysis should be performed assuming Prandtl-Reuss material behavior with biaxial load for various crack lengths. From this analysis \sqrt{J} versus crack length curves can be plotted for various applied loads. These curves should be used along with the $\sqrt{J_R}$ resistance curve, obtained under biaxial loading, to predict the residual strength for skin critical cases.

IV SUMMARY OF OVERALL PROGRAM AND PREDICTION METHOD

In an attempt to summarize the activity conducted during the time span of this program it is believed that by listing the major tasks, and including a summary of each, a fuller understanding of the scope can be appreciated. Therefore each major task will be listed in this Section along with the significant findings of the various phases.

4.1 PROGRAM SUMMARY

The objective of Phase I of this study was to analyze and evaluate the state-of-the-art of plane stress fracture analysis and to define the strong and weak points of those available methods.

It was determined that the methods could not adequately treat the problems of slow stable tear (prior to fracture) and associated crack tip plasticity, which is prevalent in higher toughness materials. The conclusion was that an ideal residual strength prediction technique should account for both of these behaviors in the method to be developed. With the ideal method in mind the development of the analytical technique and proposed failure criterion were part of the tasks of Phase II.

Phase II represented one level of complexity for the developed residual strength prediction method which was intended to treat problems of cracks in complex, uniaxially loaded structural components. To achieve this objective crack growth resistance data were developed for a wide range of aluminum and titanium alloys. These data were eventually used to establish a skin critical fracture stress in the six zee stiffened panels examined during Phase II. The six panels were grouped in three sets of two each containing the same crack size but three different methods of attachment (riveted, bolted, and bonded). This allowed for refinement of the fastener model and procedural steps. The conditions for a skin or stiffener critical situation were also established. During the development of the analytical method the path independency of the J integral for stiffened panels was demonstrated along with the first complete elastic-plastic analysis of a stiffened structure assuming both Dugdale and Prandtl-Reuss material behavior. In order to establish an elastic-plastic data base, a nonlinear analysis was performed on the crack line wedge loaded specimen geometry which permitted the introduction of the J_R resistance curve for skin critical structure. The results of several fracture criterion sub-studies indicated that crack extension occurs at very low values of stress intensity for anticipated plane stress material behavior and the specimen independency of the crack growth resistance curve.

A ten step residual strength predictive procedure was established based on the results of Phase II of the program.

The Phase III objective, reported on in this report, was to test, evaluate, and verify the capability of the residual strength predictive technique of Phase II. This involved one additional level of panel complexity and the addition of a biaxial loading condition for fuselage structure. During the course of the analysis of these biaxially loaded panels the effect of load transfer to intact stringers was determined and the ability to predict crack

arrest was verified using the J-integral approach. The question of a biaxial crack growth resistance curve for use as the failure criterion under this type of loading has been explored.

Six complex structural panels have been fracture tested (two biaxial panels) and predictions made of their residual strength. The predicted values were in good agreement with the experimental data.

4.2 PREDICTIVE PROCEDURE (STEPS)

Reference 1 (Section 8.1) detailed the steps involved in the residual strength prediction method and will not be repeated here except in summary form. It should be noted that the inclusion of biaxial or multiaxial states of stress have required additions to the basic procedure (see e.g., Steps 3 and 8). However, the basic outline remains the same and Reference 1 should be consulted for additional details

Step

- 1) Make a detailed finite element model.
- 2) Select crack length(s) for evaluation.
- 3) Perform the analysis based on Dugdale or Prandtl-Reuss material behavior - stress state dependent.
- 4) Determine stresses in the intact stiffeners.
- 5) Determine the value of \sqrt{J} for each applied stress to material yield strength ratio (p/F_{ty}) for each crack length.
- 6) Cross plot the data of Step 5 to form the crack driving force curves.
- 7) Determine the value of normalized applied stress in the intact stiffeners at stiffener ultimate strength.
- 8) Obtain crack growth resistance data for the skin material in uniaxial tension or biaxial loading.
- 9) Plot $\sqrt{J_R}$ versus Δa_{PHY} . curve from the data of Step 8.
- 10) Overlay the data from Step 9 on the crack driving force curves of Step 6 and determine the amount of slow stable tear - if minimal (≥ 0.25 inches) a stiffener critical condition is operative otherwise it becomes a skin critical case and both residual strength, slow tear, and crack arrest can be determined from tangency conditions.

V CONCLUSIONS

The following conclusions have been reached based on the studies undertaken in Phase III of this study. Following the conclusions a Table is given in Section 5.2 which summarizes the accuracy of the prediction technique for both Phase II and Phase III panels.

5.1 GENERAL TRENDS

The flexible fastener model developed in Reference 1 can be used to treat load transfer in complex structural arrangements under complex loading conditions. Dugdale material behavior can be assumed for uniaxially loaded panels, Prandtl-Reuss assumptions must be used for biaxial loading conditions.

For elastic and elastic-plastic analysis, an increase in square root of J occurs under increasing biaxial load, however the stress transferred to the intact stringer decreases. Accompanying this behavior is an increase in crack opening displacement for increasing ratio of biaxiality. This influence is opposite of that observed in unstiffened sheets. There is a decreasing trend in plastic zone size with increasing biaxial loads.

The procedure outlined in Section 4.2 can be used to predict the residual strength of typical aircraft structure loaded in uniaxial tension. The extension of this procedure to biaxially loaded panels has also been explored using certain limiting assumptions with a good degree of success.

The phenomenon of crack arrest can be predicted by using the proposed residual strength prediction technique. It was determined that the resistance curve of the material must be replotted at the new crack length after crack arrest occurs.

5.2 OVERALL ACCURACY OF THE METHOD

Table XV is a summary of all structural panels tested during Phases II and III of this study. The average difference between predicted and measured residual strength for all panels is seen to be 3.1 percent which is well within the accuracy expected of the technique and well within the materials data scatter of ± 5 percent. As noted previously a prediction was not made for the biaxial panel tested at 1:2/3 load ratio due to failure in the attached doublers.

The residual strength of Phase II panels was predicted within 10 percent for some panels. The variation between predicted and actual failure stresses could be due to residual stresses in the panel accentuated by the chem-milling process. The predicted failure load of the panel is also dependent on the assumed yield stress of the material. In the analysis an average yield stress obtained from coupon tests was used. The yield stress of individual panels may vary. Therefore, an accurate estimate of yield stress is required for a higher degree of accuracy in predicting residual strength as noted in Reference 2.

TABLE XV COMPARISON OF PREDICTED AND MEASURED RESIDUAL STRENGTHS FOR PHASE II AND PHASE III PANELS

TYPE OF PANEL	RESIDUAL STRENGTH (ksi)		PERCENTAGE DIFFERENCE
	PREDICTED	MEASURED	
<u>Phase II (Short Crack)</u>			
• Riveted Zee Stiffeners with Lands	40.05	37.25	+ 7.5%
• Bolted Zee Stiffeners with Lands	40.05	36.39	+ 10.1%
• Adhesively Bonded Zee Stiffeners with Lands	43.8	42.03	+ 4.2%
<u>Phase II (Long Crack)</u>			
• Riveted Zee Stiffeners with Lands	27.5	25.98	+ 5.85%
• Bolted Zee Stiffeners with Lands	27.0	26.41	+ 2.2%
• Adhesively Bonded Zee Stiffeners with Lands	28.8	28.98	- 0.625%
<u>Phase III (Uniaxial Tension)</u>			
• Intact Stringer - Thin Skin (-15)	39.73	37.37	+ 6.32%
• Broken Stringer - Thin Skin (-23)	34.36	34.51	- 0.44%
• All Titanium Panel	78.86	76.45	+ 3.15%
• Aluminum Panel - Thick Skin (-1)	37.02	38.78	- 4.75%
<u>Phase III (Biaxial Loading)</u>			
• 1:1/3	40	39.87	+ 0.33%
• 1:2/3	—	36.98	—

REFERENCES

1. Ratwani, M. M. and Wilhem, D. P., "Development and Evaluation of Methods of Plane Stress Fracture Analysis - Part II, Vol. I, A Technique for Predicting Residual Strength of Structure," AFFDL-TR-73-42, Part II, Volume I, April 1975.
2. Wilhem, D. P. and FitzGerald, J. H., "Development and Evaluation of Methods of Plane Stress Fracture Analysis, Part II, Vol. II, Fracture Resistance and Material Property Characterization," AFFDL-TR-73-42, Part II, Volume II, April 1975.
3. Swift, T., "The Effects of Fastener Flexibility and Stiffener Geometry on the Stress Intensity in Stiffened Cracked Sheet," Proceedings of an International Conference on Prospects of Fracture Mechanics, Delft University of Technology, The Netherlands, G. C. Sih, H. C. van Elst, and D. Broek, editors, June 1974, pp. 389-404.
4. Hilton, P. D., "Plastic Intensity Factors for Cracked Plates Subjected to Biaxial Loading," International Journal of Fracture, Vol. 9, No. 2, June 1973, pp. 149-156.
5. Kibler, J. J., "Cylindrical and Spherical Shells with Cracks," Ph.D. Thesis, Department of Mechanical Engineering and Mechanics, Lehigh University, 1969.